UNIVERSITÉ GRENOBLE ALPES

THÈSE

Pour obtenir le grade de

DOCTEUR DE L'UNIVERSITÉ GRENOBLE ALPES

Spécialité : **Chimie et Biologie**

Arrêté ministériel : 7 août 2006

Présentée par

« Dhruv THAKAR »

Thèse dirigée par **« Liliane COCHE-GUERENTE »** et
codirigée par **« Ralf P. RICHTER »** et **« Didier BOTURYN »**

préparée au sein du **Département Chimie Moléculaire**
UJF-CNRS UMR5250
dans **l'École Doctorale Chimie et Science du Vivant**

Surfaces biomimétiques pour caractériser les interactions induites par les glycosaminoglycanes aux niveaux moléculaire, supramoléculaire et cellulaire

Thèse soutenue publiquement le **« 07 septembre 2015 »**,
devant le jury composé de :

Mme Dorothe SPILLMANN
Assistant professeur, Uppsala, Rapporteur
Mme Sofia SVEDHEM
Assistant professeur, Göteborg, Rapporteur
M David FERNIG
Professeur, Liverpool, Membre
Mme Corinne ALBIGES-RIZO
Professeur, Grenoble, Membre
Mme Liliane COCHE-GUERENTE
Maître de Conférences, Grenoble, Membre
M Ralf P. RICHTER
Professeur, San Sebastián, Membre

UNIVERSITÉ GRENOBLE ALPES

THÈSE

Pour obtenir le grade de

DOCTEUR DE L'UNIVERSITÉ GRENOBLE ALPES

Spécialité : **Chimie et Biologie**

Arrêté ministériel : 7 août 2006

Présentée par

« Dhruv THAKAR »

Thèse dirigée par **« Liliane COCHE-GUERENTE »** et
codirigée par **« Ralf P. RICHTER »** et **« Didier BOTURYN »**

préparée au sein du **Département Chimie Moléculaire**
UJF-CNRS UMR5250
dans **l'École Doctorale Chimie et Science du Vivant**

Well-defined biomimetic surfaces to characterize glycosaminoglycan-mediated interactions on the molecular, supramolecular and cellular levels

Thèse soutenue publiquement le **« 07 septembre 2015 »**,
devant le jury composé de :

Mme Dorothe SPILLMANN
Assistant professeur, Uppsala, Rapporteur
Mme Sofia SVEDHEM
Assistant professeur, Göteborg, Rapporteur
M David FERNIG
Professeur, Liverpool, Membre
Mme Corinne ALBIGES-RIZO
Professeur, Grenoble, Membre
Mme Liliane COCHE-GUERENTE
Maître de Conférences, Grenoble, Membre
M Ralf P. RICHTER
Professeur, San Sebastián, Membre

It is not the answers you give, but the questions you ask

- Voltaire

A mes parents

Acknowledgement

This thesis work would not have been possible without the help and support of the people around me, who in one way or another have assisted in the completion of this project, to only some of whom it is possible to give particular mention here.

Foremost, I would like to express my sincere gratitude to my supervisors Liliane Guerente, Ralf Richter and Didier Boturyn. First of all, I am grateful to Ralf Richter for giving me the opportunity to carry out an exciting PhD project in his Chair of Excellence "GAG2D" project. From the beginning of my PhD you all have constantly challenged me and there by inspired me to further develop my scientic knowledge. You have always given me the freedom to venture upon newer ideas and techniques, and always bestowed me with confidence. You have been a huge source of knowledge and inspiration. Your high scientific requirements, deep understanding of matter and perfect organization will be a benchmark for my future work. *Thanks to all of you!!*

I am grateful to Dorothe Spillmann and Sofia Svedhem for reviewing my thesis and to Corrine Albiges-Rizo, David Fernig, Liliane Coche-Guerente and Ralf Richter for being members of my examination board.

Another thanks goes to Didier Boturyn, Catherine Picart and Hugues Lortat-Jacob for joining my thesis committee, supporting my thesis, and fruitful discussions.

I would like to express my gratitude to Corrine Albiges-Rizo and Alan Le-Goff for reviewing my PhD every year and for providing various directions where I could orient my work.

I also would like to express my sincere gratitude to Hugues Lortat-Jacob, Catherine Picart and Ralf Richter for providing me with the opportunity to carry out this PhD project in an interdisciplinary collaboration with their laboratory. These collaborations led to inspiring and stimulating discussions and, furthermore, strongly supported my research with the supply of essential material. Special thanks to Rabia Sadir for many fruitful discussions, for supplying me with HS and proteins for my project and for helping me with the synthesis and Dot-blot measurements. I am also grateful to Fabien Dalonneau for introducing me to cell culture, and helping me in all the cell assays. Another thanks goes to Nico Eisele and Galina Dubacheva for introducing and teaching me ellipsometry measurements. *Merci beaucoup, Thanks, Danke!*

Another thanks goes to Olivier Renaudet for allowing me to work in his lab and for helping me in the oxime ligation.

Special thanks goes to Elisa Migliorini, for all the nice time that we spent, sharing the office and the project, and for all the fruitful discussions during this project. I had a lot to learn from you. *Grazie mille!!*

Moreover, I would like to express my gratitude to Christophe Travelet for the help with DLS measurements, Romain Vives for the help with HS functionalization.

The work would have been less pleasant and more difficult without the support of my friends and current and former colleagues at the Department of Molecular Chemistry (DCM), CICbiomaGUNE, SAGAG group and IMBM group, for all the nice time spent and the discussions that were valuable in the progress of the project.

I am grateful to Regine Rozand and Veronique Gineste who were always helpful with the administrative stuff. *Merci Regine et Vero!*

Another thanks goes to many of the collaborators already mentioned in my thesis.

Something which I am going to surely miss is the “mercredi midi foot” and the “interlabo tournament”. I am glad, I was a part of the team that brought the trophy to DCM. My special thanks goes to the football team, Fabien, Laurent, Alan, Thomas, Kamal, Serge, Bertrand, Nouredine, Damien and Thibaut. You made it special for me, thanks a lot guys!!

Un grand merci à Hugues, Adrien, Michaël, Fabien, Jerôme, Elisa, Laurent et les autres pour tous les pause café, c'était une source de recharge d'énergie pour moi.

This thesis would not have been possible without the financial support from the Nanoscience Foundation.

I would also like to thank my second family in France, my friends Adrien, Hélène, Fabien, Hugues, Meenakshi, Priyanka, Safeer, Sidhartha, Marc, Noémie, Fatima, Carlo…. for their support and all the nice time that we spent during my entire stay in France, and my French friends for teaching me French, specially Adrien. *Merci!!*

Last but certainly not the least; I thank my family for their unconditional love and support, and their unwavering faith on my abilities. Thanks for providing me courage and motivation all the time.

I am thankful to all those who have been a part of this wonderful journey.

Table of Contents

Abbreviations

Biomolecules

BSA	Bovine serum albumin
CS	Chondroitin sulfate
CRS	Chemokine recognition site
DS	Dermatan sulfate
ECM	Extracellular matrix
ERK	Extracellular signal-regulated kinase
GAG	Glycosaminoglycan
GPCR	G protein-coupled receptor
GlcA	Glucuronic acid
GlcN	Glucosamine
GlcNAc	N-acetyl glucosamine
HA	Hyaluronic acid
IdoA	Iduronic acid
ICAM-1	Intercellular adhesion molecule
KS	Keratan sulfate
MCP-1	Monocyte chemoattractant protein 1
MIP	Macrophage inflammatory protein
MAPK	Mitogen-activated protein kinase
OEG	Oligo ethylene-glycol
PG	Proteoglycan
RGD	Arginine-glycine-aspartic acid
RANTES	Regulated on activation normal T cell expressed and secreted
SAM	Self-assembled monolayer
SLB	Supported lipid bilayer
SDF-1α	Stromal cell-derived factor–1α CXCL12α
wt	wild type

Cell Culture

ANOVA	Analysis of variance
DAPI	4',6-Diamidino-2-phenylindole
DMEM	Dulbecco's modified eagle's medium
FBS	Fetal bovine serum

Techniques and equipment

HPLC	High performance liquid chromatography
NMR	Nuclear magnetic resonance
QCM-D	Quartz crystal microbalance with dissipation monitoring
SE	Spectroscopic ellipsometry
SPR	Surface plasmon resonance

Others

Hepes	(4-(2-Hydroxyethyl)-1-piperazineethane sulfonic acid)
M_w	Molecular weight
PBS	Phosphate buffered saline
POI	Plane of incidence
RT	Room temperature
RU	Resonance units
SDS	Sodium dodecyl sulfate
TIR	Total Internal Reflection
TRIS	2-Amino-2-hydroxymethyl-propane-1,3-diol

Objectives and outline

The adhesion and migration of cells are important for many physiological and pathological processes, including development, immune response, tissue remodeling and repair, arthritis, tumor metastasis and angiogenesis [1, 2]. In particular, they are key in muscle development and repair where myoblasts (muscle precursor cells) are activated and migrate to the desired site to promote muscle formation [3, 4]. The adhesion and migration of myoblasts is guided by signaling proteins (chemokines and growth factors) that reside in the extracellular space. Polysaccharides of the glycosaminoglycan family (heparan sulfate (HS) in particular) bind signaling proteins. By doing so, they help organizing and presenting signaling proteins in the extracellular matrix (ECM) and on the cell surface, and are thus important modulators of chemokine and growth factor function.

Despite their functional importance, GAGs have so far been largely neglected in *in vitro* models mimicking the extracellular environment due to their limited availability in sufficiently pure and suitably functionalized form, and a lack of methodologies to integrate them into assemblies. The objective of this PhD thesis was to develop biomimetic surfaces that are highly defined and tunable, for mechanistic studies of GAG-protein interactions on the molecular and supramolecular levels, and to probe cellular responses to defined biochemical and biophysical cues to better understand GAG-mediated cell-cell and cell-matrix communications.

The outline of thesis is as follows:

Chapter I provides a general introduction into the biological context. It covers muscle development and repair, extracellular matrix (ECM), and constituents of the ECM that are of particular importance for this thesis work, i.e. GAGs (HS in particular), chemokines (SDF-1α/CXCL12α in particular) and their receptors, and cell adhesion ligands (RGD in particular) and their receptors. Chapter I also covers the methodology adopted to attain the objectives, providing an introduction to surface functionalization and characterization techniques.

Chapter II covers methodological developments on the molecular level. Novel methods are presented for the site-selective functionalization of GAGs at the reducing end, and to characterize GAG conjugates.

Chapters III and IV cover the supramolecular level. Chapter III presents a versatile strategy to create biomimetic surfaces that present GAGs together with chemokines and other cell surface or extracellular matrix molecules in a highly defined and tunable way. First examples are provided as to how these surfaces can be used for mechanistic studies on the molecular, supramolecular and cellular levels.

Chapter IV covers the application of well-defined model surfaces to study the supramolecular interaction between HS and soluble signaling molecules (including chemokines). It is shown that such proteins can cross-link and rigidify HS films, and the functional implications are discussed.

Chapter V is dedicated to the application of well-defined surfaces for mechanistic studies with myoblasts in the context of muscle development and repair. We find that myoblasts respond to HS-bound CXCL12α (chemokine) through adhesion and motility, and that the mode of chemokine presentation strongly affects cell behavior. In addition, a synergistic effect between cell-surface CXCR4 (i.e. the CXCL12α receptor) and integrins (i.e. the RGD receptors) was observed on co-presentation of respective ligands.

Last but not least, concluding remarks and perspectives are covered in Chapter VI.

The research work accomplished is presented in Chapters II to V in the form of articles and manuscripts in preparation for peer-reviewed journals. Each of these chapters also contains more detailed introductions, as well as detailed descriptions of the materials and methods used. The works presented in Chapters II and III are already published; the work in Chapter IV is submitted and under revision, and Chapter V represents a manuscript in preparation.

Objectives and outline (en français)

L'adhésion et la migration des cellules sont importantes pour de nombreux processus physiologiques et pathologiques, comprenant le développement, la réponse immunitaire, le remodelage et la réparation tissulaire, l'arthrite, les métastases et l'angiogenèse tumorales [1, 2]. Ces processus sont essentiels en particulier dans le développement et la réparation musculaire où les myoblastes (cellules précurseurs du muscle) sont activés et migrent vers le site concerné pour favoriser la formation du muscle [3, 4]. L'adhésion et la migration des myoblastes sont guidées par des protéines de signalisation (les chimiokines et les facteurs de croissance) qui se trouvent dans l'espace extracellulaire. Les polysaccharides de la famille des glycosaminoglycanes (GAGs), -l'héparane sulfate (HS) en particulier- se lient aux protéines de signalisation. Ce faisant, ils aident à l'organisation et à la présentation des protéines de signalisation dans la matrice extracellulaire (ECM) et à la surface de la cellule, et sont donc des modulateurs importants des chimiokines et des facteurs de croissance.

Malgré leur importance fonctionnelle, les GAGs ont jusqu'ici été largement négligés dans les modèles *in vitro* mimant le milieu extracellulaire en raison de la disponibilité limitée des formes suffisamment pures et convenablement fonctionnalisées, et un manque de méthodologies à les intégrer dans des assemblages. L'objectif de cette thèse est de développer des surfaces biomimétiques bien définies et modulables, pour l'étude mécanistique des interactions protéine-GAG aux niveaux moléculaire et supramoléculaire. Il s'agira également de sonder la réponse cellulaire à des signaux biochimiques et biophysiques spécifiques pour mieux comprendre les communications cellule-cellule et cellule-matrice induites par les GAGs.

Ces travaux de thèse sont exposés de la manière suivante:

Le chapitre I présente une introduction générale dans le contexte biologique. Il couvre le développement et la réparation musculaires, la matrice extracellulaire (ECM), et les constituants de l'ECM. Ces constitutants sont d'une importance particulière pour ce travail de thèse: les GAGs (HS en particulier), les chimiokines (SDF-1α / CXCL12α en particulier) et leurs récepteurs, des ligands d'adhésion cellulaire (RGD) et leurs récepteurs. Le chapitre I expose également la méthodologie adoptée pour atteindre les objectifs, en fournissant une introduction des stratégies de fonctionnalisation de surface et des techniques de caractérisation.

Le chapitre II présente les développements méthodologiques au niveau moléculaire. Des nouvelles méthodes de fonctionnalisation sélective des GAGs à leur extrémité réductrice et de caractérisation des conjugués résultants sont présentées.

Les chapitres III et IV couvrent le niveau supramoléculaire. Le chapitre III présente une stratégie versatile pour créer des surfaces biomimétiques permettant d'assembler les GAGs les chimiokines et d'autre molécules contenues à la surface cellulaire ou dans la matrice extracellulaire, d'une manière bien définie et modulable. Les premiers exemples d'application de ces surfaces fonctionnelles pour des études mécanistiques aux niveaux moléculaire, supramoléculaire et cellulaire sont présentées.

Le chapitre IV couvre en particulier l'application de ces surfaces modèles à l'étude de l'interaction supramoléculaire entre le HS et des molécules de signalisation solubles (dont les chimiokines). Il est montré que ces protéines peuvent réticuler les chaines de HS conduisant à une rigidification des films. Les incidences fonctionnelles de la réticulation sont ensuite discutées.

Le chapitre V est dédié à l'application de ces surfaces fonctionnelles bien définies aux études mécanistiques avec des myoblastes dans le contexte du développement et de la réparation musculaires. Nous constatons que les myoblastes répondent à la chimiokine CXCL12α liée aux HS. La présentation des chimiokines par les chaînes de HS affecte le comportement des cellules, ce qui se traduit par une motilité cellulaire plus marquée. De plus, un effet synergique entre les récepteurs cellulaires, CXCR4 (le récepteur de la CXCL12α) et les intégrines (les récepteurs des ligands RGD) a été observé lors de la co-présentation des ligands respectifs.

Les observations finales sont formulées et les perspectives discutées dans le chapitre VI.

Le travail de recherche accompli est présenté dans les chapitres II à V sous la forme d'articles et de manuscrits en préparation pour des journaux à comité de lecture. Chacun de ces chapitres contient également des introductions plus détaillées, ainsi que des descriptions détaillées des matériaux et des méthodes utilisées. Les travaux présentés dans les chapitres II et III sont déjà publiés; le texte du chapitre IV a été soumis et est actuellement en cours de révision, et le chapitre V constitue un manuscrit en préparation.

I. Introduction

I.1. State of the art

I.1.1. Muscle development and repair

Skeletal muscle constitutes one of the major parts of the human body: around 640 skeletal muscles account for ~38% and 30% of total body mass for men and for women, respectively [5]. Muscles display a hierarchical structure (Figure I.1.1). They are comprised of long cylindrical fibres called myofibres that generate force by contraction. Myofibres in turn are composed of myofibrils, and myofibrils are packed with thousands of sarcomeres (Figure I.1.1) that contain the actin and myosin filaments that interact to produce the force [6, 7].

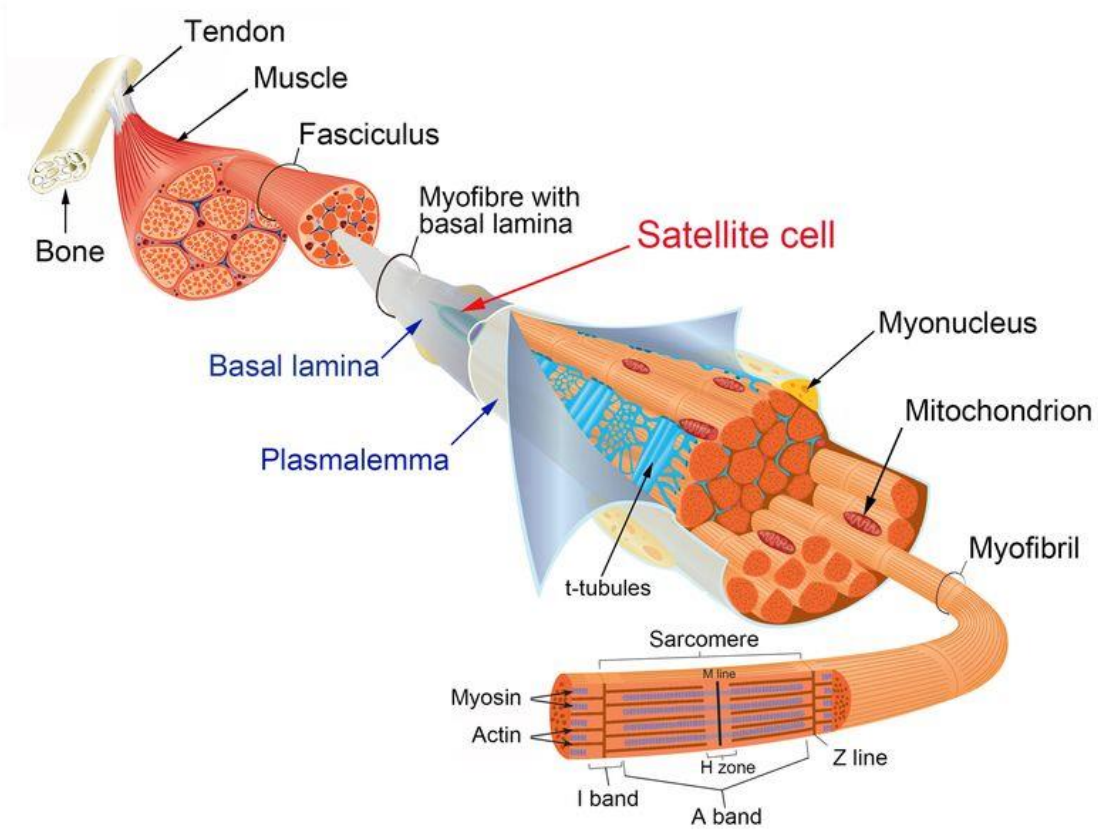

Figure I.1.1: Basic structure of skeletal muscle. Image adapted from ref [6, 7].

During the development of muscle cells, muscle precursor cells called myoblasts fuse to form myocytes which in turn fuse to give myotubes [6, 8]. These myotubes gives rise to the myofibres which then grow in size and form the skeletal muscle. Adult mammalian muscle retains a stable morphology under normal conditions yet undergoes continuous turnover to compensate for regular wear and tear, but excessive use or accidents can

lead to injury [9]. Skeletal muscle has a remarkable ability to regenerate. In response to injury, skeletal muscle undergoes a highly orchestrated regenerative process that involves the activation of satellite cells [9]. Satellite cells are stem cells and are located in a niche on the surface of the myofibre (Figure I.1.1). In response to injury, they get activated, proliferate, and differentiate into myoblasts. These then form myotubes (Figure I.1.2) and thus recover the injured muscle [6, 7, 9, 10]. These satellite cells are the source responsible for the generation of myoblasts in the postnatal skeletal muscle development and repair [11].

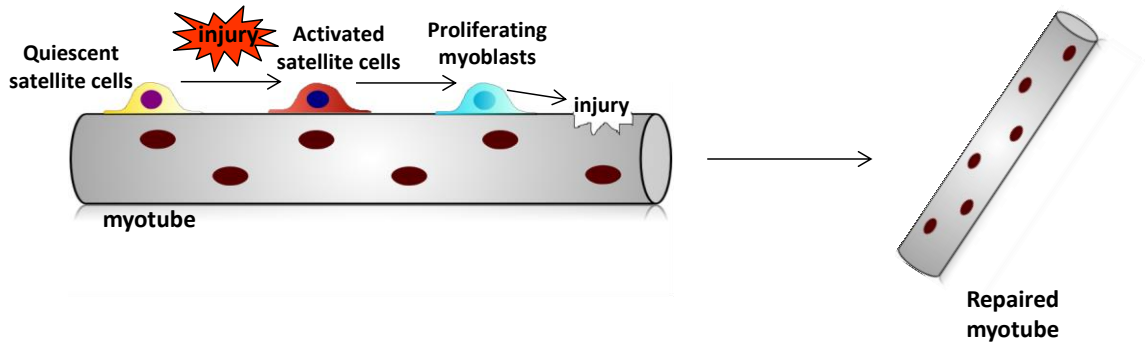

Figure I.1.2: Muscle regeneration. The repair of muscle in response to an injury involves the activation, proliferation, differentiation and fusion of myoblasts that are derived from the satellite cells to form myotubes.

The regenerative activity greatly relies on the dynamic interplay of satellite cells with their environment (i.e. the stem cell niche). An important part of the environment is the extracellular matrix (ECM) (Figure I.1.4) [12]. The ECM, described in detail in the next section, provides various signals thus guiding activities from maintenance of quiescence and stem cell potential to the regulation of proliferation and differentiation [13].

Even though satellite cells hold particular importance in muscle development and repair, their application in clinical practice is limited. This is due to the rapid loss of their muscle stem cell properties once they are removed from their *in vivo* environment [14]. For the purpose of studying myogenic differentiation, muscle cell lines have appeared as interesting candidates in *in vitro* studies [15, 16]. Access to a muscle cell line that serves as a tool to study certain aspects of myogenesis and muscle biology [16, 17], was crucial in the context of this thesis to study muscle development and repair.

I.1.2. Extracellular matrix (ECM)

Tissue formation, function and regeneration after damage are the result of a balanced interaction of numerous cellular processes, in which the cell is guided by signals originating from the extracellular environment. Signals in the cellular microenvironment originate either from the ECM (cell-matrix interactions) or from neighboring cells (cell-cell interactions) (Figure I.1.3). The ultimate decision of a cell to proliferate,

differentiate, migrate, undergo cell death (apoptosis) or perform other specific functions is a coordinated response to these signals [18].

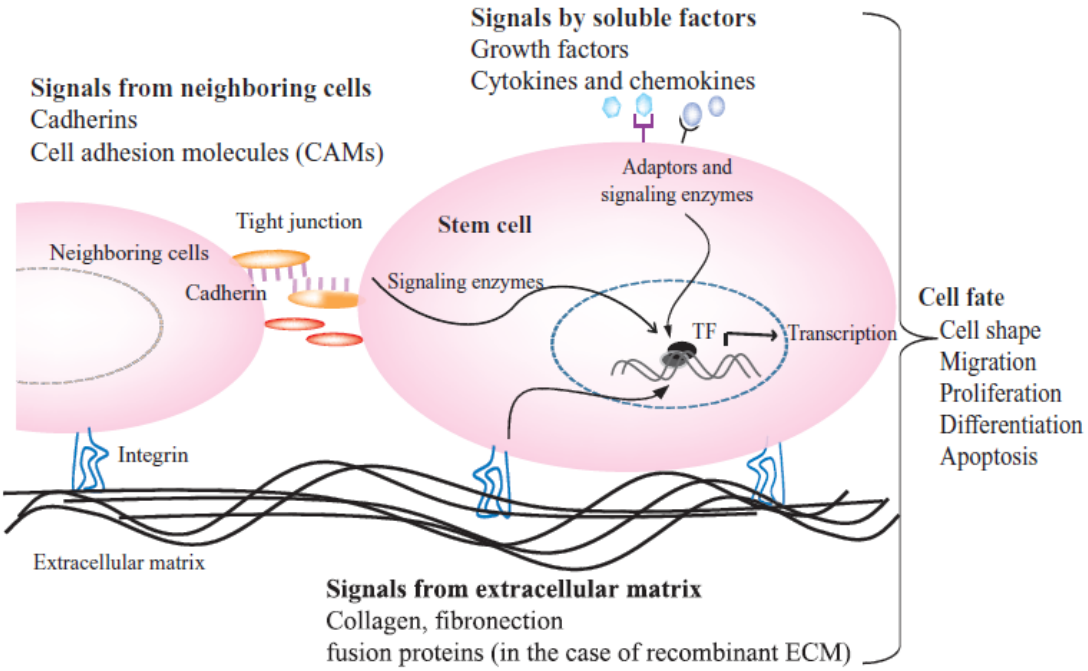

Figure I.1.3: Interactions of cells (stem cells as an example) with their microenvironment and the effect on cell behavior. Image taken from ref [18].

The ECM is the non-cellular component present within all tissues and organs. It provides essential physical scaffolding for the cellular constituents and signals in the form of biochemical and biomechanical cues (Figure I.1.4) [19]. The ECM directly influences cell behavior through ECM-specific receptors on the cell surface. By binding to the ECM through these receptors, cells sense their surroundings and actively modulate their behavior depending on ECM composition [20, 21].

The ECM is composed of various biochemically distinct components including proteins, (e.g. collagens, laminins, fibronectin, vitronectin, elastin, growth factors and small matricellular proteins), proteoglycans, and polysaccharides. The precise composition of ECM in contrast varies from tissue to tissue. Both the protein-rich and polysaccharide-rich (glycosaminoglycans (GAGs) and proteoglycans) molecules of the ECM are secreted by cells and are assembled into an organized meshwork, adapted to the functional requirements of the particular tissue [19].

In the context of cellular adhesion and migration, the highly hydrated network formed by proteoglycans and GAGs serves an important role by sequestering and storing soluble signaling molecules and presenting them to receptors on the cell surface (Figure I.1.4) [22]. This network binds and helps in the formation of gradients of signaling proteins

(chemokines) which is then sensed by the receptors on the cell surface, which in turn leads to internal signalization initiating cellular adhesion and migration [23-26].

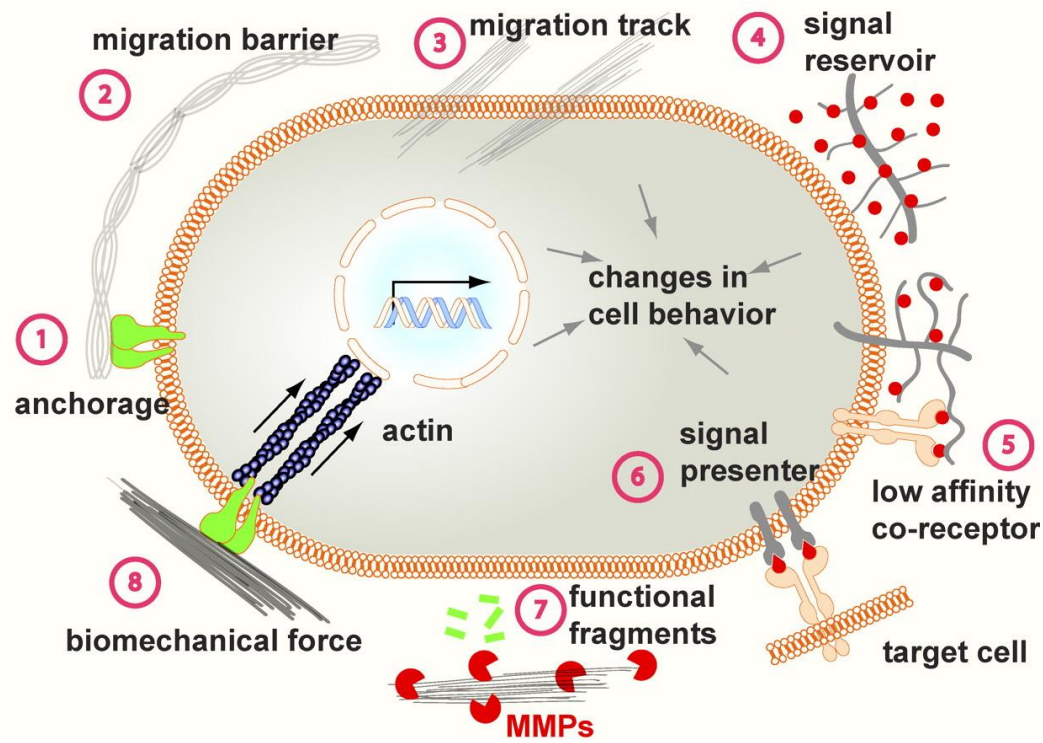

Figure I.1.4: Mechanisms of ECM function. The versatile functions of the ECM depend on its diverse physical, biochemical, and biomechanical properties. (1) Anchorage to the basement membrane; depending on contexts, the ECM may serve to block (2) or facilitate cell migration (3); In addition, by binding to chemokines and preventing their otherwise free diffusion, the ECM acts as a sink for these signals and helps shape a concentration gradient (4); certain ECM components, including heparan sulfate proteoglycans and the hyaluronic acid receptor CD44 selectively bind to different chemokines and function as a signal co-receptor (5) or a presenter (6). The ECM also directs signals to the cell by using its endogenous growth factor domains (7); finally, cells directly sense the biomechanical properties of the ECM, including its stiffness, and change a wide variety of behaviors accordingly (8). Image taken from ref [27].

The ECM is however not a static entity. It is modified, degraded and reassembled during development and even during wound healing [19, 20, 28]. This remodeling of ECM is mediated enzymatically or non-enzymatically, during which its components undergo a series of modifications. ECM dynamics/remodeling is important for various physiological processes, and misregulation can leads to pathologies [29, 30].

There are two major types of ECMs, the interstitial and pericellular matrices:

- **Interstitial matrix** is a matrix of connective tissue and consists of a tissue-specific mixture of a variety of collagen types, elastins, fibronectin, as well as proteoglycans and GAGs [19]. The negatively charged proteoglycans and GAGs

form a hydrated network where the fibrous proteins, soluble signaling proteins are embedded. This network allows the diffusion of bioactive molecules, while the embedded proteins strengthen and organize the matrix.

- **Pericellular matrices** are matrices present in close contact with cells that have a different molecular composition than the surrounding interstitial matrix. Basement membranes, for example, which are prototypes of pericellular matrices are primarily composed of laminins, collagen type IV, and perlecan (a heparan sulphate proteoglycan) [31].

For the work presented in this PhD thesis, glycosaminoglycans, chemokines and cell adhesion ligands are of particular importance. These will be presented one by one in detail in the following.

I.1.3. Glycosaminoglycans (GAGs)

GAGs are a group of acidic and linear polysaccharides ubiquitously present on the cell surface (glycocalyx) and in the ECM. They are crucial for matrix assembly, cell-cell and cell-matrix interactions. Each tissue produces specific repertoires of GAGs, some of which are known to interact with structural (e.g. collagen, fibronectin) and signaling (e.g. chemokines, growth factors) proteins and extracellular matrix, or adhesion molecules, and thereby regulate matrix assembly and remodeling, as well as cell-matrix and cell-cell interactions [32, 33]. They are usually found attached covalently through their reducing end to core proteins, forming the proteoglycan [34, 35] family (Figure I.1.5). Proteoglycans occur as an integral component of cell and basement membrane in probably all the mammalian tissues. Interaction of GAGs with other ECM components contribute to the general architecture and permeability properties of basement membranes, and thus these GAGs play a structural role. Typically, GAG function relies on the integration of its multiple interactions with proteins. For example, GAGs control the remodeling of extracellular matrices by binding to structural proteins [36, 37], crosslinking proteins [38, 39] or bulky GAG-binding proteoglycans [40-42]. Moreover, GAGs sequester [43, 44] and regulate the mobility [45] of chemokines or growth factors in matrix. Finally, the presentation of chemokines at controlled densities or in the form of gradients is controlled by GAGs to promote distinct cellular responses such as adhesion or directed migration [46, 47].

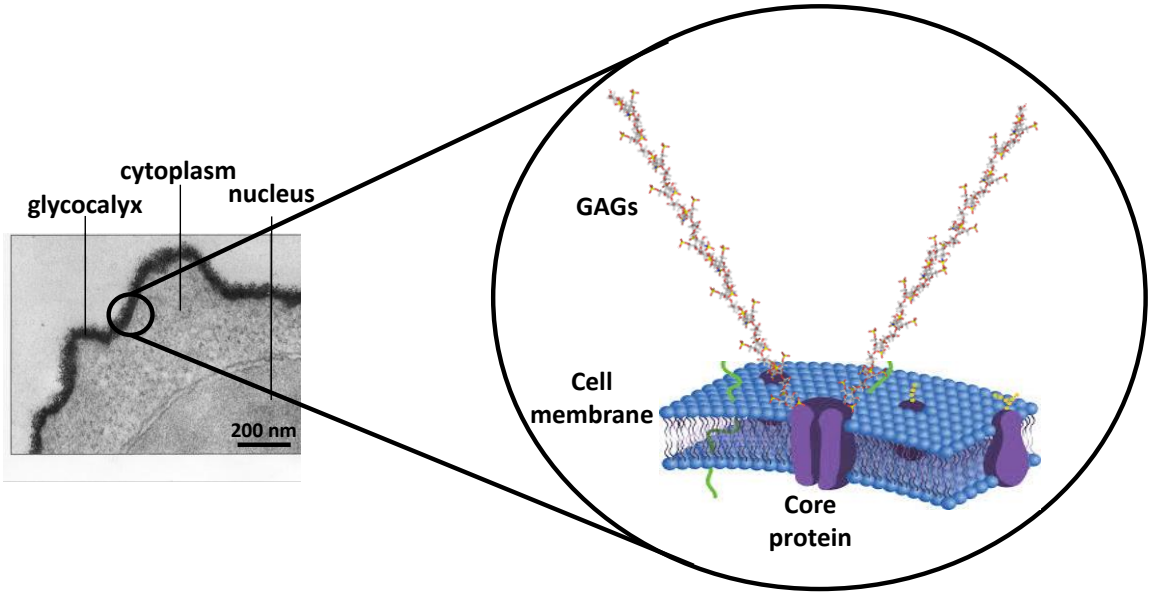

Figure I.1.5: An electron micrograph depicting a lymphocyte cell stained in ruthenium red showing the glycocalyx layer, which can reach up to 0.5 µm in thickness. The scheme demonstrates that the glycocalyx consists of polysaccharides (GAGs) bound to core proteins. This is the interface through which the cell conducts its liaison for all biological processes. The scheme is not to scale.The electron micrograph was taken from ref [48].

I.1.3.a. Structure of GAGs:

GAGs consist of a succession of disaccharide units comprising a hexuronic acid (either a β-D glucuronic acid [GlcA] or a α-L iduronic acid [IdoA]) and a hexosamine residue (either a glucosamine [GlcN] or a galactosamine [GalN]), either or both of which (except for hyaluronan) could be sulfated on different positions. With such a basic disaccharide constituent unit, an enormous molecular diversity is generated on three different levels for GAGs; firstly, the length of these chains can vary (chain lengths can range from few to few thousand of disaccharide units); secondly, individual monosaccharides can be structurally modified (N- and O-sulfations and epimerizations); finally the number and combinations of sulfated regions along an oligosaccharide chain can vary (Figure I.1.6). The members of GAG family are: hyaluronan (HA), chondroitin (CS)/dermatan sulfate (DS), heparan sulfate (HS)/ heparin, and keratan sulfate (KS) (Figure I.1.6).

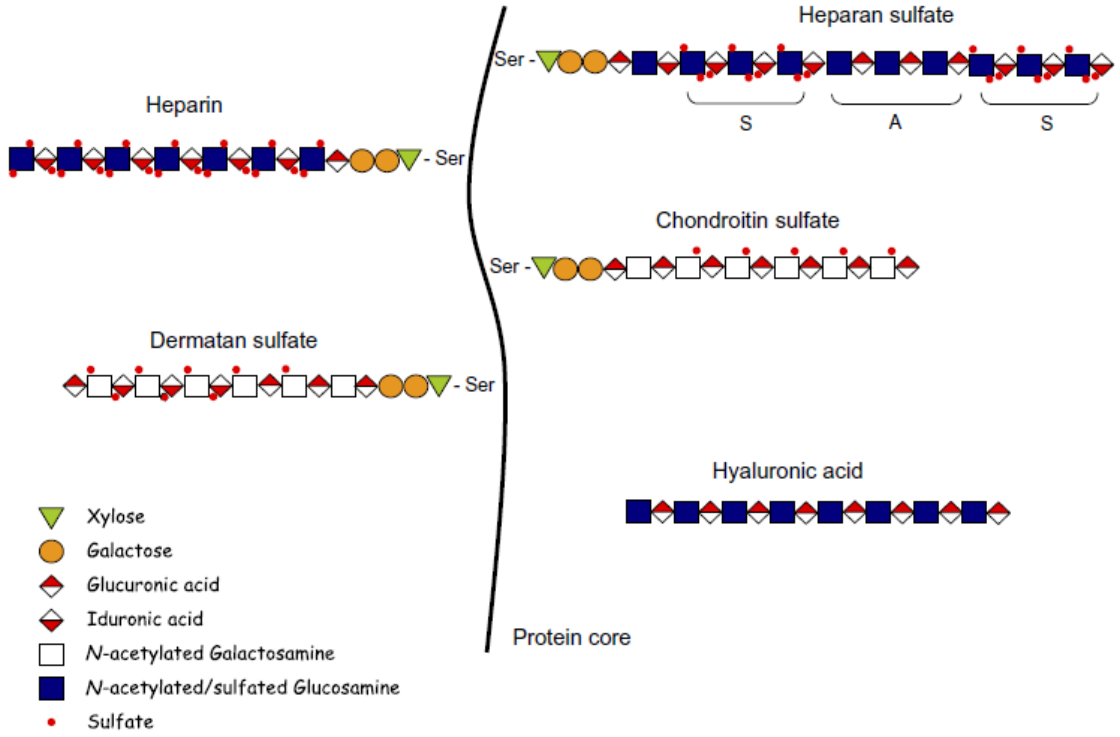

Figure I.1.6: Schematic representation of different GAGs. (Image from Imberty et al. [49])

Hyaluronan (HA) is the only GAG which is not covalently linked to a protein core in the form of a proteoglycan, but instead interacts non-covalently with selected proteoglycans such as aggrecan. It also interacts with other proteins *via* their hyaluronan-binding motifs. In addition, it has the simplest structure out of all GAGs as it is not sulfated; it is composed of β-D-glucuronic acid (GlcA) (1-3)-linked to N-acetyl glucosamine (GlcNAc) (linkages between disaccharide units are 1-3). Keratan sulfate (KS) disaccharides consists of β-D-galactose (1-4)-linked to N-acetyl glucosamine. In chondroitin sulfate (CS), the disaccharide unit is a β-D-glucuronic acid (1-3)-linked to N-acetyl galactosamine (linkages between disaccharide units are 1-4). Galactosamine can be sulfated on the C-4 or C-6 (or both) positions. β-D-Glucuronic acid in CS is converted to α-L-iduronic acid in dermatan sulfate (DS) by C-5 epimerization.

I.1.3.b. Heparan sulfate (HS)

Heparan sulfate (HS) is the structurally most complex member of the GAG family. This GAG is of particular interest for this thesis work, and is thus described in further details in this section. HS is ubiquitously found in the form of HS proteoglycans (HSPGs) [34, 35, 50]. HSPGs are widely distributed throughout animal tissues and are primarily localized as associated with the plasma membrane or with basement membranes [51, 52], where they interact with a plethora of ligands. In particular, HSPGs bind circulating growth factors and chemokines that regulate cell growth and migration [32]. Being present at

the interface between a cell and its microenvironment, HS plays important roles in cell-cell and cell-matrix interactions.

HSPGs have been located on the cell surface with a typical concentrations of around 10^5-10^6 molecules/cell [53]. HS chains vary in size from ~5 to 70 kDa while the protein cores vary in size from ~32 to 500 kDa [54]. Individual HS molecules can be imagined as relatively flexible chains. For a mean M_w of 30 kDa, the corresponding contour length is around 50 nm [53]. With these dimensions and mobility of the chains around the anchored core proteins, ~ 10^5 HS proteoglycans would encompass the entire surface of a spherical cell of 15 µm radius [53]. This corresponds to an average distance of around a few nanometers between HS molecules on the cell surface.

I.1.3.b.i. Biosynthesis of HS:

The biosynthesis of HS can be divided into three steps: chain initiation, polymerization and polymer modification. The biosynthesis is initiated by the formation of the tetrasaccharide linker between the core protein Ser-Gly and the polysaccharide chain. Addition of the first hexosamine decides whether the chain becomes CS (GalNAc) or HS (GlcNAc) [55]. HS polymerization then begins with the alternating addition of GlcA and GlcNAc (1–4 linked) to the non-reducing end of the chain by the enzymes EXT1 and EXT2 in the golgi apparatus where they form the HS polymerase [56].

I.1.3.b.ii. Structure of HS:

The polymer is subsequently modified by a series of localized, enzyme-mediated reactions that begins by N-deacetylation/N-sulfation of the GlcNAc and is followed by C-5 epimerization of GlcA to iduronic acid (IdoA) and O-sulfation at different positions (C3 or C6 position for the GlcN and C2 for the GlcA/IdoA residues) [57, 58]. These modifications give rise to distinctive and highly sulfated domains (S-domains) of variable size and extreme sequence diversity, which act as protein binding motifs, separated by regions of low sulfation (A-domains) enriched in N-acetylated disaccharide units (Figure I.1.7) [59]. Depending on the nature, the extent and the position of sulfate groups along the chain; these molecules can display a very large variety of structures. Jastrebova *et al.* have demonstrated that the effects of HS on FGF2 signaling are determined by both the structure of the highly sulfated domains and by the organization of such domains within the HS chain [60]. On average, HS contains less than 1 sulfate per disaccharide. Heparin is similar to HS but with a much higher degree of sulfation and with the sulfations homogeneously distributed along the chain.

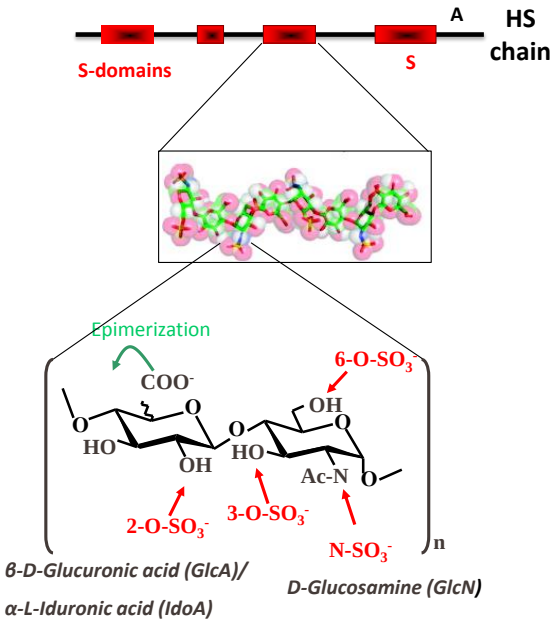

Figure I.1.7: HS chain is polymerized as a linear succession of disaccharide units comprising alternating D-glucuronic (GlcA) and D-glucosamine (GlcN) residues. Consecutive stretches of these units are modified by the concerted activities of multiple biosynthesis enzymes (red and green arrows), giving rise to motifs of appropriate sulfation pattern (S-domains; in red) that constitute protein binding sites). Along the chain, these S-domains alternate with regions of low sulfation (A-domains; in black). Figure adapted from ref [61, 62].

HS (and other GAGs) assume extended structures in aqueous solutions because of their strong hydrophilic nature based on their extensive sulfation patterns, which is further enhanced when they are covalently linked to core proteins. Through their S-domains, HS bind to a plethora of proteins including chemokines. It is *via* these interactions with chemokines, that HS (and GAGs in general) control the adhesion and migration of cells.

I.1.4. Chemokines

Chemokines are small proteins (8-12 kDa in their monomeric form) which possess chemoattractant properties. These proteins bind to and trigger the activation of cell-surface receptors, and thus regulate many cellular functions. Chemokines and their receptors are important in various biological processes such as dendritic cell maturation [63], and T and B cell development [64, 65]. Thus they are essential to many developmental and physiological possesses. In particular chemokines being chemoattractant proteins in nature, control and direct the orientated migration of cells during development, routine immune surveillance, development, angiogenesis, neuronal patterning, hematopoiesis, wound healing, inflammation, viral infection, and metastasis [66, 67].

The chemokine family comprises more than 50 members. In contrast, there exist approximately a total of 20 chemokine receptors, meaning that there are many

receptors which bind more than one chemokine. HS plays a vital role in binding of chemokines to its receptors, it binds and presents chemokines to the receptor at adequate orientation and thereby regulates chemokine binding to the cell receptor. Chemokine receptors are G protein-coupled, seven-helix transmembrane receptors (GPCRs) [67]. Chemokines are the only members of the cytokine family that act on GPCRs, where cytokines are small proteins which are important for cell signalling.

According to the latest nomenclature, chemokines are classified as CC, CXC, CX3C, or C chemokines depending on the presence and structure of the first two conserved cysteine motifs in the amino-terminal region of the molecule [68]. The first two cysteines are adjacent in CC chemokines (as in CCL5, commonly known as RANTES), are separated by residues in CXC (as in CXCL8 (interleukin-8, IL-8) and CXCL12 (commonly known as stromal cell-derived factor-1, SDF-1)). While C chemokines (XCL1, commonly known as lymphotactin) possess only a single cysteine motif [69, 70]. This motif is followed by an L (for ligand) and an identifying number (CCLn or CXCLn for example). Similarly chemokine receptors are named by the chemokine class they recognize and numbered by their order of discovery (CCR1 and CXCR1, for example, are the first discovered receptors specific for CC and CXC chemokines, respectively).

I.1.4.b. Migration in response to chemokines

Chemokines, once secreted in response to different stimuli, are presented to cells in form of gradients which initiates cell migration [71]. This directional migration of cells in response to soluble, freely diffusing chemoattractants (chemokines) is termed chemotaxis (Figure I.1.8). GAGs interact with chemokines and thus fulfill several roles. They protect secreted chemokines from proteolysis [72]; prevent them from diffusing away from their sites of production and dispersing under the influence of flow, and instead retain them; and finally present them to chemokine receptors [73]. The directed migration of adhered cells in response to gradients of chemoattractants on a surface (2D, left) or on tissue structures (3D, right) is termed haptotaxis.

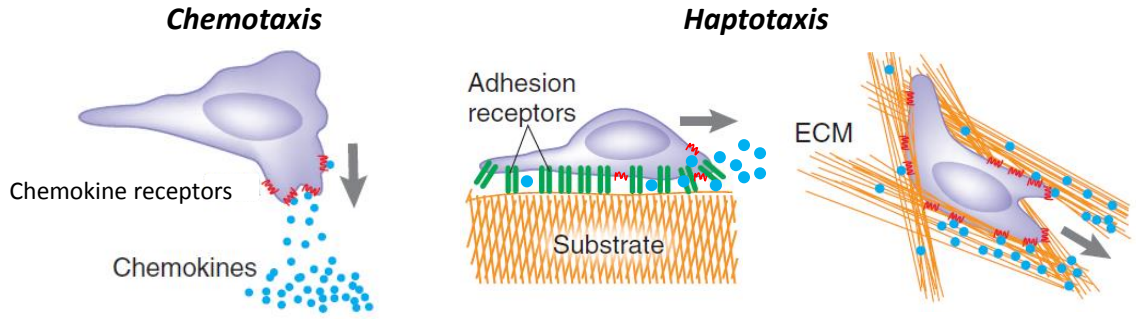

Figure I.1.8: Different modes of cellular migration. Chemotaxis is the directional migration of cells in response to soluble, freely diffusing chemoattractants (chemokines) while haptotaxis is the directed migration of adhered cells toward chemoattractants on a surface (2D, left) or on tissue structures (3D, right). Image adapted from ref [74].

On binding to its receptor (GPCRs), chemokines activate various signaling pathways such as the mitogen-activated protein kinase pathway (MAPK pathway) [75-77]. The activation and successful signaling of GPCRs is detected by the phosphorylation of extracellular signal-regulated kinases (ERK), one type of MAPK. These complex signaling cascades regulate the adhesion and migration of cells [77]. In order for a cell to initiate migration, it must undergo a polarization in its morphology which will enable it to convert cytoskeletal forces into a net cell-body displacement. These morphological changes involve the rearrangement of the cytoskeleton, changes in filamentous F-actin and the formation of integrin-mediated focal adhesions. The cell binds and detaches from the substrate in a coordinated manner with extension and retraction of pseudopods executing the directional migration [78, 79].

GAGs play an important role in the migration of cells. They help in organizing and presenting signaling proteins in the extracellular matrix (ECM) and on the cell surface, thus providing the appropriate molecular cues for migrating cells (Figure I.1.9).

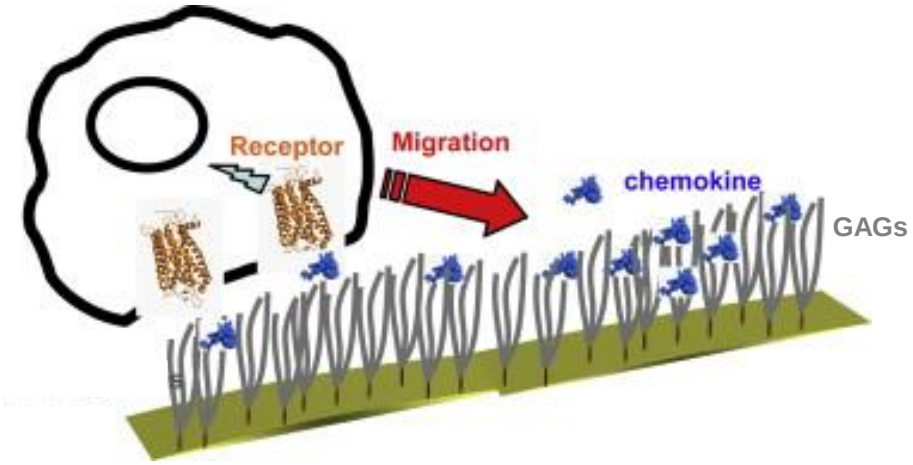

Figure I.1.9: Schematic representation of cellular migration along the extracellular matrix or cell surface. At the cell surface or extracellular matrix, GAGs sequester chemokines and help maintaining chemokine gradients and/or modulate their presentation to their G-coupled protein receptor. Image taken from ref [61].

I.1.4.c. Stromal cell-derived factor (SDF-1 also known as CXCL12)

Stromal cell-derived factor-1 (SDF-1) is a member of the CXC chemokine family, and hence called CXCL12 [69, 80]. CXCL12 has been shown to be important in cellular adhesion and migration in the context of muscle development and repair, and in inflammation, and is hence described in details here. It exists in predominantly three different isoforms: α, β and γ. The α form encodes a 68 amino acid peptide [81, 82]. The other two isoforms also contain this sequence. Specifically, the β isoform contains four additional amino acids at the C terminus, while the γ isoform has an elongated 30 amino

acid C-terminal with multiple HS binding domains (BBXB like sequences, where B and X stand for basic and neutral/hydrophobic amino acids) [62].

I.1.4.c.i. CXCL12α

CXCL12α is a potent chemo-attractant for a variety of cells, including monocytes and T-cells during inflammation [83, 84], and muscle precursor cells during embryonic myogenesis [4, 85, 86]. The main functions of CXCL12α thus include leukocyte and muscle precursor cell migration which it controls by interacting with its receptors, predominantly CXCR4 and CXCR7. The CXCL12α/CXCR4 pair is important, as mice lacking either the CXCL12α or the CXCR4 gene die *in utero*, with a number of defects including severe developmental abnormalities [87]. Unlike most other chemokines, the production of which is induced by cytokines or mitogenic stimuli, CXCL12α is constitutively expressed in a large variety of tissues [88-90].

Structure of CXCL12α:

The ternary structure of CXCL12α as reported by Crump *et al.* [91] consist of a disordered N-terminal domain (residues 1 to 8), followed by a long flexible loop, a 3_{10} helix, and a triple-stranded antiparallel β-sheet overlaid by a C-terminal α-helix (Figure I.1.10). Disulfide bonds stabilize the overall topology [92].

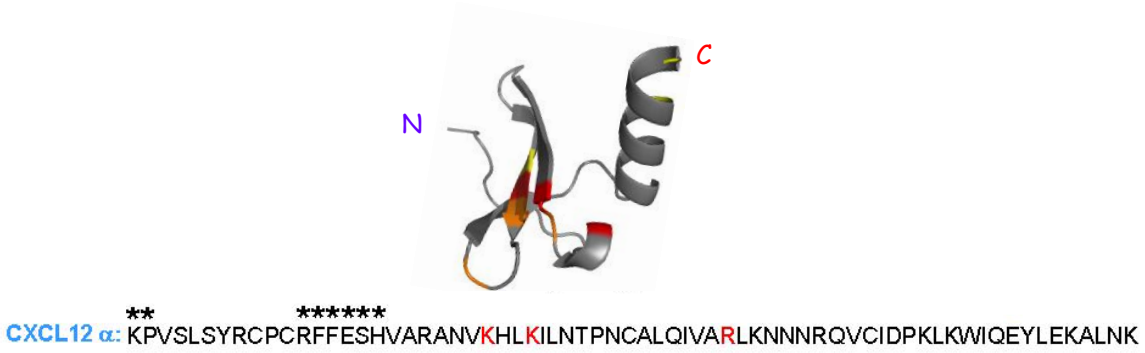

*Figure I.1.10: Structure of CXCL12α. The basic amino acids (K and R) that are highlighted in red in the sequences are amino acids that have been shown to be implicated in GAG-binding. ** KP signalling residues, ****** RFFESH initial contact/docking site with receptor. Chemical shift variations upon GAG addition (dp4) are represented in color; Red residues bind the most to GAGs and orange residues bind less and yellow residues bind the least [43, 61].*

I.1.4.c.ii. CXCL12γ

The elongated 30 amino acid C-terminal of the γ-isoform consists of as much as 18 basic residues (B), 9 of which being clustered into three putative BBXB HS-binding domains with multiple HS binding domains (BBXB) which are unique to this isoform (Figure I.1.11). The presence of the elongated C-terminal reduces the interaction of the γ-isoform with the CXCR4 receptor compared to the α isoform [43], but in contrast broadens the spectrum of GAGs to which it binds. Moreover, this domain also stabilizes

the CXCL12/HS complex and, in cooperation with the K24-R41 epitope, provides the γ-isoform with a higher affinity for GAGs compared to the α-isoform [43].

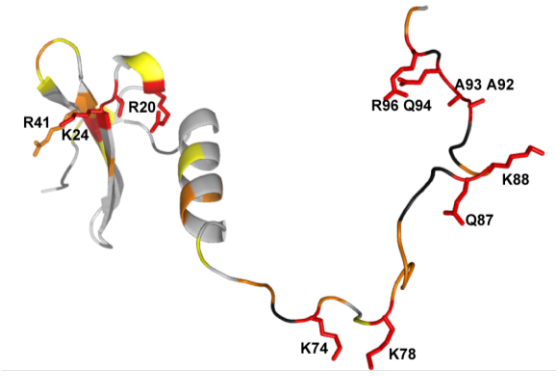

γ KPVSLSYRCPCRFFESHVARANVKHLKILNTPNCALQIVARLKNNNRQVCIDPKLKWIQEYLEKALNKGRREEKVGKKEKIGKKKRQKKRKAAQKRKN

Figure I.1.11: Structure of CXCL12γ. In addition to the 68 amino acid residues, the γ isoform has an elongated 30 amino acid C-terminal where GAG-binding domains (BBXB) are indicated by black brackets. Image adapted from ref [43].

I.1.5. HS-chemokine interactions

HS hold a significant biological importance as they are key role players in various important biological functions *via* their interactions with chemokines. The study of these interactions (structural studies, dynamics and functional studies) is paramount to understanding the biological phenomena associated with GAGs as well as harnessing their properties for therapeutic applications.

At the site of secretion, chemokines (usually highly basic proteins) bind to HS (or other GAGs) (high density of negative charge) through ionic interactions. These ionic interactions between GAGs and chemokines have been demonstrated *in vitro [93, 94]* and *in vivo [95]*. In the absence of such interactions, diffusion would occur, dissipating directional gradients and ceasing cell migration [44]. In addition, surface-confined i.e. GAG-bound chemokines elicit different responses than soluble chemokines. For example, inside-out signaling of integrins requires surface-confined chemokines [96-99]. Paradoxically, chemokines are simple and small proteins yet they orchestrate multiple biological functions. Their interactions with GAGs may explain the ability of such simple proteins to have access to such a wide range of functions.

However, regulation of chemokine functions by HS goes well beyond just the localization of chemokine and includes effects on chemokine processing, oligomerization, receptor recognition and specificity:

- **Chemokine processing.** Interaction of chemokines with membrane serine protease that mediates the removal of the N-terminal dipeptide of chemokine, leading to chemokine inactivation, is prevented by CXCL12α association with HS

[72]. In addition to this protease, GAGs also prevent degradation of chemokines by other metalloproteinases [100, 101].

- **Oligomerization.** HS or HS-derived oligosaccharides have been shown to induce dimerization and even larger oligomerization states of most chemokines [62], modulate the monomer–dimer equilibrium, or even promote chemokine heterodimerization [102], thus promoting local high concentrations of chemokines in the vicinity of the GPCRs [93]. HS favors dimerization by increasing the local concentration of the chemokines. The oligomeric state of the chemokine is functionally important [103, 104] but how these oligomerization and clustering effects modulate chemokine activity is not yet well understood.
- **Receptor recognition.** HS may also differentially regulate chemokine activity on which receptor it signals through, depending on the respective localization of HS and receptor binding sites on the chemokine surface and their potential overlap. For example, mutation of the basic residues that form the principal CCL5 HS binding site significantly decreases CCR1 binding while binding to CCR5 remains unaffected [105, 106].
- **Specificity.** Each tissue or cell type produces specific repertoires of HS structure [107, 108]) and as chemokine binding to HS depends on the HS structure, this may significantly contribute to the specificity of the cellular response in addition to the specificity of chemokine–receptor interaction itself [109].

The presence of immobilized HS is essential for the biological activity of chemokines as soluble heparin has been shown to inhibit the biological effects of chemokines as demonstrated *in vitro* [94] and *in vivo* [110]. Recently, soluble heparin and HS were shown to negatively affect chemotaxis *in vitro* mediated by CXCL12α [111]. In addition, treatment of cells with heparitinases (enzymes that degrade HS and heparin) also induces a significant reduction of CXCL12α binding to cells [112, 113].

I.1.5.a. Structural aspects of HS-CXCL12α interactions

The interaction between HS and CXCL12α is primarily electrostatic, involving interactions between anionic sites on the HS and cationic side chains within the protein (ammonium, guanidinium or imidazolium groups of lysine, arginine or histidine). The isoelectric point of CXCl12α is close to 9, hence it possesses a net positive charge under physiological conditions. Since the interactions between chemokines (and other heparin binding proteins) and negatively charged HS are electrostatic, this may lead to the false perception that chemokines bind HS in a non-specific manner. However, it has been shown that certain residues in the chemokine sequence have specific interactions with the sulfated domains of HS, and that these interactions result in the regulation of CXCL12α function [81]. These are described in detail below.

A technique to determine the GAG binding sites on chemokines is to mutate basic residues within linear sequences which contain the GAG-binding motif. Despite existing as monomers under biological conditions in solutions, CXCL12α tends to dimerise/oligomerise upon interaction with GAGs [114]. This oligomerisation may increase the affinity for GAG binding as a larger binding surface is created [115].

A few years ago, Lys24 and Lys27 were identified as essential binding sites of CXCL12α on heparin by Amara *et al.* and Sadir *et al.* [72, 81, 82]. Arg41 and Lys43 were also involved in the interaction, however are not essential. The authors also confirmed the involvement of Lys1 along with Lys24, Lys27 in the binding for the polysaccharide (Figure I.1.12). In addition, an octasaccharide of HS was demonstrated as the smallest HS fragment able to bind CXCL12α efficiently [81].

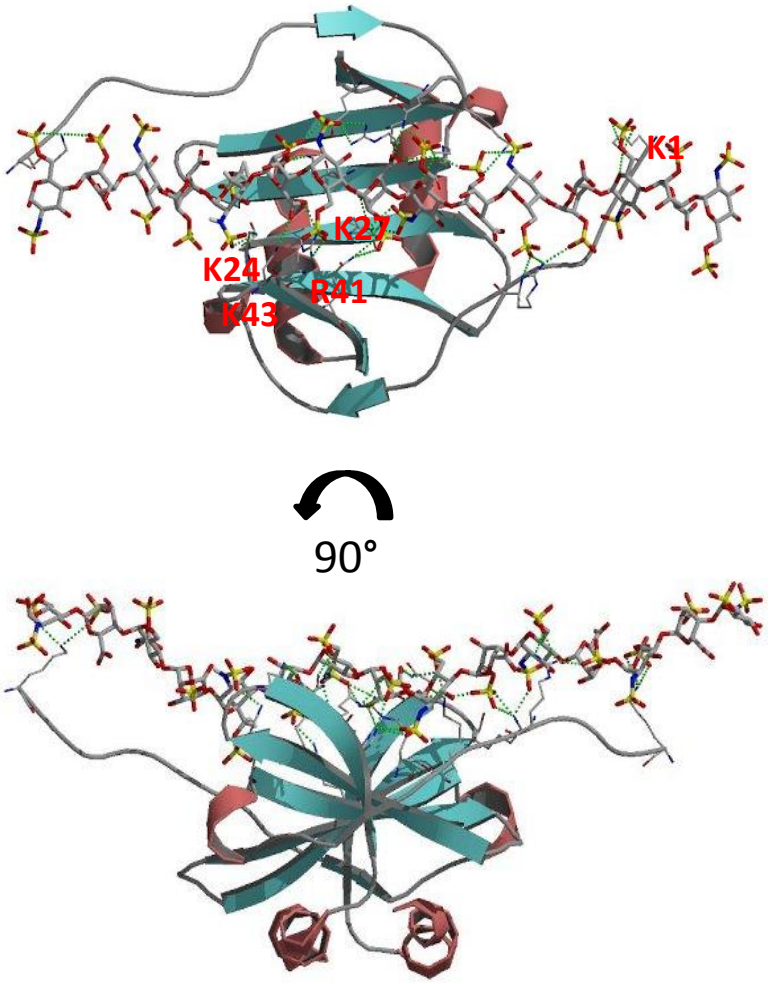

Figure I.1.12: Orthogonal representations of the model for the interaction of heparin with CXCL12α dimer. The protein is represented as a ribbon. The heparin polysaccharide, together with the basic amino acids involved in the interaction, is represented as sticks. Image taken from ref [81].

More recently, Laguri *et al.* followed the binding interaction by NMR spectroscopy and revealed a structural model of the CXCL12α-HS complex (Figure I.1.13) [116]. With this

tool, a more accurate and detailed map of the GAG binding residues on chemokines was obtained. Significant chemical shifts were detected in the same HS binding site that were observed in the previous model from Sadir *et al.*, in addition to another 20 other residues on CXCL12α that occur outside the HS binding site. This observation was attributed to a heparin-induced dimerization event as has been observed previously [114]. An advantage of the NMR method was the use of ^{13}C labelled octasaccharide which permitted defining also the residues on the sugars that participated in the interaction.

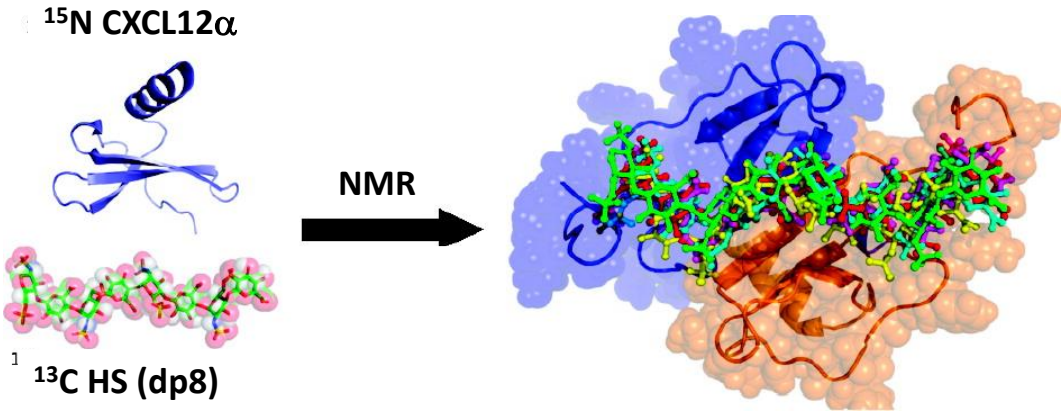

Figure I.1.13: Structure of CXCL12α dimer (ribbon structure) induced by ^{13}C labelled octasaccharide. Image taken from ref [116].

The above studies have shown that the heparin was present at the CXCL12α dimer interface (Figure I.1.14A). Based on NMR, combined with SPR analysis of point-mutated CXCL12, Ziarek *et al.* have identified additional amino acids involved in the binding, and proposed that heparin binds nearly orthogonal to the dimerization interface (Figure I.1.14) [117]. The differences in the structural aspects of heparin-CXCL12α interactions reported in different studies suggest that there is some flexibility in how the sugar and protein interacts, i.e. the interaction does not occur through a well-defined binding site.

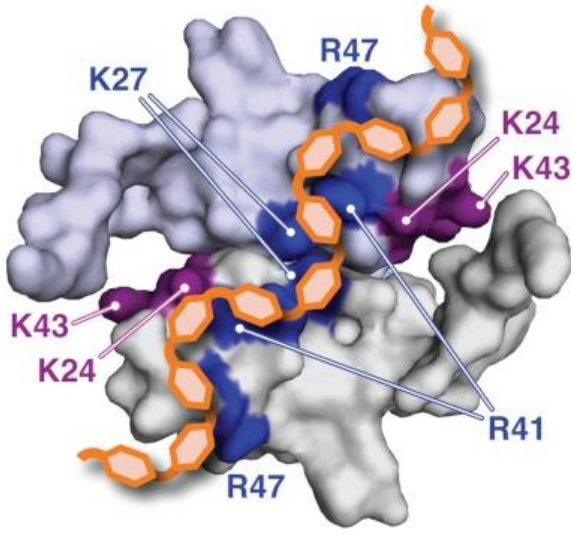

Figure I.1.14: Schematic representation of the heparin-CXCL12α binding model proposed by Ziarek et al. where heparin promotes CXCL12α dimerization by contacting residues along the entire six-stranded sheet. The highlighted CXCL12α residues associate with heparin as determined by two-dimensional NMR, mutagenesis, SPR (blue), and three-dimensional NMR (purple). Image taken from ref [117].

However, unlike the α-isoform no work has appeared on the ability of γ-isoform to form dimers, which suggests that the extended C-terminal of the γ-isoform may hinder the formation of dimers.

I.1.6. CXCL12α interactions with its receptor CXCR4

Chemokines which are first bound to cell-surface or ECM-bound GAGs, are then presented to their receptors. Binding to the receptor induces conformational changes in the receptor, and thus trigger intracellular signaling pathways implicated in cell movement and activation, explained in more detail below.

A common factor identified from different studies on the chemokine-receptor interactions is that the N-terminus is a key receptor binding domain involved in receptor signaling [118-120]. A few years ago, a two-site model for binding and receptor activation was proposed by Crump *et al.* [91]. They proposed that at first the chemokine core (RFFESH) (Figure I.1.10) binds to the exposed N-terminus of CXCR4; this serves as the initial docking step (chemokine recognition site 1 (CRS1); “site one”). Then the N-terminal residues of the CXCL12α bind to the more hidden pocket between the extracellular loops 2 or 3 within the co-receptor (signal trigger, chemokine recognition site 2 (CRS2); “site two”) (Figure I.1.15). They found that the receptor activation requires Lys1 and Pro2 residues within the N-terminal region of the chemokine. These two residues (Lys1 and Pro2) were found to activate the receptor through binding to the transmembrane helices, which was demonstrated by deletion or modification of the N-termini which resulted in chemokines that do not induce signaling [121-123]. This “two-site” binding model was a few years later also confirmed by Kofuku *et al* [124].

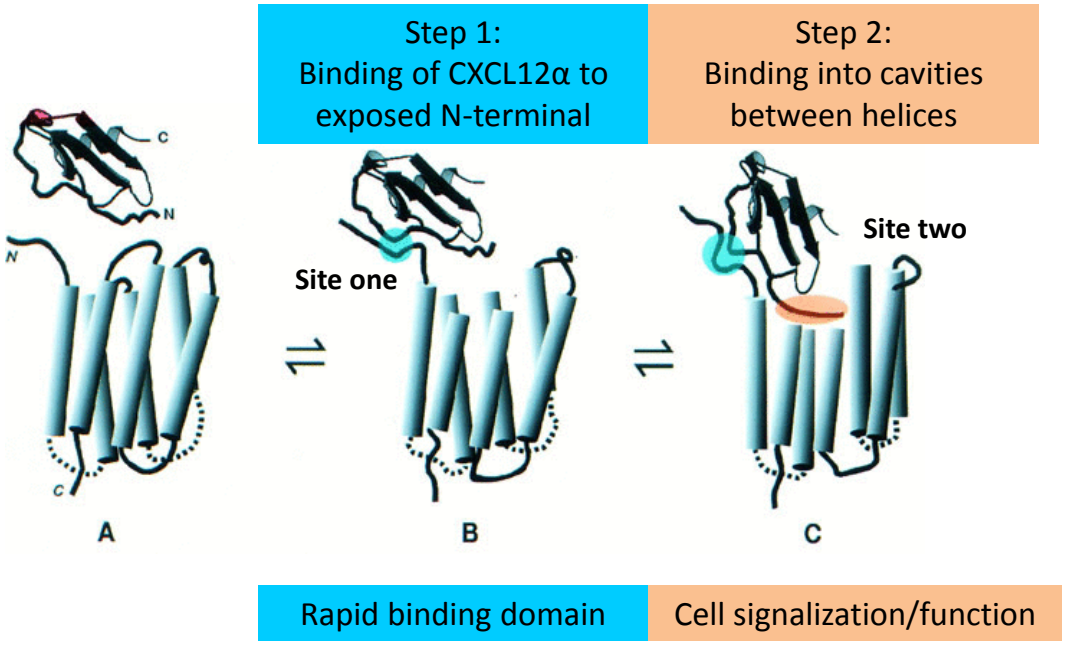

Figure I.1.15: The "two site" binding model for the CXCL12α-CXCR4 interaction. (A) CXCL12α and CXCR4 separately prior to interaction. CXCR4 is shown with the seven helices represented as cylinders, which are connected by the surface and cytoplasmic loops. The N-terminal and C-terminal segments of the receptor, and the N- and C-terminus of CXCL12α, are annotated as N and C. (B) Interaction of the CXCL12α RFFESH loop ("site one") with the N-terminal segment of the receptor. The contact region is shown in blue. Two of the helices are truncated [compare with (A)] to highlight the binding groove of the receptor. (C) N-terminal region ("site two") of CXCL12α bound in the groove at the top of the helices (orange). Binding of the N-terminal region results in activation of the receptor, which is depicted in (C) by the change in conformation of the receptor helices compared with (B). Figure adapted from ref [91].

This paradigm has guided the field for many years. Consistent with this model, an NMR study of CXCL12α in the presence of solubilized CXCR4 demonstrated that a small molecule compound, AMD3100 specifically dislodged the CXCL12α N-terminus from its binding site on CXCR4 without displacing the bound chemokine core domain [124]; hence providing structural evidence supporting the two-independent site theory. In addition to dislodging CXCL12α N-terminus, AMD3100 has also been shown to prevent CXCL12α induced signalization, hindering biological processes [17, 125]. These antagonist properties of AMD3100 motivated its use as a CXCR4-antagonist during this thesis to check the specificity of CXCL12α-CXCR4 interactions.

I.1.6.b.i. Stochiometry of CXC12α-CXCR4 interactions

In 2006, Veldkamp *et al.*, showed that a single sulfotyrosine-containing N-terminal CXCR4 peptide has an increased affinity for CXCL12α [126], and that the monomer-dimer equilibrium of CXCL12α is shifted towards a dimer in the presence of the sulfated peptide, as shown for CXCL12α in the presence of HS [114]. A couple of years later, Veldkamp *et al.* showed that the CXCR4 N-terminus bridges the CXCL12α dimer interface between the N-loop and the β_3 strand and makes both polar and electrostatic contacts

which are not observed with the monomer CXCL12α [71]. They showed that the N-terminal sulfopeptide derived from CXCR4 bound to a 'disulfide-locked' dimer of CXCL12 in 2:2 complexes [71]. While Wu *et al.* have proposed three models (1:1, 1:2 or 2:2 ligand:receptor complexes), two of which constitute a CXCL12α monomer which binds either a monomer of CXCR4 or a homodimer of CXCR4 [127]. Very recently, Kufareva *et al.* showed that the receptor:chemokine stoichiometry is 1:1 (Figure I.1.16) rather than previously observed 2:1 [128]. Thus these models are not in full agreement. The conformationally flexible and unstructured nature of the N-terminal of CXCR4 has rendered structural studies involving this region challenging, and the understanding of this binding mechanism difficult.

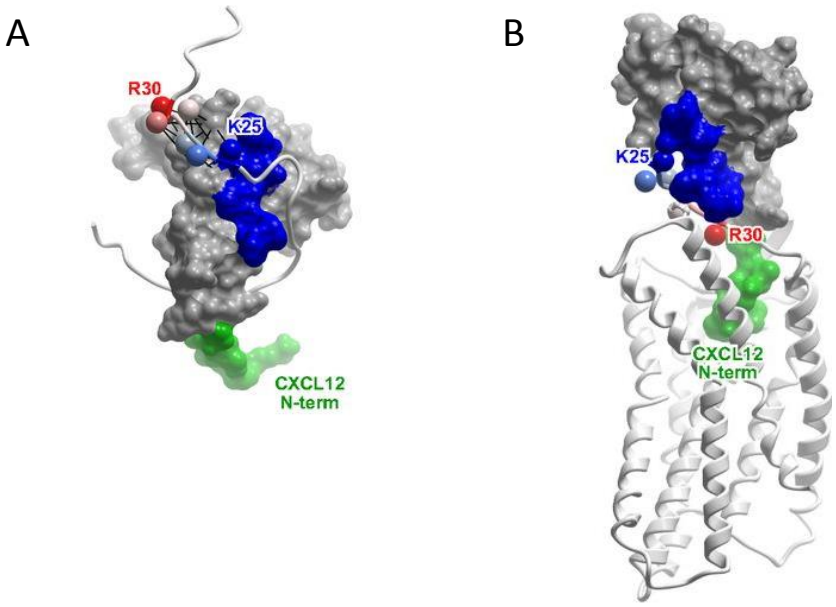

Figure I.1.16: (A) NMR structure of CXCL12α in complex with the N-terminus of CXCR4 (residues M1–K38, ribbon). Chemokine N terminus (green) and N-loop (blue) correspond to the expected interactions in CRS2 and CRS1, respectively. Receptor residues K25–R30 are shown as spheres, labeled, and colored in order from blue to red. (B) A 1:1 CXCR4: CXCL12α model consistent with the two-site interaction hypothesis. Images taken from ref [128].

I.1.6.b.ii.Effect of chemokine oligomerization on signaling

Recently, Drury *et al.* showed that CXCL12α monomers and dimers exert opposing effects on migration. Low concentrations of wild type (wt) CXCL12α induced migration, however, low concentrations of constitutively dimeric CXCL12α or high concentrations of wt-CXCL12α, failed to initiate migration [129]. Importantly, both the monomer and the dimer of CXCL12α activated the CXCR4 receptor to a similar extent. The authors demonstrated that the first 10 N-terminal residues of CXCR4 are more flexible when bound to the CXCL12α dimer in comparison to the monomer, leading to the hypothesis that different oligomers of CXCL12α lead to different signaling pathways [129]. However, this model is highly speculative due to the forced creation of the monomer and dimer CXCL12α forms and thus their plausibility is questionable.

These dimers do not depict the natural presentation of CXCL12α i.e. HS-bound, as these dimers were formed by forced disulfide bonds between two monomers in a locked conformation, which are different from the dimers induced by HS attachment where the dimers may dissociate upon binding to the receptor. In addition, the physiological relevance of the chemokine monomer-dimer equilibrium and the simultaneous interactions between GAG-bound chemokines and receptors are all not yet fully understood and highly controversial and not further discussed here.

I.1.7. Cell adhesion ligands

An important requisite for haptotaxis is the presence of adhesion sites. The adhesion is provided by cell-adhesion ligands, in the ECM or on the surface of another cell, that bind to cell-adhesion receptors. This interaction provides traction to the moving cell (on the surface), in the absence of which the cells may be dragged away, e.g. by the blood flow in the context of the leukocyte migration at the inner walls of blood vessels. Various cell-adhesion ligands and receptors have been identified, and those relevant for this work will be presented in the following.

I.1.7.a. RGD (Arg-Gly-Asp)

In an attempt to reduce complex macromolecular ligands to small and simple recognition sequences, the triad sequence RGD (Arg-Gly-Asp) was discovered by Pierschbacher and Ruoshlati [130-132] as a basic motif for cell adhesion in fibronectin. Subsequently it was also isolated in other adhesion proteins such as vitronectin, osteopontin, collagens, thrombospondin, fibrinogen, and von Willebrand factor [133, 134]. The RGD sequence is the most frequently employed peptide sequence for stimulated cell adhesion on synthetic surfaces. A likely reason for this is the simplicity of producing it compared to the full length protein, facilitating its widespread distribution permitting exploitation of its biological impact on cell anchoring, behavior and survival. RGD peptides are capable of mimicking the cell adhesion functionality of fibronection.

As adhesion to fibronectin is associated with the proliferative phase of myoblasts [135], RGD peptides hold importance in muscle development and repair. Mooney and co-workers showed that RGD coupling improved the initial adhesion and enabled the differentiation of myoblasts cultured on the surface of (2D) or inside (3D) alginate gels [136]. In another study, RGD peptides were found to significantly improve myoblast cell adhesion onto grooved polystyrene substrates [137]. Kessler *et al.* demonstrated that the cyclic analogue c[-RGD*f*V-]) showed 20- to 100-fold more affinity and specificity towards the $\alpha_v\beta_3$ integrin (receptors of RGD) over its linear analogue [138, 139]. This integrin has been shown to be expressed by myoblasts and their interaction with RGD is important in controlling adhesion of cells during myogenic differentiation [140, 141]. Hence, it is of particular interest for this thesis towards the study of muscle development and repair, and described in details later.

I.1.7.b. Intercellular adhesion molecule 1 (ICAM-1)

Another cell-adhesion ligand is intercellular adhesion molecule 1 (ICAM-1). ICAM-1 is a member of the immunoglobulin family of proteins. ICAM-1 is an endothelial- and leukocyte-associated transmembrane protein known for its importance in stabilizing cell-cell interactions and facilitating leukocyte endothelial transmigration. ICAM-1 interaction with the $\alpha_L\beta_2$ receptor on T-lymphocytes is responsible for the attachment of T-lymphocytes to the vascular endothelium, a precursor step towards migration [142].

I.1.7.c. Integrins (receptors of cell adhesion ligands)

Integrins are proteins that traverse the cytoplasmic membranes of the cells. Their extracellular domain binds cell adhesion ligands and their intracellular domain forms the link to the cytoskeleton inside the cells. The name “integrin” was given to denote the importance of these receptors for maintaining the integrity of the cytoskeletal-ECM linkage [143, 144].

Integrins are a family of membrane glycoproteins, each consisting of two non-covalently associated transmembrane subunits, termed α and β. To date 18 α and 8 β subunits are known, that form 24 different heterodimers (Figure I.1.17) [145]. The combination of the particular α and β subunits determines the ligand specificity of the integrin. Some integrins such as $\alpha_v\beta_3$ integrin bind to ECM proteins such as vitronectin and fibronectin. The cell adhesion ligands used in this thesis work bind to distinct integrins [146, 147]: RGD bind to $\alpha_v\beta_3$ and $\alpha_5\beta_1$, cRGD binds predominantly to $\alpha_v\beta_3$ and ICAM-1 binds to $\alpha_L\beta_2$ (Figure I.1.17).

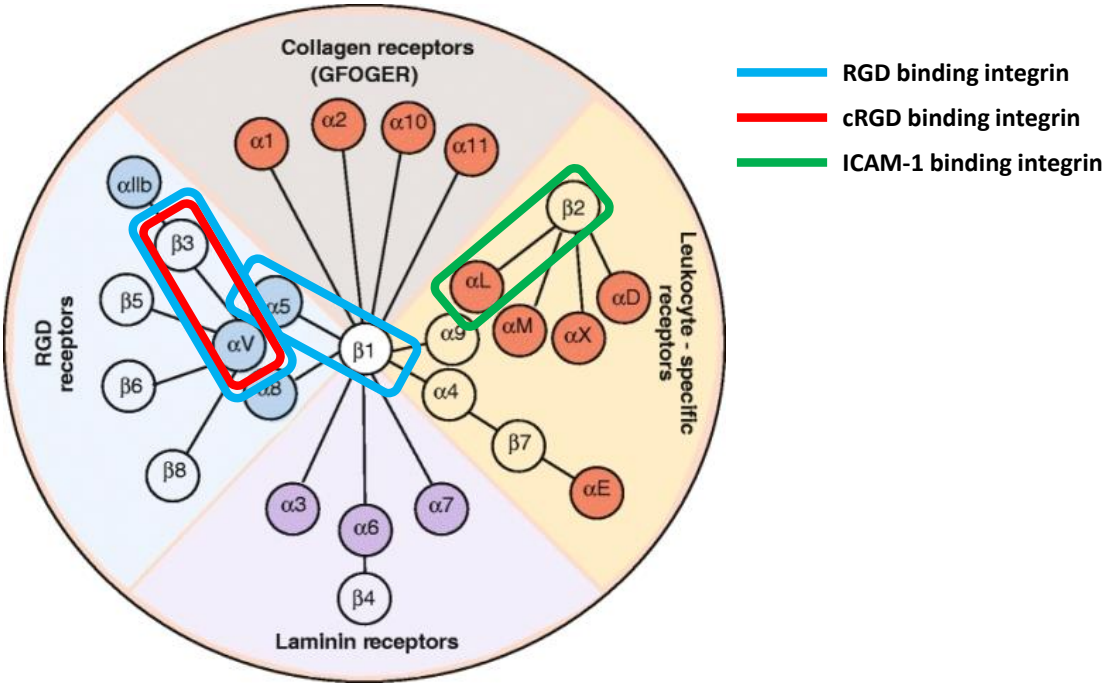

Figure I.1.17: The integrin receptor family. Integrins are heterodimers; each subunit crosses the membrane. Different integrins specific to RGD, cRGD and ICAM-1 are highlighted. Image taken from ref [148].

Although not all integrins have the same extremes in activation potential, most integrins, including integrins expressed on endothelial cells, have "on" and "off" states. The extracellular domain of $\alpha_v\beta_3$ integrin is bent or folded, thereby hiding the RGD-binding site and preventing ligand binding. Conversely, RGD-bound $\alpha_v\beta_3$ integrin has an unbent or straighter extracellular domain (Figure I.1.18). Although integrin cytoplasmic tails are much smaller than their extracellular domains, they can play pivotal roles in integrin signaling events, with separation, twisting, and hinging of the tails all considered mechanisms to allow activation [149].

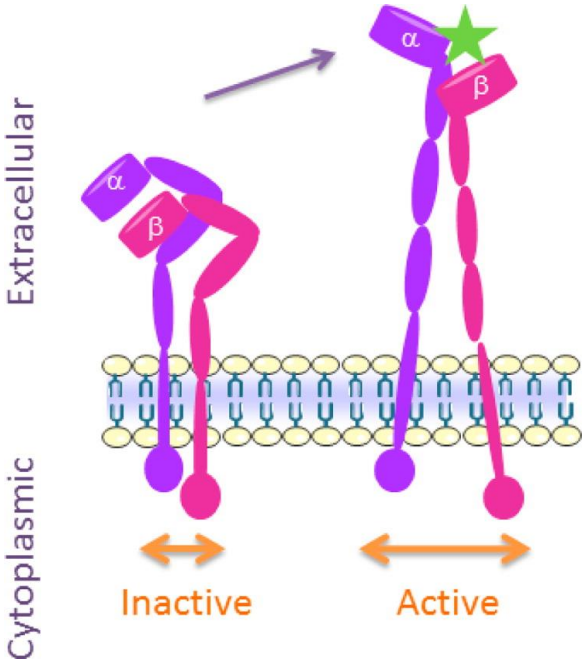

Figure I.1.18: Conformational changes in $\alpha_v\beta_3$ integrin. Upon activation, the extracellular domains extend and straighten, exposing the RGD binding domain (star). Image taken from ref [150].

ICAM-1 is presented by the endothelial cell surface and binds to the leucocyte function-associated antigen-1 (LFA-1; also called integrin $\alpha_L\beta_2$). This interaction is responsible for the attachment of T-lymphocytes to the vascular endothelium, a precursor step towards transmigration of leukocytes across vascular endothelia in processes such as extravasation and the inflammatory response [142].

In the context of this PhD thesis, cRGD was used as cell-adhesion ligands to design biomimetic surfaces in the context of myoblast adhesion and migration under muscle regeneration and repair (Chapter V). As an initial demonstration of concept, data with ICAM-1 in the context of leukocyte adhesion and migration is also briefly presented (Chapter III).

I.1.8. Biological questions and methodological approach

The objective of the PhD thesis was to develop biomimetic surfaces that are highly defined and tunable, for mechanistic studies of GAG-protein interactions on the molecular and supramolecular levels, and to probe cellular responses to defined biochemical and biophysical cues to better understand GAG-mediated cell-cell and cell-matrix communications.

Our approach consisted in reconstituting GAGs and other cell membrane and extracellular matrix components (cell adhesion ligands and proteins) into tailor-made and well-defined model surfaces (described in chapter III). The model surfaces can be tailored down to the nm-scale, and characterized with a toolbox of surface-sensitive *in*

situ analysis techniques. They permit tightly controlled and quantitative experiments on several levels of complexity of the biological system: molecular (chapter II), supramolecular (chapters III and IV) and cellular (chapter III and V).

The fundamental biological questions that we were interested in addressing pertain to the role of the GAG family of heparan sulfates in chemokine-mediated cell adhesion and migration:

- How do chemokines re-organize cell-surface GAGs, and what are the functional implications?
- How do immobilized GAGs modulate chemokine-mediated cell adhesion and migration? Of particular interest is myoblast adhesion and migration in the context of muscle development and regeneration.

I.1.9. GAGs are neglected in *in vitro* models

On the molecular level, it is clear that the interaction kinetics between a given chemokine and individual binding sites on the GAG chains, and the structure of the complex, will be functionally important. The local density and arrangement of chemokine binding sites, for example, will affect re-binding and thereby modulate the residence time and diffusion of chemokines. Also, chemokine oligomers will not only bind with enhanced avidity to GAGs, due to multivalent binding, but they may also induce cross-linking and clustering of several GAG chains. With other words, we hypothesized that the supramolecular presentation of the GAG chains - their local density, orientation and mobility – is an important parameter in the function of GAGs in cell migration. This thesis started with the realization that GAGs do not play the role that they deserve in model systems, and that the ability to control and characterize the supramolecular presentation of GAG chains, *in vivo* or *in vitro*, is very limited.

On the cellular level, cell migration is today a very active research field [74, 96]. Substantial progress has been made in the understanding of the cellular processes that ensue upon exposure to chemokines. An understanding is also emerging as to how 2-D cell migration (e.g. on the surface of blood vessels) differs from the 3-D migration (e.g. within a tissue) [74]. For quantitative investigations and mechanistic understanding, *in vitro* studies have proven essential in which the chemokines are presented in well-defined spatial gradients to the cell, without the presence of GAGs [151]. Despite strong indications for their functional importance, GAGs have so far been largely neglected in the design of *in vitro* cell chemotaxis or haptotaxis assays. Two studies with HS-containing matrigels have recently been reported for *in vitro* 3D chemotaxis assays [46, 152], but control over the HS presentation remained very limited. A likely reason for the limited use of GAGs is the limited commercial availability of sufficiently pure and suitably functionalized GAGs, and of methodologies to integrate GAGs into assemblies that

mimic the presentation at the cell surface or in the ECM well. A significant portion of this thesis was devoted to improve upon this situation. To this end, we adopted a biomimetic nano-approach, which is described in detail later.

I.2. Methodology

As outlined above, poor control over the supramolecular presentation of GAGs currently represents a technical bottleneck. To overcome this limitation, we propose a biomimetic approach. The approach consists in reconstituting GAGs, and other cell membrane and extracellular matrix components, into tailor-made and multifunctional model surfaces that recapitulate selected aspects of the *in vivo* situation. Such model surfaces enable a large range of novel and quantitative biomolecular and cell biological studies, to understand the role of GAGs in cell migration and in cell-cell and cell-ECM communication in general. They also open novel avenues for the development of biosensor applications, and for the control of cellular fate.

I.2.1. Bottom-up approach

For mechanistic studies, it would be desirable to be able to arrange GAGs, together with other relevant biomolecules, in such a way that the orientation, density and lateral mobility of the exposed biomolecules can be controlled and tuned. To this end, the biofunctionalization of solid surfaces i.e. designing biomimetic surfaces is an attractive route. The development of such surfaces was a main objective of this thesis work. To form biomimetic surfaces, we adopted a bottom-up approach with design steps covering different levels of complexity.

Molecular level: To functionalize surfaces with biomolecules, an important requisite is the availability of specific molecular building blocks. Many building blocks were already available but a few needed to be prepared.

Supramolecular level: The molecular building blocks were assembled into biomimetic surfaces, with tight control on the molecular organization down to the nanometer scale. These surfaces were used to study supramolecular HS-chemokine interactions.

Cellular level: The biomimetic surfaces were also designed such that they can be readily interfaced with living cells. In this thesis, this was demonstrated by studying the function of GAGs in chemokine-mediated cellular adhesion and motility.

The different levels of complexity are described in detail in the following. Our approach is original in that we combined synthesis strategies, state-of-the-art surface functionalization techniques, a toolbox of sophisticated surface-sensitive characterization techniques, biochemistry and cell biology in an unconventional way to study biological processes.

I.2.2. Molecular level

We aimed for a generic platform to immobilize functional molecules (i.e. a 'molecular breadboard', described in detail later). The platform of choice was a streptavidin monolayer, to which molecules with a biotin tag can be stably attached. It was thus necessary to conjugate biofunctional molecules of interest with biotin.

Reducing-end biotinylation of GAGs

For GAGs, site-specific conjugation through the reducing end is desirable, as this effectively mimics the cell surface presentation of GAG motifs and avoids alteration of GAG–protein interactions by chemical modifications along the GAG chain, or by surface-imposed conformational or spatial constraints [153].

At the outset of this thesis work, we used HS that was biotinylated at the reducing end *via* so-called hydrazone ligation. This method was already established in the collaborating laboratory of Hugues Lortat-Jacob and applications had frequently been reported [82, 154, 155]. However, we found these conjugates to be unstable. This hindered the immobilization of HS at reproducible surface coverage, and thus greatly reduced the control of surface functionalization. To overcome this limitation, I adopted oxime ligation as an alternative strategy to synthesize biotin-HS conjugates. This method revealed to be a facile, broadly applicable method for the reducing-end conjugation of glycosaminoglycans that overcomes the limited stability and yield of hydrazone ligation. The method, as well as the quantitative comparison of yield and stability of hydrazone and oxime ligations, will be described in detail in Chapter II.

Biotinylation of the cell adhesion ligand cRGD

Biotin was connected to cRGD through a linear polyethylene glycol (PEG) linker. To this end, amide-coupling and a PEG chain with a biotin at one end and an N-Hydroxysuccinimide (NHS) group at the other was used. The method is described in detail in Annex (A.1). The PEG linker between biotin and cRGD enabled control of the thickness of cRGD film adsorbed on the molecular breadboard.

I.2.3. Supramolecular level

We combine state-of-the-art surface functionalization strategies with a toolbox of sophisticated surface-sensitive characterization techniques. To reconstitute the biological structure, the molecular building blocks should be brought on the surface in proper order and at the right concentrations. The preparation of well-defined and tunable GAG assemblies remains challenging, while the biofunctionalization of solid surfaces is an attractive route, for several reasons:

- Solid surfaces naturally reproduce the 2-D confinement of the cellular surface.

- Surface science has developed a panoply of methods that enables the creation of a diversity of chemical and topographical patterns, including gradients, on surfaces with inherent length scales that cover a continuous range from a few nanometres to the macroscopic level. In combination with suitable bioconjugation methods, they can be employed as templates for the controlled 'bottom up' assembly of biomolecular architectures on surfaces. Such surface biofunctionalization approaches are now commonly applied to proteins, nucleic acids and lipids, and they are emerging for carbohydrates [156-158], including GAGs [159].
- The native environment of biomolecules is water. To avoid perturbation or destruction of the sample, *in situ* characterization is mandatory. Over the last decades, a large range of sophisticated methods for the nanoscale analysis of surface-confined films in aqueous environments have been developed. This 'toolbox' of surface-sensitive techniques is exquisitely suited for the detailed and quantitative characterization of soft and hydrated films at the solid-liquid interface, mostly without the need for labels. Parameters that can be quantified include the thickness, hydration, permeability, topography and mechanical properties of the model films, as well as the amount, mobility and orientation of incorporated molecules, and the kinetics of their self-organization.

The main advantages of these model systems are their simplicity and the fact that they permit a control over orientation and densities. The reduced complexity compared to the native system allows for highly controlled measurements and to derive quantitative information on specific interactions. On the other hand, the translation of the properties of model systems to the functions of real biological systems remains a bottle neck. The synergy of the knowledge gathered in the model systems with the real biological system is essential to fill the gap between the simple approach of the models systems and the complexity of the real biological systems. However, starting from a simplified point of view on a specific question, the entire puzzle of the biological assembly can potentially be solved. Taken together, surface science and bioengineering can today provide the nanoscience tools for the creation and detailed characterization of *in vitro* biomimetic surfaces.

I.2.3.a. Preparation of well-defined model surfaces

I.2.3.a.i. Strategies for surface functionalization

One of the paramount challenges of developing biomimetic surfaces is the correct choice of a solid support and the development of surface chemistry that is compatible with a diverse set of biomolecules while maintaining their integrity, native conformation, and biological function. Various surface functionalization strategies have been used over the last century to modify surfaces with biomolecules [160]. All the functionalization strategies have advantages and limitations, and the choice of a

particular strategy depends on the envisaged application. To design biomimetic surfaces for this thesis work, I employed two different surface functionalization platforms: oligo ethylene-glycol (OEG) monolayers and supported lipid bilayers (SLBs) (Figure I.2.1). The choice of these particular functionalization strategies and their introduction is described below. Self-assembled monolayers (SAMs) [161-167] of alkanethiolates on gold is a robust and one of the most used strategies over the last century for surface functionalization. SAM formation provides one of the easiest and robust ways to obtain ordered monolayers through strong chemisorption between the thiol group and the gold surface leading to the preparation of thermodynamically stable monolayers. This is in contrast to LB (Langmuir–Blodgett) and other techniques, where only physisorbed, mono/multilayer films are obtained. Upon adsorption, the thiols deprotonate to create strong gold thiolate bonds:

$$R\text{-}SH + Au \rightarrow R\text{-}S\text{-}Au + 1/2H_2 \qquad 1.1$$

These SAMs exhibit highly organized molecular structures [168]. The molecular terminal group of the thiols provides chemical functionality to the SAM and can be used to tailor the physical properties of the functionalized surfaces [165].

An important advantage of these SAMs is that these SAMs present a useful methodology for incorporation of different functionalities by forming “mixed” SAMs, which are monolayers comprising a well-defined mixture of molecules. Mixed SAMs can be easily formed by either co-adsorption from solutions containing mixtures of thiols (RSH + R’SH), or adsorption of asymmetric disulfides (RSSR’). The most common way of forming mixed SAMs is to use a mixture of thiols where one thiol possesses a particular functionality which can be exploited for futher surface modification.

In the context of this thesis, we used an OEG monolayer based on gold-thiol adsorption as developed by Svedhem *et al.* [169, 170]. Even though these OEG monolayers are unlikely to have the thiol groups arranged orderly, they work equally well as SAMs of alkanethiolates on gold, i.e. it is also robust and leads to a reproducible monolayer. In the context of this thesis, we formed a mixed OEG monolyer by using a mixture of thiols where one thiol was slightly longer in length comparison to the other and possessed a biotin tag. This is described in more details in Chapter III.

Another asset of these OEG monolayers (and also SAMs of alkanethiolates) is that these monolayers provide passivation against non-specific adsorption of proteins [171-173]. It has been hypothesized that the ability of OEG monolayers to bind large amounts of interfacial water presents them the non-fouling or protein resistant property [173]. In addition to passivation against proteins, the OEG monolayers also provide passivation against non-specific adhesion of cells [174, 175]. This aspect of non-specific adsorption

of proteins and adhesion of cells was particularly important in the context of this thesis for cell mechanistic studies. We thus exploited OEG monolayers for cellular assays.

Supported lipid bilayers (SLBs) have also become popular [176, 177] as model systems for the cell membrane [178, 179] and as a building block for biofunctional surfaces [180, 181]. The creation of SLBs by adsorption and spreading of vesicles on hydrophilic supports [182, 183] is attractive by its simplicity. Important insights into the nature of this self-organization process have been gained a few years ago [184-187] and a detailed picture of the structural intermediates in the SLB formation process is now available. Richter *et al.* have provided an integrated view of the formation of SLBs and have provided evidence that the solid support plays a determinant role in the lipid deposition process, giving rise to a multitude of SLB-formation pathways or even preventing SLB-formation [184, 185].

SLBs were used to study the molecular dynamics at the biological interface as these bilayers provide lateral mobility to anchored molecules whereas anchored molecules are immobile on OEG monolayers. The lateral mobility was studied using fluorescence recovery after photobleaching (FRAP).

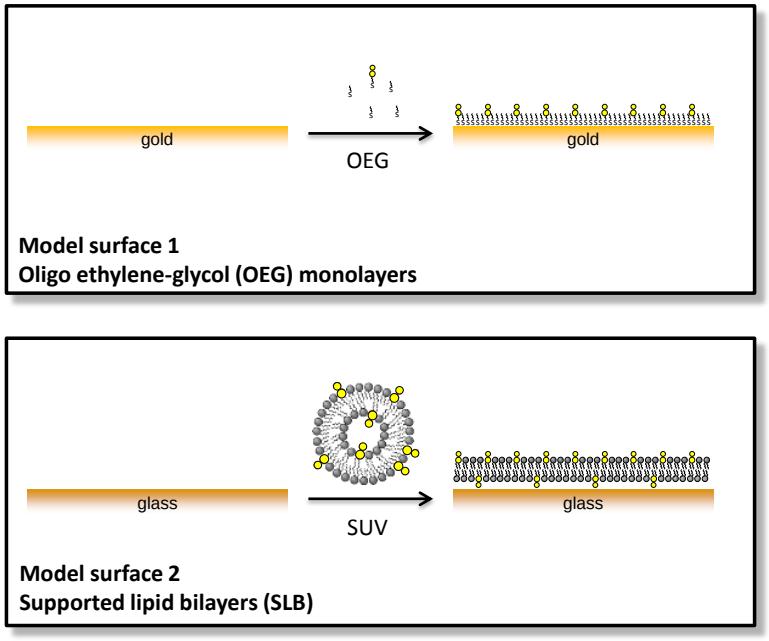

Figure I.2.1: Main surface functionalization strategies selected for this thesis work. These are based on oligo ethylene-glycol (OEG) monolayers on gold and supported lipid bilayers (SLB) on glass.

These platforms provide tight control on the orientation, density, two-dimensional mobility and distribution of biomolecules, and a background of low unspecific binding. Another advantage of these strategies is that they are supported on either Au or Si

which are suitable for characterization using quartz crystal microbalance measurements as well as using optical techniques such as ellipsometry. This point is very important for the characterization of the model surfaces. These surfaces were used as platforms for subsequent injection of biomolecules.

I.2.3.a.ii. SAv molecular breadboard

Our method to form biomimetic surfaces relies on an intermediate monolayer of streptavidin (SAv) between the surface and the biomolecule to be grafted (Figure I.2.2). This strategy provides tight control on the attachment of biomolecules to the surface and tunability of the grafting density, where multiple biomolecules can be simultaneously grafted permitting multifunctionality. In addition, the SAv monolayer acts as a passive background which is inert to the nonspecific binding of proteins. Specifically, OEG monolayers or SLBs exposing biotin served as a platform for the attachment of SAv monolayer exploiting self-assembly through strong and specific biotin-SAv interactions, as previously developed [38, 155, 169, 188]. In this case, we expect SAv to be immobilized such that two of its four biotin-binding sites are facing the surface for immobilization while the other two binding sites are facing the solution to accommodate target molecules embedded in a background that is largely inert to the undesired nonspecific adhesion of biomolecules or cells, the SAv monolayer thus serves as a molecular breadboard for the selective attachment of biotinylated molecules (Figure I.2.2).

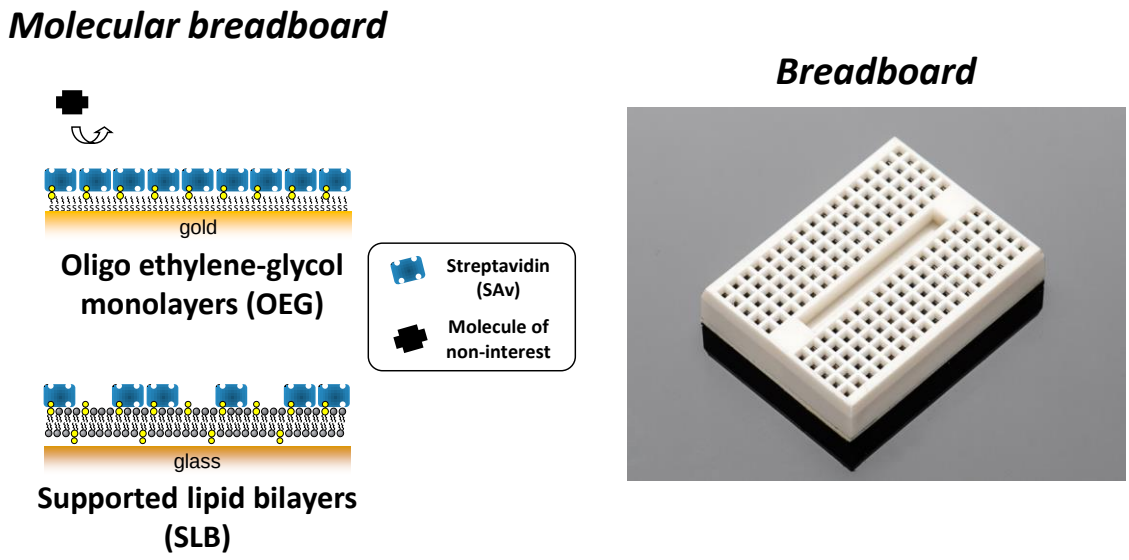

Figure I.2.2: Schematic representation of a molecular breadboard formed by a SAv monolayer on OEG monolayers and SLBs (left), similar to the breadboard used in electronics providing an array of attachment sites (right).

This strategy presents a controlled manner of biomolecular grafting compared to conventional deposition methods. For example, grafting of biomolecules directly to the surface *via* thiol groups permits only a poor control over orientation and density of

attached molecules, as many biomolecules tend to interact non-specifically with gold, i.e. immobilization does not occur exclusively through the thiol groups (Figure I.2.3).

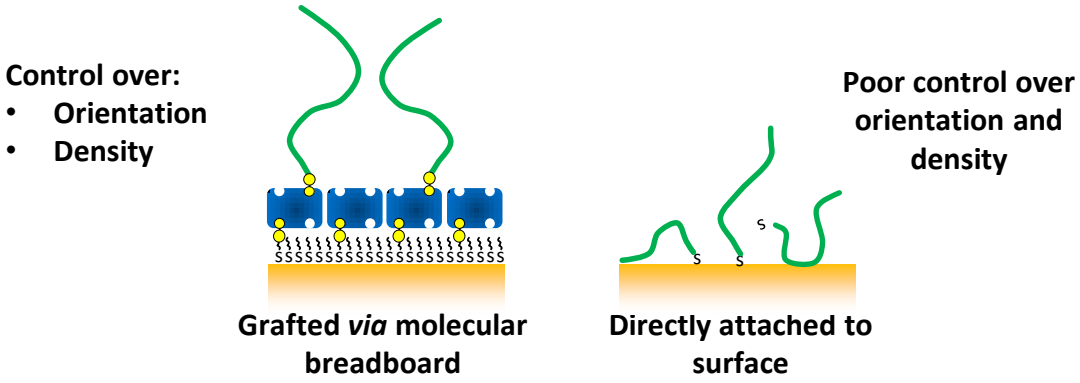

Figure I.2.3: Schematic representation of biomolecules grafted on surfaces via the molecular breadboard (left) in comparison to directly attached (right).

Our method is generic in the sense that various biomolecules can be (co-) immobilized at tunable surface densities, either through a site-specifically attached biotin tag, or if that is not available, through biotinylated adapter molecules. In particular, GAGs were immobilized with controlled orientation through a biotin tag introduced at the reducing end (Figure I.2.4). Similarly, biotinylated cell-adhesion ligands, chemokines and other molecules were also grafted on the surface.

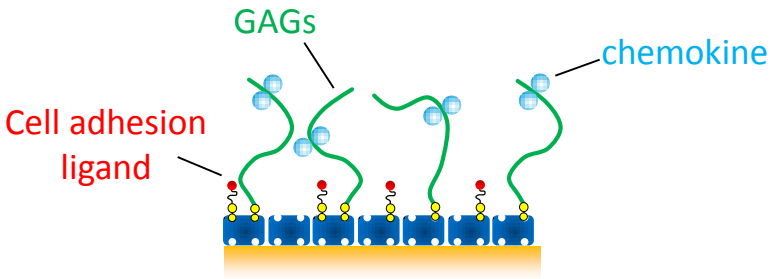

Figure I.2.4: Schematic representation of biomimetic surfaces presenting a GAG, a chemokine and a cell adhesion ligand on a molecular breadboard.

The development of model surfaces is covered in detail in Chapter III. These model surfaces presenting GAGs were used to study supramolecular GAGs-chemokine interactions. This is covered in Chapters III and IV.

I.2.3.b. Surface-characterization techniques

Our surface-confined model films are a few nanometers thick and strongly hydrated. *In situ* characterization is mandatory. A large range of sophisticated methods for the nanoscale analysis of surface-confined films in aqueous environments is available. Each technique by itself is powerful in that it can provide quantitative information about one (or a few) specific parameters, e.g. the films biomolecular mass or thickness. No single method alone, however, can provide a comprehensive picture of complex architectures. Instead, we employ a 'toolbox' of techniques for the detailed interrogation of the created biomolecular assemblies. With this toolbox of techniques, parameters such as thickness, hydration, and mechanical properties of the model films, as well as the amount and orientation of incorporated molecules, and the kinetics of their self-organization can be quantified. The main techniques employed for this thesis work are briefly described below.

I.2.3.b.i. Quartz crystal microbalance with dissipation monitoring (QCM-D)

The quartz crystal microbalance (QCM) is a nanogram sensitive technique based on inverse piezoelectric effect discovered by Curies in the 19th century [189]. This technique utilizes acoustic waves generated by oscillating a piezoelectric, single crystal quartz plate to measure mass. There are several ways to perform QCM measurements [190-193]. One way is to examine the polarization at the crystal surface as a function of the frequency of the applied voltage, the so-called impedance analysis, which along with resonance frequency f_i yields another parameter called bandwidth Γ_i [194, 195]. The alternative method is the "ring-down" method which led to the development of the QCM-D technique by Rodahl *et al.* [196]. The QCM-D method was used in the work presented in this thesis, and its working principle is described in details below.

QCM-D [190, 191, 197] is now widely used to study soft and solvated interfaces. QCM-D affords monitoring of adsorption processes in real time in liquids, providing detailed information about the binding kinetics, and the morphology and stability of surface-confined films without requiring labels. In addition, fitting of QCM-D data with viscoelastic model provided quantitative information about thickness and viscoelastic properties of the film.

Working principle

The QCM-D sensor is made of a quartz crystal that is sandwiched between two electrodes and excited into a shear oscillatory movement by applying an AC electric field at a frequency close to the resonant frequency (f_1) or to odd overtones (f_i; i = 3, 5, 7, …) of the resonance frequency (Figure I.2.5A-C). The resonance frequency is related to the thickness of the quartz crystal, d_q as:

$$d_q = i\frac{\lambda}{2} = i\frac{v_q}{2f_n} \qquad 1.\ 2$$

where v_q is the speed of sound in quartz and λ is the wavelength of sound.

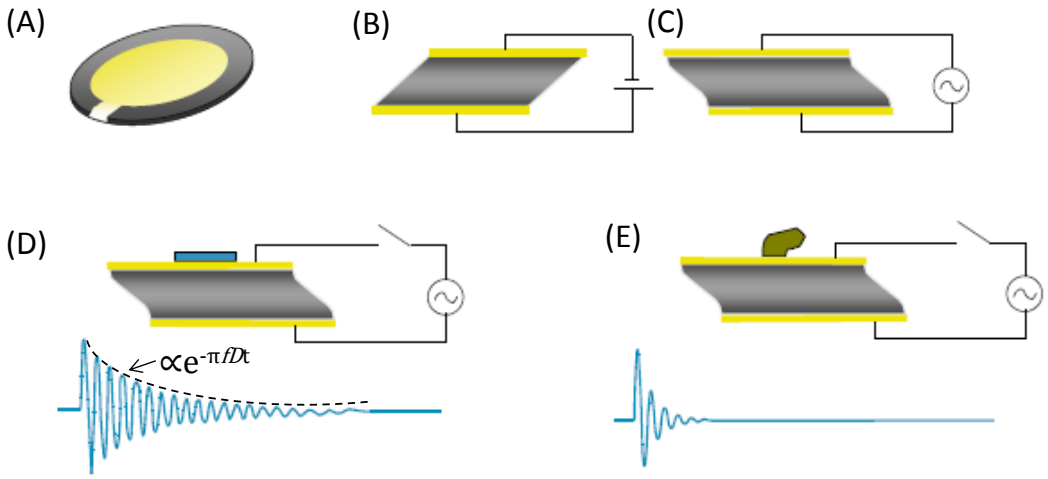

Figure I.2.5: Schematic presentation of the QCM-D working principle. A picture of quartz crystal sensor where the piezoelectric quartz crystal is sandwiched between two gold electrodes (A). The application of an electric field results in shear motion of the crystal (B). Application of oscillatory voltage results in resonance in the shear motion, where top and bottom surfaces move tangentially in an anti-parallel fashion (C). QCM-D uses a so-called ring-down method. After cutting the driving circuit, the freely decaying oscillation of the crystal is monitored (D, E). From the decay curve, the resonance frequency f and the energy dissipation D can be extracted. Attachment of a rigid mass (D) to the crystal's surface will only lead to a decreases in f, while a soft (viscoelastic) mass (E) will also affect D. Monitoring changes in f and D allows thus to follow interfacial processes in real time.

Cutting off the external electric field results in a dampened oscillation of the crystal. By fitting an exponentially decaying oscillating curve to the data (Figure I.2.5D), the resonance frequency (*f)* of the crystal and the energy dissipation (*D)*, are extracted. The envelope of the decaying oscillation, u_i, is decaying exponentially over time:

$$u_i \propto e^{-\pi f_i D_i t} \qquad 1.\ 3$$

The damping factor, D_i, is called dissipation, which is defined as

$$D_i = \frac{E_{dissipated}}{2\pi E_{stored}} \qquad 1.\ 4$$

It is obvious from equation (1. 4) that the dissipation will increase if the sensor quickly dissipates the energy of oscillation. To a first approximation, the changes in dissipation, Δ*D*, relate to the mechanical (typically viscoelastic) properties of the material bound to or situated in the close vicinity of the surface, while the changes in resonance frequency,

Δ*f*, relate to the mass (including hydrodynamically coupled water) or alternatively to the thickness of the adsorbed film.

QCM-D measures the changes, Δ*f* and Δ*D* in real time by the reverse piezo-electrical effect, i.e. the oscillation of the quartz crystal translates into an oscillating voltage. The presented way to extract frequency and dissipation from a decaying curve after cutting voltage is called ring-down approach and is characteristic for QCM-D. The resolution in frequency is currently in the range of 0.2 Hz (in liquid), corresponding to a resolution in areal mass density of a few ng·cm^{-2}. The time resolution of the QCM-D technique is typically better than 1 s.

Determination of areal mass density

The Sauerbrey equation [198] relates the adsorbed mass per surface of the sensor crystal (areal mass density), m_{QCM} with the changes in frequency, Δ*f*:

$$m_{\mathrm{QCM}} = \Delta m = -\frac{v_{\mathrm{q}}\rho_{\mathrm{q}}}{2f_o^2}\frac{\Delta f_i}{i} = -C\frac{\Delta f_i}{i} \qquad 1.5$$

where *C* is the mass sensitivity constant, and ρ_q and v_q are the density of quartz and speed of sound in quartz, respectively. The mass sensitivity constant *C* depends solely on the material properties of the sensor crystal and is thus independent from the adsorbate. For a sensor with a fundamental frequency of $f_0 \approx 4.95$ MHz, *C* = 18 ng·cm^{-2}·Hz^{-1}. Although originally derived for applications in air or vacuum, the Sauerbrey equation is also valid for films immersed in Newtonian liquids such as water. However, the film needs to be homogeneous and sufficiently rigid for the Sauerbrey equation to be applicable. Sufficiently rigid films follow the oscillation of the sensor crystal with little dissipative losses. Specifically, for homogeneous films, the Sauerbrey equation can give a good approximation if the ratio $\Delta D/(-\Delta f_i/i)$ is much smaller than 0.4×10^{-6} Hz^{-1} [190].

Coupled Solvent

A primary film parameter that is in many cases quantitatively accessible through QCM-D is the areal mass density. In contrast to optical mass-sensitive techniques, QCM-D measures all material that is mechanically excited, and hence it measures the hydrodynamically coupled solvent, $m_{solvent}$ in addition to the areal biomolecular mass density (or areal adsorbate density), m_{ads}.

$$m_{\mathrm{QCM}} = m_{\mathrm{ads}} + m_{\mathrm{solvent}} \qquad 1.6$$

As a consequence, structural changes of the adsorbed layers that are accompanied by a change of the hydrodynamically trapped liquid can be easily monitored by QCM-D.

Viscoelastic modeling

In some of the applications, the adsorbed film is not rigid and the Sauerbrey relation becomes invalid. A film that is sufficiently soft ($\Delta D > 0$) will not fully couple to the oscillation of the crystal; hence the Sauerbrey equation will underestimate the real mass of the layer. Under these conditions, QCM-D is also sensitive to viscoelastic properties of the film [190]. Soft and highly hydrated films can be treated as a homogeneous layer with a given thickness, density and effective viscoelastic properties. Viscoelastic models can be used to fit the QCM-D data (at several overtones), which relates the shifts in f and D to the film thickness and viscoelastic properties.

For fitting, the film can be modeled as a homogeneous viscoelastic layer with acoustic thickness d, density ρ, while the viscoelastic properties are usually expressed as storage modulus, $G'(f)$, which correlates to the materials elasticity and the loss modulus, $G''(f) = 2\pi f\eta$, which is a measure of the film's viscosity η. In the case of this thesis, QTM [199] software (D. Johannsmann, Technical University of Clausthal, Germany; option "small load approximation") was used to fit the data at selected time points to obtain the thickness and viscoelastic properties of HS and HS-bound CXCL12α films. For a detailed description of the viscoelastic modeling procedure, including the determination of joint confidence regions please refer elsewhere [200].

ΔD *vs* Δf plot

Another representation of QCM-D data is the ΔD *vs* Δf plot which reveals invariant curve shapes related to the film morphology (at a given surface coverage). Minor differences in the adsorption behavior and in particular its coverage dependence are best visualized in the ΔD *vs* Δf plot, and can serve as a marker for anomalous adsorption. For examples, please refer to Chapter II.

I.2.3.b.ii. Spectroscopic ellipsometry (SE)

Spectroscopic ellipsometry (SE) is an optical technique that is versatile for the characterization of interfaces [201, 202]. For biomolecular films it can provide quantitative information about the surface density of biomolecules, and the thickness and refractive index of adsorbed layers. In this thesis work, SE was used to quantify surface densities of biomolecules (such as HS, chemokines and cell adhesion ligands), as well as binding affinities and kinetics of HS-chemokine interactions.

Working Principle

Ellipsometry is based on the measurement of changes in the polarization of light upon reflection at an interface. Spectroscopic ellipsometry measures the polarization changes over a spectrum of wavelengths. Polarization is parameterized in the form of two ellipsometric angles, Δ and Ψ. The polarization changes sensibly when a thin films of

organic material is deposited at the interface which is due to the change in the refractive index imparted by the film. From the ellipsometric angles, the thickness, *d*, and the refractive index, *n*, of the adsorbed layer can be extracted. From these parameters, the areal biomolecular mass density, m_{SE}, can be extracted. The presence of biomolecules at areal mass densities down to a few ng·cm^{-2} can readily be detected. For comparison, a dense monolayer of SAv would equal an areal mass density of well above 200 ng·cm^{-2}. The detection limit thus corresponds to a small fraction of a protein monolayer.

Polarization of light

According to Maxwell theory, light is an electromagnetic wave represented by two vectors: $\overrightarrow{E}$ represents the electric field, and $\overrightarrow{B}$ the magnetic field. $\overrightarrow{E}$ and $\overrightarrow{B}$ are oriented perpendicular to each other and to the direction, z, of light propagation.

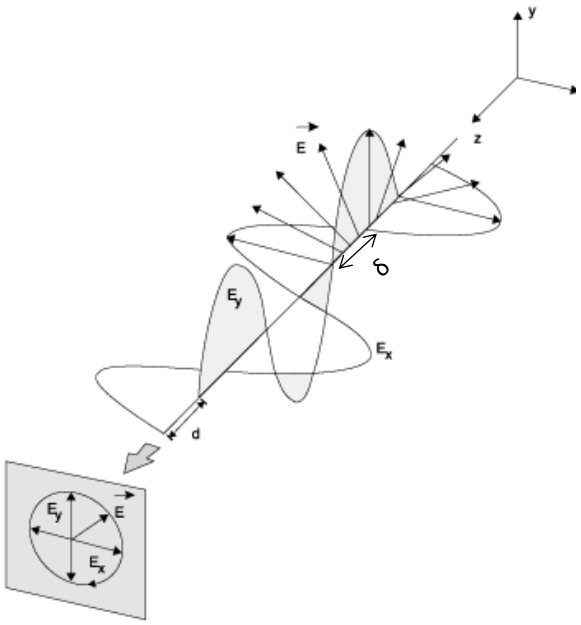

Figure I.2.6: Polarization of light: The electric field vector, $\overrightarrow{E}$, can be described as a superposition of two electric field vectors perpendicular to each other, $\overrightarrow{E_x}$ and $\overrightarrow{E_y}$. The polarization of the light depends on the ratio of E_x and E_y, and on the phase shift between them. Here, circular polarized light is depicted, i.e. E_x and E_y have the same amplitude and the phase shift is a multiple of π/2. Adapted from Goncalves et al. [203].

To understand the principles of polarization, consider the electric field vector, $\overrightarrow{E}$, which can be expressed as a superposition of two orthogonal components, E_x and E_y:

$$E_x = E_x^0 \cos(qz - \omega t + \delta_x)$$
$$E_y = E_y^0 \cos(qz - \omega t + \delta_y) \qquad 1.7$$

where *q* is the wave number (2π/*λ*), *ω* is the angular frequency, *t* is the time, δ_x and δ_y are phase constants, and E_x^0 and E_y^0 are the amplitudes of the components E_x and E_y,

respectively. The variation with time of the orientation of $\overrightarrow{E}$ along the propagation direction at a fixed location is called polarization. The polarization of the light depends on the phase shift between E_x and E_y and their ratio. When $\overrightarrow{E_x}$ and $\overrightarrow{E_y}$ are in phase, the resulting light will be linearly polarized. The relative amplitudes determine the resulting orientation. If the two components are 90° out of phase and equal in amplitude, the resultant light is circularly polarized. More generally, i.e. for orthogonal waves of arbitrary amplitude and phase, the resulting vector describes an ellipse in the *x*-*y*-plane. This is where ellipsometry gets its name.

Changes in polarization upon reflection

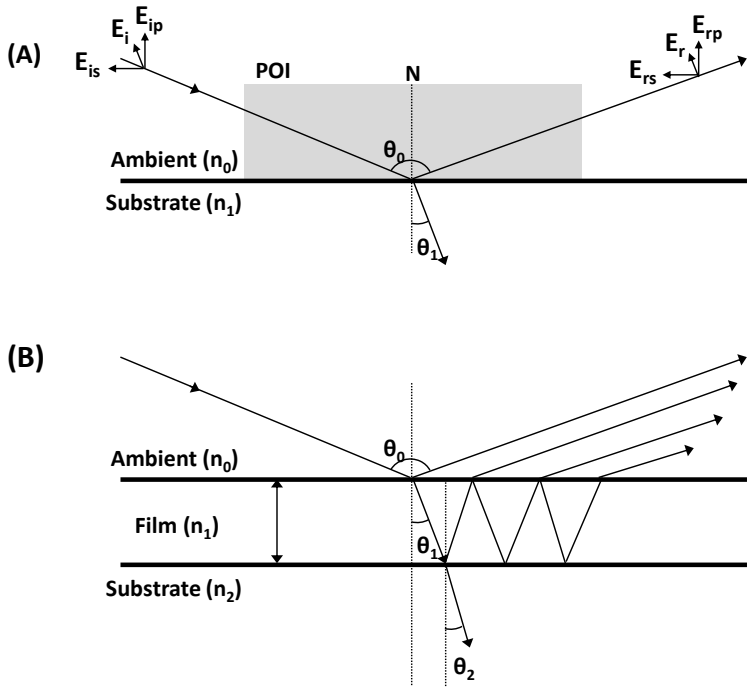

Figure I.2.7: Reflection of polarized light from a bare surface (A) and a film-covered surface (B). When a light beam hits a bare surface it will be partly refracted (and potentially absorbed) and partly reflected. In both cases (A and B), a change in the phase shift and in the amplitudes of lights parallel (E_p) and perpendicular (E_s) (to the plane of incidence) components will occur. These changes depend on the surface properties and can be measured by ellipsometry. Adapted from Goncalves et al. [203].

Figure I.2.7 illustrates how a beam of linearly polarized light incident (index *i*) on a bare surface (a) and a film-covered surface (b) is reflected (index *r*). Incident and reflected light span the plane of incidence (POI), which is in the plane of the paper. The vector of the electric field can then be expressed as a superposition of a component parallel, E_p, and a component perpendicular, E_s, to the POI. The polarization of the light will change upon reflection. This change in polarization can be measured by ellipsometry and related to the ellipsometric angles by the fundamental equation of ellipsometry:

$$\tan(\psi)\exp(j\Delta) = \frac{E_{\mathrm{rp}}/E_{\mathrm{ip}}}{E_{\mathrm{rs}}/E_{\mathrm{is}}} \quad 1.8$$

ψ and Δ express the amplitude ratio and phase difference between p- and s-polarizations, respectively:

$$\Delta = \delta_{rp} - \delta_{rs} \quad \text{and} \quad |\tan(\psi)| = \frac{|E_{rp}/E_{ip}|}{|E_{rs}/E_{is}|} \quad 1.9$$

where δ_{rp} and δ_{rs} are phase shifts in parallel and perpendicular vectors.

The relation between Ψ and Δ can thus be expressed in the form of the ratio of the Fresnel coefficients (r_{p} and r_{s}), which for a model substrate/film/ambient is obtained as:

$$\rho = \tan(\psi)\exp(j\Delta) = \frac{r_p}{r_s} = f(n_0, n_1, n_2, \lambda, d, \theta_0) \quad 1.10$$

The ratio $r_{\mathrm{p}}/ r_{\mathrm{s}}$ depends on the wavelength (λ) of the incident light, the thickness of the film (d), the angle of incidence (θ_0), and the complex refractive indices of the ambient, the adsorbed film and the substrate (n_0, n_1, and n_2, respectively). Typically, n_0, n_2, λ and $\theta_0$are known parameters or can be independently obtained. Moreover, we work with transparent films, i.e. the refractive index of the film is real ($n_1 = n$). The measured Ψ and Δ can then be directly related to the properties of the film (n and d), i.e. the refractive index n and the film thickness d can be calculated through a fit to the experimental data. In particular for thick films, the thickness and refractive index of adsorbed layer can be fitted independently with good accuracy. In spectroscopic ellipsometry (SE), Ψ and Δ are measured over a range of wavelengths, and n can then also be determined as a function of wavelength.

Determination of adsorbed mass

Based on the measured n and d, the surface density (Γ) can be calculated, to a good approximation for biomolecular films [201], according to de Feijter [204]:

$$\Gamma = \frac{d_{\mathrm{film}}(n_{\mathrm{film}} - n_{\mathrm{solvent}})}{dn_{\mathrm{adsorbate}}/dc} \quad 1.11$$

where d_{film} is the effective thickness of the film, n_{film} is the refractive index of the film, and $n_{solvent}$ the (real) refractive index of the solution. $dn_{\mathrm{adsorbate}}/dc$ is the so-called refractive-index increment of the molecules that constitute the film in the solvent. To a

good approximation, the refractive index increment is constant over the relevant concentration range.

Fitting of SE data requires careful consideration of the optical properties of the substrate and the solution. Detailed information about the models and data analysis that we employed can be found in the materials and methods part of the chapter III.

I.2.3.b.iii. Surface plasmon resonance (SPR)

Surface plasmon resonance (SPR) is an optical biosensing technology, which is popular in the areas of biochemistry, biology, and medical sciences [205-208]. It provides quantitative information about biomolecular interactions in real time and label free. In the frame of this thesis, SPR was used to quantify binding affinities and kinetics of HS-chemokine interactions.

Working Principle

When a beam of light meets the interface from a material with a higher refractive index (e.g. glass) to a material with a lower refractive index (e.g. water), the light is either reflected or refracted depending on the angle of incidence, θ_i. When the angle of incidence θ_i is equal to or greater than a critical angle (θ_C), total internal reflection occurs, and thus no light is refracted.

If the surface of the glass is coated with a thin film of a noble metal (e.g. gold or silver), instead of being internally reflected, some of the light may couple with the electron cloud (plasma) in the metal and propagate along the metal surface. This absorption process leads to a reduction in the amount of reflected light. There exists a second angle, greater than the critical angle, at which this loss is greatest and the intensity of reflected light reaches a minimum or 'dip' (Figure I.2.8). This angle is called the surface plasmon resonance angle (θ_{SPR}). The electron plasma waves are called surface plasmons, and θ_{SPR} represents a resonance condition at which the wave vector of the incident light matches the wavelength of the surface plasmons, hence the term surface plasmon resonance.

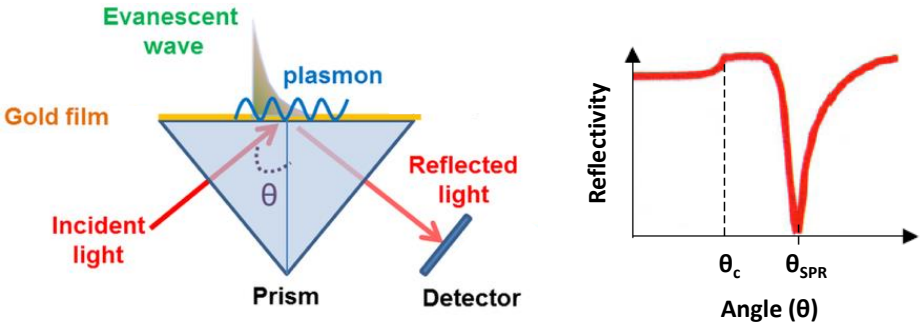

Figure I.2.8: Schematic diagram of the principles of SPR. Image adapted from ref [209].

The energy of the light coupled to the surface electron cloud creates an evanescent electric field at the interface between the metallic film and the adjacent medium. The amplitude of the wave field decays exponentially with the distance from the metal surface, with a decay length of typically 300 nm.

The optical phenomenon of SPR can be used to monitor interactions between biomolecules. This sensing application relies on the fact that changes in the refractive index of the medium in the vicinity of the metal surface upon binding of molecules sensitively affect the resonance angle. Under specific cases, the change in resonance angle (output signal) can be quantitatively related to the areal mass density of molecules in contact with the biospecific interface [207].

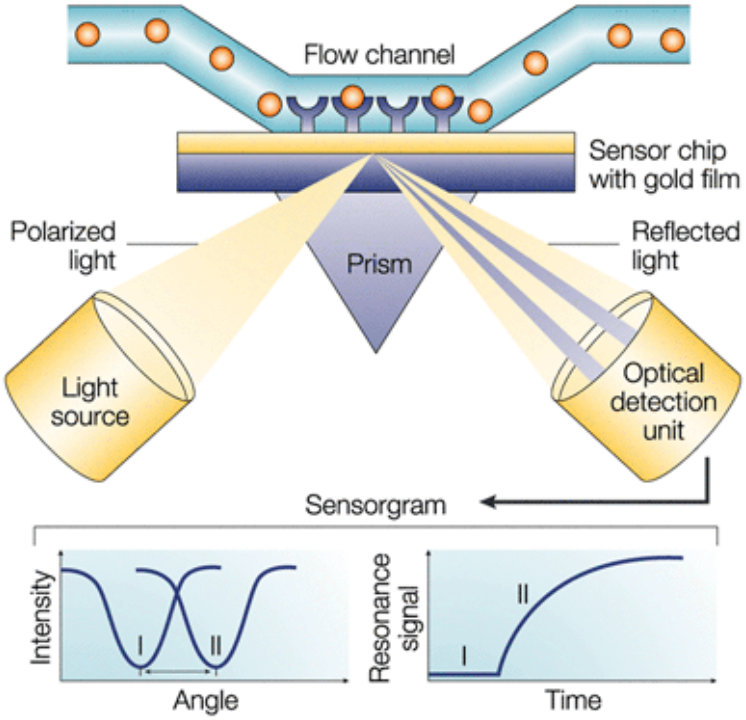

Figure I.2.9: Surface plasmon resonance (SPR) detects changes in the refractive index in the immediate vicinity of the surface layer of a sensor chip. SPR is observed as a sharp 'dip' in the intensity of reflected light at an angle θ_{SPR} that is dependent on the refractive index, and thus the areal mass density of material, at the surface. The SPR angle shifts (from I to II in the lower left-hand diagram) when biomolecules bind to the surface and thus increase the local refractive index. The change in resonant angle is monitored in real time in the form the resonance signal (proportional to mass change, lower right-hand diagram). Figure adapted from ref [210].

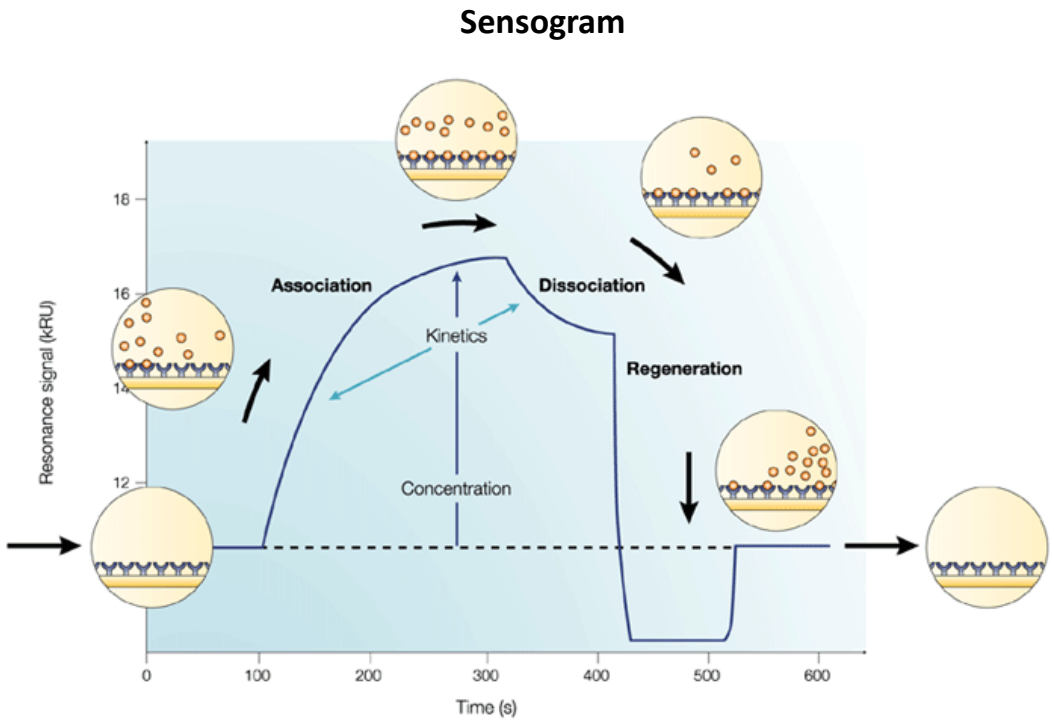

Figure I.2.10: A typical sensogram representing the different steps involved in a kinetic analysis of the interaction between an analyte in solution and its corresponding immobilized ligand. Adapted from ref [210].

SPR measurements were performed with a BIAcore T200 device. This device, equipped with a micro fluidic system, is especially dedicated to determination of binding affinities and kinetics of interactions between an immobilized ligand and an analyte in solution (Figure I.2.9). For this application, ligand (the GAG, HS in our case) was immobilized on a gold-covered surface so as to form the internal surface of a flow cell. The corresponding analyte (the chemokine CXCL12α in our case) was then injected into the flow cell in buffer solution, and binding monitored. As more analyte binds to the surface, the change in θ_{SPR} increases in magnitude giving rise to the association curve recorded in the sensorgram. In the experimental setup, the change in resonance angle is quantified in resonance units or response units (RUs), with 1 RU equivalent to a shift of 10^{-4} degrees. As the amount of analyte associating with the surface equilibrates with the amount of analyte dissociating, equilibrium is reached. During the post-injection phase, only buffer passes through the flow cell and the analyte dissociates from the surface leading to a decrease in the signal and the dissociation curve. This association and dissociation cycle is typically repeated for several analyte concentrations. At the end of each association/dissociation cycle, a regeneration step is performed to ensure a similar initial surface for the following cycles (Figure I.2.10). Simultaneous injections are performed on a reference flow cell consisting of a substrate without ligand (SAv monolayer without HS in our case), in order to remove bulk and non-specific contributions to the signal.

The sensorgrams are then subjected to fitting with a kinetic model using analysis software in order to extract association and dissociation rates and, if possible, equilibrium binding constants. To obtain equilibrium binding constants, the response signals at equilibrium ($RU_{anal,max}$) can be plotted against the analyte concentration, and analyzed. In the simplest case of a 1:1 ligand:analyte interaction, these data can be fitted with a Langmuir isotherm to obtain the binding constant K_D.

In this thesis, two distinct optical mass-sensitive techniques *i.e.* SPR and SE were used. SPR was used to study the binding kinetics between GAGs and chemokines. Main advantages of SPR over SE are superior sensitivity, an automated and purpose-designed fluid handling system, and low sample consumption, and these features are particularly attractive for the study of binding kinetics. However, quantification of absolute areal mass densities of molecules using SPR is not trivial, because being based on an evanescent wave, the SPR response depends sensitively on the distance from the gold surface at which molecules bind. The SE response, on the other hand, is rather insensitive to the exact location of the molecules, and SE was therefore preferred to quantify areal mass densities.

I.2.3.b.iv. Combination of QCM-D and SE

Our surface-confined model films are a few nanometers thick and strongly hydrated due to which *in situ* characterization is mandatory. Because of their different working principles, QCM-D and SE are highly complementary, providing insight into optical and mechanical properties, respectively.

As explained above, QCM-D measures all material that is mechanically excited, including the hydrodynamically coupled solvent, $m_{solvent}$ (equation (1. 6)). In contrast, the areal mass density measured by SE, m_{SE}, represents exclusively the adsorbate ($m_{SE} = m_{ads}$).

By exploiting this difference in mass sensitivity, information about the solvent content (e.g. hydration or porosity) of solvated films as a function of time can be extracted from combined SE/QCM-D measurements, a quantity that cannot generically be obtained with either technique alone. The hydration can be obtained as:

$$H = 1 - \frac{m_{\mathrm{SE}}}{m_{\mathrm{QCM-D}}} \qquad 1.\ 12$$

In addition, the combined SE/QCM-D measurement permits a correlation between m_{ads} (measured by SE) and Δf (measured by QCM-D). In this way, it is possible to establish a 'calibration curve' that connects frequency shifts to adsorbed amounts. This was crucial for the quantitative control on biomolecular surface densities by QCM-D. For the routine control of surface functionalization, QCM-D was preferred over SE. The main reason is that dissipation and frequency measured by QCM-D provide information about the morphology of surface-confined films that is not readily accessible by SE and valuable,

e.g. to ascertain correct orientation of surface-bound molecules. Moreover, the QCM-D setup permitted 4 measurements in parallel, thus significantly enhancing throughput compared to SE or combined SE/QCM-D measurement which are not parallelized. Last but not least, the complexity of the measurement and a relatively large sample consumption make the combined QCM-D/SE impractical for routine analysis. Taken together, a combination of selected QCM-D/SE measurements (to obtain Δf vs. m_{ads} calibration curves) with simple QCM-D measurements for routine analysis thus proved the most practical and informative characterization strategy.

I.2.4. Cellular level

The model surfaces with a well-defined presentation of HS, chemokines and cell adhesion ligands were employed to investigate cellular responses to extracellular cues in a highly defined environment (Figure I.2.11).

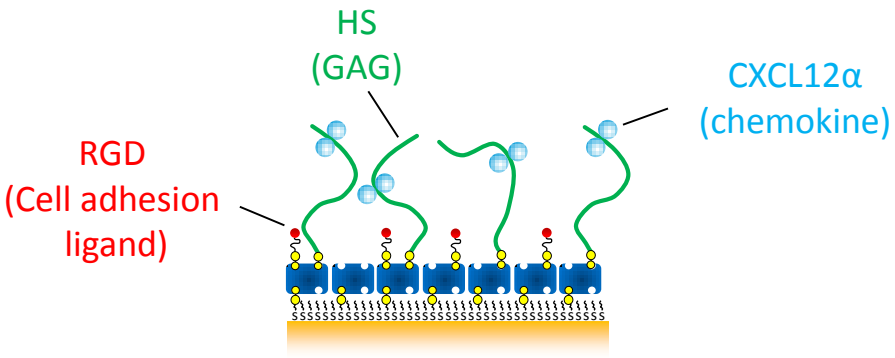

Figure I.2.11: Schematic representation of biomimetic surface presenting a selected GAG (i.e. HS), a selected chemokine (i.e. CXCL12α) and a selected cell-adhesion ligand (i.e. RGD) on a molecular breadboard based on an OEG monolayer.

The questions that we intended to answer performing cellular studies on these model surfaces were:

- What is the role of HS in chemokine-mediated cellular adhesion and motility?
- How does the presentation of chemokines in the HS-bound form affect the interaction with its cell-surface receptor?
- How do cell adhesion ligands along with HS-bound chemokines affect cellular responses?

My thesis work on the cellular level focused on myoblasts (C2C12). It was performed in collaboration with the team of Catherine Picart (IMBM, LMGP, Grenoble), and is covered in Chapter V. To establish the use of HS-presenting biomimetic surfaces in cellular assays, these were also employed for studies with a leukocyte cell model (Jurkat) by Elisa Migliorini in collaboration with the team of Hugues Lortat-Jacob (SAGAG, IBS, Grenoble), and this is covered in Chapter III.

In the context of this thesis two cell lines C2C12 (myoblasts) and Jurkat (leuckocytes) were used. C2C12 is a mouse myoblast cell line which was originally obtained from the thigh muscle of mice [211]. This cell line serves as a tool to study aspects of myogenesis, metabolism and muscle biology [16, 17]. Jurkat cells are human T lymphocyte cells that are used to study T cell signaling, leukemia and the expression of various chemokine receptors susceptible to viral entry, particularly HIV [82, 212].

To perform the cellular assays a novel approach was adopted. A gold-coated glass coverslip was attached to the bottom of a custom-designed teflon holder thus forming wells. The bottom surface of the wells was functionalized as desired, and the cells were then plated and cellular responses monitored by optical and fluorescence microscopy (Figure I.2.12).

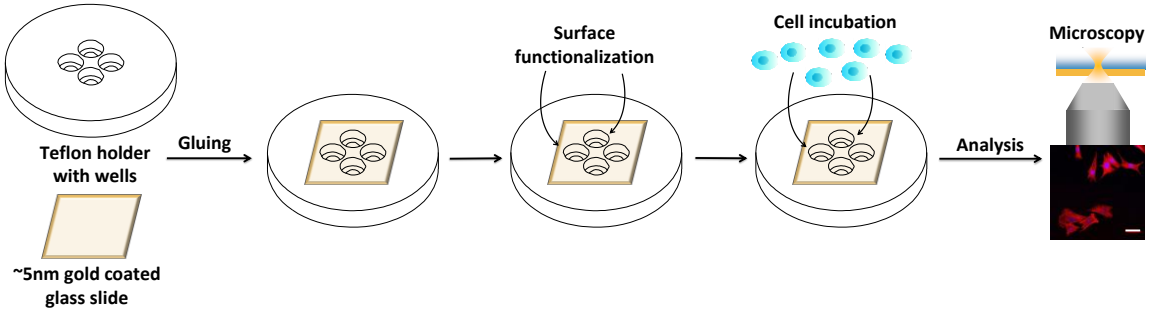

Figure I.2.12: Schematic representation of cellular assays.

The cellular response to the molecular cues presented by the biomimetic surface was characterized by various measures of the cell phenotype. Specificilly, the cellular responses were tracked by optical imaging and cell biological assays such as:

- Cell adhesion assays: For the quantification of cellular adhesion, the fraction of cells resisting gentle rinsing was quantified.
- Cell spreading assays: For this purpose the cells were fixed, stained and then visualized by fluorescence microscopy to obtain quantitative information about cell area and circularity [15].
- Cell motility assays: Time-lapse live cell imaging was employed to track cell motility.

References

[1] Ridley AJ, Schwartz MA, Burridge K, Firtel RA, Ginsberg MH, Borisy G, et al. Cell Migration: Integrating Signals from Front to Back. Science. 2003;302:1704-9.
[2] Friedl P, Gilmour D. Collective cell migration in morphogenesis, regeneration and cancer. Nat Rev Mol Cell Biol. 2009;10:445-57.
[3] Robertson TA, Papadimitriou JM, Grounds MD. Fusion of myogenic cells to the newly sealed region of damaged myofibres in skeletal muscle regeneration. Neuropathol Appl Neurobiol. 1993;19:350-8.
[4] Griffin CA, Apponi LH, Long KM, Pavlath GK. Chemokine expression and control of muscle cell migration during myogenesis. J Cell Sci. 2010;123:3052-60.
[5] Janssen I, Heymsfield SB, Wang Z, Ross R. Skeletal muscle mass and distribution in 468 men and women aged 18–88 yr. J Appl Physiol. 2000;89:81-8.
[6] Tajbakhsh S. Skeletal muscle stem cells in developmental versus regenerative myogenesis. J Intern Med. 2009;266:372-89.
[7] Relaix F, Zammit PS. Satellite cells are essential for skeletal muscle regeneration: the cell on the edge returns centre stage. Development. 2012;139:2845-56.
[8] Salvatore D, Simonides WS, Dentice M, Zavacki AM, Larsen PR. Thyroid hormones and skeletal muscle—new insights and potential implications. Nat Rev Endocrinol. 2014;10:206-14.
[9] Yin H, Price F, Rudunicki MA. Satellite cells and the muscle stem cell niche. Physiol Rev. 2013;93:23-67.
[10] Hawke TM, Garry DJ. Myogenic satellite cells: physiology to molecular biology. J Appl Physiol. 2001;91:534-51.
[11] Mauro A. Satellite cell of skeletal muscle fibres. J Biophys Biochem Cytol. 1961:493-5.
[12] Thorsteinsdottir S, Deries M, Cachaco AS, Bajanca F. The extracellular matrix dimension of skeletal muscle development. Dev Biol. 2011;354:191-207.
[13] Lund DK, Cornelison DD. Enter the matrix: shape, signal and superhighway. The FEBS journal. 2013;280:4089-99.
[14] Cosgrove BD, Sacco A, Gilbert PM, Blau HM. A home away from home: challenges and opportunities in engineering in vitro muscle satellite cell niches. Differentiation. 2009;78:185-94.
[15] Dalonneau F, Liu XQ, Sadir R, Almodovar J, Mertani HC, Bruckert F, et al. The effect of delivering the chemokine SDF-1alpha in a matrix-bound manner on myogenesis. Biomaterials. 2014;35:4525-35.
[16] Ratajczak MZ, Majka M, Kucia M, Drukala J, Pietrzkowski Z, Peiper S, et al. Expression of Functional CXCR4 by Muscle Satellite Cells and Secretion of SDF-1 by Muscle-Derived Fibroblasts is Associated with the Presence of Both Muscle Progenitors in Bone Marrow and Hematopoietic Stem/Progenitor Cells in Muscles. Stem Cell. 2003;21:363-71.
[17] Ödemis V, Boosmann K, Dieterlen MT, Engele J. The chemokine SDF1 controls multiple steps of myogenesis through atypical PKC. J Cell Sci. 2007;120:4050-9.
[18] Haque MA, Nagaoka M, Hexig B, Akaike T. Artificial extracellular matrix for embryonic stem cell cultures: a new frontier of nanobiomaterials. Sci Technol Adv Mater. 2010;11:014106.

[19] Frantz CS, K. M., Weaver VM. The extracellular matrix at a glance. J Cell Sci. 2010;123:4195-200.
[20] Daley WP, Peters SB, Larsen M. Extracellular matrix dynamics in development and regenerative medicine. J Cell Sci. 2008;121:255-64.
[21] Ghajar CM, Bissell MJ. Extracellular matrix control of mammary gland morphogenesis and tumorigenesis: insights from imaging. Histochem Cell Biol. 2008;130:1105-18.
[22] Kirkpatrick CA, Selleck SB. Heparan sulfate proteoglycans at a glance. J Cell Sci. 2007;120:1829-32.
[23] Weber M, Hauschild R, Schwarz J, Moussion C, de Vries I, Legler DF, et al. Interstitial Dendritic Cell Guidance by Haptotactic Chemokine Gradients. Science. 2013;339:328-32.
[24] Middleton J, Patterson AM, Gardner L, Schmutz C, Ashton BA. Leukocyte extravasation: chemokine transport and presentation by the endothelium. Blood. 2002;100:3853-60.
[25] Handel TM, Johnson Z, Crown SE, Lau EK, Proudfoot AE. Regulation of protein function by glycosaminoglycans--as exemplified by chemokines. Annu Rev Biochem. 2005;74:385-410.
[26] Proudfoot AEI. The biological relevance of chemokine–proteoglycan interactions. Biochem Soc Trans. 2006;34:422-6.
[27] Lu P, Weaver VM, Werb Z. The extracellular matrix: a dynamic niche in cancer progression. J Cell Biol. 2012;196:395-406.
[28] Lu P, Takai K, Weaver VM, Werb Z. Extracellular matrix degradation and remodeling in development and disease. Cold Spring Harb Perspect Biol. 2011;3.
[29] Egeblad M, Rasch MG, Weaver VM. Dynamic interplay between the collagen scaffold and tumor evolution. Curr Opin Cell Biol. 2010;22:697-706.
[30] Kass L, Erler JT, Dembo M, Weaver VM. Mammary epithelial cell: influence of extracellular matrix composition and organization during development and tumorigenesis. Int J Biochem Cell Biol. 2007;39:1987-94.
[31] LeBleu VS, Macdonal B, Kalluri R. Structure and function of basement membranes. Exp Biol Med (Maywood). 2007;232:1121-9.
[32] Bernfield M, Gotte M, Park PW, Reizes O, Fitzgerald ML, Lincecum J, et al. Functions of cell surface heparan sulfate proteoglycans. Annu Rev Biochem. 1999;68:729-77.
[33] Kreuger J, Spillmann D, Li JP, Lindahl U. Interactions between heparan sulfate and proteins: the concept of specificity. J Cell Biol. 2006;174:323-7.
[34] Hacker U, Nybakken K, Perrimon N. Heparan sulphate proteoglycans: the sweet side of development. Nat Rev Mol Cell Biol. 2005;6:530-41.
[35] Sarrazin S, Lamanna WC, Esko JD. Heparan sulfate proteoglycans. Cold Spring Harb Perspect Biol. 2011;3.
[36] Cain SA, Baldock C, Gallagher J, Morgan A, Bax DV, Weiss AS, et al. Fibrillin-1 interactions with heparin. Implications for microfibril and elastic fiber assembly. J Biol Chem. 2005;280:30526-37.
[37] Cain SA, Baldwin AK, Mahalingam Y, Raynal B, Jowitt TA, Shuttleworth CA, et al. Heparan sulfate regulates fibrillin-1 N- and C-terminal interactions. J Biol Chem. 2008;283:27017-27.
[38] Baranova NS, Nileback E, Haller FM, Briggs DC, Svedhem S, Day AJ, et al. The inflammation-associated protein TSG-6 cross-links hyaluronan via hyaluronan-induced TSG-6 oligomers. J Biol Chem. 2011;286:25675-86.

[39] Day AJ, de la Motte CA. Hyaluronan cross-linking: a protective mechanism in inflammation? Trends Immunol. 2005;26:637-43.
[40] Attili S, Richter RP. Self-assembly and elasticity of hierarchical proteoglycan–hyaluronan brushes. Soft Matter. 2013;9:10473.
[41] Lee GM, Johnstone B, Jacobson K, Caterson B. The Dynamic Structure of the Pericellular Matrix on Living Cells. J Cell Biol. 1993;123:1899-907.
[42] Knudson W, Knudson CB. Assembly of a chondrocyte-like pericellular matrix on non-chondrogenic cells. Role of the cell surface hyaluronan receptors in the assembly of a pericellular matrix. J Cell Sci. 1991;99:227-35.
[43] Laguri C, Sadir R, Rueda P, Baleux F, Gans P, Arenzana-Seisdedos F, et al. The novel CXCL12gamma isoform encodes an unstructured cationic domain which regulates bioactivity and interaction with both glycosaminoglycans and CXCR4. PloS one. 2007;2:e1110.
[44] Johnson Z, Proudfoot AE, Handel TM. Interaction of chemokines and glycosaminoglycans: a new twist in the regulation of chemokine function with opportunities for therapeutic intervention. Cytokine Growth Factor Rev. 2005;16:625-36.
[45] Duchesne L, Octeau V, Bearon RN, Beckett A, Prior IA, Lounis B, et al. Transport of fibroblast growth factor 2 in the pericellular matrix is controlled by the spatial distribution of its binding sites in heparan sulfate. PLoS biology. 2012;10:e1001361.
[46] Rueda P, Balabanian K, Lagane B, Staropoli I, Chow K, Levoye A, et al. The CXCL12gamma chemokine displays unprecedented structural and functional properties that make it a paradigm of chemoattractant proteins. PloS one. 2008;3:e2543.
[47] Hesselgesser J, Liang M, Hoxie J, Greenberg M, Brass LF, Orsini MJ, et al. Identification and Characterization of the CXCR4 Chemokine Receptor in Human T Cell Lines: Ligand Binding, Biological Activity, and HIV-1 Infectivity. J Immunol. 1998;160:877-83.
[48] Alberts B, Johnson A, Lewis J, Raff M, Roberts K, Walter P. Molecular Biology of the Cell, 4th edition. New York: Garland Science. 2002.
[49] Imberty A, Lortat-Jacob H, Perez S. Structural view of glycosaminoglycan-protein interactions. Carbohydr Res. 2007;342:430-9.
[50] Li J-P, Spillmann D. Heparan Sulfate Proteoglycans as Multifunctional Cell Regulators: Cell Surface Receptors. Methods Mol Biol 2011;836:239-55.
[51] Hook M, Kjellen L, Johansson S, Robinson J. Cell-surface glycosaminoglycans. Ann Rev Biochem. 1984;53:847-69.
[52] Noonan DM, Fulle A, Valente P, Cai S, Horigan E, Sasaki M, et al. The Complete Sequence of Perlecan, a Basement Membrane Heparan Sulfate Proteoglycan, Reveals Extensive Similarity with Laminin A Chain, Low Density Lipoprotein-Receptor, and the Neural Cell Adhesion Molecu. J Biol Chem. 1991;266:22939-47.
[53] Yanagishita M, Hascall VC. Cell Surface Heparan Sulfate Proteoglycans. J Biol Chem. 1992;267:9451-4.
[54] Iozzo RV. Heparan sulfate proteoglycans: intricate molecules with intriguing functions. J Clin Invest. 2001;108:165-7.
[55] Holmborn K, Habicher J, Kasza Z, Eriksson AS, Filipek-Gorniok B, Gopal S, et al. On the roles and regulation of chondroitin sulfate and heparan sulfate in zebrafish pharyngeal cartilage morphogenesis. J Biol Chem. 2012;287:33905-16.

[56] McCormick C, Duncan G, Goutsos KT, Tufaro F. The putative tumor suppressors EXT1 and EXT2 form a stable complex that accumulates in the Golgi apparatus and catalyzes the synthesis of heparan sulfate. Proc Natl Acad Sci USA. 2000;97:668-73.
[57] Esko JD, Selleck SB. Order out of chaos: assembly of ligand binding sites in heparan sulfate. Annu Rev Biochem. 2002;71:435-71.
[58] Rabenstein DL. Heparin and heparan sulfate: structure and function. Nat Prod Rep. 2002;19:312-31.
[59] Murphy KJ, Merry CL, Lyon M, Thompson JE, Roberts IS, Gallagher JT. A new model for the domain structure of heparan sulfate based on the novel specificity of K5 lyase. J Biol Chem. 2004;279:27239-45.
[60] Jastrebova N, Vanwildemeersch M, Lindahl U, Spillmann D. Heparan sulfate domain organization and sulfation modulate FGF-induced cell signaling. J Biol Chem. 2010;285:26842-51.
[61] Laguri C, Arenzana-Seisdedos F, Lortat-Jacob H. Relationships between glycosaminoglycan and receptor binding sites in chemokines-the CXCL12 example. Carbohydr Res. 2008;343:2018-23.
[62] Lortat-Jacob H. The molecular basis and functional implications of chemokine interactions with heparan sulphate. Curr Opin Struct Biol. 2009;19:543-8.
[63] Sozzani S, Allavena P, D'Amico G, Walter L, Bianchi G, Kataura M, et al. Cutting Edge: Differential Regulation of Chemokine Receptors During Dendritic Cell Maturation: A Model for Their Trafficking Properties. J Immunol. 1998;161:1083-6.
[64] Forster R, Emrich T, Kremmer E, Lipp M. Expression of the G-Protein-Coupled Receptor BLRl Defines Mature, Recirculating B Cells and a Subset of T-Helper Memory Cells. Blood. 1994;84:830-40.
[65] Vicari A, Figueroa DJ, Hedrick JA, Foster JS, Gilbert DJ, Jenkins NA, et al. TECK: A Novel CC Chemokine Specifically Expressed by Thymic Dendritic Cells and Potentially Involved in T Cell Development. Immunity. 1997;7:291-301.
[66] Gerard C, Rollins BJ. Chemokines and disease. Nat Immunol. 2001;2:108-15.
[67] Rossi D, Zlotnik A. The Biology of chemokines and their receptors. Annu Rev Immunol. 2000;18:217-42.
[68] Zlotnik A, Yoshie O. Chemokines: A New Classification System and Their Role in Immunity. Immunity. 2000;12:121-7.
[69] Rollins BJ. Chemokines. Blood. 1997;90:909-28.
[70] Baggiolini M, Dewald B, Moser B. Human Chemokines: An Update. Annu Rev Immunol. 1997;15:675-705.
[71] Veldkamp CT, Seibert C, Peterson FC, De la Cruz NB, Haugner JC, 3rd, Basnet H, et al. Structural basis of CXCR4 sulfotyrosine recognition by the chemokine SDF-1/CXCL12. Sci Signal. 2008;1:ra4.
[72] Sadir R, Imberty A, Baleux F, Lortat-Jacob H. Heparan sulfate/heparin oligosaccharides protect stromal cell-derived factor-1 (SDF-1)/CXCL12 against proteolysis induced by CD26/dipeptidyl peptidase IV. J Biol Chem. 2004;279:43854-60.
[73] Ali S, Palmer ACV, Banerjee B, Fritchley SJ, Kirby JA. Examination of the Function of RANTES, MIP-1a, and MIP-1b following Interaction with Heparin-like Glycosaminoglycans. J Biol Chem. 2000;275:11721-7.
[74] Friedl P, Weigelin B. Interstitial leukocyte migration and immune function. Nat Immunol. 2008;9:960-9.

[75] Ganju RK, Brubaker SA, Meyer J, Dutt P, Yang Y, Qin S, et al. The a-Chemokine, Stromal Cell-derived Factor-1a, Binds to the Transmembrane G-protein-coupled CXCR-4 Receptor and Activates Multiple Signal Transduction Pathways. J Biol Chem. 1998;273:23169-75.
[76] Vlahakis SR, Villasis-Keever A, Gomez T, Vanegas M, Vlahakis N, Pay CV. G Protein-Coupled Chemokine Receptors Induce Both Survival and Apoptotic Signaling Pathways. J Immunol. 2002:5546-54.
[77] Alsayed Y, Ngo H, Runnels J, Leleu X, Singha UK, Pitsillides CM, et al. Mechanisms of regulation of CXCR4/SDF-1 (CXCL12)–dependent migration and homing in multiple myeloma. Blood. 2007;109:2708-17.
[78] Bokoch GM. Chemoattractant Signaling and Leukocyte Activation. Blood. 1995;86:1649-60.
[79] Ward SG, Bacon K, Westwick J. Chemokines and T Lymphocytes: More than an Attraction. Immunity. 1998;9:1-11.
[80] Yu L, Cecil J, Peng SB, Schrementi J, Kovacevic S, Paul D, et al. Identification and expression of novel isoforms of human stromal cell-derived factor 1. Gene. 2006;374:174-9.
[81] Sadir R, Baleux F, Grosdidier A, Imberty A, Lortat-Jacob H. Characterization of the stromal cell-derived factor-1alpha-heparin complex. J Biol Chem. 2001;276:8288-96.
[82] Amara A, Lorthioir O, Valenzuela A, Magerus A, Thelen M, Montes M, et al. Stromal Cell-derived Factor-1a Associates with Heparan Sulfates through the First b-Strand of the Chemokine. J Biol Chem. 1999;274:23916-25.
[83] Bleul CC, Fuhlbrigge RC, Casasnovas JM, Aiuti A, Springer TA. A Highly Efficacious Lymphocyte Chemoattractant, Stromal Cell-derived Factor 1 (SDF-1). J Exp Med. 1996;184:1101-9.
[84] Oberlin E, Amara A, Bacheleria F, Bessia C, Virelizier J-L, Arenzana-Seisdedos F, et al. The CXC chemokine SDF-1 is the ligand for LESTR/fusin and prevents infection by T-cell-line-adapted HIV-1. Nature. 1996;382:833-5.
[85] Vasyutina E, Stebler J, Brand-Saberi B, Schulz S, Raz E, Birchmeier C. CXCR4 and Gab1 cooperate to control the development of migrating muscle progenitor cells. Genes Dev. 2005;19:2187-98.
[86] Yusuf F, Rehimi R, Morosan-Puopolo G, Dai F, Zhang X, Brand-Saberi B. Inhibitors of CXCR4 affect the migration and fate of CXCR4+ progenitors in the developing limb of chick embryos. Dev Dyn. 2006;235:3007-15.
[87] Tachibana K, Hirota S, Iizasa H, Yoshida H, Kawabata K, Kataoka Y, et al. The chemokine receptor CXCR4 is essential for vascularization of the gastrointestinal tract. Nature. 1998;393:591-4.
[88] Coulomb-L'Hermine A, Amara A, Schiff C, Durand-Gasselin I, Foussat A, Delaunay T, et al. Stromal cell-derived factor 1 (SDF-1) and antenatal human B cell lymphopoiesis: Expression of SDF-1 by mesothelial cells and biliary ductal plate epithelial cells. Proc Natl Acad Sci U S A. 1999;96:8585-90.
[89] Pablos JL, Amara A, Bouloc A, Santiago B, Caruz A, Galindo M, et al. Stromal-Cell Derived Factor Is Expressed by Dendritic Cells and Endothelium in Human Skin. Am J Pathol. 1999;155:1577-85.
[90] Agace WW, Amara A, Roberts AI, Pablos JL, Thelen S, Uguccioni M, et al. Constitutive expression of stromal derived factor-1 by mucosal epithelia and its role in HIV transmission and propagation. Curr Biol. 2000;10:325-8.

[91] Crump M, Gong J-H, Loetscher P, Rajarathnam K, Amara A, Arenzana-Seisdedos F, et al. Solution structure and basis for functional activity of stromal cell-derived factor-1; dissociation of CXCR4 activation from binding and inhibition of HIV-1. EMBO J. 1997;16:6996-7007.
[92] Allen SJ, Crown SE, Handel TM. Chemokine: receptor structure, interactions, and antagonism. Annu Rev Immunol. 2007;25:787-820.
[93] Hoogewerf AJ, Kuschert GSV, Proudfoot AEI, Borlat F, Clark-Lewis I, Power CA, et al. Glycosaminoglycans Mediate Cell Surface Oligomerization of Chemokines. Biochemistry. 1997;36:13570-8.
[94] Kuschert GSV, Coulin F, Power CA, Proudfoot AEI, Hubbard RE, Hoogewerf AJ, et al. Glycosaminoglycans Interact Selectively with Chemokines and Modulate Receptor Binding and Cellular Responses. Biochemistry. 1999;38:12959-68.
[95] Rot A. Neutrophil attractant/activation protein-1 (interleukin-8) induces in vitro neutrophil migration by haptotactic mechanism. Eur J Immunol. 1993;23:303-6.
[96] Ley K, Laudanna C, Cybulsky MI, Nourshargh S. Getting to the site of inflammation: the leukocyte adhesion cascade updated. Nat Rev Immunol. 2007;7:678-89.
[97] Campbell JJ, Qin S, Bacon KB, Mackay CR, Butcher EC. Biology of Chemokine and Classical Chemoattractant Receptors: Differential Requirements for Adhesion-triggering versus Chemotactic Responses in Lymphoid Cells. J Cell Biol. 1996;134:255-66.
[98] Schumann K, Lammermann T, Bruckner M, Legler DF, Polleux J, Spatz JP, et al. Immobilized chemokine fields and soluble chemokine gradients cooperatively shape migration patterns of dendritic cells. Immunity. 2010;32:703-13.
[99] Campbell JJ, Hedrick J, Zlotnik A, Siani MA, Thompson DA, Butcher EC. Chemokines and the Arrest of Lymphocytes Rolling Under Flow Conditions. Science. 1998;279:381-4.
[100] Cadene M, Boudier C, Daney de Marcillac G, Bieth JG. Influence of low molecular mass heparin on the kinetics of neutrophil elastase inhibition by mucus proteinase inhibitor. J Biol Chem. 1995;270:13204-9.
[101] Webb LMC, Ehrengruber MU, Clark-Lewis I, Baggiolini M, Rot A. Binding to heparan sulfate or heparin enhances neutrophil responses to interleukin 8. Proc Natl Acad Sci U S A. 1993;90:7158-62.
[102] Crown SE, Yu Y, Sweeney MD, Leary JA, Handel TM. Heterodimerization of CCR2 chemokines and regulation by glycosaminoglycan binding. J Biol Chem. 2006;281:25438-46.
[103] Proudfoot AE, Handel TM, Johnson Z, Lau EK, LiWang P, Clark-Lewis I, et al. Glycosaminoglycan binding and oligomerization are essential for the in vivo activity of certain chemokines. Proc Natl Acad Sci U S A. 2003;100:1885-90.
[104] Salanga CL, O'Hayre M, Handel T. Modulation of chemokine receptor activity through dimerization and crosstalk. Cell Mol Life Sci. 2009;66:1370-86.
[105] Proudfoot AE, Fritchley S, Borlat F, Shaw JP, Vilbois F, Zwahlen C, et al. The BBXB motif of RANTES is the principal site for heparin binding and controls receptor selectivity. J Biol Chem. 2001;276:10620-6.
[106] Martin L, Blanpain C, Garnier P, Wittamer V, Parmentier M, Vita C. Structural and Functional Analysis of the RANTES-Glycosaminoglycans Interactions. Biochemistry. 2001;40:6303-18.
[107] Shi X, Zaia J. Organ-specific heparan sulfate structural phenotypes. J Biol Chem. 2009;284:11806-14.

[108] Bulow HE, Hobert O. The Molecular Diversity of Glycosaminoglycans Shapes Animal Development. Annu Rev Cell Dev Biol. 2006;22:375-407.
[109] Massena S, Christoffersson G, Hjertstrom E, Zcharia E, Vlodavsky I, Ausmees N, et al. A chemotactic gradient sequestered on endothelial heparan sulfate induces directional intraluminal crawling of neutrophils. Blood. 2010;116:1924-31.
[110] Johnson Z, Kosco-Vilbois MH, Herren S, Cirillo R, Muzio V, Zaratin P, et al. Interference with Heparin Binding and Oligomerization Creates a Novel Anti-Inflammatory Strategy Targeting the Chemokine System. J Immunol. 2004;173:5776-85.
[111] Murphy JW, Cho Y, Sachpatzidis A, Fan C, Hodsdon ME, Lolis E. Structural and functional basis of CXCL12 (stromal cell-derived factor-1 alpha) binding to heparin. J Biol Chem. 2007;282:10018-27.
[112] Mbemba E, Benjouad A, Saffar L, Gattegno L. Glycans and Proteoglycans Are Involved in the Interactions of Human Immunodeficiency Virus Type 1 Envelope Glycoprotein and of SDF-1a with Membrane Ligands of CD4+ CXCR4+ Cells. Virology. 1999;265:354-64.
[113] Mbemba E, Gluckman JC, Gattegno L. Glycan and glycosminoglycan binding properties of stromal cell-derived factor (SDF)-1a. Glycobiology. 2000;10:21-9.
[114] Veldkamp CT, Peterson FC, Pelzek AJ, Volkman BF. The monomer-dimer equilibrium of stromal cell-derived factor-1 (CXCL 12) is altered by pH, phosphate, sulfate, and heparin. Protein Sci. 2005;14:1071-81.
[115] Salanga CL, Handel TM. Chemokine oligomerization and interactions with receptors and glycosaminoglycans: the role of structural dynamics in function. Exp Cell Res. 2011;317:590-601.
[116] Laguri C, Sapay N, Simorre JP, Brutscher B, Imberty A, Gans P, et al. 13C-labeled heparan sulfate analogue as a tool to study protein/heparan sulfate interactions by NMR spectroscopy: application to the CXCL12alpha chemokine. J Am Chem Soc. 2011;133:9642-5.
[117] Ziarek JJ, Veldkamp CT, Zhang F, Murray NJ, Kartz GA, Liang X, et al. Heparin oligosaccharides inhibit chemokine (CXC motif) ligand 12 (CXCL12) cardioprotection by binding orthogonal to the dimerization interface, promoting oligomerization, and competing with the chemokine (CXC motif) receptor 4 (CXCR4) N terminus. J Biol Chem. 2013;288:737-46.
[118] Clark-Lewis I, Dewald B, Loestscher M, Moser B, Baggiolini M. Structural Requirements for Interleukin-8 Function Identified by Design of Analogs and CXC Chemokine Hybrids. J Biol Chem. 1994;269:16075-81.
[119] Clark-Lewis I, Kim K-S, Rajarathnam K, Gong J-H, Dewald B, Moser B, et al. Structure-activity relationships of chemokines J Leukocyte Biol. 1995;57:703-11.
[120] Loetscher P, Clark-Lewis I. Agonistic and antagonistic activities of chemokines. J Leukocyte Biol. 2001;69:881-4.
[121] Clark-Lewis I, Gong J-H. Antagonists of Monocyte Chemoattractant Protein 1 Identified by Modification of Functionally Critical NH2-terminal Residues. J Exp Med. 1995;181:631-40.
[122] Hemmerich S, Paavola C, Bloom A, Bhakta S, Freedman R, Grunberger D, et al. Identification of Residues in the Monocyte Chemotactic Protein-1 That Contact the MCP-1 Receptor, CCR2. Biochemistry. 1999;38:13013-25.

[123] Jarnagin K, Grunberger D, Mulkins M, Wong B, Hemmerich S, Paavola C, et al. Identification of Surface Residues of the Monocyte Chemotactic Protein 1 That Affect Signaling through the Receptor CCR2. Biochemistry. 1999;38:16167-77.
[124] Kofuku Y, Yoshiura C, Ueda T, Terasawa H, Hirai T, Tominaga S, et al. Structural basis of the interaction between chemokine stromal cell-derived factor-1/CXCL12 and its G-protein-coupled receptor CXCR4. J Biol Chem. 2009;284:35240-50.
[125] Griffin CA, Apponi LH, Long KK, Pavlath GK. Chemokine expression and control of muscle cell migration during myogenesis. J Cell Sci. 2010;123:3052-60.
[126] Veldkamp CT, Seibert C, Peterson FC, Sakmar TP, Volkman BF. Recognition of a CXCR4 sulfotyrosine by the chemokine stromal cell-derived factor-1alpha (SDF-1alpha/CXCL12). J Mol Biol. 2006;359:1400-9.
[127] Wu B, Chien EYT, Mol CD, Fenalti G, Liu W, Katritch V, et al. Structures of the CXCR4 Chemokine GPCR with Small-Molecule and Cyclic Peptide Antagonist. Science. 2010;330:1066-71.
[128] Kufareva I, Stephens BS, Holden LG, Qin L, Zhao C, Kawamura T, et al. Stoichiometry and geometry of the CXC chemokine receptor 4 complex with CXC ligand 12: molecular modeling and experimental validation. Proc Natl Acad Sci U S A. 2014;111:E5363-72.
[129] Drury LJ, Ziarek JJ, Gravel S, Veldkamp CT, Takekoshi T, Hwang ST, et al. Monomeric and dimeric CXCL12 inhibit metastasis through distinct CXCR4 interactions and signaling pathways. Proc Natl Acad Sci U S A. 2011;108:17655-60.
[130] Pierschbacher MD, Ruoslahti E. Cell attachment activity of fibronectin can be duplicated by small synthetic fragments of the molecule. Nature. 1984;309:30-3.
[131] Pierschbacher MD, Ruoslahti E. Variants of the cell recognition site of fibronectin that retain attachment-promoting activity. Proc Natl Acad Sci U S A. 1984;81:5985-8.
[132] Ruoslahti E, Pierschbacher MD. New perspectives in cell adhesion: RGD and integrins. Science. 1987;238:491-7.
[133] Humphries MJ. The molecular basis and specificity of integrin-ligand interactions. J Cell Sci. 1990;97:585-92.
[134] Albelda SM, Buck CA. Integrins and other cell adhesion molecules. FASEB J. 1990;4:2868-80.
[135] Gullberg D, Ekblom P. Extracellular matrix and its receptors during development Int J Dev Biol. 1995;39:845854.
[136] Rowley JA, Mooney DJ. Alginate type and RGD density control myoblast phenotype. J Biomed Mater Res. 2002;60:217-23.
[137] Wang P-Y, Thissen H, Tsai W-B. The Roles of RGD and Grooved Topography in the Adhesion, Morphology, and Differentiation of C2C12 Skeletal Myoblasts. Biotechnol Bioeng. 2012;109:2104-15.
[138] Aumailley M, Gurrath M, Muller G, Calvete J, Timpl R, Kessler H. Arg-gly-Asp constrained within cyclic pentapeptides, strong and selective inhibitors of cell adhesion to vitronectin and laminin fragment P1. FEBS. 1991;291:50-4.
[139] Haubner R, Gratias R, Diefenbach B, Goodman SL, Jonczyk A, Kessler H. Structural and Functional Aspects of RGD-Containing Cyclic Pentapeptides as Highly Potent and Selective Integrin avb3 Antagonists. J Am Chem Soc. 1996;118:7461-72.
[140] Ren K, Fourel L, Rouviere CG, Albiges-Rizo C, Picart C. Manipulation of the adhesive behaviour of skeletal muscle cells on soft and stiff polyelectrolyte multilayers. Acta Biomater. 2010;6:4238-48.

[141] Gribova V, Gauthier-Rouviere C, Albiges-Rizo C, Auzely-Velty R, Picart C. Effect of RGD functionalization and stiffness modulation of polyelectrolyte multilayer films on muscle cell differentiation. Acta Biomater. 2013;9:6468-80.
[142] Hogg N, Laschinger M, Giles K, McDowall A. T-cell integrins: more than just sticking points. J Cell Sci. 2003;116.
[143] Tamkin JW, DeSimone DW, Fonda D, Patel RS, Buck C, Horwitz AF, et al. Structure of Integrin, a Glycoprotein Involved in the Transmembrane Linkage between Fibronectin and Actin. Cell Mol Life Sci. 1986;46:271-82.
[144] Hynes RO. The emergence of integrins: a personal and historical perspective. Matrix Biol. 2004;23:333-40.
[145] Hynes RO. Integrins: Bidirectional, Review Allosteric Signaling Machines. Cell. 2002;110:673-87.
[146] van der Flier A, Sonnenberg A. Function and interactions of integrins. Cell Tissue Res. 2001;305:285-98.
[147] Plow EF, Haas TA, Zhang L, Loftus J, Smith JW. Ligand binding to integrins. J Biol Chem. 2000;275:21785-8.
[148] Barczyk M, Carracedo S, Gullberg D. Integrins. Cell Tissue Res. 2010;339:269-80.
[149] Hodivala-Dilke KM, Reynolds AR, Reynolds LE. Integrins in angiogenesis: multitalented molecules in a balancing act. Cell Tissue Res. 2003;314:131-44.
[150] Danhier F, Le Breton A, Preat V. RGD-based strategies to target alpha(v) beta(3) integrin in cancer therapy and diagnosis. Mol Pharm. 2012;9:2961-73.
[151] Zigmond SH. Ability of polymorphonucleur leukcytes to orient in gradients of chemotactic factors. J Cell Biol. 1977;75:606-16.
[152] Haessler U, Pisano M, Wu M, Swartz MA. Dendritic cell chemotaxis in 3D under defined chemokine gradients reveals differential response to ligands CCL21 and CCL19. Proc Natl Acad Sci U S A. 2011;108:5614-9.
[153] Altgarde N, Becher J, Moller S, Weber FE, Schnabelrauch M, Svedhem S. Immobilization of chondroitin sulfate to lipid membranes and its interactions with ECM proteins. J Colloid Interface Sci. 2013;390:258-66.
[154] Saesen E, Sarrazin S, Laguri C, Sadir R, Maurin D, Thomas A, et al. Insights into the mechanism by which interferon-gamma basic amino acid clusters mediate protein binding to heparan sulfate. J Am Chem Soc. 2013;135:9384-90.
[155] Altgarde N, Nileback E, de Battice L, Pashkuleva I, Reis RL, Becher J, et al. Probing the biofunctionality of biotinylated hyaluronan and chondroitin sulfate by hyaluronidase degradation and aggrecan interaction. Acta Biomater. 2013;9:8158-66.
[156] Albertorio F, Daniel S, Cremer PS. Supported Lipopolymer Membranes as Nanoscale Filters: Simultaneous Protein Recognition and Size-Selection Assays. J Am Chem Soc. 2006;128:7168-9.
[157] Kikkeri R, Kamena F, Gupta T, Hossain LH, Boonyarattanakalin S, Gorodyska G, et al. Ru(II) glycodendrimers as probes to study lectin-carbohydrate interactions and electrochemically measure monosaccharide and oligosaccharide concentrations. Langmuir. 2010;26:1520-3.
[158] Kaindl T, Oelke J, Pasc A, Kaufmann S, Konovalov OV, Funari SS, et al. Regulation of adhesion behavior of murine macrophage using supported lipid membranes displaying tunable mannose domains. J Phys Condens Matter. 2010;22:285102.

[159] Richter RP, Hock KK, Burkhartsmeyer J, Boehm H, Bingen P, Wang G, et al. Membrane-Grafted Hyaluronan Films: A Well-Defined Model System of Glycoconjugate Cell Coats. J Am Chem Soc. 2007;129:5306-7.
[160] Jonkheijm P, Weinrich D, Schroder H, Niemeyer CM, Waldmann H. Chemical strategies for generating protein biochips. Angew Chem Int Ed Engl. 2008;47:9618-47.
[161] Ulman A. Formation and Structure of Self-Assembled Monolayers. Chem Rev. 1996;96:1533-54.
[162] Schreiber F. Self-assembled monolayers: from simple model systems to biofunctionalized interfaces. J Phys: Condens Matter. 2004;16:R881-R900.
[163] Bain CD, Whitesides GM. Modeling Organic Surfaces with Self-Assembled Monolayers. Angew Chem Int Ed Engl. 1989;28:506-12.
[164] Vericat C, Vela ME, Corthey G, Pensa E, Cortés E, Fonticelli MH, et al. Self-assembled monolayers of thiolates on metals: a review article on sulfur-metal chemistry and surface structures. RSC Adv. 2014;4:27730.
[165] Christopher Love J, Estroff LA, K. KJ, Nuzzo RG, Whitesides GM. Self-Assembled Monolayers of Thiolates on Metals as a Form of Nanotechnology. Chem Rev. 2005;105:1103-69.
[166] Samanta D, Sarkar A. Immobilization of bio-macromolecules on self-assembled monolayers: methods and sensor applications. Chem Soc Rev. 2011;40:2567-92.
[167] Chaki NK, Vijayamohanan K. Self-assembled monolayers as a tunable platform for biosensor applications. Biosens Bioelectron. 2002;17:1-12.
[168] Dubois LH, Nuzzo RG. Synthesis, structure, and properties of model organic surfaces. Annu Rev Phys Chem. 1992;43:437-63.
[169] Nileback E, Westberg F, Deinum J, Svedhem S. Viscoelastic Sensing of Conformational Changes in Plasminogen Induced upon Binding of Low Molecular Weight Compounds. Anal Chem. 2010;82:8374-6.
[170] Nileback E, Feuz L, Uddenberg H, Valiokas R, Svedhem S. Characterization and application of a surface modification designed for QCM-D studies of biotinylated biomolecules. Biosens Bioelectron. 2011;28:407-13.
[171] Prime KL, Whitesides GM. Adsorption of Proteins onto Surfaces Containing End-Attached Oligo(ethylene oxide): A Model System Using Self-Assembled Monolayers. J Am Chem Soc. 1993;115:10714-21.
[172] Hoffmann J, Groll J, Heuts J, Rong H, Klee D, Ziemer G, et al. Blood cell and plasma protein repellent properties of Star-PEG-modified surfaces. J Biomater Sci, Polym Ed. 2006;17:985-96.
[173] Chen S, Zheng J, Li L, Jiang S. Strong Resistance of Phosphorylcholine Self-Assembled Monolayers to Protein Adsorption: Insights into Nonfouling Properties of Zwitterionic Materials. J Am Chem Soc. 2005;127:14473-8.
[174] Deng L, Mrksich M, Whitesides GM. Self-Assembled Monolayers of Alkanethiolates Presenting Tri(propylene sulfoxide) Groups Resist the Adsorption of Protein. J Am Chem Soc. 1996;118:5136-7.
[175] Ostuni E, Yan L, Whitesides GM. The interaction of proteins and cells with self-assembled monolayers of alkanethiolates on gold and silver. Colloids Surf, B. 1999;15:3-30.
[176] Sackmann E. Supported Membranes: Scientific and Practical Applications. Science. 1996;271:43-8.

[177] Boxer SG. Molecular transport and organization in supported lipid membranes. Curr Opin Chem Biol. 2000;4:704-9.
[178] Salafsky JG, J. T., Boxer SG. Architecture and Function of Membrane Proteins in Planar Supported Bilayers: A Study with Photosynthetic Reaction Centers. Biochemistry. 1996;35:14773-81.
[179] Milhiet P-E, Giocondi M-C, Baghdadi OR, F., Roux B, Le Grimellec C. Spontaneous insertion and partitioning of alkaline phosphatase into model lipid rafts. EMBO Rep. 2002;3:485-90.
[180] Sapuri AR, Baksh MM, Groves JT. Electrostatically Targeted Intermembrane Lipid Exchange with Micropatterned Supported Membranes. Langmuir. 2003;19:1606-10.
[181] Kam L, Boxer SG. Spatially Selective Manipulation of Supported Lipid Bilayers by Laminar Flow: Steps Toward Biomembrane Microfluidics. Langmuir. 2003;19:1624-31.
[182] Watts TH, Brian AA, Kappler JWM, P., McConnell HM. Antigen presentation by supported planar membranes containing affinity-purified I-Ad. Proc Natl Acad Sci USA. 1984;81:7564-8.
[183] Brian AA, McConnell HM. Allogeneic stimulation of cytotoxic T cells by supported planar membranes. Proc Natl Acad Sci USA. 1984;81:6159-63.
[184] Richter RP, Berat R, Brisson AR. Formation of Solid-Supported Lipid Bilayers: An Integrated View. Langmuir. 2006;22:3497-505.
[185] Richter RP, Brisson AR. Following the formation of supported lipid bilayers on mica: a study combining AFM, QCM-D, and ellipsometry. Biophys J. 2005;88:3422-33.
[186] Reviakine I, Brisson A. Formation of Supported Phospholipid Bilayers from Unilamellar Vesicles Investigated by Atomic Force Microscopy. Langmuir. 2000;16:1806-15.
[187] Reimhult E, Höök F, Kasemo B. Vesicle adsorption on SiO2 and TiO2: Dependence on vesicle size. J Chem Phys. 2002;117:7401.
[188] Haussling L, Ringsdorf H, Schmitt F-J, Knoll W. Biotin-Functionalized Self - Assembled Monolayers on Gold: Surface Plasmon Optical Studies of Specific Recognition Reactions. Langmuir. 1991;7:1837-40.
[189] Curie J, Curie P. Comput Rend Acad Sci Paris. 1880;91:294-7.
[190] Reviakine I, Johannsmann D, Richter RP. Hearing what you cannot see and visualizing what you hear: interpreting quartz crystal microbalance data from solvated interfaces. Analytical chemistry. 2011;83:8838-48.
[191] Johannsmann D. Viscoelastic, mechanical, and dielectric measurements on complex samples with the quartz crystal microbalance. Phys Chem Chem Phys. 2008;10:4516-34.
[192] Kanazawa K, Cho N-J. Quartz Crystal Microbalance as a Sensor to Characterize Macromolecular Assembly Dynamics. J Sens. 2009;2009:1-17.
[193] Marx KA. Quartz crystal microbalance: a useful tool for studying thin polymer films and complex biomolecular systems at the solution-surface interface. Biomacromolecules. 2003;4:1099-120.
[194] Wudy F, Multerer M, Stock C, Schmeer G, Gores HJ. Rapid impedance scanning QCM for electrochemical applications based on miniaturized hardware and high-performance curve fitting. Electrochim Acta. 2008;53:6568-74.
[195] Sabot A, Krause S. Simultaneous Quartz Crystal Microbalance Impedance and Electrochemical Impedance Measurements. Investigation into the Degradation of Thin Polymer Films. Anal Chem. 2002;74:3304-11.

[196] Rodahl M, Höök F, Krozer A, Brzezinski P, Kasemo B. Quartz crystal microbalance setup for frequency and Q-factor measurements in gaseous and liquid environments. Rev Sci Instrum. 1995;66:3924.
[197] Marx KA. Quartz Crystal Microbalance: A Useful Tool for Studying Thin Polymer Films and Complex Biomolecular Systems at the Solution-Surface Interface. Biomacromolecules. 2003;4:1099-120.
[198] Sauerbrey G. Z Phys. 1959;155:206–22.
[199] Johannsmann D. http://www2.pc.tu-clausthal.de/dj/software_en.shtml.
[200] Eisele NB, Andersson FI, Frey S, Richter RP. Viscoelasticity of thin biomolecular films: a case study on nucleoporin phenylalanine-glycine repeats grafted to a histidine-tag capturing QCM-D sensor. Biomacromolecules. 2012;13:2322-32.
[201] Richter RP, Rodenhausen KB, Eisele NB, Schubert M. Coupling Spectroscopic Ellipsometry and Quartz Crystal Microbalance to Study Organic Films at the Solid-Liquid Interface. Springer Ser Surf Sci. 2014;52:223-48.
[202] Fujiwara H. Spectroscopic Ellipsometry, Principles and Applications. John Wiley & Sons. 2007.
[203] Goncalves D, Irene EA. Fundamentals and Applications of Spectroscopic Ellipsometry. Quim Nova. 2002;25:794-800.
[204] De Feijter JA, Benjamins J, Veer FA. Ellipsometry as a Tool to Study the Adsorption Behavior of Synthetic and Biopolymers at the Air-Water Interface. Biopolymers. 1978;17:1759-72.
[205] Zhang J, Zhang L, Xu W. Surface plasmon polaritons: physics and applications. J Phys D: Appl Phys. 2012;45:113001.
[206] Gopinath SCB. Biosensing applications of surface plasmon resonance-based Biacore technology. Sens Actuators, B. 2010;150:722-33.
[207] Jung LS, Campbell CT, Chinowsky TM, Mar MN, Yee SS. Quantitative Interpretation of the Response of Surface Plasmon Resonance Sensors to Adsorbed Films. Langmuir. 1998;14:5636-48.
[208] Myszka DG. Kinetic analysis of macromolecular interactions using ssurface plasmon resonance biosensors. Curr Opin Biotechnol. 1997;8:50-7.
[209] Yanase Y, Hiragun T, Ishii K, Kawaguchi T, Yanase T, Kawai M, et al. Surface plasmon resonance for cell-based clinical diagnosis. Sensors. 2014;14:4948-59.
[210] Cooper MA. Optical biosensors in drug discovery. Nat Rev Drug Discovery. 2002;1:515-28.
[211] Yaffe D, Saxel O. Serial passing and differentiation of myogenic cells isolated from dystrophic mouse muscle. Nature. 1977;270:725-7.
[212] Abraham RT, Weiss A. Jurkat T cells and development of the T-cell receptor signalling paradigm. Nat Rev Immunol. 2004;4:301-8.

II. Terminal functionalization of glycosaminoglycans

This chapter was published in *Chem. Commun*., 2014, 50, 15148-15151 as:

A quartz crystal microbalance method to study the terminal functionalization of glycosaminoglycans

Dhruv Thakar[a,b], Elisa Migliorini[a,b], Liliane Coche-Guerente[a,b], Rabia Sadir[c,d,e], Hugues Lortat-Jacob[c,d,e], Didier Boturyn[a,b], Olivier Renaudet[a,b], Pierre Labbe[a,b] and Ralf P. Richter[a,b,f,g]

[a]Universite Grenoble Alpes, DCM, 38000 Grenoble, France; [b]CNRS, DCM, 38000 Grenoble, France; [c]Universite Grenoble Alpes, Institut de Biologie Structurale (IBS), 38027 Grenoble, France; [d]CNRS, IBS, 38027 Grenoble, France; [e]CEA, DSV, IBS, 38027 Grenoble, France; [f]CIC biomaGUNE, Paseo Miramon 182, 20009 Donostia - San Sebastian, Spain; [g]Max Planck Institute for Intelligent Systems, 70569 Stuttgart, Germany.

Significance: We have established oxime ligation as a facile, one-step, superior in yield and stability compared to the popular hydrazone ligation, and versatile method for the functionalization of GAGs. The method should find broad use, as a tool in the glycosciences and in biotechnological applications. The control over and stability of GAG conjugates proved crucial for the reliable preparation of GAG-functionalized surfaces described in Chapter III.

My contribution: I co-designed research (together with Liliane Coche-Guerente, Didier Boturyn, Olivier Renaudet and Ralf P. Richter). I performed all measurements and analysis except for the synthesis of b-OEG-ONH_2 (compound 5). I contributed to data interpretation, and figure preparation. I wrote the first draft of the article and helped to complete the article for publication.

Résumé

La conception de puces à sucres nécessite la fixation de GAGs sur des surfaces solides. À cet égard, la conjugaison d'un site spécifique par l'extrémité réductrice est souhaitable. Ce mode de fonctionnalisation mime efficacement la présentation des motifs de GAG à la surface des cellules et permet d'éviter l'altération des interactions GAG-protéine par des modifications chimiques de la chaîne de GAG, ou par des contraintes conformationnelles ou spatiales.

La ligation chimiosélective par formation de lien oxime s'avère être une méthode de couplage simple qui est largement applicable à la conjugaison de l'extrémité réductrice des glycosaminoglycanes qui permet de remédier au manque de stabilité et au rendement limité du couplage par formation de lien hydrazone. Ce procédé peut être largement appliqué à la fonctionnalisation d'oligosaccharides et de différents types de GAG dont les GAGs polymériques de poids moléculaire élevé. La caractérisation par QCM-D de l'adsorption des conjugués préparés à partir de molécules chimiquement complexes tels que les GAG, a fourni des informations pertinentes sur les rendements de réaction de couplage et la dégradation des échantillons qui est difficile à évaluer en utilisant des techniques analytiques classiques, en particulier lorsque la quantité d'analyte est limitée à quelques microgrammes.

La ligation chimiosélective par formation de lien oxime pourra être utilisée largement comme outil de fonctionnalisation dans le domaine des glycosciences et dans des applications de biotechnologie. Pour des applications en ingénierie tissulaire ou pour des études biologiques fondamentales, le contrôle et la stabilité de conjugués de GAG s'avèrent déterminants pour la préparation fiable des surfaces fonctionnalisées.

ChemComm

COMMUNICATION

A quartz crystal microbalance method to study the terminal functionalization of glycosaminoglycans†

Cite this: *Chem. Commun.*, 2014, **50**, 15148

Received 1st September 2014,
Accepted 16th October 2014

DOI: 10.1039/c4cc06905f

www.rsc.org/chemcomm

Dhruv Thakar,[ab] Elisa Migliorini,[ab] Liliane Coche-Guerente,[ab] Rabia Sadir,[cde] Hugues Lortat-Jacob,[cde] Didier Boturyn,[ab] Olivier Renaudet,[ab] Pierre Labbe[ab] and Ralf P. Richter*[abfg]

We demonstrate the quartz crystal microbalance as a novel method to quantify the reaction yields and stability of the terminal conjugation of chemically complex molecules. Oxime ligation is identified as a facile, broadly applicable method for the reducing-end conjugation of glycosaminoglycans that overcomes the limited stability and yield of popular hydrazone ligation.

Linear polysaccharides known as glycosaminoglycans (GAGs) are ubiquitous cell surface and extracellular matrix components and fulfill crucial biological functions. Advanced screening applications (*e.g.* glycan microarrays[1,2]), functional molecular and cellular assays,[3] as well as biosensors and biomaterials[4] require the attachment of GAGs to surfaces or other scaffolds (*e.g.* with a biotin that can be anchored to biotin-binding proteins). In this regard, site-specific conjugation through the reducing end is desirable, as it effectively mimics the cell surface presentation of GAG motifs and avoids alteration of GAG–protein interactions by chemical modifications along the GAG chain, or by surface-imposed conformational or spatial constraints.[5]

An important but still underestimated challenge with the conjugation of GAG-derived oligosaccharides, and in particular polymeric GAGs, is the characterization of the reaction products. The often low isolated yields from natural sources, the GAG's hydrophilic nature and lack of a suitable chromophore, and the GAG's acidity, fragility, polydispersity and heterogeneous sulfation make their characterization not readily amenable by NMR, reverse-phase HPLC and mass spectrometry,[6] respectively.

Here, we demonstrate that quartz crystal microbalance with dissipation monitoring (QCM-D), a surface-sensitive technique popular for biosensing applications, enables quantitative analysis of conjugation yields and stability with a few micrograms of GAGs of arbitrary complexity. To this end, we compared the biotinylation of GAGs *via* two different chemoselective ligation chemistries (Scheme 1A).[7] Hydrazone ligation has become the most frequently used strategy for GAG functionalization.[1,8–10,11] Oxime ligation (for selected references, see ref. 12), on the other hand, has only rarely been applied to polysaccharides,[13] and to our knowledge not to GAGs.

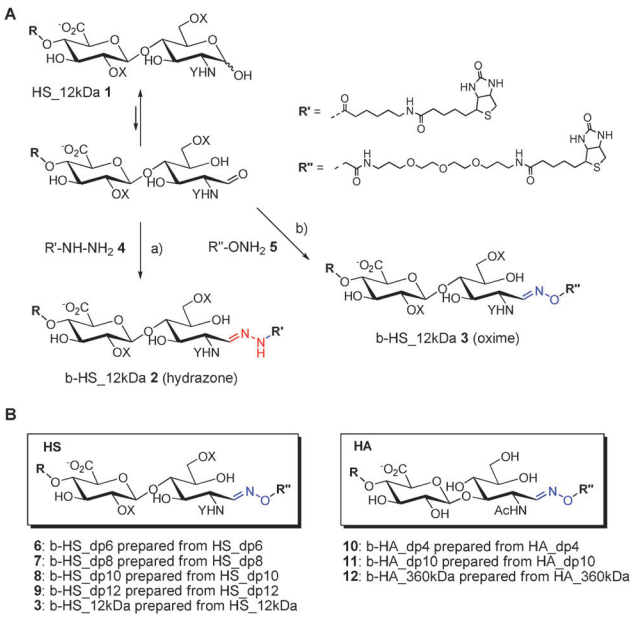

Scheme 1 (A) Strategies adopted for the biotinylation of GAGs at their reducing end, exemplified with a selected HS. Conditions: (a) **1** (0.33 mM), **4** (10 mM), PBS, pH 7.4, RT, 48 h; (b) **1** (4 mM), **5** (3.4 mM), aniline (100 mM), acetate buffer (100 mM), pH 4.5, 37 °C, 48 h. (B) Library of biotin conjugates of the GAGs HS and HA of various sizes, prepared using oxime ligation. HS consists of GlcA $\beta(1 \rightarrow 4)$ GlcNAc $\alpha(1 \rightarrow 4)$ disaccharides; X can be either H or SO_3H; Y can be either Ac or SO_3H. HA is unsulfated and consists of GlcA $\beta(1 \rightarrow 3)$ GlcNAc $\beta(1 \rightarrow 4)$ disaccharides. R = remaining GAG chain.

[a] *Université Grenoble Alpes, DCM, 38000 Grenoble, France*
[b] *CNRS, DCM, 38000 Grenoble, France*
[c] *Université Grenoble Alpes, Institut de Biologie Structurale (IBS), 38027 Grenoble, France*
[d] *CNRS, IBS, 38027 Grenoble, France*
[e] *CEA, DSV, IBS, 38027 Grenoble, France*
[f] *CIC biomaGUNE, Paseo Miramon 182, 20009 Donostia - San Sebastian, Spain. E-mail: rrichter@cicbiomagune.es; Tel: +34 943 00 53 29*
[g] *Max Planck Institute for Intelligent Systems, 70569 Stuttgart, Germany*

† Electronic supplementary information (ESI) available: Supplementary materials and methods, synthesis of a precursor, supplementary figures and references. See DOI: 10.1039/c4cc06905f

We show that conventional hydrazone ligation is inefficient, in particular for long GAGs, due to a low yield, and confirm that hydrazone conjugates are unstable in an aqueous environment.[14,15] In contrast, oxime ligation emerges as a facile, rapid and efficient method that provides conjugates with higher stability and can be broadly applied, *i.e.* for different GAG types and for oligosaccharides as well as polymeric GAGs of high molecular weight.

The reducing terminus of GAGs can selectively react with biotin derivatives presenting aminooxy or hydrazide groups to provide oxime and hydrazone linkage, respectively. For oxime ligation, the reaction was successful only by using aniline as a catalyst as described previously.[16] To reproduce a commonly reported protocol,[1,8,10,11] we did not use aniline for hydrazone ligation, although this compound is also known to enhance this reaction.[17] We created a library of biotin-conjugates through oxime ligation, containing GAGs of different types and defined chain lengths (Scheme 1B): hyaluronic acid (HA; oligosaccharides with 2 and 5 disaccharide units (dp4, dp10), and a 360 kDa polysaccharide) and heparan sulfate (HS; dp6, dp8, dp10, dp12, and a 12 kDa polysaccharide).

For b-HA_dp4 **10**, mass analysis (Fig. S1, ESI†) demonstrated that one biotin molecule is attached per HA while NMR analysis (Fig. S2, ESI†) confirmed that the biotin is attached at the reducing end, forming *E* and *Z* oxime isomers in a 73/27 ratio. Notably, these conventional characterization methods did not provide useful information on any of the other compounds produced.

To characterize the conjugation of more complex GAGs, we exploited the high affinity of the streptavidin (SAv)–biotin interaction,[8,18] and followed the binding of GAGs to surfaces displaying a SAv monolayer (Fig. 1B, inset) by QCM-D (Fig. S3, ESI†). Fig. 1A and B illustrates the differences in the stability of biotinylated HS (b-HS made from **1**, ~22 disaccharides) prepared through hydrazone and oxime ligation, **2** and **3**, respectively, as a function of storage time (up to two months) at 4 °C. The binding of b-HS samples was evaluated using two different parameters: the QCM-D frequency shift at saturation (Δf_{sat}; proportional to the areal mass density of immobilized b-HS (Fig. S4, ESI†)) and the maximal binding rate ($\Delta f/\Delta t$; proportional to the concentration of b-HS in the sample solution (Fig. S5A, ESI†)). The magnitudes of Δf_{sat} and $\Delta f/\Delta t$ decreased appreciably with increasing storage time for b-HS hydrazone (Fig. 1A), whereas only minor changes were observed for b-HS oxime (Fig. 1B). Moreover, the magnitudes of Δf and $\Delta f/\Delta t$ for **2** were lower than for **3**, even when de-frozen aliquots were used immediately. We argue that these effects are the result of the release of biotin upon degradation of the conjugates, *i.e.* the hydrazone but not the oxime is already appreciably degraded immediately after purification, and further degrades upon storage at 4 °C.

To understand this, we note that the QCM-D responses in Fig. 1 are exclusively due to binding of intact b-HS. Biotin-free HS did not bind (Fig. S3, ESI†) and free biotin (produced as the result of degradation) did not by itself give rise to a measurable signal (Fig. S6, ESI†). A decrease in the magnitude of Δf_{sat}, therefore, is consistent with partial occupancy of the surface with b-HS and saturation of the remaining binding sites by free biotin (Fig. S7, ESI†). Further analysis of the QCM-D responses,

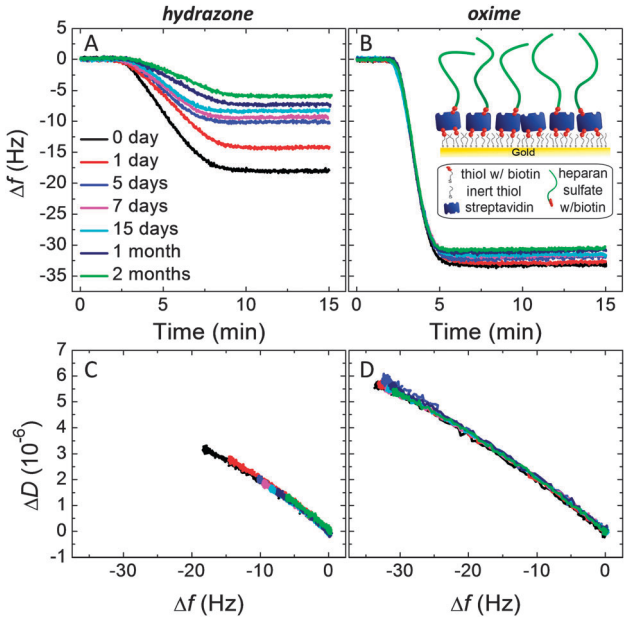

Fig. 1 Binding assay to study the yield and stability of hydrazone and oxime conjugation. (A, B) QCM-D frequency shifts, Δf, obtained for the specific binding of **2** (A) and **3** (B), stored at 4 °C for variable times (as indicated), on streptavidin-coated surfaces (schematically shown in the inset). Samples were incubated for 10 min (from 2 to 12 min) at a total GAG concentration of 50 μg mL^{-1}, which was followed by exposure to buffer solution. (C, D) Parametric plots of QCM-D dissipation shifts, ΔD (not previously shown) *vs.* Δf (from A and B, respectively). The plots inform about the evolution of the HS film mechanical properties and morphology with increasing surface coverage. All curves had comparable shapes, indicating that all compounds tested generate comparable film morphologies at a given surface coverage.

including the dissipation shift ΔD, in terms of so-called ΔD *vs.* Δf curves (Fig. 1C and D) revealed invariant curve shapes, indicating that the film morphology (at a given surface coverage) was comparable for all compounds tested. A plausible explanation is that the composition of the film in terms of the HS molecular conformation or size distribution is not altered by the degradation or the type of conjugation. This implies that degradation of b-HS occurs exclusively through cleavage of the bond that links biotin to HS, which is due to the hydrolysis of hydrazone (and to a much lesser extent oxime) under physiological conditions.[14]

We note in passing that the biotin released upon degradation would occupy a fraction of the available binding site on any biotin-capturing surface. This influences the surface density of immobilized GAGs, and thus entails a limited reproducibility of surface functionalization. This shortcoming needs to be considered, for example, in solid-phase molecular binding assays such as by surface plasmon resonance.[11,19]

For a quantitative analysis of reaction yields and degradation rates, we determined steady-state binding rates (Fig. 2A and Fig. S5A, ESI†) through linear fits to appropriate portions of the binding curves in Fig. 1A and B. At steady state, binding is mass-transfer limited, and with total HS concentrations and flow conditions remaining unchanged in our assay, any decrease in the binding rate reflects a proportional decrease in the concentration of intact b-HS in the probed solution.[20] From the binding rate of freshly

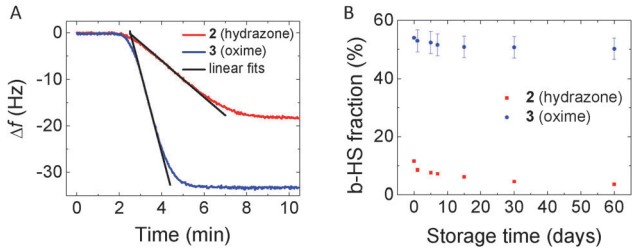

Fig. 2 (A) Quantification of active analyte concentrations from QCM-D binding assays. The ratio of the slopes of the extended linear binding regimes (black lines are linear fits), here shown by way of example for freshly de-frozen b-HS hydrazone **2** (red line) and b-HS oxime **3** (blue line) (data from Fig. 1), is proportional to the ratio of the analytes' active concentrations. (B) Fraction of intact b-HS as a function of storage time at 4 °C for **2** (red squares) and **3** (blue circles), determined through comparison of binding rates (data from Fig. 1). Error bars represent variations in the slopes observed for three independent measurements under identical conditions. Freshly de-frozen b-HS oxime **3**, for which the active analyte concentration was determined independently (Fig. S5, ESI†), was used as a reference.

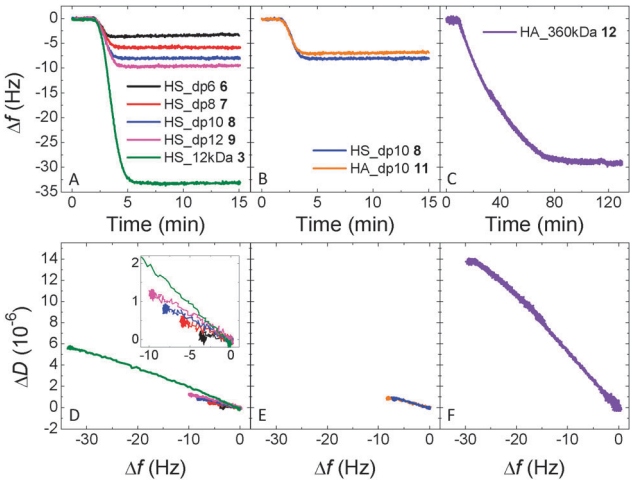

Fig. 3 QCM-D binding assays for HS (A) and HA (B, C) of various sizes (as indicated). All GAGs were conjugated with biotin *via* oxime ligation. Data for **8** are also shown in (B) to facilitate comparison with **11**. Incubation conditions were as described in Fig. 1, except for **12**, which was incubated from 5 to 110 min. (D–F) ΔD *vs.* Δf curves corresponding to (A–C), respectively; the inset in (D) shows a part of the data at a higher magnification. The magnitude of the slope of the ΔD *vs.* Δf curves increases as a function of GAG size, indicating that larger GAGs generate a softer film.[21]

de-frozen **3** and through comparison with a reference molecule of known concentration we could estimate the reaction yield of oxime ligation (Fig. S5, ESI†); comparison of the binding rates in Fig. 1 then yielded the fraction of intact b-HS in all probed solutions (Fig. 2). The fraction of the biotinylated analyte in the freshly de-frozen **3** was 54 ± 8%. This value was confirmed by weighing **10** (which in contrast to larger GAGs could be readily separated from non-biotinylated GAGs; Fig. S1, ESI†). The activity of freshly defrozen **2** was almost 5-fold smaller than that of **3**, indicating that reaction yields are considerably improved for oxime ligation (Fig. 2B). The 5-fold improvement in yield was confirmed by dot-blot analysis (Fig. S8, ESI†). Moreover, the fraction of intact **2** decreased by another 5-fold over 60 days of storage at 4 °C, indicating substantial degradation, whereas **3** was only marginally degraded over the same time interval (Fig. 2B).

Concerning the GAGs of various chain lengths, a clear trend in the Δf values at saturation (Fig. 3A for HS and Fig. 3B and C for HA) and in the ΔD *vs.* Δf curves (Fig. 3D–F) as a function of size confirmed that QCM-D curves are indeed sensitive to variations in molecular weight. Differences in molecular weight, as small as one disaccharide for oligomeric GAGs, can be readily distinguished through ΔD *vs.* Δf curves (Fig. 3D, inset). Thus, the ΔD *vs.* Δf curves represent a useful tool that provides insight into sample composition. HA_dp10 **8** bound to SAv monolayers with a response similar although not identical to HS_dp10 **11** (Fig. 3B and E). We propose that the slightly stronger Δf shift for **8** over **11** reflects an increased film thickness, resulting from a stronger repulsion between the sulfated and thus more highly charged HS chains in **8**. Notably, even the long HA polymer **12** with ~900 disaccharides could be readily biotinylated (Fig. 3C), indicating that the polymer length does not affect conjugation.

In summary, QCM-D together with a suitably functionalized sensor surface has proven to be instrumental for the characterization of conjugates made from chemically complex molecules such as GAGs, providing information about reaction yields, sample degradation and sample composition that is difficult to assess using conventional analytical techniques, in particular when the amount of sample is limited to a few micrograms. Moreover, we have established oxime ligation as a facile, one-step method for the selective conjugation of GAGs at the reducing end. The method is superior in yield and stability to the commonly used hydrazone ligation, and versatile in that it can be applied to GAGs of various (most likely any) types and sizes. The methods should find broad use, as tools in the glycosciences and in biotechnological applications. In particular, the control over and stability of GAG conjugates are crucial for the reliable preparation of GAG-functionalized surfaces and scaffolds for tissue engineering and fundamental biological studies.[22]

We thank C. Travelet (Cermav, Grenoble, France) and G. Dubacheva (CIC biomaGUNE) for support with DLS and SE measurements, respectively, E. Defrancq and N. Spinelli (DCM) for oligonucleotide synthesis and R. Vivés (IBS) for preparation of HS oligomers. This work was supported by the Nanosciences Foundation (Grenoble) through the Chair of Excellence Project GAG2D (to R.P.R.) and a PhD scholarship (to D.T.), the NanoBio programme, the ICMG FR 2607 and the LabEx ARCANE (ANR-11-LABX-0003-01).

Notes and references

1 E. Mercey, R. Sadir, E. Maillart, A. Roget, F. Baleux, H. Lortat-Jacob and T. Livache, *Anal. Chem.*, 2008, **80**, 3476–3482.
2 W. Takada, M. Fukushima, P. Pothacharoen, P. Kongtawelert and K. Sugahara, *Anal. Biochem.*, 2013, **435**, 123–130; E. Clo, O. Blixt and K. J. Jensen, *Eur. J. Org. Chem.*, 2010, 540–554; S. Park, J. C. Gildersleeve, O. Blixt and I. Shin, *Chem. Soc. Rev.*, 2013, **42**, 4310–4326.
3 M. Morra, *Biomacromolecules*, 2005, **6**, 1205–1223.
4 J. A. Burdick and G. D. Prestwich, *Adv. Mater.*, 2011, **23**, H41–56.
5 N. Altgarde, J. Becher, S. Moller, F. E. Weber, M. Schnabelrauch and S. Svedhem, *J. Colloid Interface Sci.*, 2013, **390**, 258–266.
6 J. Zaia, *Biomacromol. Mass Spectrom.*, 2005, **1**, 3–36.

7 J. A. Prescher and C. R. Bertozzi, *Nat. Chem. Biol.*, 2005, **1**, 13–21.
8 N. Altgarde, E. Nileback, L. de Battice, I. Pashkuleva, R. L. Reis, J. Becher, S. Moller, M. Schnabelrauch and S. Svedhem, *Acta Biomater.*, 2013, **9**, 8158–8166.
9 K. Godula and C. R. Bertozzi, *J. Am. Chem. Soc.*, 2010, **132**, 9963–9965.
10 H. Ichijo, N. Sugiura and K. Kimata, *Polymers*, 2013, **5**, 254–268; T. Mori, T. Kodera, H. Yoshimine, Y. Kakuta, N. Sugiura, K. Kimata and Y. Okahata, *Chemistry*, 2012, **18**, 7388–7393.
11 E. Saesen, S. Sarrazin, C. Laguri, R. Sadir, D. Maurin, A. Thomas, A. Imberty and H. Lortat-Jacob, *J. Am. Chem. Soc.*, 2013, **135**, 9384–9390.
12 F. Peri, P. Dumy and M. Mutter, *Tetrahedron*, 1998, **54**, 12269–12278; R. D. Goff and J. S. Thorson, *Med. Chem. Commun.*, 2014, **5**, 1036–1047; F. Lin, J. Zheng, J. Yu, J. Zhou and M. L. Becker, *Biomacromolecules*, 2013, **14**, 2857–2865.
13 T. J. Styslinger, N. Zhang, V. S. Bhatt, N. Pettit, A. F. Palmer and P. G. Wang, *J. Am. Chem. Soc.*, 2012, **134**, 7507–7515; A. Richard, A. Barras, A. B. Younes, N. Monfilliette-Dupont and P. Melnyk, *Bioconjugate Chem.*, 2008, **19**, 1491–1495; T. T. Beaudette, J. A. Cohen, E. M. Bachelder, K. E. Broaders, J. L. Cohen, E. G. Engleman and J. M. J. Frechet, *J. Am. Chem. Soc.*, 2009, **131**, 10360–10361.
14 J. Kalia and R. T. Raines, *Angew. Chem., Int. Ed.*, 2008, **47**, 7523–7526.
15 A. A. Kale and V. P. Torchilin, *Bioconjugate Chem.*, 2007, **18**, 363–370; B. Levrand, Y. Ruff, J.-M. Lehn and A. Herrmann, *Chem. Commun.*, 2006, 2965–2967.
16 M. B. Thygesen, H. Munch, J. Sauer, E. Clo, M. R. Jorgensen, O. Hindsgaul and K. J. Jensen, *J. Org. Chem.*, 2010, **75**, 1752–1755.
17 J. Y. Byeon, F. T. Limpoco and R. C. Bailey, *Langmuir*, 2010, **26**, 15430–15435.
18 N. S. Baranova, E. Nileback, F. M. Haller, D. C. Briggs, S. Svedhem, A. J. Day and R. P. Richter, *J. Biol. Chem.*, 2011, **286**, 25675–25686.
19 R. I. W. Osmond, W. C. Kett, S. E. Skett and D. R. Coombe, *Anal. Biochem.*, 2002, **310**, 199–207.
20 W. T. Hermens, M. Benes, R. Richter and H. Speijer, *Biotechnol. Appl. Biochem.*, 2004, **39**, 277–284.
21 I. Reviakine, D. Johannsmann and R. P. Richter, *Anal. Chem.*, 2011, **83**, 8838–8848.
22 E. Migliorini, D. Thakar, R. Sadir, T. Pleiner, F. Baleux, H. Lortat-Jacob, L. Coche-Guerente and R. P. Richter, *Biomaterials*, 2014, **35**, 8903–8915.

Supporting Information

A Quartz Crystal Microbalance Method to Study the Terminal Functionalization of Glycosaminoglycans

Dhruv Thakar, Elisa Migliorini, Liliane Coche-Guerente, Rabia Sadir, Hugues Lortat-Jacob, Didier Boturyn, Olivier Renaudet, Pierre Labbe, and Ralf P. Richter*

Table of Contents

Supplementary Materials and Methods

GAGs and proteins

HS with an average molecular weight of 12 kDa and a polydispersity of 1.59,[1] derived from porcine intestinal mucosa, was obtained from Celsus Laboratories (Cincinnati, Ohio). HS oligosaccharides (HS_dp6, HS_dp8, HS_dp10, HS_dp12) presenting GlcNAc at their reducing end were prepared as previously described.[2] HA oligosaccharides (HA_dp4, HA_dp10) presenting GlcNAc at their reducing end were purchased from Hyalose (Oklahoma, OK, USA). Lyophilized streptavidin (SAv) and bovine serum albumin (BSA) were purchased from Sigma-Aldrich (Saint-Quentin Fallavier, France), suspended in autoclaved Hepes buffer (10 mM Hepes (Fisher, Illkirch, France), pH 7.4, 150 mM NaCl (Sigma-Aldrich)) and stored at -20°C.

An oligonucleotide ($^{5'}$X AAT TCG CTA GCT GGA GCT TGG ATT GAT GTG GTG TGT GAG TGC GGT GCC C$^{3'}$, X represents the 5' amino linker; M_w = 15 440 Da) and an equivalent oligonucleotide with a biotin ($^{5'}$AAT TCG CTA GCT GGA GCT TGG ATT GAT GTG GTG TGT GAG TGC GGT GCC C X$^{3'}$, X represents the 3' biotin tetraethyleneglycol linker; M_w = 15595.3 Da) were synthesized at 0.2 µmol scale using standard β-cyanoethyl phosphoramidite chemistry on a DNA synthesizer (ABI 3400). After elongation, oligonucleotides were cleaved from the solid support and released into solution by treatment with 28% ammonia (1.5 mL) for 2 h and finally deprotected by keeping in ammonia solution for 16 h at 55 °C. Purifications were carried out by denaturing polyacrylamide gel electrophoresis and oligonucleotides were desalted by SEC on NAP-10 columns (GE Healthcare, Velizy-Villacoublay, France). Quantifications were performed at 260 nm using a CARY 400 Scan UV-Visible Spectrometer (L-tym: 16 nmoles, 13 %, ε_{260nm}= 463600 $M^{-1}cm^{-1}$); ε was estimated according to the nearest neighbour model.

Biotinylation of GAGs

For oxime ligation, the GAGs (4 mM) were suspended in 100 mM acetate buffer, made from glacial acetic acid (Fisher, Illkirch, France) and sodium acetate (Sigma-Aldrich), at pH 4.5. They were then reacted with b-OEG-ONH_2 ***5*** (3.4 mM; synthesized as described on page S3) in the presence of aniline (100 mM; Sigma-Aldrich) for 48 h at 37°C. Hydrazone ligation was performed as previously described.[3] Briefly, HS suspended in phosphate-buffered saline (PBS; Sigma Aldrich), pH 7.4 at 0.33 mM was reacted for 48 h at room temperature with 10 mM biotin-LC-hydrazine (Pierce, Rockford, USA). The final mixtures for both reactions were purified either by extensively dialyzing against water through membranes with a molecular weight cutoff (MWCO) of 1000 Da (Spectra/Por, France) or by using a desalting column (Pd-10 G-25M with MWCO = 5000 Da; GE Healthcare), depending on the molecular weights used, to remove unreacted biotin and aniline. The final products, typically containing a mixture of unreacted and biotin-conjugated GAGs, were then lyophilized and stored at -20°C, either as is or re-solubilized in Hepes buffer or ultrapure water at a concentration of 10 mg/mL. Under these storage conditions, none of the samples was found to degrade appreciably. For further use, the conjugates were diluted to desired concentrations in Hepes buffer.

Quartz crystal microbalance with dissipation monitoring (QCM-D)

QCM-D measures the changes in resonance frequency, Δf, and dissipation, ΔD, of a sensor crystal upon molecular binding events on its surface. The QCM-D response is sensitive to the mass (including hydrodynamically coupled water) and the mechanical properties of the surface-bound layer. Measurements were performed with a Q-Sense E4 system equipped with 4 independent Flow Modules (Biolin Scientific, Västra Frölunda, Sweden). Before use, the walls of the liquid handling system were passivated against biomolecular binding with bovine serum albumin (BSA). The system was operated in flow mode with a flow rate of typically 10 µL/min using a peristaltic pump (ISM935C, Ismatec, Zurich, Switzerland). The working temperature was 24°C. Δf and ΔD were measured at six overtones (n = 3, 5, ..., 13), corresponding to resonance frequencies of $f_n \approx$ 5, 15, 25, ..., 65 MHz; changes in dissipation and normalized frequency, $\Delta f = \Delta f_n/n$, of the third overtone (n = 3) are presented. Any other overtone would have provided comparable information.

Synthesis of b-OEG-ONH$_2$ 5

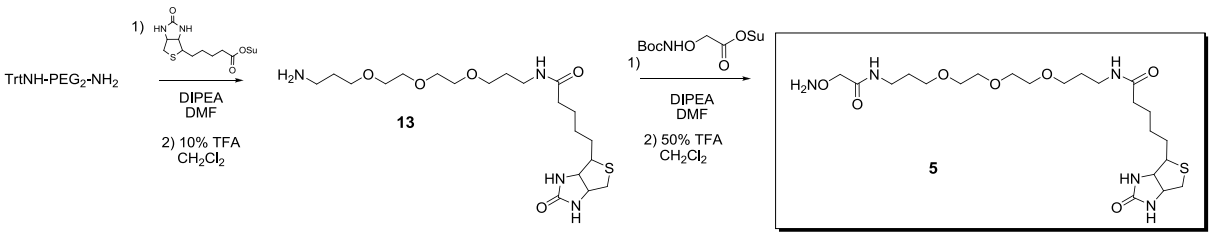

Scheme Syn1. Steps for the synthesis of the bi-functional linker b-OEG-ONH$_2$ **5**, presenting a biotin and an oxyamine moiety (–ONH$_2$).

The synthesis route is schematically shown in Scheme Syn1. Unless otherwise stated, chemical reagents were purchased from Sigma Aldrich (Saint Quentin Fallavier, France) or Acros (Noisy-Le-Grand, France) and were used without further purification. Analytical RP-HPLC was performed on a Waters system equipped with a Waters 600 controller and a Waters 2487 Dual Absorbance Detector. Analysis was carried out at 1.0 mL/min (EC 125/3 nucleosil 300-5 C_{18}) with UV monitoring at 214 nm and 250 nm using a linear A–B gradient (buffer A: 0.09% CF_3CO_2H in water; buffer B: 0.09% CF_3CO_2H in 90% acetonitrile). Preparative separation was carried out at 22 mL/min (VP 250/21 nucleosil 300-7 C18) with UV monitoring at 214 nm and 250 nm using a linear A–B gradient (buffer A: 0.09% CF_3CO_2H in water; buffer B: 0.09% CF_3CO_2H in 90% acetonitrile). Mass spectrometry was performed using electrospray ionization on an Esquire 3000+ Bruker Daltonics in positive mode. ^{1}H NMR spectra were recorded in D_2O at 400 MHz with a Bruker Avance 400 spectrometer.

Synthesis of compound **13**. TrtNH-PEG$_2$-NH$_2$ (200 mg, 0.43 mmol; Calbiochem-Novabiochem (Merck Biosciences - VWR, Limonest, France)) and biotin-OSu (220 mg, 0.65 mmol; Calbiochem-Novabiochem) were dissolved in dry DMF (10 mL) containing DIPEA (75 µL, 0.43 mmol) and the solution was stirred at room temperature. After 45 min RP-HPLC analysis indicated complete reaction (R_t = 12.29 min, 5-100% B in 20 min). The solvent was then evaporated under reduced pressure and the crude oily residue was taken up with a solution of 10% TFA in CH_2Cl_2 (10 mL) containing 0.1% of triisopropylsilane. The solution was evaporated after 1 h and diethyl ether was added to precipitate compound **13** which was obtained as a white powder after centrifugation. Yield: 77% (149 mg); R_t = 7.97 min (5-100% B in 20 min); ESI-MS: *m/z* calcd. for $C_{20}H_{39}N_4O_5S$ $(M + H)^+$ 447.3, found 447.5.

Synthesis of compound **5**. Compound **13** (50 mg, 0.11 mmol) was dissolved in dry DMF (5 mL) containing DIPEA (19.5 µL, 0.11 mmol). Boc-Aoa-OSu (39 mg, 0.13 mmol) was added to the solution and the mixture was stirred at room temperature until complete disappearance of the starting material observed by analytical HPLC (R_t = 10.17 min, 5-100% B in 20 min). The solvent was removed and the residue was precipitated in diethyl ether. The resulting white powder was next stirred 30 min at room temperature in 50% TFA in CH_2Cl_2 (5 mL). After solvent evaporation, the crude mixture was purified by preparative RP-HPLC to afford compound **5** (Fig. Syn1). Yield: 74% (43 mg); R_t = 7.96 min (5-100% B in 20 min); ESI-MS (Fig. Syn2): *m/z* calcd. for $C_{22}H_{42}N_5O_7S$ $(M + H)^+$ 520.3, found 520.5.

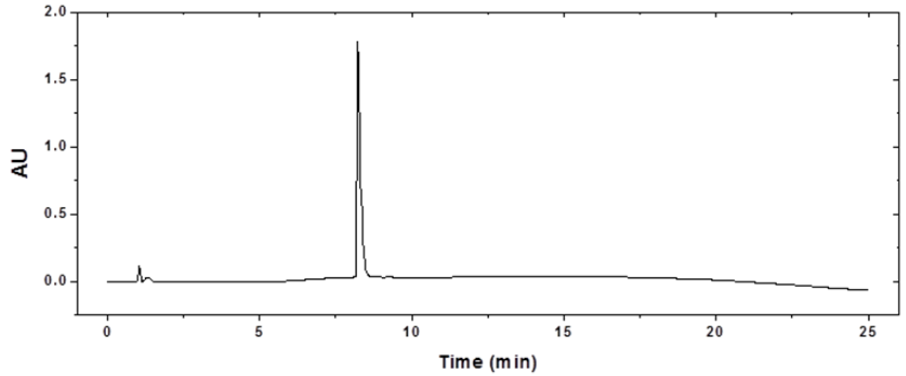

Figure Syn1. Crude RP-HPLC profile (5 to 100% B in 100 min, λ = 214 nm) of compound **5**.

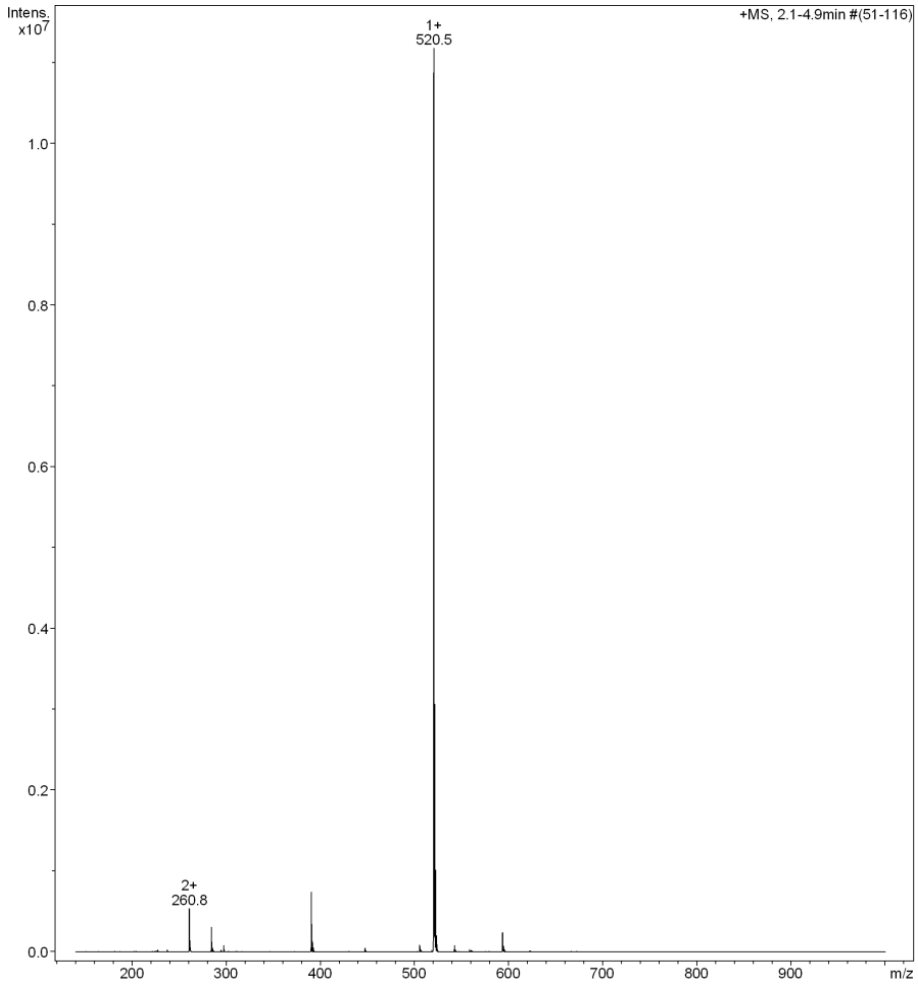

Figure Syn2. ESI-MS (positive mode) of compound **5**.

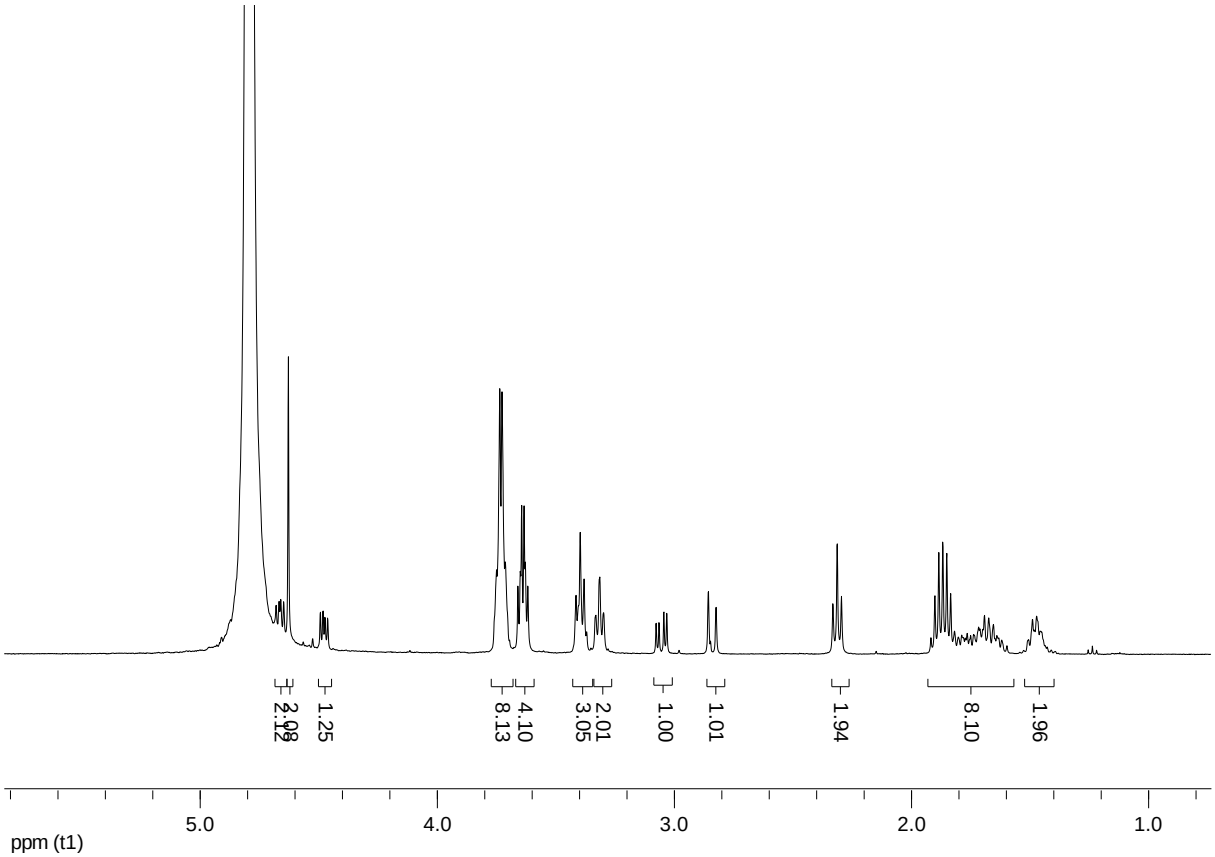

Figure Syn3. ^{1}H NMR spectrum (400 MHz, D_2O) of compound **5**.

Supplementary Figures

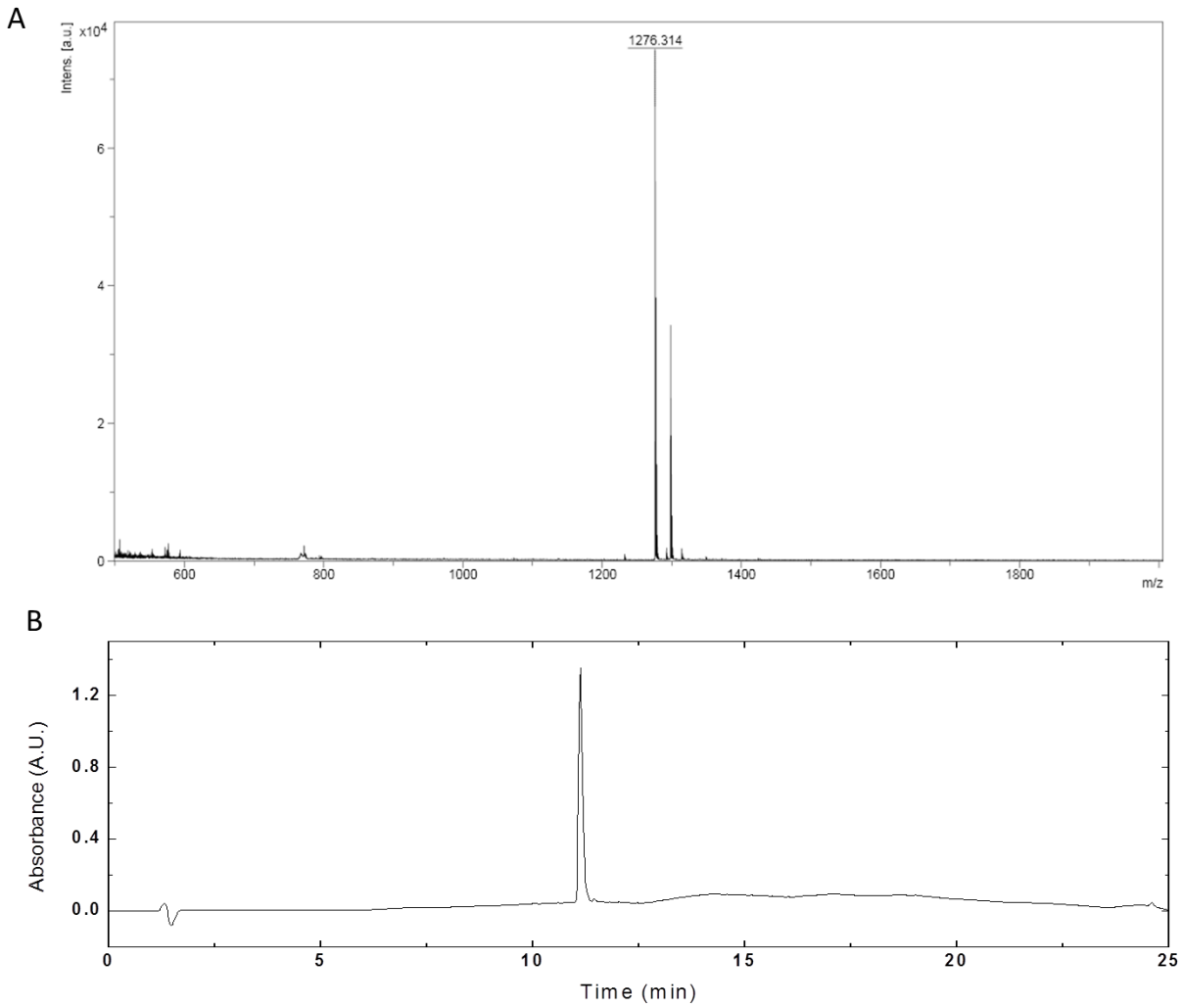

***Figure S1*. Analysis of biotinylated HA_dp4.** (A) Mass spectrum (ESI-MS, negative mode) of biotinylated HA_dp4 (b-HA_dp4 **10**), m/z calcd for $C_{50}H_{83}N_7O_{29}S$: 1278.3; found m/z: 1277.3, the peak at 1298.3 corresponds to $[M+Na-H]^-$. This confirms the attachment of one biotin group per HA chain. (B) HPLC Chromatogram (5 to 100% B in 100 min, λ= 214 nm) of **10**. The peak at 11.1 min corresponds to the final product. HA_dp4 (1.4 mg, 1.8 μmol) was mixed with b-OEG-ONH_2 **5** (3.4 mM) and aniline (100 mM) in acetate buffer (100 mM), pH 4.5, 37°C for 48 h. The reaction mixture was purified using HPLC to obtain **10** (1.3 mg, 1.0 μmol, yield = 56%) as a white powder after freeze-drying.

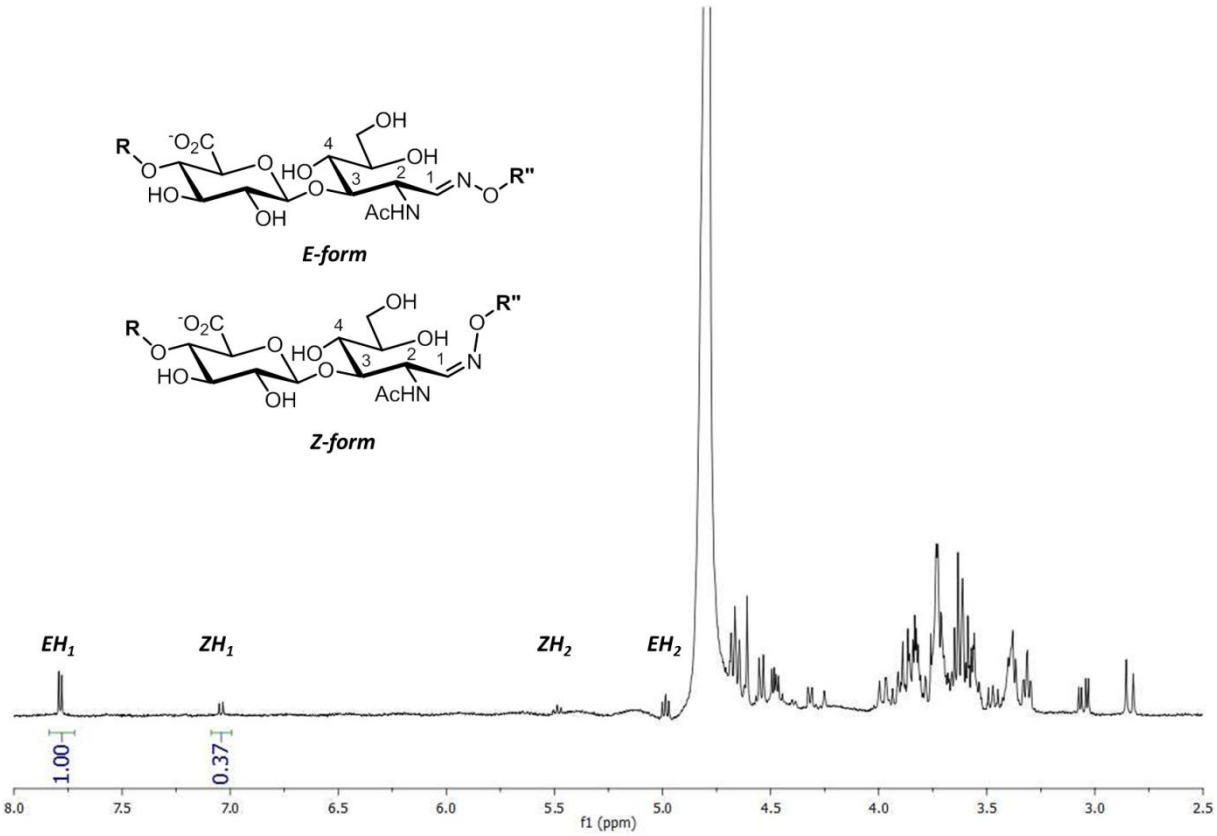

Figure S2. **NMR analysis of b-HA_dp4 10.** The ^{1}NMR analysis shows the formation of E and Z conformations of **10**, indicating that the attachment of biotin occurs at the reducing end of HA which leads to both the open and closed forms. Integrating the signals corresponding to the two conformations, the oxime link was found to be 73% and 27% in E and Z conformation, respectively. R is a GlcA β(1→3) GlcNAc β(1→4) disaccharide, and R" is defined in Scheme 1.

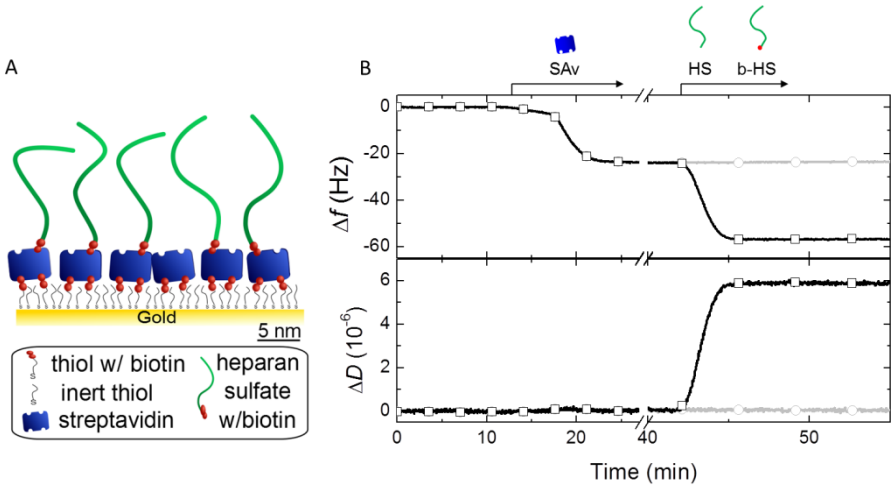

Figure S3. **QCM-D binding assay.** (A) Schematic presentation of the streptavidin (SAv)-presenting surface used to study the yield and stability of GAG biotinylation. (B) Representative QCM-D binding assay with frequency shifts, Δf, and dissipation shifts, ΔD. Prior to each QCM-D measurement, QCM-D sensors with a new gold coating (QSX301, Biolin Scientific) were cleaned by rinsing with ultrapure water, blow-drying with N_2 and exposure to UV/ozone (Jelight, Irvine, CA, USA) for 10 min; within 5 min after UV/ozone treatment, the sensors were immersed in an ethanolic solution (Fisher) of oligo ethyleneglycol (OEG) disulfide and biotinylated OEG thiol (Polypure Oslo, Norway), at a total concentration of 1 mM and a molar ratio of thiol equivalents of 999:1; after overnight incubation, the sensor surfaces were rinsed with ethanol and blow-dried with N_2, before being installed in the QCM-D modules. Start and duration of sample incubation steps are indicated by arrows on top of the plot; during remaining times, the surface was exposed to Hepes buffer solution. SAv was initially incubated at a concentration of 1 µg/mL at a small flow rate (6 µL/min) for 4 min, and then at 20 µg/mL at standard flow rate (10 µL/min). At equilibrium, SAv generated frequency shifts $\Delta f = -23 \pm 1$ Hz and dissipation shifts $\Delta D < 0.4 \times 10^{-6}$ which are characteristic for the formation of a dense protein monolayer. The injection at low concentration was routinely performed to confirm the absence of protein depletion resulting from undesired adsorption to the walls of the tubing or the QCM-D flow module due to insufficient passivation: any depletion of SAv from the solution would result in a decreased binding rate. GAGs were incubated at 50 µg/mL. End-biotinylated HS (b-HS_12kDa **3** (oxime), black lines with square symbols) readily bound to the free biotin-binding sites on the SAv monolayers. The ensuing shift in frequency and the strong increase in dissipation indicate the formation of a soft and hydrated layer as would be expected for a film of end-grafted HS chains. Biotin-free GAGs (grey lines with circle symbols) showed no response, confirming that the immobilization of GAGs on the SAv monolayer occurs exclusively through the biotin moiety at the GAG's reducing end.

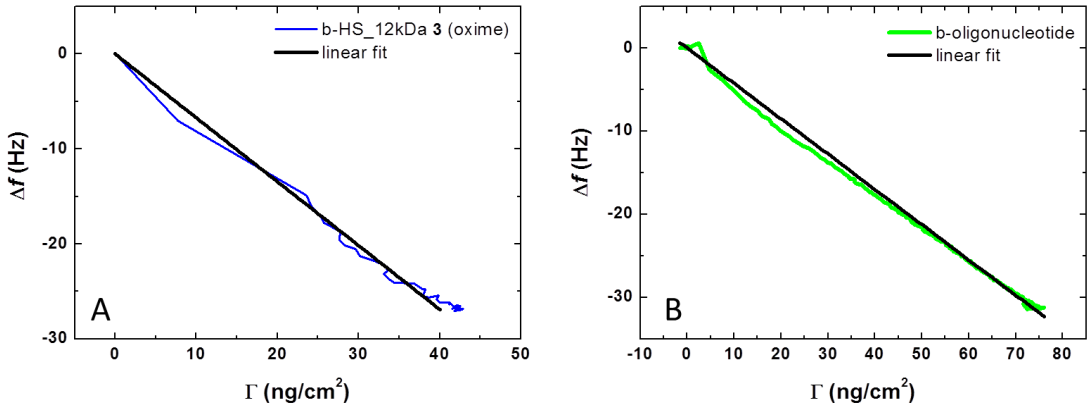

Figure S4. **Relationship between the QCM-D frequency shift and areal mass density.** Data were acquired through a combined QCM-D and spectroscopic ellipsometry (SE; M2000V, J. A. Woollam, Lincoln, NE, USA) measurement. The graph shows Δf (from QCM-D) *vs.* areal mass density Γ (from SE) for the adsorption under static conditions of **3** (A, blue line; at a total HS concentration of 1 µg/mL), and of a biotinylated oligonucleotide (B, green line; at 1.56 µg/mL) that served as a reference molecule in Fig. S5. The data are well approximated by straight lines through the origin (black lines) confirming that the relationship between Δf and Γ is roughly linear for these compounds. The slopes of the linear fits $\Delta f / \Delta\Gamma$ were –0.67 ± 0.01 Hz/(ng/cm^2) for **3** and –0.42 ± 0.01 Hz/(ng/cm^2) for the biotinylated oligonucleotide (mean ± S.E.M. from three independent measurements). The combined QCM-D and SE measurement was performed with a custom-built open fluid cell as described earlier.[4, 5] Before use, the walls of the fluid cell were passivated against biomolecular binding with BSA. SE measures changes in the polarization of light upon reflection at a planar surface, from which the areal mass density can be quantified through fitting of the SE data to an optical model. Fitting was performed, as described in detail elsewhere;[6] the opaque gold film with the OEG monolayer was treated as a single isotropic layer and fitted as a B-spline substrate; SAv and b-HS film were considered as separate transparent Cauchy layers; b-HS areal mass densities were determined through de Fejter's equation,[4] using a refractive index increment of dn/dc = 0.15 cm^3/g.

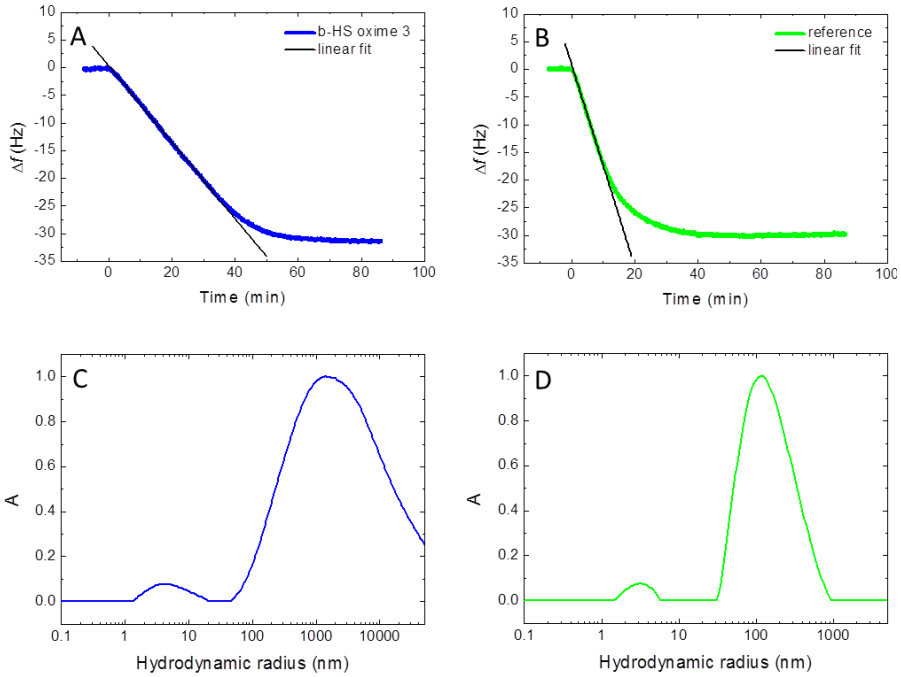

Figure S5. **Quantification of active analyte concentrations from QCM-D binding assays.** (A-B) QCM-D responses (Δf) for the adsorption of **3** (freshly defrozen and incubated at 1 µg/mL total HS concentration; A) and a biotinylated oligonucleotide (incubated at c_{ref} = 1.56 µg/mL; B) to a SAv monolayer. The oligonucleotide served as reference molecule to determine the concentration of intact b-HS, $c_{\text{b-HS}}$, in the HS solution, as described in the following. Binding of an analyte (b-HS in our case) to a ligand (SAv) on the QCM-D sensor surface is a two-step event, consisting of mass transfer to the sensor surface followed by the actual binding to the ligand. Since the biotin-SAv bond forms rapidly, the first step is rate limiting in our assay, except at high coverage were the scarcity of available binding sites limits binding. For mass-transfer limited binding, the binding rate depends exclusively on the flow conditions (i.e. flow-cell geometry and flow rate, maintained constant in our assay) and the analyte's active concentration (i.e. the concentration of HS being effectively biotin-conjugated, $c_{\text{b-HS}}$) and diffusion coefficient, $D_{\text{b-HS}}$.[7] Considering the flow conditions in our experimental setup (i.e. laminar flow in a slit), the binding rate is given by

$$\left.\frac{\Delta\Gamma}{\Delta t}\right|_{\text{b-HS}} \propto D_{\text{b-HS}}^{2/3} c_{\text{b-HS}} \qquad \text{[Eq. S1]}$$

in steady state.[7] From a comparative measurement with a reference molecule of known concentration c_{ref} and diffusion coefficient D_{ref}, the analyte's active concentration can be determined through

$$c_{\text{b-HS}} = c_{\text{ref}} \left(\frac{D_{\text{ref}}}{D_{\text{b-HS}}}\right)^{2/3} \left.\frac{\Delta\Gamma}{\Delta t}\right|_{\text{b-HS}} \Big/ \left.\frac{\Delta\Gamma}{\Delta t}\right|_{\text{ref}} \qquad \text{[Eq. S2A]}$$

The ratio $D_{\text{ref}}/D_{\text{b-HS}}$ is identical to the ratio of the molecules' hydrodynamic radii $r_{\text{h,b-HS}}/r_{\text{h,ref}}$ due to the Stokes-Einstein equation. Moreover, the relationship between Γ and Δf is linear for the molecules of inerest (Fig. S4), and hence

$$c_{\text{b-HS}} = c_{\text{ref}} \left(\frac{r_{\text{h,b-HS}}}{r_{\text{h,ref}}}\right)^{2/3} \left(\left.\frac{\Delta f}{\Delta t}\right|_{\text{b-HS}} \Big/ \left.\frac{\Delta f}{\Delta t}\right|_{\text{ref}}\right) \left(\left.\frac{\Delta f}{\Delta\Gamma}\right|_{\text{ref}} \Big/ \left.\frac{\Delta f}{\Delta\Gamma}\right|_{\text{b-HS}}\right) \qquad \text{[Eq. S2B]}$$

The extended linear binding regimes in A and B (black solid lines are fits with slopes $\Delta f/\Delta t|_{\text{b-HS}}$ = -0.82 ± 0.03 Hz/min and $\Delta f/\Delta t|_{\text{ref}}$ = -1.86 ± 0.03 Hz/min (mean ± S.E.M. from three independent measurements)) confirm mass-transfer limited binding in steady state. Equation S2B, with $\Delta f/\Delta\Gamma$ taken from Fig. S4 and r_{h} determined through dynamic light scattering (see C-D below), resulted in $c_{\text{b-HS}}$ = 0.54 ± 0.08 µg/mL. Finally, comparison with the total HS concentration employed reveals that 54 ± 8% of the HS chains were effectively biotinylated. This value is in excellent agreement with the yield obtained through weighing of purified HA_dp4 **10** (Fig. S1).

Equation S1 shows that, during mass-transfer limited binding, the binding rate is directly proportional to the analyte's active concentration, and a reduction in the binding rate (e.g. in Fig. 1) reflects a proportional decrease in the analyte's active concentration (since the analyte's diffusion coefficient is unchanged). To obtain the fractions of b-HS in Fig. 2, relative changes in the slopes in Fig. 1 were compared, and combined with the value of 54% for freshly defrozen **3**.

(C-D) Quantification of hydrodynamic radii by dynamic light scattering (DLS). Mass-weighted distributions (A) of hydrodynamic radii (r_{h}) of HS_12kDa **1** (C) and the reference oligonucleotide (D) with peaks at $r_{\text{h,b-HS}}$ = 4.7 ± 0.2 nm and $r_{\text{h,ref}}$ = 3.3 ± 0.1 nm (mean ± S.E.M. from 6 independent measurements; we estimate that addition of the small biotin moiety to polymeric HS and oligonucleotide does not affect r_{h} appreciably) corresponding to the size of individual molecules. Secondary peaks at 100 nm and more are likely to correspond to aggregates; although these peaks dominate the mass-weighted distribution, their contribution in numbers is very small (less than 0.1%). Measurements were performed as described in detail elsewhere.[8] Autocorrelaton functions were collected at 25.0 ± 0.1 °C for a counting time of 60 s at 90 degrees scattering angle. Radius distributions were obtained using CONTIN analysis[9] of the autocorrelation functions.

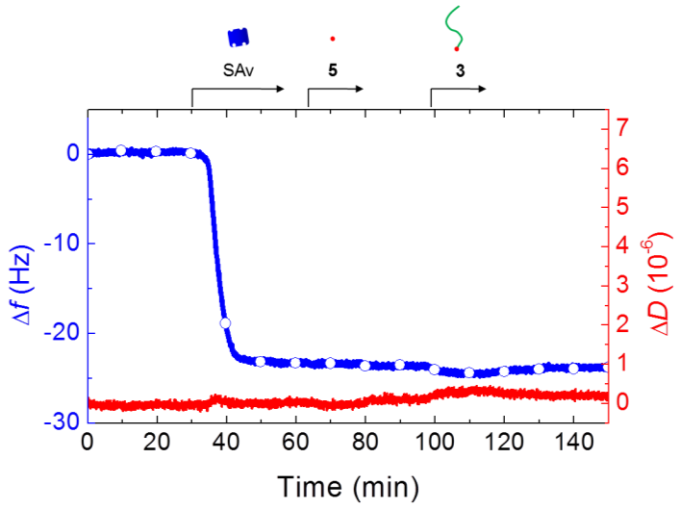

Figure S6. **Binding of free biotin to streptavidin monolayers does not elicit a measurable QCM-D response.** QCM-D responses (Δf – blue lines with circle symbols, ΔD – red lines) during the formation of a SAv monolayer (conditions as in Fig. S3) followed by sequential exposure to b-OEG-ONH_2 **5** (50 µg/mL) and **3** (50 µg/mL). Start and duration of sample incubation steps are indicated by arrows on top of the plot; during remaining times, the surface was exposed to Hepes buffer solution. The absence of b-HS binding confirms that free biotin saturated all biotin-binding sites on the SAv monolayer. Yet, the SAv-bound biotin (i.e. **5**) did not by itself give rise to a measurable QCM-D response, presumably due to the compound's low molecular weight and the location of the biotin-binding pocket deep inside SAv.

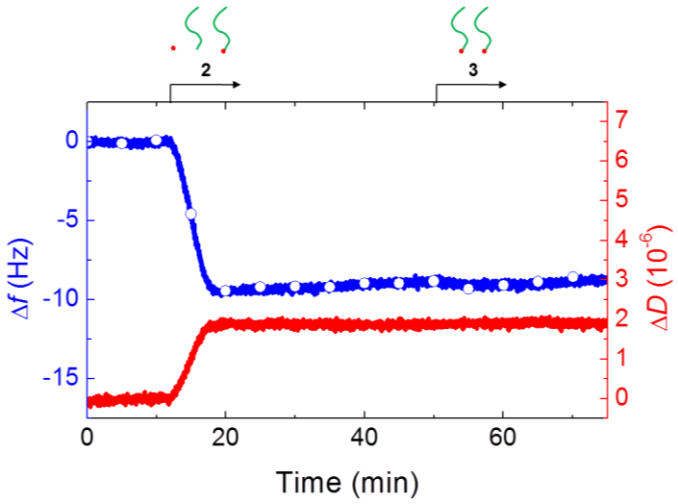

Figure S7. **Free biotin, released upon degradation, contributes to the occupation of binding sites in streptavidin monolayers.** QCM-D responses (Δf – blue lines with circle symbols, ΔD – red lines) during the adsorption of a partially degraded sample (**2**, 7 days storage at 4°C; 50 µg/mL) to a SAv monolayer followed by incubation of a non-degraded sample (**3**, freshly de-frozen; 50 µg/mL). Start and duration of sample incubation steps are indicated by arrows on top of the plot; during remaining times, the surface was exposed to Hepes buffer solution. Incubation with the non-degraded sample did not lead to significant additional binding. This confirms that no free biotin binding sites were available after incubation with the supposedly degraded sample, i.e. the biotin released due to degradation saturates all available biotin binding pockets.

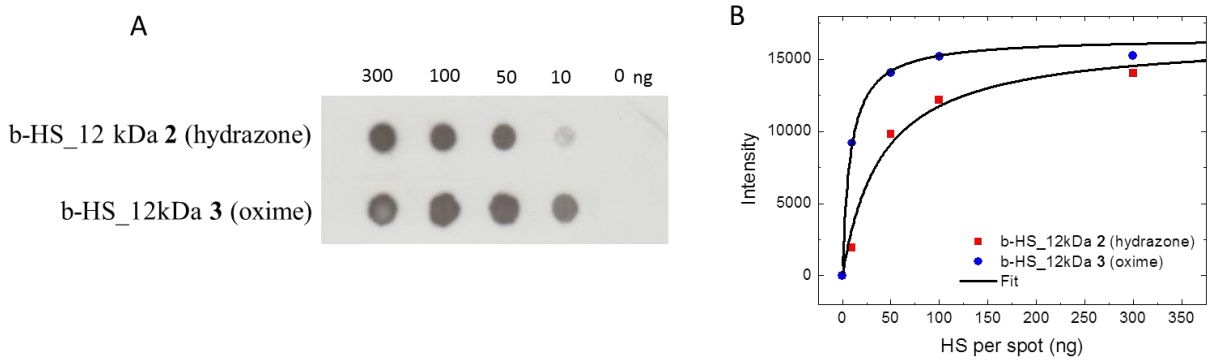

Figure S8. **Dot-blot analysis confirms HS biotinylation.** 50 µL of b-HS samples at a range of total HS concentrations were spotted on a (positively charged) nitrocellulose membrane (Genomic Zeta-Probe; Bio-Rad, Marnes-la-Coquette, France) which retains (negatively charged) HS but not free biotin. Membranes were pre-washed with PBS at pH 7.4 using a vacuum-assisted dot-blot apparatus, rinsed twice with PBS, blocked for 30 min at 37°C in a 5% (w/v) dry milk solution in Tris-buffered saline (TBS; Sigma-Aldrich) at pH 7.4, and extensively rinsed with TBS. The blots were probed with extravidin-labeled horseradish peroxidase (exAvHRP; Sigma-Aldrich) diluted 1:3000 in TBS with 0.05% (w/v) Tween20 for 45 min under shaking. After 6 cycles of washing (5 min each) with TBS and 0.05% (w/v) Tween20 at RT, the biotinylated samples were revealed by incubation of the membrane with hydrogen peroxide and the chemiluminescent detection reagent (Luminata Classico Western HRP Substrate; Millipore, Molsheim, France) for 1 min, followed by autoradiography (Amersham Hyperfilm ECL; GE Healthcare). (A) Autoradiograph of membranes spotted with **2** and **3** with total HS quantities per spot (in ng) indicated. (B) Dot intensities, quantified by densitometry using ImageJ software, for b-HS hydrazone 2 (red squares) and b-HS oxime (blue circles) from the membrane displayed in A. Intensities were offset by the intensity of the control samples lacking b-HS (0 ng). Both data sets were well approximated by the expression $I = I_{\max}[\mathrm{HS}]/([\mathrm{HS}] + [\mathrm{HS}]_{1/2})$, where $I_{\max}$ is the intensity at saturation, [HS] the total HS quantity per spot and $[\mathrm{HS}]_{1/2}$ the total HS quantity at which half-maximal intensity is attained. Black lines are best fits, giving $I_{\max}$ = 16500 (set to be identical for both curves) and $[\mathrm{HS}]_{1/2}$ = 40.6 and 8.3 ng for **2** and **3**, respectively. The ratio of the two $[\mathrm{HS}]_{1/2}$ values is 4.9, confirming that the concentration of biotinylated HS in the oxime conjugate **3** is about 5 times larger than in the equivalent hydrazone conjugate **2**, as determined from the analysis of the QCM-D data (Figs. 2 and S5).

Supplementary References

1. B. Mulloy, C. Gee, S. F. Wheeler, R. Wait, E. Gray and T. W. Barrowcliffe, *Thromb. Haemost.*, 1997, **77**, 668–674.
2. E. Saesen, S. Sarrazin, C. Laguri, R. Sadir, D. Maurin, A. Thomas, A. Imberty and H. Lortat-Jacob, *J. Am. Chem. Soc.*, 2013, **135**, 9384−9390.
3. A. Amara, O. Lorthioir, A. Valenzuela, A. Magerus, M. Thelen, M. Montes, J.-L. Virelizier, M. Delepierre, F. Baleux, H. Lortat-Jacob and F. Arenzana-Seisdedos, *J. Biol. Chem.*, 1999, **274**, 23916-23925.
4. R. P. Richter, K. B. Rodenhausen, N. B. Eisele and M. Schubert, in *Ellipsometry of Functional Organic Surfaces and Films*, Springer Series in Surface Sciences, 2014, vol. 52, pp. 223-248.
5. I. Carton, A. R. Brisson and R. P. Richter, *Anal. Chem.*, 2010, **82**, 9275-9281.
6. G. V. Dubacheva, T. Curk, B. M. Mognetti, R. Auzely-Velty, D. Frenkel and R. P. Richter, *J. Am. Chem. Soc.*, 2014, **136**, 1722-1725.
7. W. T. Hermens, M. Benes, R. Richter and H. Speijer, *Biotechnol. Appl. Biochem.*, 2004, **39**, 277-284.
8. C. Travelet, M. Stemmelen, V. Lapinte, F. Dubreuil, J.-J. Robin and R. Borsali, *J. Nanopart. Res.*, 2013, **15**.
9. J. Bodycomb and M. Hara, *Macromolecules*, 1995, **28**, 8190-8197.

III. Well-defined biomimetic surfaces

This chapter was published in *Biomaterials*, 2014, 35, 8903-8915 as:

Well-defined biomimetic surfaces to characterize glycosaminoglycans-mediated interactions on the molecular, supramolecular and cellular levels

Elisa Migliorini[a,b,*], Dhruv Thakar[a,b,*], Rabia Sadir[c,d,e], Tino Pleiner[f], Françoise Baleux[g], Hugues Lortat-Jacob[c,d,e], Liliane Coche-Guerente[a,b], Ralf P. Richter[a,b,h,i]

[a]Univ. Grenoble Alpes, Departement de Chimie Moleculaire (DCM), Grenoble, France; [b]CNRS, DCM, Grenoble, France; [c]Univ. Grenoble Alpes, Institut de Biologie Structurale (IBS), Grenoble, France; [d]CNRS, IBS, Grenoble, France; [e]CEA, DSV, IBS, Grenoble, France, [f]Department of Cellular Logistics, Max Planck Institute for Biophysical Chemistry, Göttingen, Germany; [g]Unite de Chimie des Biomolecules, Departement de Biologie Structurale et Chimie, Institut Pasteur, Paris, France; [h]CIC biomaGUNE, Biosurfaces Unit, San Sebastian, Spain; [i]Max Planck Institute for Intelligent Systems, Stuttgart, Germany.

* - authors contributed equally

Significance: We present here a generic platform for the immobilization of biomolecules. It is based on a SAv monolayer that serves as a 'molecular breadboard' to present biomolecules at controlled orientations and tunable densities, in a background of low non-specific interactions. These surfaces were exploited to study GAG-mediated interactions on the molecular, supramolecular (in this chapter and Chapter IV) and cellular levels (in this chapter and Chapter V), and should find great potential in mimicking the extracellular matrix by grafting different biomolecules.

My contribution: I co-designed research (together with Elisa Migliorini, Liliane Coche-Guerente and Ralf P. Richter). I performed and analyzed the QCM-D measurements (together with Elisa Migliorini), and the spectroscopic ellipsometry and surface plasmon resonance measurements. I contributed to data interpretation and figure preparation, except for the cellular assays. I contributed to the article writing for the publication.

Résumé

Les glycosaminoglycanes (GAGs) omniprésents à la surface des cellules et dans la matrice extracellulaire jouent un rôle essentiel pour l'assemblage de la matrice et dans les interactions cellule-cellule et cellule-matrice. La présentation supramoléculaire des chaînes de GAGs avec d'autres composants de la matrice extracellulaire, est susceptible d'être fonctionnellement important, mais reste difficile à contrôler et à caractériser, *in vivo* et aussi *in vitro*.

Nous présentons une méthode pour créer des surfaces biomimétiques bien définies qui portent des GAGs, seuls ou accompagnés de ligands d'adhesion, sur un substrat qui supprime les interactions non-spécifiques. Grâce à la conception d'une plate-forme d'immobilisation - une monocouche de streptavidine qui sert de plateforme moléculaire modulable à la fixation de divers ligands biotinylés - et d'un ensemble de techniques d'analyse *in situ* de surface sensibles (microbalance à quartz et ellipsométrie spectroscopique), les surfaces biomimétiques sont réalisées sur mesure avec un contrôle étroit de l'orientation biomoléculaire, de la densité de surface et de la mobilité latérale.

En analysant les interactions entre un GAG sélectionné (l'héparane sulfate, HS) et la chimiokine CXCL12α (également appelé SDF-1α) qui se lie au HS, nous avons démontré que ces surfaces sont polyvalentes pour réaliser l'étude des interactions biomoléculaires et cellulaires. Les lymphocytes-T adhérent spécifiquement aux surfaces présentant la chimiokine CXCL12α, liée réversiblement au HS ou irréversiblement lorsqu'elle est immobilisée sur le substrat inerte, y compris en l'absence d'un ligand d'adhésion cellulaire. La présence simultanée sur les surfaces fonctionnelles de la chimiokine CXCL12α liée au HS et du ligand d'adhésion ICAM-1 (molécule d'adhésion intercellulaire 1) exerce un effet synergique qui favorise l'adhésion cellulaire. Notre stratégie de biofonctionnalisation de surface devrait être largement applicable à des études fonctionnelles qui nécessitent une présentation supramoléculaire bien définie des GAGs avec d'autres composants de la matrice extracellulaire ou de la surface cellulaire.

Biomaterials 35 (2014) 8903–8915

Contents lists available at ScienceDirect

Biomaterials

journal homepage: www.elsevier.com/locate/biomaterials

Well-defined biomimetic surfaces to characterize glycosaminoglycan-mediated interactions on the molecular, supramolecular and cellular levels

Elisa Migliorini [a, b, 1], Dhruv Thakar [a, b, 1], Rabia Sadir [c, d, e], Tino Pleiner [f], Françoise Baleux [g], Hugues Lortat-Jacob [c, d, e], Liliane Coche-Guerente [a, b], Ralf P. Richter [a, b, h, i, *]

[a] Univ. Grenoble Alpes, Departement de Chimie Moléculaire (DCM), Grenoble, France
[b] CNRS, DCM, Grenoble, France
[c] Univ. Grenoble Alpes, Institut de Biologie Structurale (IBS), Grenoble, France
[d] CNRS, IBS, Grenoble, France
[e] CEA, DSV, IBS, Grenoble, France
[f] Department of Cellular Logistics, Max Planck Institute for Biophysical Chemistry, Göttingen, Germany
[g] Unité de Chimie des Biomolécules, Département de Biologie Structurale et Chimie, Institut Pasteur, Paris, France
[h] CIC biomaGUNE, Biosurfaces Unit, San Sebastian, Spain
[i] Max Planck Institute for Intelligent Systems, Stuttgart, Germany

ARTICLE INFO

Article history:
Received 21 May 2014
Accepted 10 July 2014
Available online 1 August 2014

Keywords:
Glycosaminoglycan
Chemokine
T-lymphocyte adhesion
Quartz crystal microbalance
Spectroscopic ellipsometry
Surface plasmon resonance

ABSTRACT

Glycosaminoglycans (GAGs) are ubiquitously present at the cell surface and in extracellular matrix, and crucial for matrix assembly, cell–cell and cell-matrix interactions. The supramolecular presentation of GAG chains, along with other matrix components, is likely to be functionally important but remains challenging to control and to characterize, both *in vivo* and *in vitro*. We present a method to create well-defined biomimetic surfaces that display GAGs, either alone or together with other cell ligands, in a background that suppresses non-specific binding. Through the design of the immobilization platform – a streptavidin monolayer serves as a molecular breadboard for the attachment of various biotinylated ligands – and a set of surface-sensitive *in situ* analysis techniques (including quartz crystal microbalance and spectroscopic ellipsometry), the biomimetic surfaces are tailor made with tight control on biomolecular orientation, surface density and lateral mobility. Analysing the interactions between a selected GAG (heparan sulphate, HS) and the HS-binding chemokine CXCL12α (also called SDF-1α), we demonstrate that these surfaces are versatile for biomolecular and cellular interaction studies. T-lymphocytes are found to adhere specifically to surfaces presenting CXCL12α, both when reversibly bound through HS and when irreversibly immobilized on the inert surface, even in the absence of any *bona fide* cell adhesion ligand. Moreover, surfaces which present both HS-bound CXCL12α and the intercellular adhesion molecule 1 (ICAM-1) synergistically promote cell adhesion. Our surface biofunctionalization strategy should be broadly applicable for functional studies that require a well-defined supramolecular presentation of GAGs along with other matrix or cell-surface components.

1. Introduction

Glycosaminoglycans (GAGs), a group of acidic and linear polysaccharides including e.g. heparan sulphates (HS) and hyaluronan (HA), are ubiquitously present at the cell surface and in extracellular matrix. They interact with many structural (e.g. collagen, fibronectin) and signalling (e.g. chemokines, growth factors) proteins and thereby regulate matrix assembly and remodelling, as well as cell-matrix and cell–cell interactions [1]. Typically, GAG

* Corresponding author. Biosurfaces Unit, CIC biomaGUNE, Paseo Miramon 182, 20009 Donostia-San Sebastian, Spain. Tel.: +34 943 00 53 29; fax: +34 943 00 53 15.
E-mail address: rrichter@cicbiomagune.es (R.P. Richter).
[1] E.M. and D.T. contributed equally to this work.

http://dx.doi.org/10.1016/j.biomaterials.2014.07.017
0142-9612/

function relies on the integration of multiple interactions rather than on individual binding events. Examples are (i) the remodelling of extracellular matrices by GAGs binding to structural proteins [2,3], by GAG-crosslinking proteins [4,5] or by bulky GAG-binding proteoglycans [6–8], (ii) the sequestration [9,10] and tightly regulated mobility [11] of chemokines or growth factors in matrix and (iii) the presentation of chemokines at controlled densities or in the form of gradients to promote distinct cellular responses such as adhesion or directed migration [12,13].

In all these cases, the local arrangement and density of GAGs, along with other cell surface or matrix components, is of key functional importance. Studies in this direction, however, are challenging because the supramolecular presentation of GAG chains is difficult to control and to characterize, not only *in vivo* but also *in vitro*. For example, GAGs have so far been largely neglected in the design of *in vitro* cell migration assays [14], despite their recognized functional importance. A likely reason is the limited commercial availability of sufficiently pure and suitably functionalized GAGs, and of methodologies to integrate GAGs into assemblies that mimic the presentation at the cell surface or in matrix well. Only few studies demonstrate, so far, the possibility to immobilize and to control GAG surface densities and/or orientations on supports [15–18]. Moreover, to the best of our knowledge the cellular interaction with such surfaces has not been studied. To study the role of GAG-protein interactions in matrix assembly and in cell behaviour *in vitro*, it would be desirable to be able to prepare materials that present GAGs together with other relevant biomolecules in such a way that the orientation, density and lateral mobility of the exposed biomolecules can be controlled and tuned.

Here, we present a method to fabricate biomimetic surfaces that display GAGs and other biomolecules of interest at well-defined orientation, density and lateral mobility (Fig. 1). The method relies on a stratified monolayer of streptavidin (SAv) and self-assembly through strong and specific interactions. Embedded in a background that is largely inert to the undesired nonspecific adhesion of biomolecules or cells, the SAv monolayer serves as a molecular breadboard for the selective attachment of biotinylated molecules. The method is generic in the sense that various biomolecules can be (co-) immobilized at tuneable surface densities, either through a site-specifically attached biotin tag, or if that is not available, through biotinylated adapter molecules. In particular, GAGs are immobilized with controlled orientation through a biotin tag introduced at the reducing end. As a prerequisite of the present work, a method for the preparation of stable and terminally functionalized GAG conjugates was recently developed (Thakar D, Migliorini E, Guerente L, Sadir R, Lortat-Jacob H, Boturyn D, Renaudet O, Labbé P, Richter, RP manuscript submitted).

Two *in situ* surface sensitive analytical techniques, quartz crystal microbalance (QCM-D) and spectroscopic ellipsometry (SE), were combined to monitor in real time the assembly of the biomimetic surfaces and to ascertain that the desired functionalities are indeed realized. In particular, QCM-D provides time-resolved information about the assembly process, including overall film morphology and mechanics [19], while SE enables time-resolved and label-free quantification of biomolecular surface densities and binding stoichiometries [20].

To demonstrate the versatility of our approach for well-controlled and quantitative biomolecular and cellular studies, we selected HS as GAG, and stromal-cell derived factor 1 (CXCL12α, also called SDF-1α) as GAG-binding chemokine [21]. We first quantify the kinetics of CXCL12α binding to HS-displaying surfaces by surface plasmon resonance and then investigate the adhesion of Jurkat cells as a CXCL12α sensitive T-lymphocyte cell line [13] to a range of biomimetic surfaces, including surfaces that present HS-bound CXCL12α along with the intercellular adhesion molecule 1 (ICAM-1). CXCL12α is known to bind with high affinity to the T cell-surface receptor CXCR4 [22,23]; the ensuing activation of T cells as well as the binding of T cells to ICAM-1 at the endothelial cell

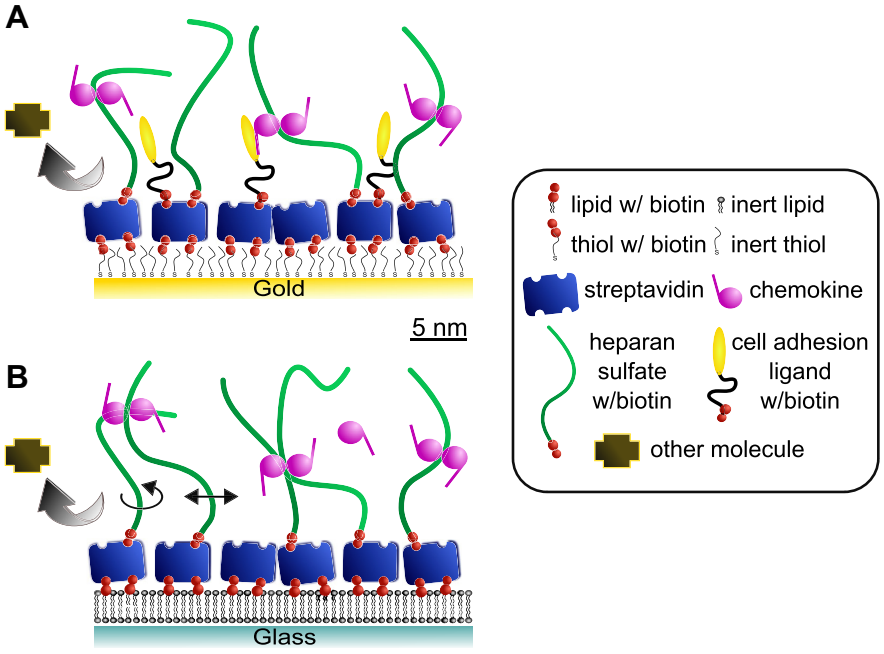

Fig. 1. Design of biomimetic surfaces that reproduce the presentation of cell-surface GAGs. Schematic presentation of well-defined model surfaces presenting heparan sulphate (HS). HS is biotinylated site-specifically at the reducing end (b-HS) and immobilized on a streptavidin (SAv) monolayer with controlled orientation. (A) Model surface based on a gold-supported OEG monolayer exposing biotin at the end of a fraction of the OEG molecules. Stable attachment to the gold is mediated by thiols. (B) Model surface based on a silica-supported lipid bilayer (SLB) exposing biotin at the head of a fraction of the lipids. All molecules are drawn approximately to scale, with the scale bar indicating the approximate size. The OEG monolayer and the SLB confer a background of low nonspecific binding. On fluid SLBs (B) but not on the OEG monolayers (A), HS chains can diffuse laterally together with the anchoring SAv (*thin arrows*).

surface of blood vessels are of particular importance in immune cell trafficking [12,24,25]. With this study, surfaces thus become available that mimic selected aspects of the endothelial cell surface, towards mechanistic cellular studies in an environment that is well-defined and tuneable.

2. Methods

2.1. Buffer, heparan sulphate and proteins

The working buffer used for all experiments and for protein dilution was made of 10 mM Hepes (Fisher, Illkirch, France) at pH 7.4 and 150 mM NaCl (Sigma Aldrich, Saint-Quentin Fallavier, France) in ultrapure water.

Heparan sulphate (HS) derived from porcine intestinal mucosa with an average molecular weight of 12 kDa and a polydispersity of 1.59 [26] (Celsus Laboratories, Cincinnati, OH, USA) was conjugated with biotin through an oligoethylene glycol linker of approximately ~1 nm length, site-specifically attached to the reducing end by oxime ligation. In contrast to the conventionally used hydrazone ligation, oxime ligation produces conjugates that are stable for many weeks in aqueous solution.

CXCL12α (amino acids 1 to 68; 8.1 kDa) was produced by solid-phase peptide synthesis as previously reported [9]. The same CXCL12α construct with a biotin conjugated to the C-terminal lysine through a tetraethylene glycol (OEG) linker (b-CXCL12α; 8.6 kDa), was also produced by solid-phase peptide synthesis. A protein construct containing two Z-domains of protein A, separated by an extended peptide spacer from an Avi-tag carrying a single biotin (b-ZZ, 31.8 kDa) was produced recombinantly in *Escherichia coli* by co-expression with the biotin ligase BirA. Lyophilized streptavidin (SAv, 60 kDa), bovine serum albumin (BSA) and fibronectin (Fn) were purchased from Sigma Aldrich. A chimera of the Fc part of IgG and two human ICAM-1 extracellular domains (Fc-ICAM-1; 152 kDa) was obtained from R&D Systems (Minneapolis, MN, USA). All proteins were diluted to concentrations between 0.2 and 1 mg/mL in autoclaved working buffer and stored at −20 °C. Thawed protein solutions were used within 5 days and further diluted as desired.

2.2. Sensors and surface preparation

QCM-D sensors with gold (QSX301) and silica (QSX303) coatings were purchased from Biolin Scientific (Västra Frölunda, Sweden). Appropriately sized silicon wafers with a native oxide layer of less than 2 nm thickness or with an optically opaque gold coating (100 nm, sputter-coated) were used for SE measurements. SPR gold-coated sensor chips (SIA Kit Au) were purchased from Biacore (GE Healthcare Bio-Sciences, Uppsala, Sweden). Glass cover slips (24 × 24 mm^2; Menzel Gläser, Braunschweig, Germany) for cellular studies were cleaned by immersion in freshly prepared piranha solution (i.e. a 1:3 (*v*/*v*) mixture of H_2O_2 (ACROS Organics, New Jersey, USA) and concentrated H_2SO_4 (Sigma Aldrich)) for 1 h, rinsing with ultrapure water, and blow-drying with N_2. They were used as such or sputter-coated with a titanium adhesion layer (~0.5 nm) and a semi-transparent gold film (~5 nm). All substrates were exposed to UV/ozone (Jelight, Irvine, CA, USA) for 10 min prior to further use.

2.2.1. Functionalization of surfaces with a biotin-displaying and otherwise inert background

Gold-coated surfaces were immersed overnight in an ethanolic solution (Fisher, Illkirch, France) of OEG disulfide and biotinylated OEG thiol (Polypure, Oslo, Norway) at a total concentration of 1 mM and a molar ratio of thiol equivalents of 999:1, and subsequently for 20 min in a stirred solution of pure ethanol, and blow-dried in N_2. Biotin-functionalized supported lipid bilayers (SLBs) were prepared by the method of vesicle spreading though exposure of small unilamellar vesicles (SUVs; at 50 μg/mL in working buffer supplemented with 2 mM $CaCl_2$ (VWR International, Leuven, Belgium)) to silica-coated surfaces, as described earlier [27]. SUVs were prepared by sonication, as described earlier [28], from mixtures of dioleoylphosphatidylcholine (DOPC) and dioleoylphosphatidylethanolamine-CAP-biotin (DOPE-CAP-b) (Avanti Polar lipids, Alabaster, AL, USA) in a molar ratio of 95:5.

2.2.2. Surface functionalization with BSA and Fn

BSA and Fn were physisorbed on uncoated glass cover slips. To this end, the cover slips were exposed to solutions of either BSA at 5 mg/mL or Fn at 5 μg/mL in working buffer for 20 min.

2.3. Assembly of biomimetic surface coatings

The rationale behind the design of the self-organized biomolecular assemblies is provided in the results section (Fig. 1). Unless indicated otherwise, the following concentrations and exposure times were used: SAv – 20 μg/mL, 20 min; b-HS – 50 μg/mL, 10 min; CXCL12α – 5 μg/mL, 20 min; Fc-ICAM-1 – 0.1 μM, 30 min. Under these conditions, binding is expected to saturate or equilibrate, irrespective of whether the solution is flown (in QCM-D and SPR measurements), stirred (in SE measurements) or still (for cell assays). In QCM-D measurements, the injection was sometimes also stopped earlier once the binding curve had reached a plateau. To obtain surfaces that display HS-bound CXCL12α together with Fc-ICAM-1, b-HS (1 μg/mL; 30 min) and b-ZZ (0.05 μM; 5 min) were sequentially exposed to the SAv-coated surfaces. Here, the concentrations and incubation times were chosen to obtain desired surface densities (see Fig. S4 for details). Fc-ICAM-1 and CXCL12α were then incubated until saturation and equilibrium, respectively, were reached.

For QCM-D measurements, exposure to 20 μg/mL SAv was routinely preceded by a first SAv injection at low concentration (1 μg/mL) and decreased flow rate (6 μL/min) for 5 min, to confirm the absence of protein depletion resulting from undesired adsorption to the walls of the tubing or the QCM-D flow module due to insufficient passivation: any depletion of SAv from the solution would result in a decreased binding rate (compared to the established standard rate of −0.5 ± 0.1 Hz/min, see Fig. 2A–B).

2.4. Quartz crystal microbalance with dissipation monitoring (QCM-D)

QCM-D measures the changes in resonance frequency, Δf, and dissipation, ΔD, of a sensor crystal upon molecular adsorption on its surface. The QCM-D response is sensitive to the mass (including hydrodynamically coupled water) and the mechanical properties of the surface-bound layer. Measurements were performed with a Q-Sense E4 system equipped with 4 independent Flow Modules (Biolin Scientific). Sensor functionalization with biotinylated OEG monolayers was performed *ex situ* before the measurement. All other surface functionalization steps proceeded *in situ*. The system was operated in flow mode with a flow rate of typically 10 μL/min using a peristaltic pump (ISM935C, Ismatec, Zurich, Switzerland). The working temperature was 24 °C. Δf and ΔD were measured at six overtones ($i = 3, 5, \ldots, 13$), corresponding to resonance frequencies of $f_i \approx 5, 15, 25, \ldots, 65$ MHz; changes in dissipation and normalized frequency, $\Delta f = \Delta f_i/i$, of the third overtone ($i = 3$) are presented; any other overtone would have provided comparable information.

For sufficiently rigid biomolecular layers at high surface coverage, the film thickness was estimated from $d = -C/\rho \times \Delta f$, where ρ is the film density and $C = 18.06$ ng/cm^2/Hz the mass sensitivity constant for a sensor with a fundamental resonance frequency of 4.95 MHz [19]. For very soft films, such as HS monolayers, this equation is not valid. Here, film thickness was determined by fitting the QCM-D data to a continuum viscoelastic model [29] with the software QTM (D. Johannsmann, Technical University of Clausthal, Germany) [30,31] as described in detail elsewhere [32]. These thickness values are provided as average ± standard deviation from at least three independent experiments.

2.5. Spectroscopic ellipsometry (SE)

SE measures changes in the polarization of light upon reflection at a planar surface. SE was employed *in situ* with a M2000V system (J. A. Woollam, Lincoln, NE, USA) to quantify the surface density of adsorbed biomolecules in a time-resolved manner [28]. The desired substrate was installed in a custom-built open cuvette featuring a magnetic stirrer for continuous homogenization of the sample solution (~150 μl; samples were pipetted into the solution) and a flow-through system for rapid solution exchange during rinsing steps. Before use, the cuvette walls were passivated against biomolecular binding with BSA [4]. Substrate functionalization with biotinylated OEG monolayers was performed *ex situ*, before the measurement. All other surface functionalization steps proceeded *in situ*. Measurements were performed at room temperature.

Surface densities were quantified through fitting of the data to optical models, as described in detail elsewhere [28,33]. The opaque metal film and the OEG monolayer on gold-coated silicon wafers were treated as a single isotropic layer and fitted as a B-spline substrate. The bulk silica of native wafers was also modelled as a B-spline substrate. The native oxide film, alone or together with a deposited SLB, were modelled as a single transparent Cauchy layer. Areal mass densities were determined through de Fejter's equation [20], using refractive index increments, dn/dc, of 0.15 cm^3/g for b-HS, 0.18 cm^3/g for all proteins and 0.17 cm^3/g for lipids.

2.6. Surface plasmon resonance (SPR)

SPR measurements were performed with a Biacore T200 (GE Healthcare Bio-Sciences) operated with Biacore T200 evaluation software (version 2.0.1). All measurements were performed at 25 °C using a working buffer solution supplemented with 0.005% (*w*/*w*) surfactant P20 (an additive employed to reduce nonspecific adsorption to flow system surfaces). The gold-covered Biacore sensor chips were first coated *ex situ* with a biotinylated OEG monolayer, and further functionalization with SAv and b-HS to saturation proceeded *in situ*. Binding experiments were performed by injecting CXCL12α at desired concentrations and at a rate of 75 μL/min for 4.5 min. Between binding assays, the surface was regenerated by two steps of exposure to 2 M NaCl for 2 min each. Upon NaCl treatment, the SPR signal returned to within 5 RU to the level before incubation with chemokine, indicating full regeneration. Reference measurements were performed in parallel on SAv monolayers lacking HS. To obtain the sensorgram shown in Fig. 4A, the reference data were subtracted from the binding curves on HS films. The responses in the reference channel were always below 10% of the total response, indicating that non-specific binding and solution effects on the SPR response were minor.

2.7. T-lymphocyte culture and adhesion assays

The Jurkat cell line was obtained from the European Collection of Cell Cultures (ECACC). Cells were maintained in Roswell Park Memorial Institute (RPMI 1640)

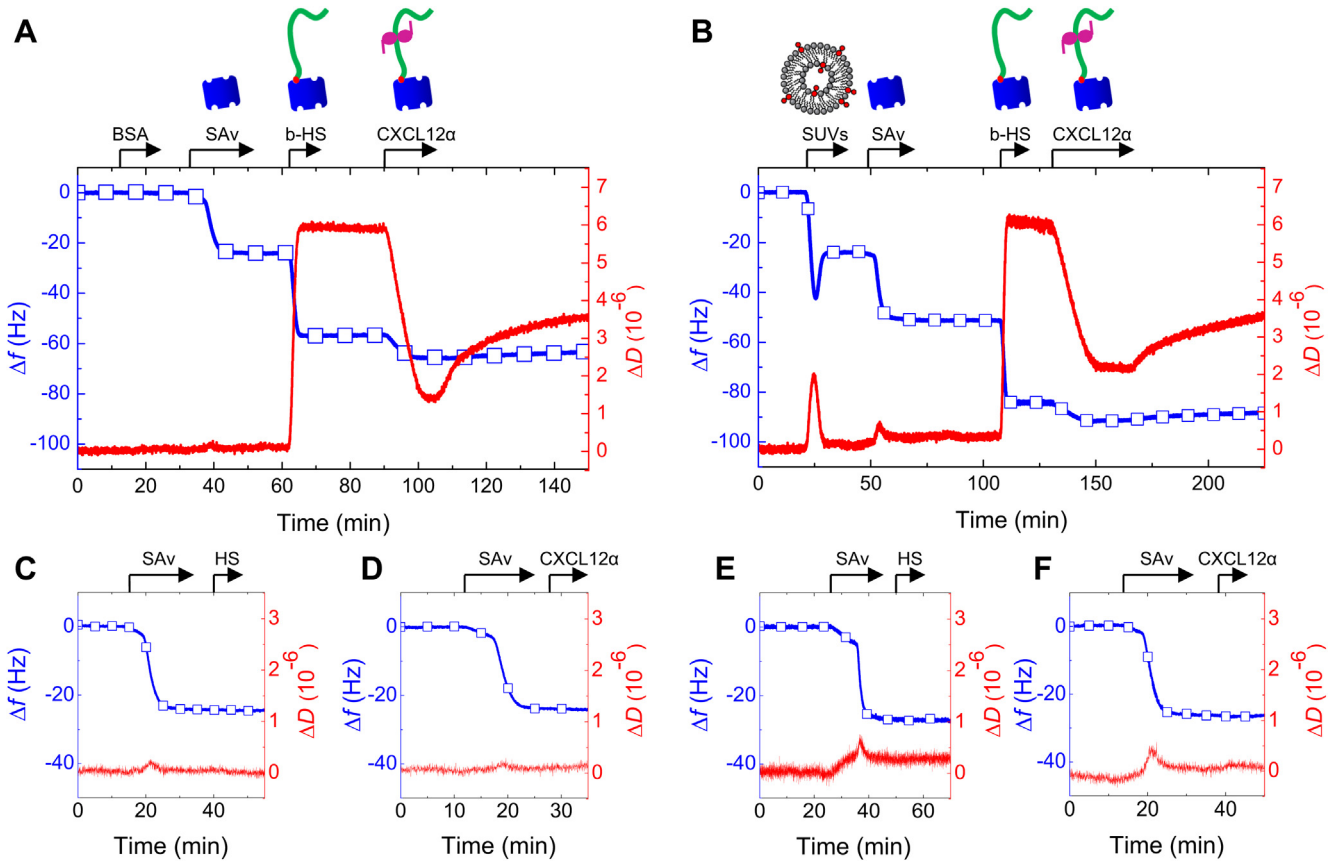

Fig. 2. Step-by-step self-assembly of GAG-presenting model surfaces. Surface functionalization was followed *in situ* by QCM-D (frequency shifts, Δf – *blue lines with square symbols*, dissipation shifts, ΔD – *red lines*) on an OEG monolayer (A) and on a SLB (B). Start and duration of incubation steps with different samples are indicated by *arrows*; during all other times, the surface was exposed to working buffer. HS lacking biotin functionality did not bind to the SAv film on OEG monolayers (C) or SLBs (E) and CXCL12α did not bind to either SAv film in the absence of HS (D, F). (For interpretation of the references to colour in this figure legend, the reader is referred to the web version of this article.)

medium, supplemented with 10% fetal calf serum, 2 mM L-glutamine, 100 units/ml penicillin, 100 μg/mL streptomycin (all from LifeTechnologies, Carlsbad, CA, USA). Cells were grown at 37 °C under a 5% CO_2 atmosphere, and passed at densities between 2×10^5 and 2×10^6 cells/mL.

For cell adhesion assays, glass coverslips – either uncoated or coated with gold and a biotinylated OEG monolayer – were attached, using a bi-component glue (Picodent, Wipperfürth, Germany), to a custom-built teflon holder, thus forming the bottom of 4 identical wells with a volume of ~50 μl each. Biomolecular samples for surface functionalization were incubated in still solution. To remove excess sample after each incubation step, the content was diluted by repeated addition of a 2-fold excess of working buffer and removal of excess liquid until the concentration of the solubilized sample, estimated from the extent of dilution, was below 10 ng/mL. Repeated aspiration and release ensured homogenization of the liquid volume at each dilution step. Care was taken to keep the substrates wet at all times. To avoid unbinding of CXCL12α from HS films, excess CXCL12α in solution was not removed and all cell suspensions were supplemented with 5 μg/mL CXCL12α prior to cell plating.

Prior to plating, cells were re-suspended at a concentration of 10^6 cells/mL in RPMI medium without serum. For life cell nuclear labelling, Hoechst 33342 (Sigma Aldrich) at a concentration of 100 ng/mL was added to the cell suspension. To test for the specificity of the cellular recognition of CXCL12α through the receptor CXCR4, T-lymphocytes were treated with the human monoclonal anti-CXCR4 antibody 12G5 (R&D Systems), which inhibits interaction with CXCL12α [13], at a concentration of 1 μg/mL for 1 h. For assays involving ICAM-1 displaying surfaces, 1 mM $MgCl_2$ and 1 mM EGTA were added to the cell suspension 10 min before plating; this treatment enhances the affinity of the ICAM-1 cell-surface receptor LFA-1 and thus promotes adhesion to ICAM-1 displaying surfaces [34].

Cells were plated at a density of 2.5×10^5 cells per cm^2 on the functionalized glass cover slips. After incubation for 1 h, non-adhesive (and weakly adhesive) cells were removed by gentle rinsing with a pipette in phosphate-buffered saline (PBS; Sigma Aldrich) at pH 7.4. Differential interference contrast (DIC) micrographs and epi-fluorescence micrographs of the nuclear labelling were taken shortly before and after the rinsing step, using an inverted microscope (IX81; Olympus, Hamburg, Germany) equipped with a 60× oil immersion objective (PlanAPoN60XO; Olympus). At least 20 locations were imaged on each sample, covering a surface area of at least 2 mm^2, and used for further quantitative analysis. The same locations were imaged before and after the rinsing step. Volocity visualization software (PerkinElmer, Wlatham, MA, USA) was used for analysis of fluorescence micrographs, to detect the cells and quantify cell surface densities. From a comparison with manual cell counts on selected samples, we estimate the error in the automated determination of cell surface densities to be below 5%. All assays were repeated at least 4 times with independent cell cultures. The percentage of adherent cells is presented as mean values ± standard deviation of four independent experiments. To evaluate the statistical significance between the mean values of more than two samples, the ANOVA test with Bonferroni correction was applied, and a p-value for $\alpha = 0.05$ was extracted for each sample combination.

3. Results

3.1. Design of well-defined biomimetic surfaces

The design of our biomimetic glycosaminoglycan-presenting surfaces is schematically shown in Fig. 1. Two different approaches were used to immobilize GAGs. Both have in common that they use biotinylated GAGs (here HS) and a monolayer of streptavidin (SAv) on a passivating background that prevents non-specific binding. The passivating background was either a gold-supported oligo(ethylene glycol) (OEG) monolayer exposing biotin at the end of a fraction of the OEG molecules (Fig. 1A) or a silica-supported lipid bilayer (SLB) exposing biotin at the head of a fraction of the lipids (Fig. 1B).

The design rules were chosen such that ensuing molecular interactions give rise to self-assembled yet stable model surfaces that are well-defined and tuneable with regard to the density, the

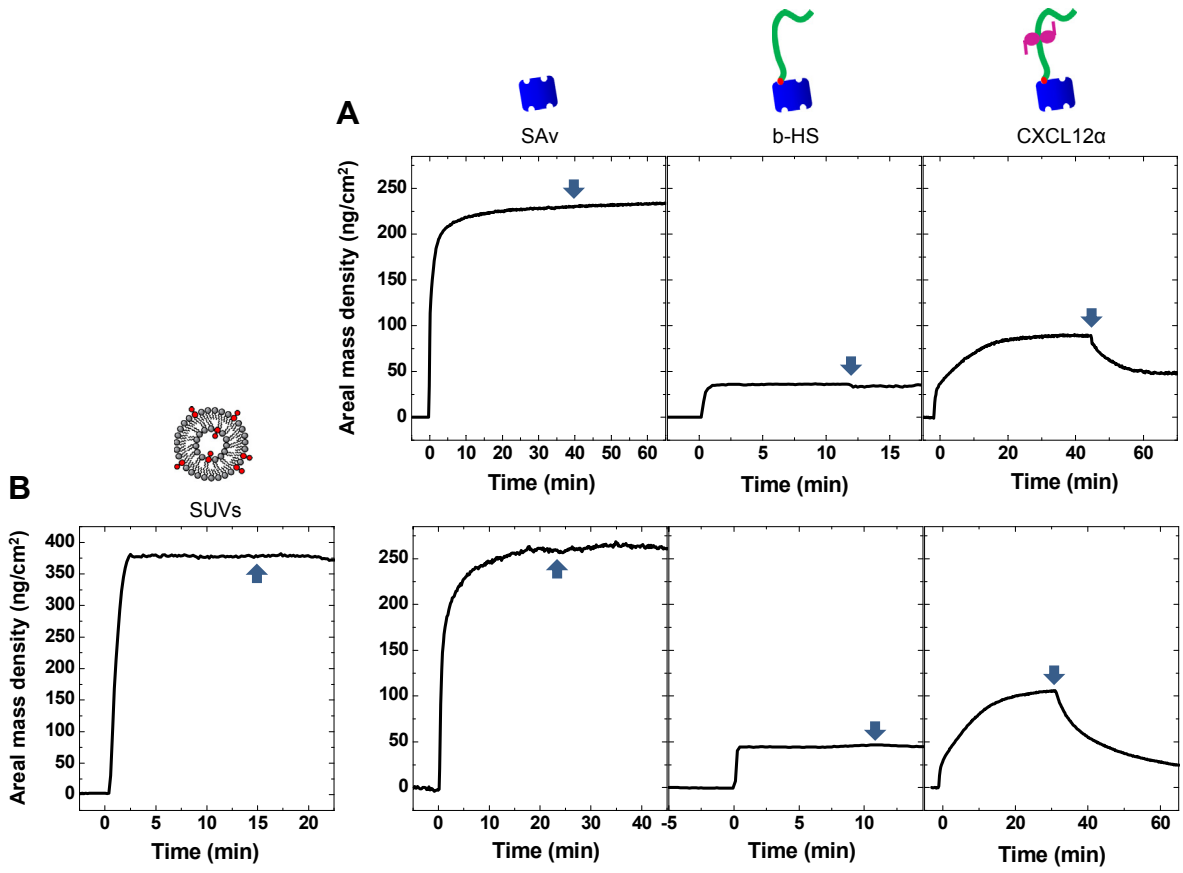

Fig. 3. Quantification of adsorbed amounts. Surface functionalization was followed *in situ* by spectroscopic ellipsometry (SE) on a gold-supported OEG monolayer (A) and a silica-supported lipid bilayer (B). Incubation steps and sample concentrations were as for Fig. 2. Each incubation step started at 0 min; the start of rinsing in working buffer is indicated by an arrow.

orientation and the lateral mobility of the displayed molecules. In particular, we expect SAv to be immobilized such that two of its four biotin-binding sites are facing the surface for immobilization while the other two binding sites are facing the solution to accommodate target molecules. In this regard, SAv performed better than neutravidin (which is perhaps more frequently used in molecular labelling applications), because neutravidin has an enhanced tendency to aggregate [35] and hence does not form well-defined monolayers. Biotin conjugation of the target molecule at a specific site affords immobilization at a well-defined and desired orientation on SAv monolayers. In the case of HS, for example, site-specific biotinylation at the reducing end ensures binding with an orientation that mimics the attachment to HS-displaying core proteins in the cell membrane [36]. Moreover, because binding is stoichiometric and very stable, more than one type of biotinylated molecules can be sequentially immobilized on SAv monolayers. Because the bond forms rapidly (i.e. binding is mass-transfer limited at sufficiently low surface densities), surface densities of target molecules can be quantitatively tuned by varying their solution concentrations and incubation times. The main difference between the two passivating backgrounds is the lateral mobility of the SAv molecules. On SLBs, SAv and any target molecule anchored to it can rotate and diffuse laterally (as illustrated by the black arrows in Fig. 1B), provided that the SAv surface density is low enough to prevent two-dimensional protein crystallization [37,38] (the latter was reported to occur at surface densities above 75% relative to that of the crystalline phase, i.e. above 200 ng/cm^2, on lipid monolayers [39]).

To validate our approach, the step-by-step assembly of our biomimetic surfaces was monitored by QCM-D (Fig. 2). OEG monolayers were prepared *ex situ* prior to installing the gold-coated sensors in the QCM-D chamber. SLBs were formed *in situ* by the method of vesicle spreading, through incubation of the silica-coated QCM-D sensor with 50 μg/mL SUVs (Fig. 2B). The final shifts in frequency ($\Delta f = -26 \pm 0.5$ Hz) and in dissipation ($\Delta D \leq 0.3 \times 10^{-6}$) indicates the formation of a confluent SLB of good quality [40]. The binding kinetics upon successive incubation with 1 μg/mL (to check for sample depletion in the fluidic system, see Methods for details) and 20 μg/mL (to rapidly saturate the surface) SAv were comparable on both surfaces. At equilibrium, SAv generated frequency shifts of -23 ± 1 Hz on OEG monolayers and -27 ± 1 Hz on SLBs, and on both supports, the shifts in dissipation were below 0.4×10^{-6}. From the frequency shifts, and assuming a mean density of 1.2 g/cm^3 for the SAv film with trapped solvent [41], a film thickness of approximately 4 nm can be determined using Sauerbrey's equation, consistent with the molecular dimensions of SAv. Overall, these responses are as expected for the formation of rather dense protein monolayers [16,41], in which each SAv molecule exposes two biotin-binding sites each towards the surface and the bulk solution, respectively.

b-HS, incubated at 50 μg/mL, readily bound to the free biotin-binding sites on the SAv monolayers, with frequency shifts at equilibrium of -31 ± 1 Hz on OEG monolayers and -33 ± 2 Hz on SLBs, and with corresponding dissipation shifts of $5.0 \pm 0.5 \times 10^{-6}$ and $5.5 \pm 0.5 \times 10^{-6}$, respectively. These responses indicate the formation of a soft and presumably highly hydrated film. The HS

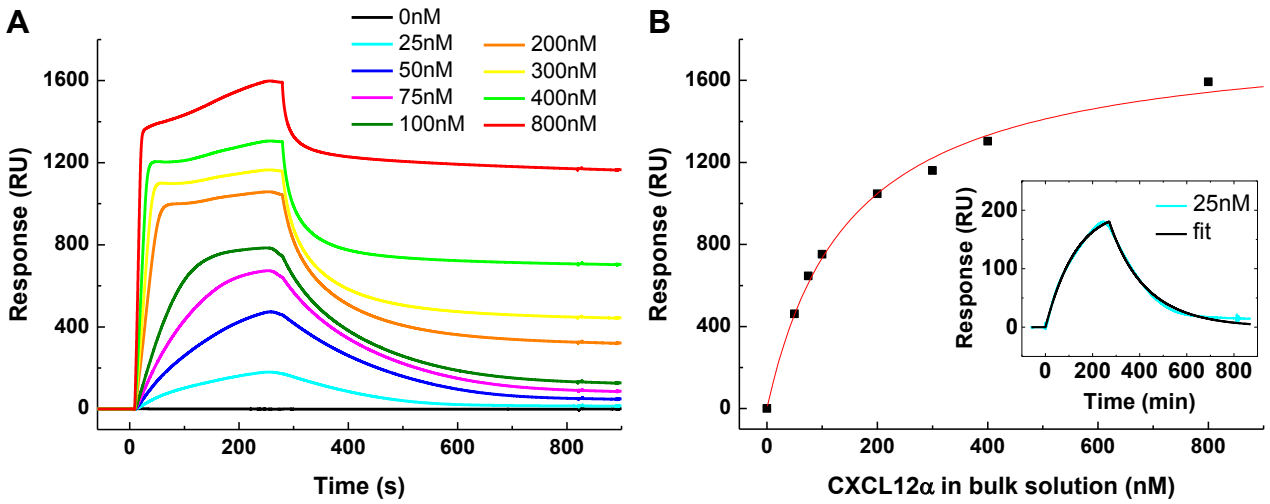

Fig. 4. SPR analysis of CXCL12α binding to HS films. (A) SPR response for the binding of CXCL12α at different concentrations (0–800 nM, as indicated, corresponding to 0–6.4 μg/mL) to a model surface presenting a dense monolayer of b-HS on a SAv-coated OEG monolayer as represented in Fig. 1A. The chemokine was injected from 0 to 270 s, followed by rinsing in buffer alone. (B) Quantitative analysis of SPR data through fitting. The binding isotherm, obtained from the SPR responses close to equilibrium in *A* (*black symbols*) was well described by a Langmuir isotherm (*red line*) with $K_D = 0.13 \pm 0.02$ μM (or 1.1 ± 0.2 μg/mL) and a maximal binding of 1910 ± 100 RU (mean ± standard deviation of 3 measurements). Data at 25 nM from a selected measurement (*inset*, *blue line*) were fit with a one-to-one Langmuir type kinetic model (*black line*), from which $k_{on} = 2.3 \times 10^5$ M^{-1} s^{-1}, $k_{off} = 1.7 \times 10^{-2}$ s^{-1}, $K_D = 73$ nM (or 0.59 μg/mL) and a maximal binding of 790 RU were extracted. (For interpretation of the references to colour in this figure legend, the reader is referred to the web version of this article.)

film was completely stable to rinsing in buffer, as expected for immobilization through the strong biotin-SAv bond. We note that the HS surface densities obtained in the present measurements correspond to the maximal attainable coverage. Lower surface densities can be readily obtained by tuning b-HS incubation time and concentration. By fitting the QCM-D responses to a viscoelastic model, the effective thickness of the HS films was estimated to be 11.6 ± 1.2 nm. In comparison, the average contour length of the employed HS chains is approximately 25 nm. The QCM-D data are hence consistent with the formation of a film of end-grafted HS, in which the individual chains are slightly coiled and/or point in random directions with respect to the surface normal.

The chemokine CXCL12α, incubated at 5 μg/mL, generated negative shifts in frequency (-9 ± 1 Hz on both surfaces), indicating binding. The strong concomitant decrease in dissipation (by $-5 \pm 1 \times 10^{-6}$ on OEG monolayers and $-4.4 \pm 1 \times 10^{-6}$ on SLBs) indicates protein-induced rigidification of the HS film. This remarkable effect merits further investigation, which will be the subject of a forthcoming study. Upon subsequent rinsing in buffer, frequency and dissipation increased slowly but did not return to the level of the virgin HS film, demonstrating that some CXCL12α was released over experimentally accessible time scales whereas a sizeable fraction remained rather stably bound and displayed by HS.

We performed several additional assays to validate the quality of our surfaces and the specificity of immobilization. Bovine serum albumin (BSA) at 100 μg/mL did not bind to the OEG monolayer (Fig. 2A), confirming that the OEG film indeed effectively blocks against access of proteins to the underlying gold surface. BSA also did not bind to the SLB or to the SAv monolayers (not shown). HS lacking biotin functionality did not bind to any of the SAv monolayers (Fig. 2C and E), confirming that b-HS is exclusively immobilized through the biotin moiety at the GAG's reducing end. CXCL12α did not bind any of the SAv monolayers in the absence of HS (Fig. 2D and F), confirming that chemokine binding to HS is specific. Moreover, the CXCL12α fraction that remained in the HS film after rinsing with buffer could be eluted, and the HS film thus fully regenerated, by exposure of the surfaces to 2 M of either guanidine hydrochloride (GuHCl; Fig. S1) or NaCl (not shown).

3.2. Quantitative analysis of surface densities of functional biomolecules

The surface densities of biomolecules during the step-by-step assembly of the biomimetic surfaces were quantified by spectroscopic ellipsometry (SE; Fig. 3). As for the QCM-D measurements, OEG monolayers were formed *ex situ*, whereas all other immobilization steps were followed *in situ*. Time-resolved data for OEG monolayers and SLBs are displayed in Fig. 3A and B, respectively, and Table 1 provides quantities extracted at equilibrium. The lipid surface density at equilibrium (380 ng/cm^2) is consistent with expectations for an SLB. At the maximal attained SAv coverage on SLBs, the average surface area available per SAv molecule was ~37 nm^2. In comparison, the projected surface area of an appropriately oriented SAv molecule was estimated to 4.3 nm × 5.4 nm ≈ 23 nm^2 [41], confirming that SAv formed a dense monolayer. Consistent with expectations from the QCM-D frequency responses (Fig. 1A–B), OEG monolayers could accommodate a similar yet slightly (18%) lower density of SAv, corresponding to an average surface area per molecule of ~45 nm^2. The increased binding on SLBs could be due to the lateral mobility of SAv on fluid SLBs, allowing reorganization into a more densely packed monolayer. Taken together, with two biotin-binding sites available per SAv molecule, the average surface area per biotin-binding site (i.e. anchor point for b-HS) on saturated SAv monolayers would be 21 ± 2 nm^2, corresponding to an average spacing of 4.5 nm (assuming packing in a square lattice).

The binding curves for b-HS in Fig. 3 reveal a constant binding rate up to approximately 80% of maximal coverage, and a rapid saturation thereafter. This indicates that HS binding is mass-transfer limited at low surface densities [42], and that kinetic limitations due to crowding of HS chains on the surface do only weakly affect HS binding even at high surface densities. This would suggest that all solution-facing biotin-binding sites (i.e. two per SAv molecule) can be occupied with b-HS. According to Table 1, and considering a SAv molecular mass of 60 kDa [41], the amount of HS bound on average per biotin-binding site is 5.2 ± 0.6 kDa. This value is inferior to the average HS molecular mass employed (12 kDa).

Table 1
Adsorbed amounts (Γ_{max}) and surface areas available per molecule (A_{min}) at equilibrium for SAv, b-HS and CXCL12α. Data was extracted from SE measurements. Mean values and standard errors from the mean were derived from 3 independent measurements. The adsorbed amount and the average surface area occupied per deposited molecule were estimated to quantify the number of SAv or HS molecules grafted per unit surface area, and the stoichiometry of chemokine binding.

Immobilization platform	SAv		b-HS		CXCL12α	
	Γ_{max} (ng/cm^2)	A_{min} (nm^2)	Γ_{max} (ng/cm^2)	A_{min} (nm^2)	Γ_{max} (ng/cm^2)	A_{min} (nm^2)
OEG monolayer on gold	235 ± 6	42.4 ± 1.1	35.5 ± 2.2	56.3 ± 3.5[a]	78 ± 7	17.4 ± 1.6
SLB on silica	273 ± 8	36.5 ± 1.5	46.8 ± 1.5	42.6 ± 1.4[a]	120 ± 20	11.5 ± 1.9

[a] Assuming an average molecular weight of 12 kDa per surface-bound b-HS. This assumption is based on the average molecular weight determined for HS in solution prior to biotinylation. In reality, the surface-binding might favour low molecular weight HS. When assuming instead that two HS chains are bound per SAv molecule, the average molecular weight per surface-bound b-HS would be 5.2 ± 0.3 kDa on SLBs and 4.6 ± 0.4 kDa on OEG monolayers and A_{min} for b-HS would correspond to 0.5 times the A_{min} for SAv.

The discrepancy is likely a consequence of the large size distribution of HS in solution, i.e. capture on SAv has selected the shortest chains in the initial HS sample. The binding of smaller molecules tends to be favoured, because of their faster diffusion and hence mass transfer to the surface [42] and because they may also penetrate an existing HS film more easily. Assuming an average molecular mass of an HS disaccharide of 500–550 Da [43], we can estimate that 10 ± 2 disaccharides are bound on average per biotin-binding site. With a length of 1.0 nm per disaccharide, the average chain contour length would then be 10 nm. The final b-HS surface density on OEG monolayers was slightly lower than on SLBs. This is most likely a consequence of the reduced SAv density on OEG monolayers. Indeed, within the experimental uncertainties, the mass ratio of b-HS to SAv was constant on both surfaces.

The binding curve for CXCL12α reproduced many features already observed by QCM-D (Fig. 2A–B), such as rapid binding and equilibration and partial release of proteins upon rinsing in buffer. Thanks to the quantification of surface densities afforded by SE (Table 1), and with a CXCL12α molecular mass of 8.1 kDa, it is possible to estimate that each CXCL12α molecule has approximately 3.5 kDa HS, corresponding to roughly 7 disaccharides, available on average at equilibrium.

3.3. Application of the biomimetic GAG-presenting surfaces to molecular interaction analysis

Surface plasmon resonance (SPR) was used to analyse thermodynamic and kinetic parameters of the interaction of CXCL12α with HS films (Fig. 4). SPR studies of CXCL12α binding to HS have previously been reported [9] using a film of carboxymethylated dextran (i.e. Biacore CM4 sensor chips) with covalently immobilized SAv as an immobilization platform. The dextran film is approximately 100 nm thick [44] and hence represents a three-dimensional environment into which b-HS was bound (at unknown volume densities). The model surfaces in our study are distinct, in that all HS molecules are presented at the same orientation in the form of a monolayer with controlled surface density. As for QCM-D (Fig. 2A) and SE (Fig. 3A) measurements, the gold-coated SPR sensor chip was first functionalized *ex situ* with an OEG monolayer, and subsequent functionalization was monitored *in situ*. At saturation, 2550 ± 25 and 330 ± 20 response units (RU) were reached for SAv and b-HS, respectively. According to Table 1, these values correspond to surface densities of approximately 235 and 35 ng/cm^2, respectively.

The sensorgram in Fig. 4A shows a response in CXCL12α binding that is dose dependent in the initial binding rates and the binding equilibrium, as expected. For low protein concentrations (≤100 nM), the binding curves were conventional and the protein could be close-to-completely removed upon rinsing in buffer. The unbinding curves at the lowest employed concentration (25 nM) were well-fitted by a one-to-one Langmuir type binding model (Fig. 4B, inset), revealing an association rate constant $k_{on} = 2.3 \times 10^5$ M^{-1} s^{-1}, a dissociation rate constant $k_{off} = 1.7 \times 10^{-2}$ s^{-1}, and hence a dissociation constant $K_D = k_{off}/k_{on} = 73$ nM (or 0.59 μg/mL), and a maximal response of 790 RU. The results of the fit varied somewhat depending on how much of the unbinding curve was included in the fit, and from these variations we estimate the K_D to be accurate to within a few 10%. The simple one-to-one binding model increasingly failed to reproduce the experimental data with increasing protein concentration. Above 100 nM, a peculiar multi-phase binding response appeared: a first fast binding was followed by a quasi-plateau and a phase of slower binding before equilibrium was reached. Moreover, a substantial fraction of the chemokine remained bound upon rinsing in buffer at these protein concentrations. The multi-phase binding response and the limited release appear to be correlated, suggesting that CXCL12α can bind to HS in at least two distinct ways.

The complex binding pattern precluded a further quantitative analysis of the kinetic SPR data. However, a binding isotherm was constructed from the SPR responses close to equilibrium (Fig. 4B). The data could be fitted with a Langmuir isotherm with $K_D = 0.13 \pm 0.02$ μM (or 1.1 ± 0.2 μg/mL) and a maximal response of 1910 ± 100 RU, both significantly larger though of the same order of magnitude as the values obtained above for a solution concentration of 25 nM. Considering the complex binding pattern observed by SPR, and the heterogeneous sulphation of HS, it is rather surprising that the binding isotherm is so well described by the simple Langmuir binding model. The agreement might well be coincidental, and we therefore suggest that the $K_D = 0.13$ μM obtained through the binding isotherm should be considered an effective value rather than representing the true binding affinity of a one-to-one binding interaction. Notably, our effective K_D value is comparable to the value of 0.20 μM, previously obtained by SPR with a film of HS-functionalized carboxymethylated dextran using an HS preparation of comparable sulphation and molecular weight [9]. The $K_D = 73$ nM obtained through analysis of the kinetic data at 25 nM, on the other hand, may be a true binding constant, representing the highest-affinity binding sites in the HS film. Since CXCL12α tends to bind to highly sulphated regions [47], one would expect this number to be comparable to the affinity of CXCL12α for the highly sulphated GAG heparin. Indeed, a similar value of 93 nM has been reported for heparin [9].

We note that the SPR responses at equilibrium upon CXCL12α binding (Fig. 4A) were several fold larger than what was previously reported on CM4 sensor chips [9]. Most likely, this is due in part to a higher HS density selected in our assays and in another part to an enhanced sensitivity of our assay (i.e. because the SPR sensitivity decays exponentially with the distance from the gold surface, and the interactions in our assay are confined to within about 20 nm whereas the CM4 chip samples approximately 100 nm). By comparing the SE data for CXCL12α binding (at 5 μg/mL or 620 nM solution concentration; Table 1) with the Langmuir isotherm

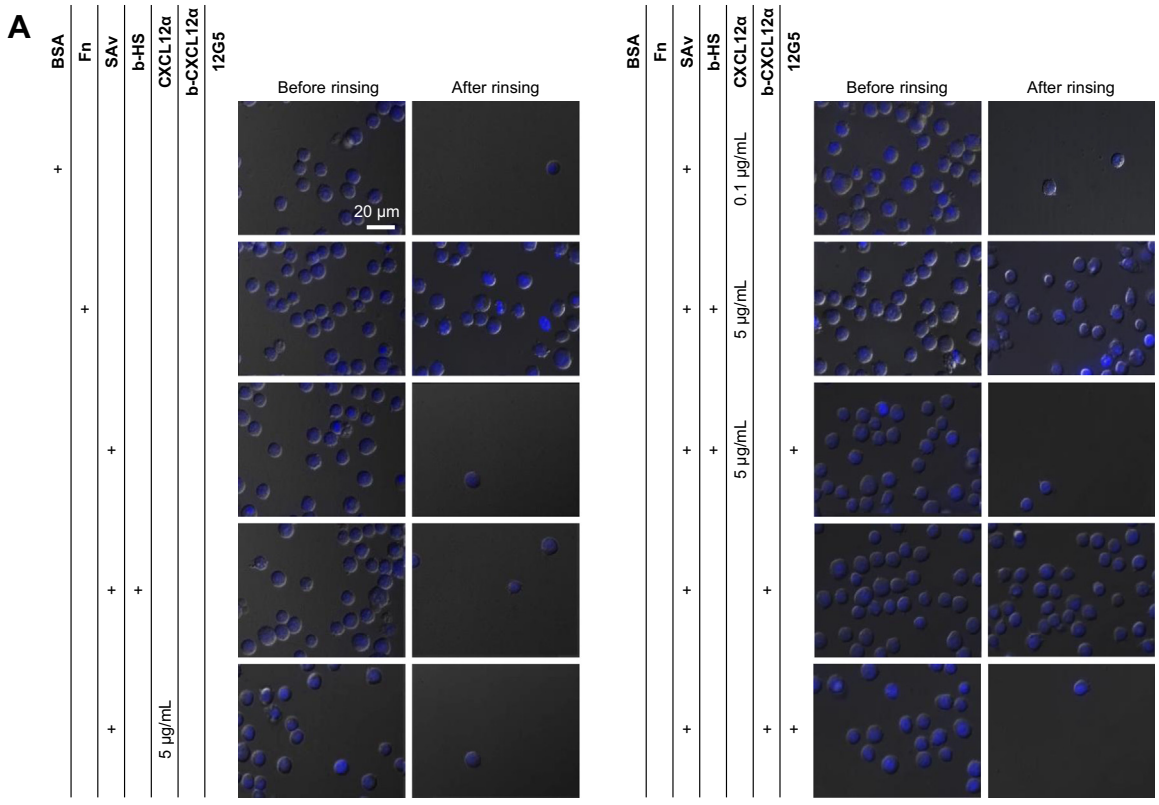

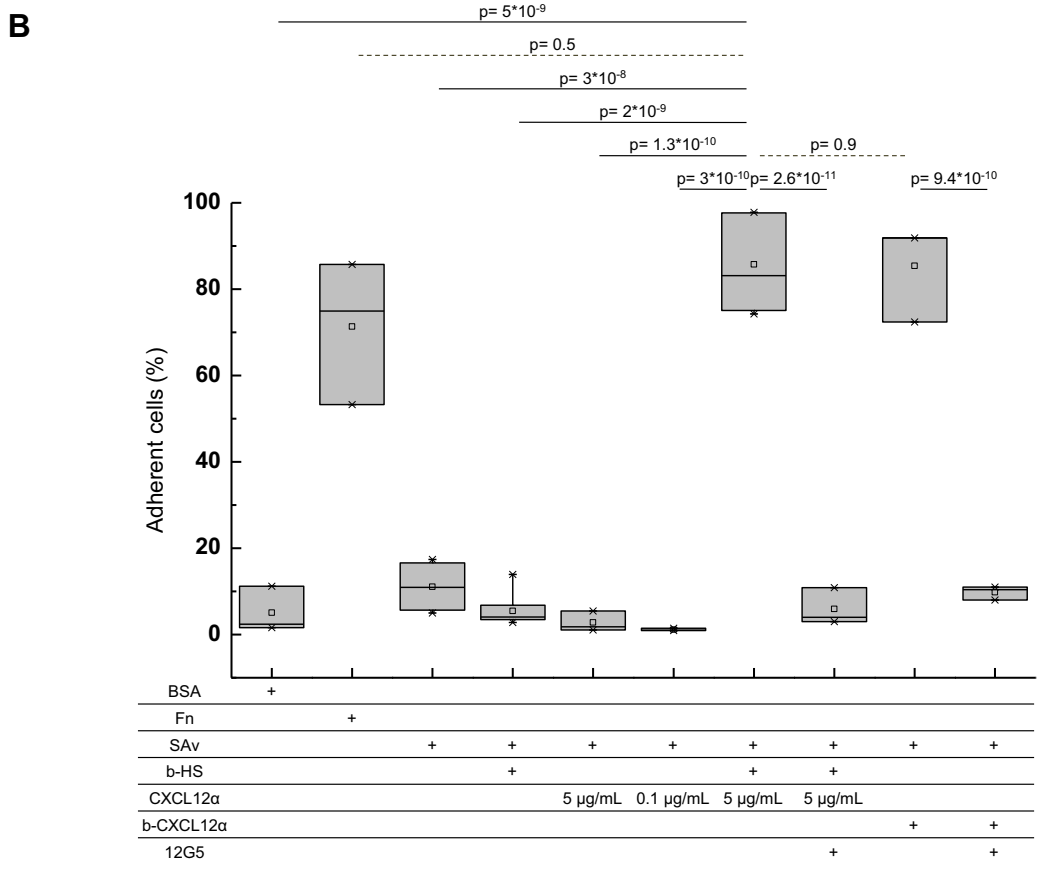

Fig. 5. T-lymphocytes adhere specifically to model surfaces presenting HS-bound chemokine. (A) Representative images of T-lymphocytes that were plated on surfaces presenting different surface functionalizations. Molecules used for functionalization are listed on the left, and "+" indicates that a compound was used on a given surface. BSA and fibronectin (Fn) were physisorbed on glass cover slips and used as the negative and positive control, respectively, for cellular adhesion. All other functionalizations were performed on OEG monolayers on coverslips coated with a 5 nm gold film. Whenever CXCL12α was used, the chemokine was maintained in the soluble phase throughout the cell adhesion assay at

derived from SPR (Fig. 4B), we can estimate that the maximal SPR response of 1910 RU corresponds to roughly 6 disaccharides available on average per CXCL12α. CXCL12α is known to dimerize upon binding to GAGs, with the GAG binding site being located at the interface between the constituent monomers [45–47], i.e. 12 disaccharides would be effectively available per CXCL12α dimer binding site. In comparison, structural models and binding data have suggested that a CXCL12α dimer occupies approximately 6 disaccharides [47,50]. Thus, if all CXCL12α are bound directly to HS and if CXCL12α binds exclusively to the highly sulphated regions, then this would mean that about one half of the HS is highly sulphated. The degree of sulfation in HS is diverse and depends on the source, but the above calculation is clearly in the range of what is possible.

3.4. Application of the biomimetic GAG-presenting surfaces to cellular interaction studies

Increasing complexity, the biomimetic GAG-presenting surfaces were used to trigger specific cellular responses. As a model system, we chose CXCL12α-loaded HS-presenting surfaces and Jurkat cells as a CXCL12α sensitive T-lymphocytes cell line [13]. In a first step, the adhesion of Jurkat cells to surfaces with different functionalizations was assessed by quantifying the fraction of cells that resisted gentle rinsing with a pipette after 1 h of exposure to the surface (Fig. 5). Less than 20% of cells adhered stably to glass cover slips with physisorbed BSA whereas more than 60% of cells remained attached on glass cover slips with physisorbed fibronectin (Fn). These surfaces served as negative and positive controls, respectively.

All other functionalizations were performed on OEG monolayers on coverslips coated with a 5 nm (i.e. semi-transparent) gold film, following the previously established protocol (Fig. 1A). Surfaces displaying a virgin SAv monolayer or a SAv monolayer with HS film showed a level of cellular adhesion that was comparable to the negative control (Fig. 5). This demonstrates that our surfaces are resistant to non-specific cellular adhesion, as desired. The presence of CXCL12α at 100 ng/ml in the bulk solution did not enhance cell adhesion to a virgin SAv monolayer. At this chemokine concentration, close to CXCL12α plasma concentration during inflammation [48], T-lymphocytes are known to become activated [49]. Even with CXCL12α at 5 μg/mL in the bulk solution, T-lymphocyte adhesion remained at baseline level on virgin SAv monolayers. We conclude that stimulation through CXCL12α in the solution does not promote significant (non-specific) cell adhesion.

In contrast, when CXCL12α was presented by the surface through HS (Fig. 5), cellular adhesion increased significantly, to levels that were comparable or even superior to Fn-displaying surfaces. Considering that CXCL12α is not known as a cell adhesion ligand and that CXCL12α binds reversibly to the HS-coated surface, this finding is surprising. When CXCL12α-binding to its cell-surface receptor CXCR4 was blocked with the anti-CXCR4 antibody 12G5 [13], cell adhesion returned to baseline levels, demonstrating that CXCL12α-mediated adhesion of Jurkat cells to HS-presenting surfaces is specific and mediated by CXCR4.

In a complementary assay, we tested if the presence of HS was required for CXCL12α-mediated cellular adhesion (Fig. 5). To this end, CXCL12α was immobilized directly on the SAv monolayer using a biotinylated protein construct (Fig. S2). Site-specific conjugation with a biotin at position 68, the C-terminal residue that is not expected to interfere with CXCL12α binding to HS (see Fig. S2A) or to the cell surface receptor CXCR4 [50], ensured close-to-stoichiometric binding of CXCL12α to SAv (i.e. two CXCL12α molecules per SAv, Fig. S2B) at appropriate orientation. There was no significant difference in the cellular adhesion between the two methods of CXCL12α presentation (Fig. 5B; *p-value* = 0.9). Therefore, under the employed conditions (including CXCL12α surface densities of similar magnitude, see Fig. 3A and Fig. S2B), the presentation of the chemokine through HS does apparently not alter the cellular response in terms of adhesion to CXCL12α as compared to chemokine presentation in the absence of HS.

3.5. Cell adhesion on surfaces presenting GAGs together with cell adhesion ligands – towards more complex cellular interaction studies

With its modular design, our surface functionalization platform can readily accommodate multiple biotinylated compounds, generating multifunctional surfaces (Fig. 1A). To demonstrate this, surfaces were created on which the intercellular adhesion molecule 1 (ICAM-1) was immobilized, either alone or in combination with HS. ICAM-1 is known to be presented by the endothelial cell surface and to bind to the leucocyte function-associated antigen-1 (LFA-1; also called integrin $\alpha_L\beta_2$). This interaction is responsible for the attachment of T-lymphocytes to the vascular endothelium, a precursor step towards migration through the endothelial barrier [51]. Here, we tested how the co-presentation of HS-bound CXCL12α and ICAM-1 affects cell adhesion.

The assembly of the new model surface was first characterized by QCM-D. A fusion protein made from two ICAM-1 extracellular domains and an immunoglobulin Fc domain (Fc-ICAM-1) could be immobilized stably and with desired orientation through an adaptor protein (b-ZZ) that contained two Z-fragments of Protein A (for binding to the Fc domain) and a site-specifically conjugated biotin (for binding to SAv) (Fig. S3). Fig. 6A confirms that b-HS and b-ZZ can be sequentially immobilized on the same SAv monolayer, and that the resulting surface can be used to co-display CXCL12α (specifically through b-HS, see also Fig. S3A) and Fc-ICAM-1 (specifically through b-ZZ, see also Fig. S3B). For the cell adhesion assays, surfaces presenting HS-bound CXCL12α together with ICAM-1 were compared with surfaces presenting either HS-bound CXCL12α or ICAM-1 alone. Surfaces displaying b-ZZ, either alone or with HS, were used as negative controls. Throughout the assay, surface densities of the incubated components were maintained constant. The surface coverage of b-HS and b-ZZ was controlled by varying the samples' solution concentrations and incubation times and exploiting the fact that binding to SAv is mass transport limited at sufficiently low b-HS and b-ZZ surface densities (Fig. S4). The surface density of b-HS was fixed to 35 ± 5% of the maximal surface density (Fig. S4A), corresponding to an average distance of about 13 nm between neighbouring HS chains. Onto this low-density HS film, CXCL12α bound with an equilibrium surface density of 35 ± 4 ng/cm^2 (Fig. S4B). b-ZZ was immobilized at 7 ng/cm^2 (Fig. S4C). This surface density, corresponding to an average distance of 28 nm

indicated concentrations. Jurkat cells were incubated for 1 h and non-adhesive cells were then removed by gentle rinsing. Micrographs (DIC (*gray scale*) overlayed with fluorescence of labeled cell nuclei (*blue*)) are representative and were taken shortly before (*left columns*) and after (*right columns*) rinsing. (B) Box plot representing the distribution of the percentage of adherent cells that remained after rinsing as a function of surface functionalization. The small square and the horizontal line inside the box indicate the mean and the median, respectively, the lower and upper boundaries of the box are determined by the 25th and 75th percentiles, respectively. The crosses correspond to the maximum and to the minimum value observed. ANOVA tests were performed to obtain *p*-values. (For interpretation of the references to colour in this figure legend, the reader is referred to the web version of this article.)

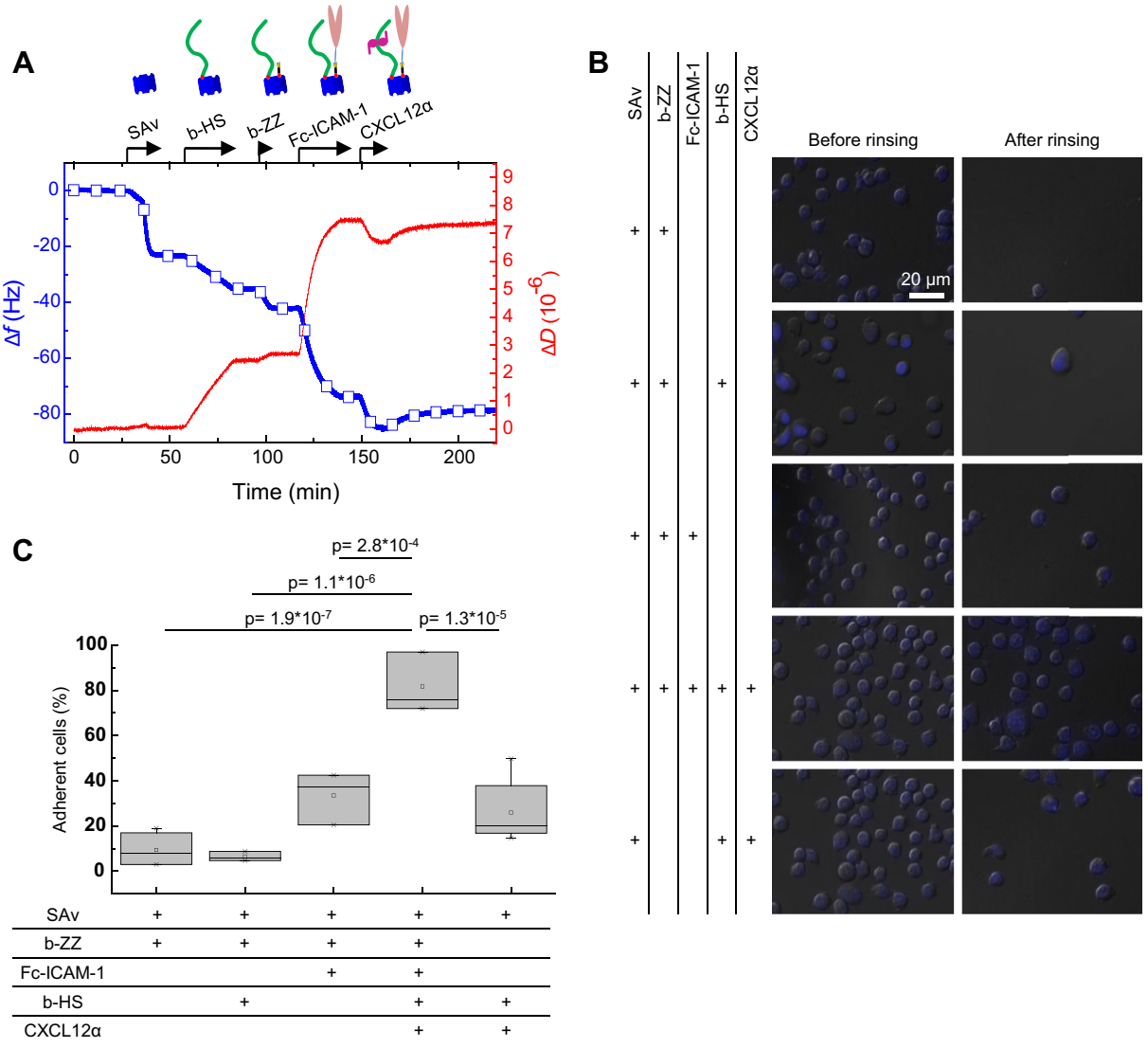

Fig. 6. T-lymphocytes differentially respond to surfaces presenting HS-bound chemokine with an integrin ligand. (A) The assembly of a biomimetic surface displaying HS-bound CXCL12α together with the cell adhesion molecule ICAM-1 on a SAv-coated gold-supported OEG monolayer was demonstrated by QCM-D (Δ*f* – *blue line with square symbols*, Δ*D* – *red line*). Start and duration of each incubation step with different samples are indicated by an arrow; during all other times, the surface was exposed to working buffer. SAv was incubated as in Fig. 2A, b-HS at 1 μg/mL, b-ZZ at 0.05 μM, Fc-ICAM-1 at 0.1 μM, and CXCL12α at 5 μg/mL. (B) Representative micrographs of Jurkat cells plated on surfaces presenting different surface functionalizations. Surface densities of all displayed molecules were kept constant throughout the assay as described in the main text. Cells were incubated, and micrographs are presented as described in Fig. 5A. (C) Box plot representing the distribution of the percentage of adherent cells that remain after rinsing as a function of surface functionalization (analysis analogous to Fig. 5B). (For interpretation of the references to colour in this figure legend, the reader is referred to the web version of this article.)

between neighbouring anchor points for Fc-ICAM-1, was chosen to have an ICAM-1 surface density not too high to be able to appreciate the effect of the co-presentation of the integrin ligand with the chemokine presented through HS.

Considering the molecular dimensions of the Fc-ICAM-1 construct – the five immunoglobulin (Ig)-like domains per each of the two ICAM-1 domains [52] and the four Ig domains of the Fc part [53] are expected to form an assembly of two bent rods aligned at the Fc part, where each rod is about 26 nm long and 2 nm in diameter – it is unlikely that steric constraints will limit the binding of Fc-ICAM-1 to b-ZZ, and the average distance between ICAM-1 dimers is therefore estimated to be also 28 nm. Moreover, with the chosen surface densities, surface crowding should not limit immobilization of any of the molecular species. In contrast to the previous assay (Fig. 5), Jurkat cells were treated with 1 mM $MgCl_2$ and 1 mM EGTA to induce high-affinity binding of LFA-1 to ICAM-1 and thus to enhance T-lymphocyte adhesion [54,55].

Results are presented in Fig. 6B–C. Only 10% of the cells adhered to the negative control surfaces, comparable to the BSA control previously used (Fig. 5B), confirming low non-specific binding. A larger fraction of cells, about 34% and 26%, adhered to surfaces displaying either Fc-ICAM-1 or HS-bound CXCL12α alone, respectively. Interestingly, the adhesion increased drastically, to about 80%, when ICAM-1 and HS-bound CXCL12α were presented together. This assay thus demonstrates that the co-presentation of an integrin ligand and a GAG-bound chemokine elicits a cellular response that is distinct from the response to each individual cue alone.

4. Discussion

We have developed a bottom-up biosynthetic approach to reconstitute GAGs and other cell membrane and extracellular matrix molecules (lipids and proteins) into well-defined model surfaces and demonstrated the application of these tailor-made

biomimetic environments for quantitative molecular and cellular studies.

The presented surface functionalization strategy is versatile. SAv monolayers serve as a molecular breadboard for the selective coupling of various biomolecules. SAv acts as a host for biotin which is site-specifically conjugated, either directly to the desired biomolecule (e.g. Fig. 2 and Fig. S2) or to an adaptor molecule that binds other tags. The latter was demonstrated here with b-ZZ and an Fc chimera (Fig. S3) and other highly specific yet stable interactions can also be exploited (e.g. multivalent NTA constructs and histidine tags [56]). Moreover, the surface density – and hence also the average molecular spacing – can be controlled (Fig. 3) and tuned (Fig. S4). Although not explicitly demonstrated in this study, the design principle also enables comparative studies on surfaces displaying immobile (Fig. 1A) *vs.* laterally mobile (Fig. 1B) molecules, e.g. to assess the importance of ligand clustering in cellular interactions. Taken together, surface functionalization combined with the design of molecular building blocks through synthetic conjugation chemistry or biochemistry thus provide a toolbox of interactions for the assembly of multifunctional surfaces in a molecular-lego-type fashion.

The employed surface design, validated by QCM-D and SE characterization, confers control on molecular orientation such that the appropriate molecular face is exposed to the solution phase. This ensures that the vast majority of immobilized molecules remains active, in contrast to conventional immobilization approaches such as physisorption (e.g. in enzyme-linked immunosorbent assays (ELISA)) or covalent coupling through random sites (e.g. carboxylic acids or primary amines *via* EDC NHS chemistry), where surface-induced denaturation and/or spatial constraints can drastically limit the activity of immobilized molecules [57,58]. Biospecific interactions are also more rapid than practically relevant covalent chemistries (including the so-called 'click' chemistries), thus enabling rapid assembly of the biomimetic surfaces. The interactions between biotin and SAv, or between Fc and Z domains, are strong enough for the surfaces to remain stable over many hours. Where required, such non-covalent yet rapid and highly specific interactions could be exploited for initial coupling to guide the subsequent formation of covalent bonds at desired sites with enhanced rates [59], thereby enhancing stability and further broadening the application range.

Several proof-of-concept measurements illustrated the use of the biomimetic surfaces for mechanistic studies. On the molecular scale, we find that CXCL12α may bind to HS in several distinct ways (Fig. 4). CXCL12α is known to dimerize upon binding to GAGs [45–47], and higher-order oligomers of this chemokine have also been reported [60]. Moreover, HS are heterogeneously sulphated and CXCL12α is known to bind preferentially to the highly sulphated domains [47]. All these factors might contribute to the complex binding behaviour, in a way that remains to be elucidated. We also find that CXCL12α rigidifies HS films (Fig. 2A–B), indicating that the interaction of this chemokine affects the supramolecular arrangement of HS chains. In future studies, the model surfaces should be versatile towards elucidating the molecular mechanism behind GAG matrix remodelling by CXCL12α and its functional consequences. More generally, it becomes possible to study directly on the supramolecular scale how extracellular proteins bind to GAG matrices and remodel them, or how the presentation of GAGs affects protein retention and dynamics (e.g. towards the formation of chemokine gradients [24,61]).

At the cellular level we demonstrate that the specific interaction between HS-bound CXCL12α and the receptor CXCR4 promotes T-lymphocyte adhesion (Fig. 5). Given that the interaction between HS and CXCL12α is reversible and considering that no other *bona fide* cell adhesion receptor is involved, this finding is remarkable. It suggests that CXCL12α can interact simultaneously and in *trans* with HS and CXCR4 and that this interaction is strong enough to confer adhesion. The CXCL12α-mediated bridging of CXCR4 and HS is consistent with the observation that in CXCL12α, the binding domains for GAG and CXCR4 are spatially distant and do not interfere functionally [62].

Although the presentation of CXCL12α through HS and in the form of b-CXCL12α is distinct – HS displays CXCL12α in dimeric form [45–47] and reversibly bound whereas b-CXCL12α is monomeric and irreversibly immobilized – no significant difference in the adhesion of T-lymphocytes was found. This observation might suggest that the specific conformation in which CXCL12α is presented is not crucial for chemokine recognition by T-lymphocytes. It has been demonstrated that, when presented in solution, both monomeric and dimeric CXCL12α are recognized by CXCR4. However, the oligomerization state has antagonistic effects on cell signalling and function [63]: low monomer concentrations enhanced chemotaxis while the dimer inhibited chemotaxis [64,65]. The assays here developed enable the presentation of CXCL12α in a matrix-bound form, mimicking in this way the endothelial cell surface, and thus provide means to test how distinct presentations of CXCL12α in a matrix-bound form affect cellular response. Future studies should investigate if the display of CXCL12α through an HS matrix, and the potential internalization of the reversibly HS-bound chemokine by the cell, leads to distinct downstream effects that are not detectable in the simple cell adhesion assay used here. It will also be interesting to analyse how the oligomerization state of CXCL12α affects the cellular response. Moreover, assays with distinct GAG conjugates would enable to study how the HS sulphation pattern or the GAG type affect chemokine-mediated cellular responses.

While integrins and L-selectin are recognized as the major adhesion receptors expressed on the surface of T cells [51], it is known that signals from homeostatic chemokine receptors are essential for stable cell adhesion and migration [66,67]. Here, we demonstrate that when chemokines and integrin ligands are co-presented, their combined effect increases the adhesion of T-lymphocytes as compared to either molecule alone (Fig. 6). Future studies should investigate if ICAM-1 and HS-bound CXCL12α promote cell adhesion independently, or if the enhanced adhesion is the consequence of any cooperative action involving cross-talk between receptors. For example, it has been proposed that the cellular signalling pathways triggered by CXCL12α and ICAM-1 cooperate, increasing LFA-1 avidity to ICAM-1 [68]. Such a study will require analysis of cell signalling processes, which is amenable with our surfaces yet outside the scope of the current work.

The discussed examples illustrate that the strategy to create biomimetic surfaces described here represents a versatile experimental platform for mechanistic studies of GAG-protein interactions on the molecular and supramolecular scale, and of GAG-mediated cell–cell and cell-matrix communication. The platform could also be useful for *in vitro* diagnostic studies and for drug development. Indeed the strategy could be used for the formation of surfaces presenting gradients of GAGs and proteins, to study the effect of specific compounds/drugs on T-lymphocyte migration during the immune response. Moreover, methods for the controlled presentation of chemokines by HS may be of key importance for the design of chemokine-loaded implantable devices for regenerative medicine or tissue remodelling purposes. For example, it was recently shown that CXCL12α-HS binding is necessary for post ischemia revascularization [69].

5. Conclusions

We have presented a versatile strategy to create biomimetic surfaces that present GAGs together with other cell surface or extracellular matrix molecules in a background of low non-specific binding. We have demonstrated that the orientation of the immobilized molecules can be controlled and their surface density tuned, thanks to the surface design and quantitative characterization by surface sensitive techniques, and how this platform can be used for functional studies on the molecular, supramolecular and cellular levels. T-lymphocytes adhere specifically to surfaces presenting CXCL12α and CXCL12α presented through HS enhanced cellular adhesion when co-immobilized with ICAM-1. The strategy to create multifunctional biomimetic surfaces should be broadly applicable for functional studies that require a well-defined supramolecular presentation of GAGs along with other matrix or cell-surface components.

Acknowledgements

We thank Nico Eisele and Luis Yate (both CIC biomaGUNE) for support with the SE measurements and for surface coatings, respectively, Damien Maurin (IBS) for producing recombinant CXCL12α, Rose-Laure Revel-Goyet, Françoise Lacroix and Jean-Philippe Kleman (IBS) for access to and support with the Microscope Platform, Nicole Thielens and Isabelle Bally (IBS) for access to and support from the SPR platform of the Partnership for Structural Biology in Grenoble, Jérôme Dejeu (DCM) for support with SPR experiments, and Pierre Labbé (DCM) for discussions. This work was supported by the Nanoscience Foundation Chair of Excellence Project "GAG2D", the NanoBio programme, the ICMG FR 2607, and LabEx ARCANE (ANR-11-LABX-0003-01).

Appendix A. Supplementary data

Supplementary data related to this article can be found online at http://dx.doi.org/10.1016/j.biomaterials.2014.07.017.

References

[1] Bernfield M, Götte M, Park PW, Reizes O, Fitzgerald ML, Lincecum J, et al. Functions of cell surface heparan sulfate proteoglycans. Annu Rev Biochem 1999;68:729–77.
[2] Cain SA, Baldock C, Gallagher J, Morgan A, Bax DV, Weiss AS, et al. Fibrillin-1 interactions with heparin. Implications for microfibril and elastic fiber assembly. J Biol Chem 2005;280:30526–37.
[3] Cain SA, Baldwin AK, Mahalingam Y, Raynal B, Jowitt TA, Shuttleworth CA, et al. Heparan sulfate regulates fibrillin-1 N- and C-terminal interactions. J Biol Chem 2008;283:27017–27.
[4] Baranova NS, Nilebäck E, Haller FM, Briggs DC, Svedhem S, Day AJ, et al. The inflammation-associated protein TSG-6 cross-links hyaluronan via hyaluronan-induced TSG-6 oligomers. J Biol Chem 2011;286:25675–86.
[5] Day AJ, De la Motte CA. Hyaluronan cross-linking: a protective mechanism in inflammation? Trends Immunol 2005;26:637–43.
[6] Attili S, Richter RP. Self-assembly and elasticity of hierarchical proteoglycan-hyaluronan brushes. Soft Matter 2013;9:10473–83.
[7] Lee GM, Johnstone B, Jacobson K, Caterson B. The dynamic structure of the pericellular matrix on living cells. J Cell Biol 1993;123:1899–907.
[8] Knudson W, Knudson CB. Assembly of a chondrocyte-like pericellular matrix on non-chondrogenic cells. Role of the cell surface hyaluronan receptors in the assembly of a pericellular matrix. J Cell Sci 1991;99(Pt 2):227–35.
[9] Laguri C, Sadir R, Rueda P, Baleux F, Gans P, Arenzana-Seisdedos F, et al. The novel CXCL12γ isoform encodes an unstructured cationic domain which regulates bioactivity and interaction with both glycosaminoglycans and CXCR4. PLoS One 2007;2:e1110.
[10] Johnson Z, Proudfoot AE, Handel TM. Interaction of chemokines and glycosaminoglycans: a new twist in the regulation of chemokine function with opportunities for therapeutic intervention. Cytokine Growth Factor Rev 2005;16:625–36.
[11] Duchesne L, Octeau V, Bearon RN, Beckett A, Prior IA, Lounis B, et al. Transport of fibroblast growth factor 2 in the pericellular matrix is controlled by the spatial distribution of its binding sites in heparan sulfate. PLoS Biol 2012;10:e1001361.
[12] Rueda P, Balabanian K, Lagane B, Staropoli I, Chow K, Levoye A, et al. The CXCL12gamma chemokine displays unprecedented structural and functional properties that make it a paradigm of chemoattractant proteins. PLoS One 2008;3:e2543.
[13] Hesselgesser J, Liang M, Hoxie J, Greenberg M, Brass LF, Orsini MJ, et al. Identification and characterization of the CXCR4 chemokine receptor in human T cell lines: ligand binding, biological activity, and HIV-1 infectivity. J Immunol 1998;160:877–83.
[14] Weber M, Hauschild R, Schwarz J, Moussion C, De Vries I, Legler DF, et al. Interstitial dendritic cell guidance by haptotactic chemokine gradients. Science 2013;339:328–32.
[15] Altgärde N, Nilebäck E, De Battice L, Pashkuleva I, Reis RL, Becher J, et al. Probing the biofunctionality of biotinylated hyaluronan and chondroitin sulfate by hyaluronidase degradation and aggrecan interaction. Acta Biomater 2013;9:8158–66.
[16] Baranova NS, Foulcer SJ, Briggs DC, Tilakaratna V, Enghild JJ, Milner CM, et al. Inter-α-inhibitor impairs TSG-6-induced hyaluronan cross-linking. J Biol Chem 2013;288:29642–53.
[17] Richter RP, Hock KK, Burkhartsmeyer J, Boehm H, Bingen P, Wang G, et al. Membrane-grafted hyaluronan films: a well-defined model system of glycoconjugate cell coats. J Am Chem Soc 2007;129:5306–7.
[18] Wolny PM, Banerji S, Gounou C, Brisson AR, Day AJ, Jackson DG, et al. Analysis of CD44-hyaluronan interactions in an artificial membrane system: insights into the distinct binding properties of high and low molecular weight hyaluronan. J Biol Chem 2010;285:30170–80.
[19] Reviakine I, Johannsmann D, Richter RP. Hearing what you cannot see and visualizing what you hear: interpreting quartz crystal microbalance data from solvated interfaces. Anal Chem 2011;83:8838–48.
[20] Richter R, Rodenhausen K, Eisele NB, Schubert M. Coupling spectroscopic ellipsometry and quartz crystal microbalance to study organic films at the solid-liquid interface. In: Hinrichs K, Eichhorn K-J, editors. Ellipsometry of functional organic surfaces and films. Berlin: Springer; 2014. pp. 223–48.
[21] Laguri C, Sapay N, Simorre J-P, Brutscher B, Imberty A, Gans P, et al. 13C-labeled heparan sulfate analogue as a tool to study protein/heparan sulfate interactions by NMR spectroscopy: application to the CXCL12α chemokine. J Am Chem Soc 2011;133:9642–5.
[22] Bleul CC, Wu L, Hoxie JA, Springer TA, Mackay CR. The HIV coreceptors CXCR4 and CCR5 are differentially expressed and regulated on human T lymphocytes. Proc Natl Acad Sci U S A 1997;94:1925–30.
[23] Nagasawa T, Hirota S, Tachibana K, Takakura N, Nishikawa S, Kitamura Y, et al. Defects of B-cell lymphopoiesis and bone-marrow myelopoiesis in mice lacking the CXC chemokine PBSF/SDF-1. Nature 1996;382:635–8.
[24] Massena S, Christoffersson G, Hjertstrom E, Zcharia E, Vlodavsky I, Ausmees N, et al. A chemotactic gradient sequestered on endothelial heparan sulfate induces directional intraluminal crawling of neutrophils. Blood 2010;116:1924–31.
[25] Lortat-Jacob H. The molecular basis and functional implications of chemokine interactions with heparan sulphate. Curr Opin Struct Biol 2009;19:543–8.
[26] Mulloy B, Gee C, Wheeler SF, Wait R, Gray E, Barrowcliffe TW. Molecular weight measurements of low molecular weight heparins by gel permeation chromatography. Thromb Haemost 1997;77:668–74.
[27] Richter R, Mukhopadhyay A, Brisson A. Pathways of lipid vesicle deposition on solid surfaces: a combined QCM-D and AFM study. Biophys J 2003;85:3035–47.
[28] Eisele NB, Frey S, Piehler J, Görlich D, Richter RP. Ultrathin nucleoporin phenylalanine-glycine repeat films and their interaction with nuclear transport receptors. EMBO Rep 2010;11:366–72.
[29] Domack A, Prucker O, Ruhe J, Johannsmann D. Swelling of a polymer brush probed with a quartz crystal resonator. Phys Rev E 1997;56:680–9.
[30] Johannsmann D, Reviakine I, Rojas E, Gallego M. Effect of sample heterogeneity on the interpretation of QCM(-D) data: comparison of combined quartz crystal microbalance/atomic force microscopy measurements with finite element method modeling. Anal Chem 2008;80:8891–9.
[31] D. Johannsmann. http://www2.pc.tu-clausthal.de/dj/software_en.shtml. n.d.
[32] Eisele NB, Andersson FI, Frey S, Richter RP. Viscoelasticity of thin biomolecular films: a case study on nucleoporin phenylalanine-glycine repeats grafted to a histidine-tag capturing QCM-D sensor. Biomacromolecules 2012;13:2322–32.
[33] Dubacheva GV, Curk T, Mognetti BM, Auzély-Velty R, Frenkel D, Richter RP. Superselective targeting using multivalent polymers. J Am Chem Soc 2014;136:1722–5.
[34] Mobley JL, Ennis E, Shimizu Y. Differential activation-dependent regulation of integrin function in cultured human T-leukemic cell lines. Blood 1994;83:1039–50.
[35] Wolny PM, Spatz JP, Richter RP. On the adsorption behavior of biotin-binding proteins on gold and silica. Langmuir 2010;26:1029–34.
[36] Sarrazin S, Lamanna WC, Esko JD. Heparan sulfate proteoglycans. Cold Spring Harb Perspect Biol 2011;3:a004952.
[37] Richter RP, Brisson A. Characterization of lipid bilayers and protein assemblies supported on rough surfaces by atomic force microscopy. Langmuir 2003;19:1632–40.
[38] Horton MR, Manley S, Arevalo SR, Lobkovsky AE, Gast AP. Crystalline protein domains and lipid bilayer vesicle shape transformations. J Phys Chem B 2007;111:880–5.

[39] Frey W, Schief WR, Vogel V. Two-dimensional crystallization of streptavidin studied by quantitative Brewster angle microscopy. Langmuir 1996;12:1312–20.
[40] Richter RP, Bérat R, Brisson AR. Formation of solid-supported lipid bilayers: an integrated view. Langmuir 2006;22:3497–505.
[41] Bingen P, Wang G, Steinmetz NF, Rodahl M, Richter RP. Solvation effects in the quartz crystal microbalance with dissipation monitoring response to biomolecular adsorption. A phenomenological approach. Anal Chem 2008;80:8880–90.
[42] Hermens WT, Benes M, Richter R, Speijer H. Effects of flow on solute exchange between fluids and supported biosurfaces. Biotechnol Appl Biochem 2004;39:277–84.
[43] Zhang Z, Xie J, Liu H, Liu J, Linhardt RJ. Quantification of heparan sulfate disaccharides using ion-pairing reversed-phase microflow high-performance liquid chromatography with electrospray ionization trap mass spectrometry. Anal Chem 2009;81:4349–55.
[44] Roussille L, Brotons G, Ballut L, Louarn G, Ausserré D, Ricard-Blum S. Surface characterization and efficiency of a matrix-free and flat carboxylated gold sensor chip for surface plasmon resonance (SPR). Anal Bioanal Chem 2011;401:1601–17.
[45] Fermas S, Gonnet F, Sutton A, Charnaux N, Mulloy B, Du Y, et al. Sulfated oligosaccharides (heparin and fucoidan) binding and dimerization of stromal cell-derived factor-1 (SDF-1/CXCL 12) are coupled as evidenced by affinity CE-MS analysis. Glycobiology 2008;18:1054–64.
[46] Murphy JW, Cho Y, Sachpatzidis A, Fan C, Hodsdon ME, Lolis E. Structural and functional basis of CXCL12 (stromal cell-derived factor-1α) binding to heparin. J Biol Chem 2006;282:10018–27.
[47] Sadir R, Baleux F, Grosdidier A, Imberty A, Lortat-Jacob H. Characterization of the stromal cell-derived factor-1α-heparin complex. J Biol Chem 2001;276:8288–96.
[48] Soriano A, Martínez C, García F, Plana M, Palou E, Lejeune M, et al. Plasma stromal cell-derived factor (SDF)-1 levels, SDF1-3'A genotype, and expression of CXCR4 on T lymphocytes: their impact on resistance to human immunodeficiency virus type 1 infection and its progression. J Infect Dis 2002;186:922–31.
[49] Ganju RK, Brubaker SA, Meyer J, Dutt P, Yang Y, Qin S, et al. The alpha-chemokine, stromal cell-derived factor-1alpha, binds to the transmembrane G-protein-coupled CXCR-4 receptor and activates multiple signal transduction pathways. J Biol Chem 1998;273:23169–75.
[50] Sadir R, Imberty A, Baleux F, Lortat-Jacob H. Heparan sulfate/heparin oligosaccharides protect stromal cell-derived factor-1 (SDF-1)/CXCL12 against proteolysis induced by CD26/dipeptidyl peptidase IV. J Biol Chem 2004;279:43854–60.
[51] Hogg N, Laschinger M, Giles K, McDowall A. T-cell integrins: more than just sticking points. J Cell Sci 2003;116:4695–705.
[52] Yang Y, Jun CD, Liu JH, Zhang R, Joachimiak A, Springer TA, et al. Structural basis for dimerization of ICAM-1 on the cell surface. Mol Cell 2003;14:269–76.
[53] Deisenhofer J. Crystallographic refinement and atomic models of a human Fc fragment and its complex with fragment B of protein A from Staphylococcus aureus at 2.9- and 2.8 Å resolution. Biochemistry 1981;20:2361–70.
[54] Semmrich M, Smith A, Feterowski C, Beer S, Engelhardt B, Busch DH, et al. Importance of integrin LFA-1 deactivation for the generation of immune responses. J Exp Med 2005;201:1987–98.
[55] Azcutia V, Routledge M, Williams MR, Newton G, Frazier WA, Manica A, et al. CD47 plays a critical role in T-cell recruitment by regulation of LFA-1 and VLA-4 integrin adhesive functions. Mol Biol Cell 2013;24:3358–68.
[56] Reichel A, Schaible D, Al Furoukh N, Cohen M, Schreiber G, Piehler J. Noncovalent, site-specific biotinylation of histidine-tagged proteins. Anal Chem 2007;79:8590–600.
[57] Nisnevitch M, Firer MA. The solid phase in affinity chromatography: strategies for antibody attachment. J Biochem Biophys Methods 2001;49:467–80.
[58] Cha T, Guo A, Zhu X-Y. Enzymatic activity on a chip: the critical role of protein orientation. Proteomics 2005;5:416–9.
[59] Chevalier S, Cuestas-Ayllon C, Grazu V, Luna M, Feracci H, De la Fuente JM. Creating biomimetic surfaces through covalent and oriented binding of proteins. Langmuir 2010;26:14707–15.
[60] Murphy JW, Yuan H, Kong Y, Xiong Y, Lolis EJ. Heterologous quaternary structure of CXCL12 and its relationship to the CC chemokine family. Proteins 2009;78:1331–7.
[61] Schumann K, Lämmermann T, Bruckner M, Legler DF, Polleux J, Spatz JP, et al. Immobilized chemokine fields and soluble chemokine gradients cooperatively shape migration patterns of dendritic cells. Immunity 2010;32:703–13.
[62] Laguri C, Arenzana-Seisdedos F, Lortat-Jacob H. Relationships between glycosaminoglycan and receptor binding sites in chemokines-the CXCL12 example. Carbohydr Res 2008;343:2018–23.
[63] Ray P, Lewin SA, Mihalko LA, Lesher-Perez S-C, Takayama S, Luker KE, et al. Secreted CXCL12 (SDF-1) forms dimers under physiological conditions. Biochem J 2012;442:433–42.
[64] Ziarek JJ, Getschman AE, Butler SJ, Taleski D, Stephens B, Kufareva I, et al. Sulfopeptide probes of the CXCR4/CXCL12 interface reveal oligomer-specific contacts and chemokine allostery. ACS Chem Biol 2013;8:1955–63.
[65] Veldkamp CT, Seibert C, Peterson FC, De la Cruz NB, Haugner 3rd JC, Basnet H, et al. Structural basis of CXCR4 sulfotyrosine recognition by the chemokine SDF-1/CXCL12. Sci Signal 2008;1:ra4.
[66] Bargatze RF, Butcher EC. Rapid G protein-regulated activation event involved in lymphocyte binding to high endothelial venules. J Exp Med 1993;178:367–72.
[67] Von Andrian UH, Mackay CR. T-cell function and migration. Two sides of the same coin. N Engl J Med 2000;343:1020–34.
[68] Weber KS, Ostermann G, Zernecke A, Schröder A, Klickstein LB, Weber C. Dual role of H-Ras in regulation of lymphocyte function antigen-1 activity by stromal cell-derived factor-1alpha: implications for leukocyte transmigration. Mol Biol Cell 2001;12:3074–86.
[69] Rueda P, Richart A, Récalde A, Gasse P, Vilar J, Guérin C, et al. Homeostatic and tissue reparation defaults in mice carrying selective genetic invalidation of CXCL12/proteoglycan interactions. Circulation 2012;126:1882–95.

SUPPLEMENTARY INFORMATION

Well-defined biomimetic surfaces to characterize glycosaminoglycan-mediated interactions on the molecular, supramolecular and cellular levels

Elisa Migliorini, Dhruv Thakar, Rabia Sadir, Tino Pleiner, Françoise Baleux, Hugues Lortat-Jacob, Liliane Coche-Guerente, and Ralf P. Richter

SUPPLEMENTARY FIGURES

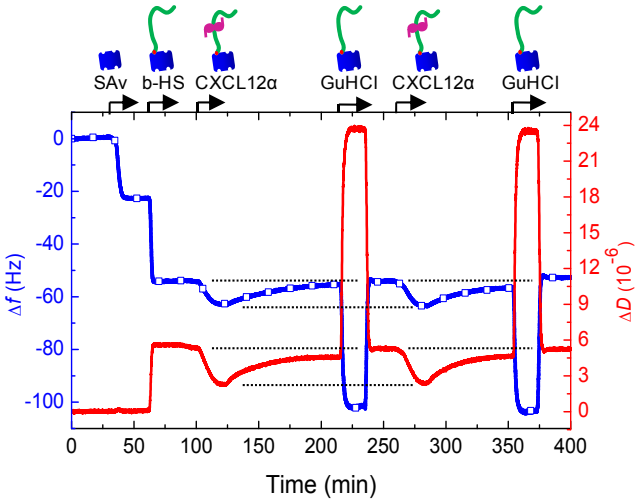

Figure S1. Regeneration of HS films by guanidine hydrochloride (GuHCl). QCM-D (Δ*f* – *blue lines with square symbols*, Δ*D* – *red lines*) was used to follow the surface functionalization on a gold-supported OEG monolayer and the effect of GuHCl on the model surface. Start and duration of each incubation step with different samples are indicated by an arrow; during all other times, the surface was exposed to working buffer. The assembly of the model surfaces, including loading with CXCL12α, was performed as in Fig. 2*A*. Upon exposure of the CXCL12α-loaded surface to 2 M GuHCl (GuHCl (Sigma Aldrich) was dissolved at 8 M in ultrapure water and then diluted in working buffer to the desired concentration), frequency and dissipation shifts recovered the values for a virgin HS film, indicating (i) total release of the protein, and (ii) that the HS film itself is not significantly affected by GuHCl. A second injection of CXCL12α generated the same shifts in frequency and dissipation as the first one, confirming that the surfaces can be effectively regenerated by 2 M GuHCl. *Horizontal black dashed lines* are provided to facilitate comparison of data at different times. The large changes in Δ*f* and Δ*D* observed during incubation with GuHCl are predominantly due to changes in the viscosity and density of the bulk solution owing to the presence of GuHCl and thus unrelated to surface processes.

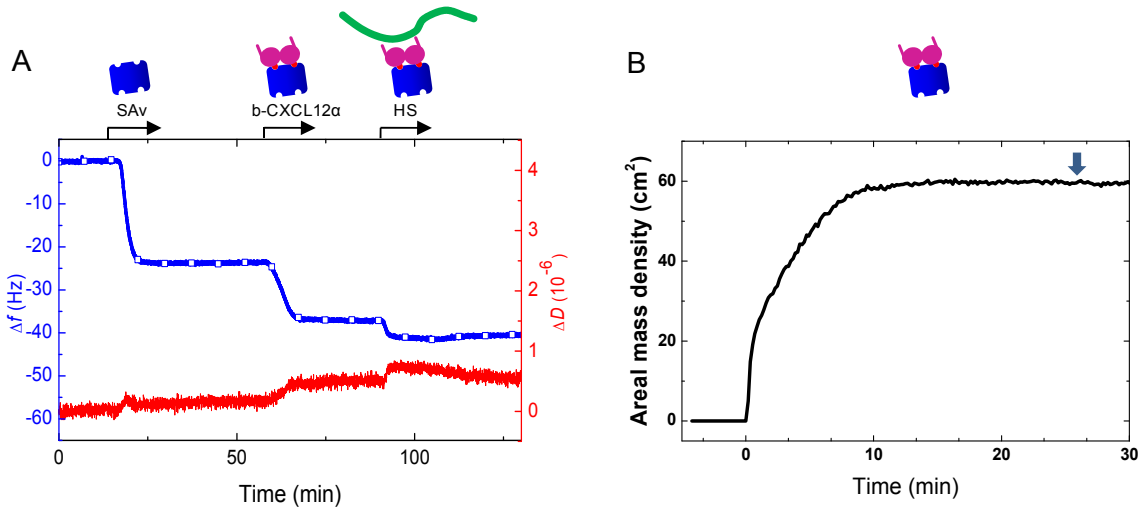

Figure S2. Assembly of surfaces presenting b-CXCL12α. (*A*) Functionalization of a gold-supported OEG monolayer was followed by QCM-D (Δ*f* – *blue lines with square symbols*, Δ*D* – *red lines*). Start and duration of incubation steps with different samples are indicated by an arrow; during all other times, the surface was exposed to working buffer. SAv was incubated at 20 µg/mL, b-CXCL12α at 5 µg/mL and HS at 50 µg/mL. b-CXCL12α bound stably with final shifts of Δf = -13 ± 0.5 Hz and $\Delta D = 0.4 \pm 0.1 \times 10^{-6}$. Assuming a density of 1.2 g/cm^3 for the b-CXCL12α film with trapped solvent, the frequency shift would correspond to a film thickness of approximately 2.0 nm, slightly lower than the dimensions of CXCL12α monomers (2.7 to 4 nm, depending on the exact orientation [1]). The QCM-D response is hence consistent with the formation of a monolayer of monomeric CXCL12α. HS (without biotin) bound readily to the CXCL12α monolayer, but not to a virgin SAv monolayer (Fig. 2*C*), confirming that the accessibility of the HS binding site was not obstructed by the immobilisation of CXCL12α through the C-terminal biotin. HS binding is partially reversible, as previously observed for CXCL12α bound to b-HS films (Fig. 2*A-B*). (*B*) Formation of a b-CXCL12α monolayer followed by SE. The surface was prepared as in *A*; incubation of b-CXCL12α started at 0 min, and the start of rinsing in working buffer is indicated by an arrow. From the molecular weights and maximal surface densities of SAv (60 kDa; 235 ng/cm^2, see Table 1) and b-CXCL12α (8.6 kDa; 59 ng/cm^2), we calculate a binding stoichiometry of 1.8. This confirms that biomolecules can be immobilized with a maximal stoichiometry close to two, provided they are small enough to avoid packing constraints, consistent with every immobilized SAv molecule exposing two binding sites as expected from the design of our immobilization platforms.

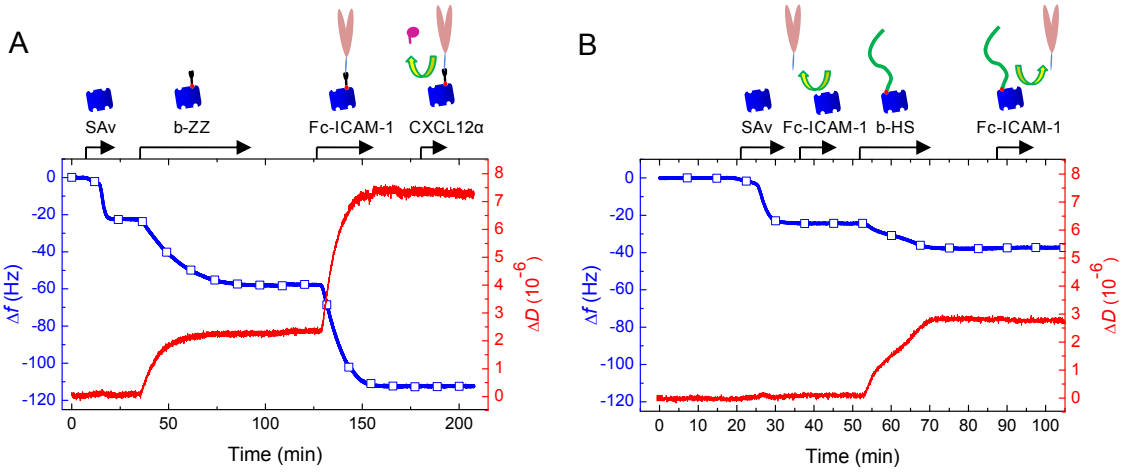

Figure S3. Assembly of surfaces presenting ICAM-1. Fc-ICAM-1 was immobilized in an oriented manner through a biotinylated linker molecule with a ZZ domain (b-ZZ) which recognizes the Fc-tag on ICAM-1. Functionalization of a gold-supported OEG monolayer was followed by QCM-D (Δ*f* – *blue lines with square symbols*, Δ*D* – *red lines*). Start and duration of incubation steps with different samples are indicated by an arrow; during all other times, the surface was exposed to working buffer. SAv was incubated as in Fig. 2*A*, b-ZZ at 0.05 µM, Fc-ICAM-1 at 0.2 µM, CXCL12α at 5 µg/mL and b-HS at 1 µg/mL. (*A*) The binding curves for b-ZZ and Fc-ICAM-1 saturated and binding was stable upon rinsing in working buffer, indicating formation of stable monolayers. The frequency shift at saturation for b-ZZ (-35.5 Hz) corresponds to a film thickness of approximately 6 nm (assuming a film density of 1.2 g/cm^3), consistent with the hydrodynamic diameter (7.1 nm; measured by dynmic light scattering) of b-ZZ. The lack of response for CXCL12α confirmed that ICAM-1 did not compromise the inertness of the surface against non-specific binding of chemokines. (*B*) In the absence of b-ZZ, Fc-ICAM-1 did not bind to a bare SAv monolayer nor to a SAv monolayer presenting b-HS (at approximately half-maximal coverage), confirming that Fc-ICAM-1 immobilization through b-ZZ is specific.

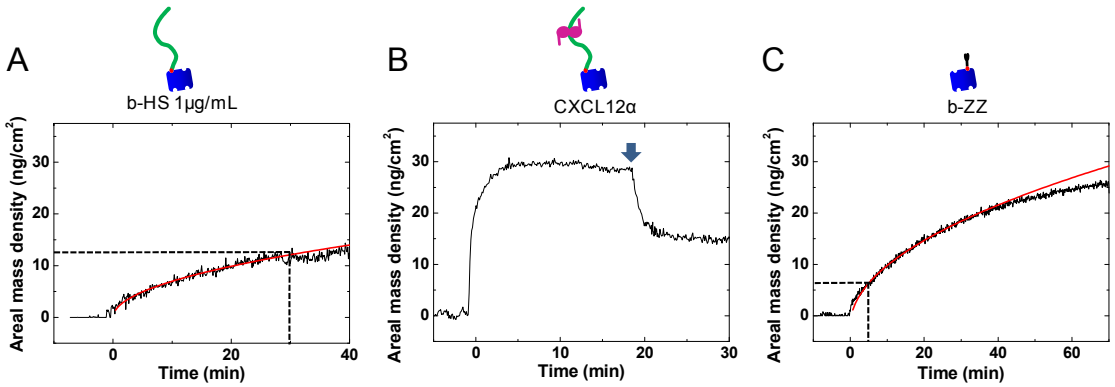

Figure S4. Tuning of biomolecular surface densities on SAv monolayers. Adsorption was followed by SE; each incubation step started at 0 min; the start of rinsing in working buffer is indicated by an arrow. (*A*) Adsorption of b-HS at a concentration of 1 µg/mL from still solution to a SAv-coated OEG monolayer. Only initial binding is shown, as adsorption did not reach saturation within reasonable times at such a low solution concentration; b-HS surface densities can be tuned by interrupting incubation at desired time points. For example, to create the surfaces used for Fig. 6*B*-*C*, b-HS was incubated for 30 min (indicated with *dotted lines*), reaching an areal mass density of 12.7 ± 1.3 ng/cm^2 (average value over 4 independent measurements, not shown), corresponding to 35 ± 5% of maximal coverage. (*B*) Representative data for the adsorption of CXCL12α at a concentration of 5 µg/mL on such a low density b-HS film. At equilibrium, the areal mass density of CXCL12α was 35 ± 4 ng/cm^2. (*C*) Adsorption of b-ZZ at a concentration of 0.05 µM from still solution to a SAv monolayer. Only initial binding is shown, as adsorption did not reach saturation within reasonable times at such a low solution concentration; b-ZZ coverage at saturation was found to be around 118.6 ± 0.2 ng/cm^2 using higher b-ZZ concentrations in solution (data not shown). To reach the b-ZZ surface density of 7 ng/cm^2, desired for Fig. 6*B*-*C* and corresponding to 6% of maximal coverage, b-ZZ was incubated for 5 min (indicated with *dotted lines*). Note that binding of b-HS and b-ZZ scales with the square root of incubation time (*red curves* are fits with square-root dependence) provided that the surface density is sufficiently low. The square-root dependence is expected for mass-transport limited binding, and indicates that surface coverages can be tuned by varying the incubation time (with square-root dependence, as shown) and/or the incubation concentration (with linear dependence, not shown). See ref. [2] for details.

SUPPLEMENTARY REFERENCES

1. Veldkamp CT, Ziarek JJ, Su J, Basnet H, Lennertz R, Weiner JJ, et al. Monomeric structure of the cardioprotective chemokine SDF-1/CXCL12. Protein Sci 2009;18:1359–69.
2. Hermens WT, Benes M, Richter R, Speijer H. Effects of flow on solute exchange between fluids and supported biosurfaces. Biotechnol Appl Biochem 2004;39:277–84.

IV. Cytokines and growth factors cross-link heparan sulfate

This chapter is submitted as a manuscript and is under revision in Open Biology as:

Cytokines and growth factors cross-link heparan sulfate

Elisa Migliorini[1,2,3], Dhruv Thakar[1,2], Jens Kühnle[4], Rabia Sadir[1,2,5], Douglas P. Dyer[6], Yong Li[7], Changye Sun[7], Brian F. Volkman[8], Tracy M. Handel[6], Liliane Coche-Guerente[1,2], David G. Fernig[7], Hugues Lortat-Jacob[1,2,5], and Ralf P. Richter[1,2,3,9]

Université Grenoble Alpes[1] and the CNRS[2], Departement de Chimie Moléculaire (DCM), Grenoble, France; the CIC biomaGUNE[3], San Sebastian, Spain; the Department of Biophysical Chemistry, University of Heidelberg[4], Heidelberg, Germany; the Université Grenoble Alpes[1], the CNRS[2] and the CEA[5], Institut de Biologie Structurale (IBS), Grenoble, France; the University of California, San Diego[6], the Skaggs School of Pharmacy and Pharmaceutical Sciences, La Jolla, CA, USA; the Department of Biochemistry, Institute of Integrative Biology[7], University of Liverpool, Liverpool, UK; Department of Biochemistry, Medical College of Wisconsin[8], Milwaukee, WI, USA; and the Max Planck Institute for Intelligent Systems[9], Stuttgart, Germany

Significance: We present here the application of the biomimetic GAG-presenting surfaces (described in Chapter III) to the analysis of supramolecular HS-protein interactions. We demonstrate that chemokines and growth factors cross-link HS chains, and that this cross-linking ability is a common feature among these proteins and depends on the architecture of the protein's HS binding sites. This finding suggests that the functions of chemokines and growth factors may not simply be confined to the activation of cognate cellular receptors.

My contribution: I co-designed research (together with Elisa Migliorini, Liliane Coche-Guerente and Ralf P. Richter) and participated in data analysis. I performed the QCM-D measurements with CXCL12α and CXCL12γ. I performed the synthesis and QCM-D measurements of b-HS oligosaccharides. I performed the QTM-analysis of QCM-D measurements for the determination of film thickness. I contributed to the preparation of figures.

Résumé

Le glycosaminoglycane, héparane sulfate (HS), présent à la surface de la plupart des cellules et omniprésent dans la matrice extracellulaire, se lie à de nombreuses molécules de signalisation extracellulaires solubles tels que les chimiokines et les facteurs de croissance, et régule la fonction de transport et la fonction effectrice. Cependant, on ignore si ces protéines liées au HS peuvent affecter la structure à long terme du HS. Pour approfondir la question, nous avons mis en oeuvre un système supramoléculaire modèle, dans lequel les chaînes de HS sont greffées sur une plateforme de streptavidine adsorbée sur une monocouche d'oligoéthylène glycol ou sur une bicouche lipidique supportée. Ces surfaces fonctionnelles de HS qui miment les matrices péricellulaires ou extracellulaires riches en HS ont été caractérisées par des techniques biophysiques comme la microbalance à quartz (QCM-D) et la redistribution de fluorescence après photoblanchiment (FRAP). Nous sommes en mesure de contrôler et de caractériser la présentation supramoléculaire des chaînes de HS - leur densité locale, leur orientation, leur conformation et leur mobilité latérale - et leur interaction avec des protéines. La chimiokine CXCL12α (ou SDF-1α) rigidifie le film de HS, cet effet est dû à la réticulation des chaînes de HS induite par les protéines. Des mesures complémentaires avec des mutants de la chimiokine CXCL12α et l'isoforme CXCL12γ ont permis de mieux comprendre le mécanisme moléculaire sous-jacent à la réticulation. Le facteur de croissance des fibroblastes 2 (FGF-2), qui possède trois sites de liaison au HS, conduit également à une réticulation du HS, mais ce n'est pas le cas du FGF-9, qui possède un seul site de liaison. Sur la base de ces données, nous proposons que la capacité à réticuler HS est une caractéristique générique de nombreuses cytokines et facteurs de croissance, qui dépend de l'architecture de leurs sites de liaison sur les HS. La possibilité de changer l'organisation de la matrice et les propriétés physico-chimiques (par exemple la perméabilité et la rigidification) implique que les fonctions des cytokines et des facteurs de croissance ne peuvent pas simplement être confinés à l'activation des récepteurs cellulaires apparentés.

Cytokines and Growth Factors Cross-link Heparan Sulfate

*Elisa Migliorini[1,2,3], Dhruv Thakar[1,2], Jens Kühnle[4], Rabia Sadir[5,6,7], Douglas P. Dyer[8], Yong Li[9], Changye Sun[9], Brian F. Volkman[10], Tracy M. Handel[8], Liliane Coche-Guerente[1,2], David G. Fernig[9], Hugues Lortat-Jacob[5,6,7], and Ralf P. Richter[1,2,3,11,]**

[1] Université Grenoble Alpes, Departement de Chimie Moléculaire (DCM), Grenoble, France

[2] CNRS, DCM, Grenoble, France

[3] CIC biomaGUNE, San Sebastian, Spain

[4] Department of Biophysical Chemistry, University of Heidelberg, Heidelberg, Germany

[5] Université Grenoble Alpes[1], Institut de Biologie Structurale (IBS), Grenoble, France

[6] CNRS, IBS, Grenoble, France

[7] CEA, IBS, Grenoble, France

[8] University of California, San Diego, Skaggs School of Pharmacy and Pharmaceutical Sciences, La Jolla, CA, USA

[9] Department of Biochemistry, Institute of Integrative Biology, University of Liverpool, Liverpool, UK

[10] Department of Biochemistry, Medical College of Wisconsin, Milwaukee, WI, USA

[11] Max Planck Institute for Intelligent Systems, Stuttgart, Germany

* Corresponding author: Ralf Richter, CIC biomaGUNE, Paseo Miramon 182, 20009 San Sebastian, Spain; phone: +34 943 00 53 29; fax: +34 943 00 53 15; email: rrichter@cicbiomagune.es

Abstract. The glycosaminoglycan heparan sulfate (HS), present at the surface of most cells and ubiquitous in extracellular matrix, binds many soluble extracellular signaling molecules such as chemokines and growth factors, and regulates their transport and effector functions. It is, however, unknown whether upon binding HS these proteins can affect the long-range structure of HS. To test this idea, we interrogated a supramolecular model system, in which HS chains grafted to streptavidin-functionalized oligoethylene glycol monolayers or supported lipid bilayers mimic the HS-rich pericellular or extracellular matrix with the biophysical techniques quartz crystal microbalance (QCM-D) and fluorescence recovery after photobleaching (FRAP). We were able to control and characterize the supramolecular presentation of HS chains - their local density, orientation, conformation and lateral mobility - and their interaction with proteins. The chemokine CXCL12α (or SDF-1α) rigidified the HS film, and this effect was due to protein-mediated cross-linking of HS chains. Complementary measurements with CXCL12α mutants and the CXCL12γ isoform provided insight into the molecular mechanism underlying cross-linking. Fibroblast growth factor 2 (FGF-2), which has three HS binding sites, was also found to cross-link HS, but FGF-9, which has just one binding site, did not. Based on these data, we propose that the ability to cross-link HS is a generic feature of many cytokines and growth factors, which depends on the architecture of their HS binding sites. The ability to change matrix organization and physico-chemical properties (e.g. permeability and rigidification) implies that the functions of cytokines and growth factors may not simply be confined to the activation of cognate cellular receptors.

Keywords. heparan sulfate; glycosaminoglycan; extracellular matrix; chemokine; growth factor; cytokine

Background

Heparan sulfate (HS)[1] is a linear polysaccharide made of variably sulfated repeating disaccharide units. Attached to extracellular matrix or cell-surface proteins (HSPGs), it pervades the intercellular space of many tissues and the periphery of virtually all mammalian cells. HS binds many soluble extracellular signaling molecules such as growth factors and chemokines, and these interactions are known to be important for various physiological and pathological processes (1–4) including organogenesis and growth control (5, 6), cell adhesion (7) and signalling (8), inflammation (9), tumour development (10), and interactions with pathogens (11).

Past studies have revealed how HS-protein interactions determine protein function. For example, HS (as well as the highly sulfated analogue heparin) plays a role in the specificity and control of the engagement of fibroblast growth factors (FGFs) with their cell-surface receptors, through the formation of stable ternary complexes (12), thus modulating cell signaling. The binding of chemokines to HS in the extracellular space, on the other hand, enables the formation of chemokine gradients (13), thus providing directional cues and guiding the migration of appropriate cells in the context of their inflammatory, developmental, and homeostatic functions.

In contrast, very little is known about the effect of signaling proteins on HS and HSPGs. HS chains are typically a few 10 nm in length (15) and, thus, possess multiple binding sites enabling simultaneous binding of several proteins. These interactions will influence the molecular structure of individual HS chains. Moreover, they may also profoundly affect the supramolecular organization of HS in the extracellular space. Such long-range effects have hitherto been difficult to test, due to the lack of appropriate structural and biochemical methods.

Here, we demonstrate that several soluble extracellular signaling proteins can effectively cross-link HS. To this end, we develop an *in vitro* binding assay that is based on films of surface-grafted HS chains, as a well-defined model of HS-rich pericellular or extracellular matrix (7) and a combination of two biophysical analysis techniques: quartz crystal microbalance (QCM-D) and fluorescence recovery after photobleaching (FRAP). These techniques provide insight into the binding of proteins to the HS film, and the concomitant changes in film morphology and HS chain mobility. Through the analysis of a set of proteins and their mutants - including chemokines, cytokines and growth factors - with this assay, we identify molecular features that determine the HS cross-linking

[1] The abbreviations used are: HS, heparan sulfate; b-HS, biotinylated HS; SDF-1/CXCL12, stromal cell-derived factor 1; GAG, glycosaminoglycan; OEG, oligo(ethylene glycol); SLB, supported lipid bilayer; SAv, streptavidin; fl-SAv, fluorescent streptavidin; FGF, fibroblast growth factor; IFN, interferon; dp, degree of polymerization; QCM-D, quartz crystal microbalance; FRAP, fluorescence recovery after photobleaching; NMR, nuclear magnetic resonance.

propensity of extracellular signaling proteins. The ability to cross-link, and thus to change matrix organization and physico-chemical properties implies that the functions of these proteins may not simply be confined to the activation of cognate cellular receptors, and we discuss possible physiological implications.

Materials and Methods

Buffer. The working buffer used for all measurements contained 10 mM HEPES (Fisher, Illkirch, France) at pH 7.4 and 150 mM NaCl (Sigma-Aldrich, Saint-Quentin Fallavier, France).

Heparan sulfate and proteins. HS polysaccharide derived from porcine intestinal mucosa (Celsus Laboratories, Cincinnati, OH, USA) was found to have an average molecular weight of 12 kDa and a polydispersity of 1.6 (16). Size-uniform HS oligosaccharides from hexasaccharide (dp6) to dodecasaccharide (dp12) were derived from this source, as previously described (17). HS was conjugated with biotin through an oligoethylene glycol (OEG) linker of approximately 1 nm length, site-specifically attached to the reducing end by oxime ligation. In contrast to the conventionally used hydrazone ligation, oxime ligation produces conjugates that are stable for many weeks in aqueous solution (18). HS conjugates were stored at a concentration of 10 mg/mL at -20°C until further use.

Recombinant CXCL12α (amino acids 1 to 68; 8.1 kDa) was prepared as previously described (20). A truncated CXCL12α construct (amino acids 5 to 67; 7.4 kDa (21)) was produced by solid-phase peptide synthesis, as previously reported (4, 22). A I55C/L58C mutant of CXCL12α with reduced dimerization propensity (‘partial monomer’) was prepared as previously described (23). A L36C/A65C mutant of CXCL12α in which the introduced cysteines promote the formation of dimers (‘locked dimer’) was prepared, as described in Veldkamp et al. (24). The cDNA of murine CXCL12γ was inserted in a pET-17b vector (Novagen, Merck Chemical Ltd., Nottingham, UK) between NdeI and SpeI restriction sites, checked by DNA sequencing and the protein (11.6 kDa) was produced by recombinant expression in *E. coli* strain BL21 Star DE3, as previously reported (14). IFNγ (17 kDa) was produced by recombinant expression in *E. coli* strain BL21 Star DE3 using a pET-11a vector (Novagen), as previously reported (25). Recombinant FGF-2 (18 kDa) and FGF-9 (26 kDa) were obtained by expression in C41 *E. coli* cells using pET-14b and pET-M11 for vectors (Novagen), respectively, as described by Xu et al. (26).

Lyophilized streptavidin (SAv), fluorescently labeled SAv (fl-SAv; with atto565) and bovine serum albumin (BSA) were obtained from Sigma-Aldrich. All proteins were stored in working buffer at -20°C until further use. Thawed protein solutions were used within 5 days.

Surfaces and surface funtionalization with a biotin-displaying and otherwise inert background. QCM-D sensors with gold (QSX301) and silica (QSX303) coatings (Biolin

Scientific, Västra Frölunda, Sweden) were used as is. Glass cover slips (24 × 24 mm^2; Menzel-Gläser, Braunschweig, Germany) for FRAP assays were cleaned by immersion in freshly prepared piranha solution (i.e. a 1:3 (*v*/*v*) mixture of H_2O_2 (Fisher Scientific) and concentrated H_2SO_4 (Sigma-Aldrich)) for 1 h, rinsing with ultrapure water, and blow-drying with N_2. All substrates were exposed to UV/ozone (Jelight Company, CA, USA) for 10 min prior to use.

Gold surfaces were functionalized with biotin-displaying monolayers of oligo(ethylene glycol) (OEG) as previously described (7). Briefly, the gold-coated surfaces were immersed overnight in an ethanolic solution of OEG disulfide and biotinylated OEG thiol (Polypure, Oslo, Norway), at a total concentration of 1 mM and a molar ratio of thiol equivalents of 999:1.

Silica (for QCM-D) and glass (for FRAP) surfaces were functionalized with biotin-displaying supported lipid bilayers (SLBs) by the method of vesicle spreading, as described in detail elsewhere (27). Briefly, the surfaces were exposed for 30 min to small unilamellar vesicles, made from a mixture of dioleoylphosphatidylcholine (DOPC) and dioleoylphosphatidylethanolamine-CAP-biotin (DOPE-CAP-b) (Avanti Polar Lipids, Alabaster, AL, USA) at the desired molar ratio (99.5:0.5 or 95:5) at a total concentration of 50 µg/mL in working buffer supplemented with 2 mM $CaCl_2$ (VWR International, Leuven, Belgium).

Assembly of HS films. Biotin-displaying surfaces were further functionalized for studies of protein interactions with well-defined HS films, as described in detail earlier (7). Briefly, the surfaces were first exposed to SAv, to form a SAv monolayer, and then to b-HS, to form a molecular film of HS that is site-specifically attached through the reducing end to the surface. This mode of attachment avoids any perturbation of protein-HS interactions through chemical modifications along the HS chain. Sample concentrations and incubation times were chosen such that binding either saturates or equilibrates, unless otherwise stated.

Quartz crystal microbalance with dissipation monitoring (QCM-D). QCM-D measurements were performed, as previously described (7). QCM-D measures changes in frequency, Δf, and in dissipation, ΔD, of a quartz sensor upon interaction of molecules with its surface. Measurements were performed with a Q-Sense E4 system equipped with Flow Modules (Biolin Scientific) with a flow rate of typically 10 µL/min and at a working temperature of 24 °C. QCM-D data were collected at six overtones (n = 3, 5, 7, 9, 11, 13, corresponding to resonance frequencies of ~15, 25, 35, 45, 55, 65 MHz). For the sake of simplicity, only changes in dissipation and normalized frequency, $\Delta f = \Delta f_n/n$ of the third overtone (n = 3) are presented. Any other overtone would have provided comparable information.

A viscoelastic model (28), implemented in the software QTM (Diethelm Johannsmann, Clausthal University of Technology (29)), was used to quantify the

thickness *d* and visoelastic properties of HS films from QCM-D data. Details of the fitting procedure are described elsewhere (30). We parametrized viscoelastic properties in terms of the elastic and viscous compliances *J*' and *J*" at a reference frequency of *f* = 15 MHz (i.e. close to the resonance frequency at *n* = 3). *J*' and *J*" are measures for the softness of the film. The elastic compliance can also be estimated directly from the QCM-D responses for the film through the approximate relationship $\Delta D/(-\Delta f) = 4\pi n\eta_1\rho_1/\rho \times J'$, where η_l = 0.89 mPa·s and ρ_l = 1.0 g/cm^3 are the viscosity and density of the aqueous bulk solution, respectively, and $\rho \approx 1.0$ g/cm^3 is the film density (31).

Fluorescence recovery after photobleaching (FRAP). For FRAP assays, cleaned glass cover slips were attached, using a bi-component glue (Picodent, Wipperfürth, Germany), to a custom-built teflon holder, thus forming the bottom of 4 identical wells with a volume of 50 µL each. All surface functionalization steps were performed in still solution. To remove excess sample after each incubation step, the content was diluted by repeated addition of a 2-fold excess of working buffer and removal of excess liquid until the concentration of the solubilized sample, estimated from the extent of dilution, was below 10 ng/mL. Repeated aspiration and release ensured homogenization of the liquid volume at each dilution step. Care was taken to keep the substrates wet at all times.

FRAP measurements were performed with a confocal laser scanning microscope (LSM 700, Zeiss, Germany) using a laser with 555 nm wavelength, a plan-apochromat 63× / 1.4 oil immersion objective and a fully opened pinhole (1 mm diameter). fl-SAv, attached to biotin-displaying SLBs was used as a fluorophore to report on the lateral mobility of SAv-bound HS.

After acquiring 3 pre-bleach images, a circular region with the radius of 10 µm in the centre of the imaged area was bleached through exposure for ~20 seconds to high laser intensity; approximately 80% bleaching in the centre of the exposed area was achieved. The fluorescence recovery due to lateral diffusion of bleached and unbleached fl-SAv was monitored through acquisition of post-bleach images over a period of typically 10 min.

The images acquired using this protocol were then analyzed by 'time-resolved profile analysis', a custom-made algorithm (32) implemented in Matlab (MathWorks, MA, USA). Briefly, each post-bleach fluorescence image was first corrected for background fluorescence, spatial aberrations and intensity fluctuations and then radially averaged. The radial intensity profiles thus obtained were compared to numerical solutions of a diffusion equation, where the first post-bleach image defined the initial conditions for the diffusion process. A lateral diffusion model with one mobile fraction and one immobile fraction was found to reproduce our data well. This model has two independent fitting parameters, namely, the size and diffusion constant of the mobile fraction. These were computed through global minimization of the root-mean-square differences between numerical predictions and all post-bleach profiles.

Results

We tested the effect of several extracellular signaling molecules on HS model matrices, namely the α and γ isoforms of the chemokine CXCL12, the cytokine IFNγ, and the growth factors FGF-2 and FGF-9. These were selected based on their known affinity for HS and distinct structural features (Fig. 1). CXCL12α forms homodimers through the association of β-sheets upon binding to HS, with the known HS binding site being located at the interface between the two monomers (Fig. 1A). CXCL12γ is distinct from CXCL12α in that it features flexible C-terminal extensions that are also involved in HS binding (Fig. 1B). IFNγ is constitutively present as a homodimer which features a very extended HS binding surface on the flexible C-termini of the monomers (Fig. 1C). The FGFs are more compact. FGF-2 has three distinct HS binding sites (Fig. 1D) that are separated from each other by borders of negatively charged and hydrophobic residues. FGF-9, in contrast, features only one HS binding site (Fig. 1E). As HS matrix model, we employed films of HS chains grafted with the reducing end to a protein-repellant surface (Fig. 2A). QCM-D allows monitoring of HS film assembly and protein binding as well as analysis of film thickness and mechanical properties (Fig. 2). FRAP allows for the lateral mobility of HS chains to be probed (Fig. 3).

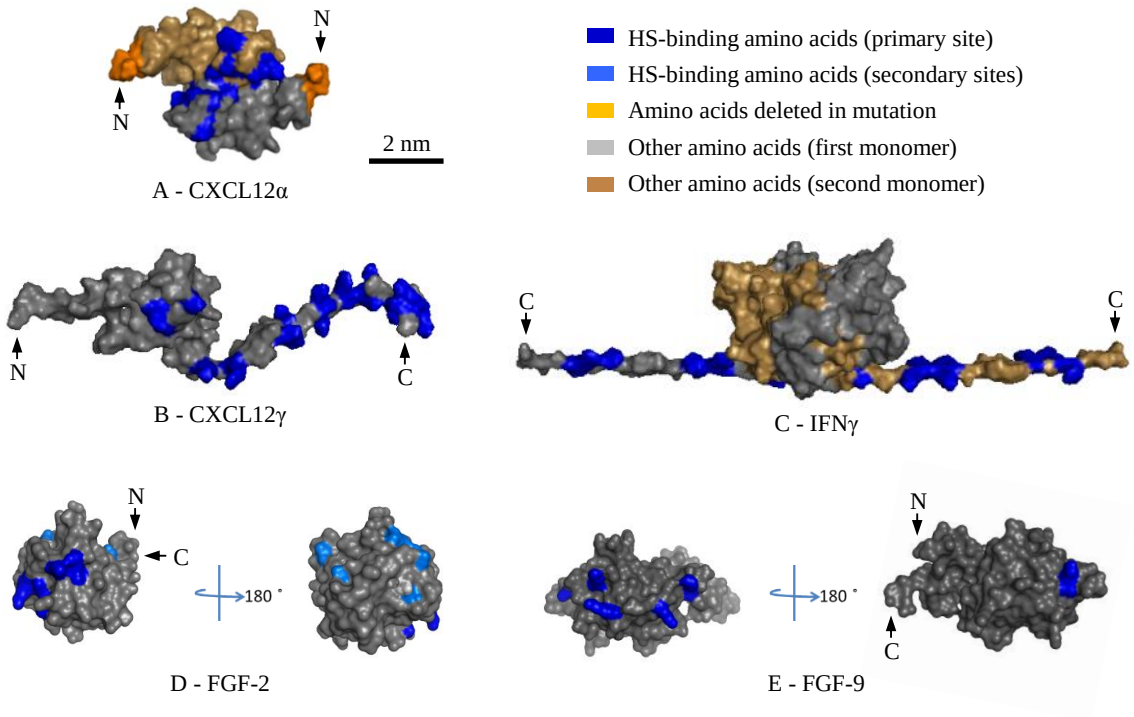

Figure 1. Structures of soluble extracellular signalling proteins used in this study. *Structures are surface plots, all drawn at the same scale (scale bar indicated in (A)). Amino acids known to contribute to primary and secondary HS-binding sites are shown in dark and light blue, respectively; the remaining protein surfaces are coloured in grey, or in light brown for the second monomer in the structures of homodimers; the position of selected N or C terminals are marked with an arrow. CXCL12α (A) is shown as a*

homodimer associated through β-sheets (PDB code: 1QG7, where missing residues were added as described in (17)) with its reported HS-binding amino acids (17, 22, 33) and the first four amino acids, lacking in the CXCL12α(5-67) mutant, indicated (orange). CXCL12γ (B) was constructed from a CXCL12α monomer and the additional 30 amino acid long N-termini modelled as previously reported (14). IFNγ (C; PDB code: 1HIG (34)) is shown as a homodimer with the C-termini (residues 120-143, absent in the structure) built as extended β-strands. FGF-2 (D; PDB code: 1FQ9 (55)) and FGF-9 (E; PDB code: 1IHK (35)) are shown as a monomers with their known HS-binding sites, i.e. three sites for FGF-2 (37) and a single, extended site for FGF-9 (26).

Design of HS model matrix. Our HS films present HS in an oriented manner and at controlled density (Fig. 2A) (7). Gold supports were first coated with a monolayer of oligo(ethylene glycol) (OEG) exposing terminal biotin groups at controlled surface density. A monolayer of streptavidin (SAv) was then formed and used to anchor HS through a biotin moiety that was conjugated to the GAG's reducing end (7). The SAv-on-OEG film inhibits non-specific protein binding to the surface, i.e. measured responses are exclusively due to specific interactions.

QCM-D was used to validate correct assembly of the model surface and to characterize the effect of protein binding on HS films. The QCM-D response is sensitive to the amount of adsorbed ligand (including coupled solvent), with a negative frequency shift Δf typically correlating with a mass increase, and to mechanical properties, as well as morphological features of the biomolecular film, typically reflected in the dissipation shift ΔD (31).

QCM-D responses upon sequential incubation of OEG monolayers with SAv and HS at saturation (Fig. 2B, curves without symbols; at 6 to 21 min and 46 to 61 min, respectively, as indicated by arrows on top of the graph) were consistent with the formation of a relatively rigid SAv monolayer (i.e. with Δf = -23 $\pm$ 1 Hz and a low dissipation shift, $\Delta D \leq 0.3 \times 10^{-6}$, at saturation) and a soft, hydrated HS layer (i.e. with Δf = -28.5 $\pm$ 1.0 Hz and a high dissipation shift, ΔD = 5.0 $\pm$ 0.2 $\times$ 10^{-6}, at saturation), respectively. As reported in our previous study (7), the frequency shift for such an HS film (henceforward called high-density HS film) corresponds to an areal mass density of 35.5 ± 2.2 ng/cm^2, and to a water content of 96.9 ± 0.5%. In this earlier work, we had also estimated the mean distance between adjacent HS anchor sites to be 5 nm, consistent with the dimensions of SAv, and the mean length of the surface-bound HS chains to be 20 monosaccharides (or 10 nm); in this regard, we note that the mean length of surface-bound b-HS chains is shorter than the mean length in the solution from which they were bound, because shorter chains bind preferentially (7). In essence these numbers indicate that, while there is plenty of space for small proteins to bind into the HS films, the pendant HS chains are long enough to make contact with their neighbors and cover the whole surface area.

Effect of CXCL12α binding on HS films. Exposure of the chemokine CXCL12α at a concentration of 0.64 µM to the high-density HS film generated a negative frequency shift (-9 ± 1 Hz; Fig. 2B, blue curve without symbols, 74 to 90 min), confirming CXCL12α binding. The concomittant change in dissipation was pronounced and negative (-3.8 ± 0.2 $\times$ 10^{-6}; Fig. 2B, red curve without symbols). Such a QCM-D response provides a strong indication that the chemokine rigidifies the HS film. Quantitative analysis of the QCM-D data through viscoelastic modelling revealed decreases in the elastic compliance *J*' and the viscous compliance *J*" upon CXCL12α binding (Fig. 2C). *J*' and *J*" are physical parameters (elastic and viscous contributions, respectively) related to film softness, and their decrease thus confirms film rigidification. This analysis also revealed that the protein induces a moderate decrease in film thickness (Fig. 2C). Upon subsequent rinsing in buffer, frequency and dissipation increased slowly, but did not return to the level of the virgin HS film (Fig. 2B, curves without symbols; from 89 min), demonstrating that some, but not all CXCL12α is released over experimentally accessible time scales, and that the HS film partially recovers its original morphology.

To test if the protein-induced morphological changes depend on HS surface density, we repeated the QCM-D assay at reduced HS surface coverage (Fig. 2B, curves with square symbols). To this end, b-HS was incubated at a lower solution concentration (1 µg/mL) and binding was interrupted after 15 min (Fig. 2B, 46 to 61 min). The frequency shift for HS (-8 ± 1 Hz) in this case (henceforward called low-density HS film) corresponds to an areal mass density of 12.0 ± 0.5 ng/cm^2 and an average distance between adjacent HS anchors of about 10 nm, according to previously reported estimates (7). CXCL12α induced a clear (albeit smaller) decrease in dissipation (Fig. 2B, 74 to 90 min), i.e. film rigidification also occured on low-density HS films.

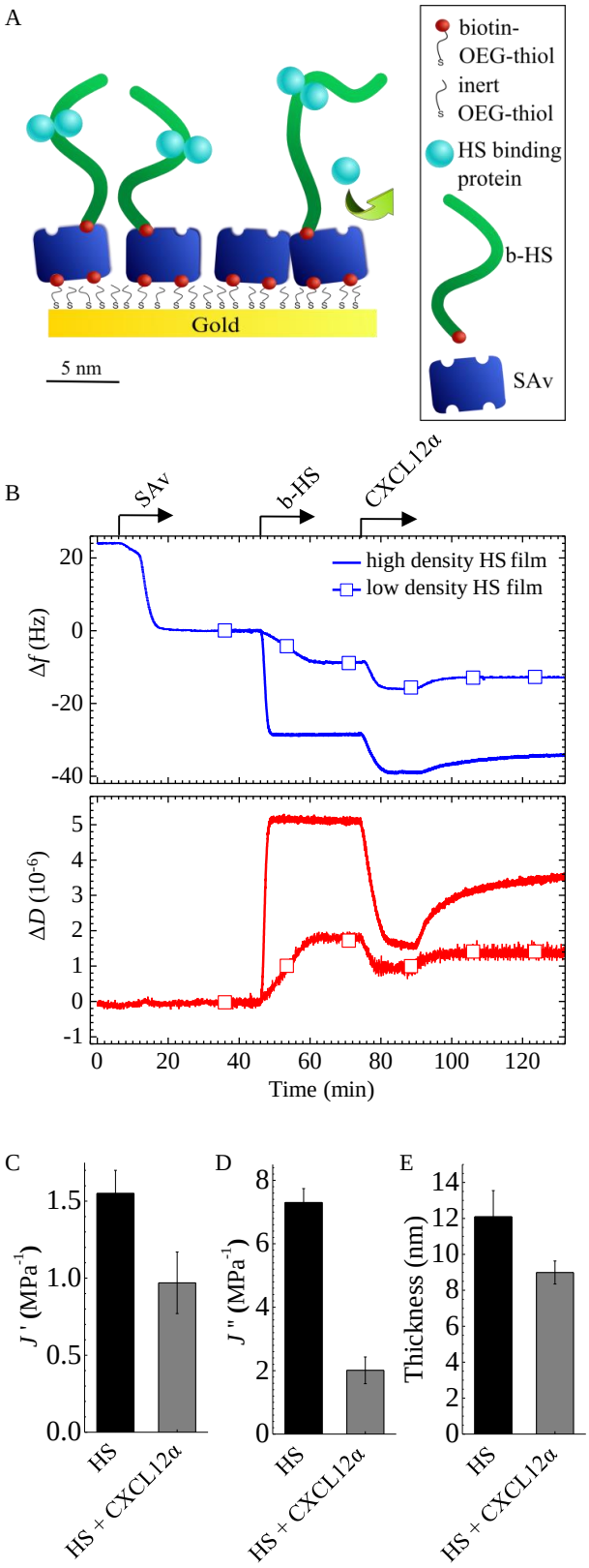

Figure 2. Design of HS films and effect of CXCL12α binding. *(A) Schematic representation with the relative sizes of all molecules approximately drawn to scale. HS is*

biotinylated at the reducing end for oriented and specific immobilization on streptavidin (SAv). SAv is specifically bound to a gold-supported monolayer of thiolated oligo(ethylene glycol) (OEG) exposing terminal biotin. (B) Surface functionalization and CXCL12α binding followed by QCM-D (frequency shifts, Δf, dissipation shifts, ΔD). Start and duration of incubation steps with different samples are indicated by an arrow; during all other times, the surface was exposed to buffer. SAv was first incubated at 1 µg/mL and then at 20 µg/mL, and responses are consistent with the formation of a dense protein monolayer (7). b-HS was incubated either at 50 µg/mL to saturation ('high density HS films', curves without symbols) or at 1 µg/mL for 15 min to reach about 30% of maximal coverage ('low density HS films', curves with square symbols). CXCL12α, incubated at 0.64 µM, induced dissipation decreases for both HS densities, indicating rigidification of the hydrated HS film upon chemokine binding. (C) Elastic compliance J', viscous compliance J" and thickness of HS films obtained from QCM-D data for high density HS films, bare and with CXCL12α at binding equilibrium. Data correspond to mean and standard error of the mean from three independent experiments. All parameters decreased upon CXCL12α incubation, confirming film rigidification and compaction.

Effect of CXCL12α binding on HS chain mobility. We hypothesized that the rigidification and thinning of HS films is due to cross-linking of HS chains by the chemokine. However, an alternative explanation could be that individual HS chains wrap around CXCL12α molecules, thereby stiffening the film and reducing the film thickness without generating any inter-chain cross-links. To distinguish between these two scenarios, we tested how the chemokine affects the lateral mobility of HS chains.

To this end, we used a modified model surface in which the gold-supported OEG monolayer was replaced by a silica- or glass-supported lipid bilayer (SLB; Fig. 3A). The oriented immobilization of HS at controlled densities is retained on these surfaces and the SAv-on-SLB film is also effectively passivating against non-specific binding of proteins (7). SLBs are distinct, however, in that they provide a fluid surface on which SAv, and the SAv-bound b-HS, have the freedom to move laterally (schematically shown in Fig. 3A).

The lateral mobility was probed by FRAP, using fluorescently labeled SAv (fl-SAv) as b-HS anchors. In this method, a limited surface area is rapidly bleached, and diffusion of fluorescent molecules into (and bleached molecules out of) the bleached area is subsequently monitored.

We verified correct surface functionalization by QCM-D (Fig. 3B). The fraction of biotinylated lipids used to form SLBs was adjusted to 0.5% such that incubation of fl-SAv at saturation (Fig. 3B, 10 to 20 min) led to a partial protein monolayer, in which the SAv molecules diffused freely, i.e. without being appreciably hindered by two-dimensional crowding. The fluorescent label did not induce any non-specific binding of CXCL12α or HS (Fig. 3B, 29 to 37 min and 44 to 51 min, respectively). The shifts in frequency (-9 ± 1 Hz) and dissipation ($2 \pm 0.2 \times 10^{-6}$) for incubation of b-HS at saturation (Fig. 3B, 58 to 68 min) were comparable to the low-density HS film shown in Fig. 2B. Moreover, the QCM-

D responses upon subsequent binding of CXCL12α (Fig. 3B, 92 to 105 min) were also similar to those observed in Fig. 2B. This indicates that the FRAP measurements can be directly correlated with QCM-D measurements on low-density HS films.

The representative fluorescence micrographs in Fig. 3C demonstrate close-to-complete recovery of virgin b-HS films within 100 s, confirming that fl-SAv with HS is indeed laterally mobile, as desired. In contrast, the bleached spot remained clearly visible after 100 s when CXCL12α was added to the HS film. Radially averaged fluorescence intensity profiles were computed from time-lapse series of micrographs after photobleaching, and analyzed to quantify lateral mobility. To this end, the pool of fl-SAv was assumed to be distributed in two distinct fractions, one immobile and the other laterally mobile with a given diffusion constant. The size of the mobile fraction and its diffusion constant are shown in Figs. 3D-E. These quantitative results confirm that virtually all (i.e. ≥ 95%) fl-SAv in a virgin SAv-monolayer was mobile, and that the mobility was unaffected by the presence of b-HS. In the presence of CXCL12α, 40% of the fl-SAv became effectively immobilized, and additionally, the diffusion constant of the retained mobile fraction was strongly reduced (by 45%). These data provide evidence that CXCL12α impedes lateral motion of HS and its fl-SAv anchor, and we propose that this immobilization is the consequence of CXCL12α-mediated HS cross-linking.

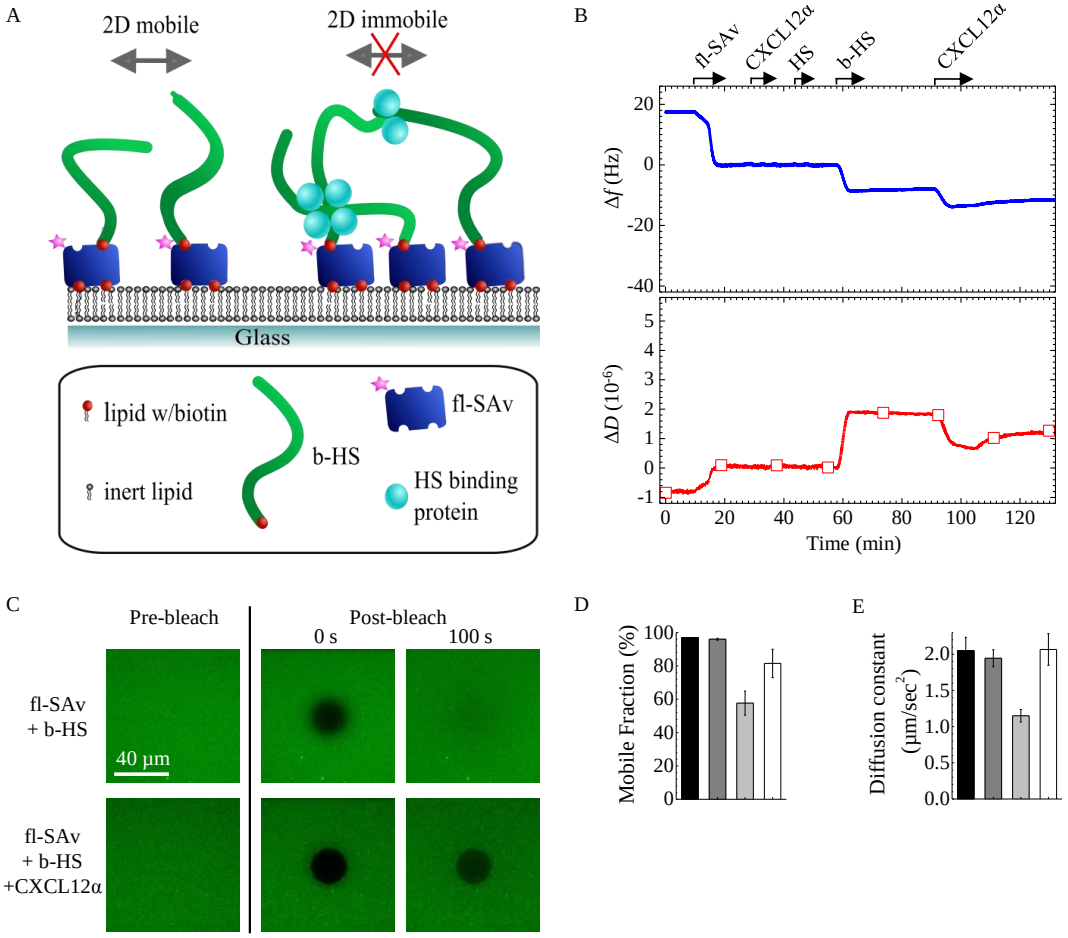

Figure 3. FRAP confirms CXCL12α mediated cross-linking of HS films. *(A) Schematic representation of HS films used for FRAP experiments. b-HS, anchored to fl-SAv, can diffuse along the surface (2D mobile) thanks to a fluid biotin-presenting supported lipid bilayer (left). Cross-linking, mediated by HS-binding proteins, is expected to lead to a reduction of HS (and hence fl-SAv) lateral mobility (right). (B) Surface functionalization and CXCL12α binding followed by QCM-D. Start and duration of each incubation step with different samples are indicated by an arrow; during all other times, the surface was exposed to buffer. fl-SAv was incubated at 20 µg/mL until saturation; the low percentage of biotinylated lipids (0.5%) limits fl-SAv binding to a sub-monolayer. CXCL12α (0.64 µM) and 50 µg/mL biotin-free HS produced no measurable response, confirming that the fluorescent label does not induce any nonspecific binding. The QCM-D responses for b-HS (incubated at 50 µg/mL to saturation), and for CXCL12α (incubated at 0.64 µM), were comparable to the low-density HS films shown in Fig. 2B. (C) Representative fluorescence micrographs demonstrating the FRAP assay to assess chemokine-mediated cross-linking. Recovery of the bleached spot is seen after 100 s for a bare HS film, but not for a CXCL12α-loaded HS film. (D-E) Quantitative analysis of FRAP data in terms of the mobile fraction (D) and its diffusion constant (E). Lateral mobility of fl-SAv was assessed in the absence of b-HS, after incubation with b-HS at saturation, after 15 min incubation of the HS film with chemokines (in the presence of 0.64 µM chemokines in solution), and after*

regeneration of the HS film by 2 M GuHCl. Data correspond to mean and standard error of the mean for three independent experiments.

After treatment with 2 M GuHCl, which we know effectively releases all CXCL12α from HS while keeping the HS film intact (7), the mobile fraction and its diffusion constant largely returned to the values observed for a virgin HS film. This confirms that HS mobility is largely restored upon chemokine release, i.e. the cross-linking is reversible and requires the presence of the chemokine. The mobile fraction though remained marginally reduced, indicating that a small fraction of fl-SAv remains permanently immobile upon GuHCl treatment. Most likely, the lack of complete regeneration is due to a weak yet irreversible perturbation of the fl-SAv film by GuHCl: detailed inspection of the fluorescent micrographs after GuHCl treatment revealed bright spots that we believe are fl-SAv aggregates.

Effect of CXCL12α mutations on HS cross-linking. CXCL12α is known to form β-sheet dimers (Fig. 1A) upon binding to HS (22). To test if this oligomerization is involved in HS cross-linking, we additionally tested two CXCL12α constructs with point mutations that leave the ternary structure of CXCL12α essentially intact, but alter the ability of the protein to form β-sheet dimers: L36C/A65C mutations result in inter-molecular disulphide bonds and formation of a 'locked dimer' (24) while I55C/L58C mutations promote an intra-molecular disulphide bond and formation of a 'partial monomer' with a reduced propensity to form dimers (23).

We tested the effect of binding of these constructs to low- and high-density HS films by QCM-D, and HS mobility in low-density HS films by FRAP. As with the wild type, both mutants bound to HS films (Fig. 4A, blue curves), but not to the supporting SAv monolayer (Fig. 4A, grey curves with triangle symbols). Binding to HS was distinct, however, with regard to the magnitude of the frequency shift at equilibrium and reversibility upon elution in buffer. The locked dimer exhibited enhanced and more stable binding, whereas binding was reduced and less stable for the partial monomer, as compared to native CXCL12α. These systematic variations reflect the importance of CXCL12α dimerization in stabilizing the interaction between the protein and HS (23).

Interestingly, both mutants also generated pronounced decreases in dissipation (Fig 4A, red curves) upon binding to HS, albeit with different magnitudes. Parametric plots of the $\Delta D/-\Delta f$ ratio as a function of $-\Delta f$, shown in Fig. 4B for high-density HS films, were very similar for all three protein constructs, except at the highest magnitudes of Δf. For thin films, the $\Delta D/-\Delta f$ ratio is proportional to the elastic compliance J' (31) and thus a simple relative measure for softness, whereas $-\Delta f$ is a relative measure for the protein surface density. The plots illustrate that the softness of HS films reduces only marginally as the HS grafting density increases during HS film formation (i.e. from $-\Delta f$ = 0 to 28.5 ± 1 Hz), and that subsequent protein binding (c.f. larger values of $-\Delta f$) reduces the softness drastically and in a coverage-dependent manner. The fact that the $\Delta D/-\Delta f$ *vs.* $-\Delta f$ curves for protein binding superimpose indicates that the mechanical properties (and hence the

morphologies) of the HS films are comparable for a given protein concentration in the film, irrespective of the quaternary state of the employed protein. This implies that the differences in the magnitude of Δ*f* and Δ*D* at equilibrium are entirely due to differences in the affinity (i.e. the adsorbed amounts), but that the intrinsic propensity of CXCL12α to cross-link HS does not depend on protein oligomerization.

Complementary FRAP assays revealed that the partial monomer and locked dimer can effectively reduce the mobile fraction (Fig. 4C) and its diffusion constant (Fig. 4D), confirming that all CXCL12α constructs can indeed cross-link HS. However, an appreciable reduction in mobility for the partial monomer could only be observed after increasing the protein solution concentration (by 6-fold). Moreover, after elution of residual partial monomer from the bulk solution with working buffer, the mobile fraction and its diffusion constant returned close to the level of a virgin HS film, whereas both parameters remained unaffected for the locked dimer. This demonstrates that an efficient cross-linking of the HS film requires a minimal protein concentration. Taken together, we conclude that the HS-induced CXCL12α dimerization (23, 24) enhances protein binding, but that this dimeric structure is dispensable for HS cross-linking if the reduced affinity is compensated by an increased protein solution concentration.

CXCL12α mutants lacking the N-terminal lysine residue have been reported to display reduced affinity for HS based on surface plasmon resonance data (22, 33), while NMR analysis found no direct evidence of interaction with heparin-derived oligosaccharides (20, 33). We hypothesized that this amino acid, which forms the end of a rather flexible protein domain and is rather distant from all other amino acids known to be involved in HS binding (17), may be important for cross-linking. To test this, we studied an additional construct with a truncated amino acid sequence, i.e. a mutant that lacked the four N-terminal amino acids (CXCL12α(5-67); Fig. 1A). The magnitudes of the QCM-D responses for this construct were comparable to native CXCL12α (Fig. 4A). In particular, the mutant also showed a negative dissipation shift, and the Δ*D*/-Δ*f vs.* -Δ*f* curves for CXCL12α(5-67) and native CXCL12α (Fig. 4B) were indistinguishable. Moreover, FRAP results (Figs. 4C-D) confirmed that the mutation does not affect HS mobility. Taken together, these data indicate that the N-terminus is also dispensable for cross-linking, which is presumably consistent with its modest and/or transient interaction with HS (17, 22, 33)

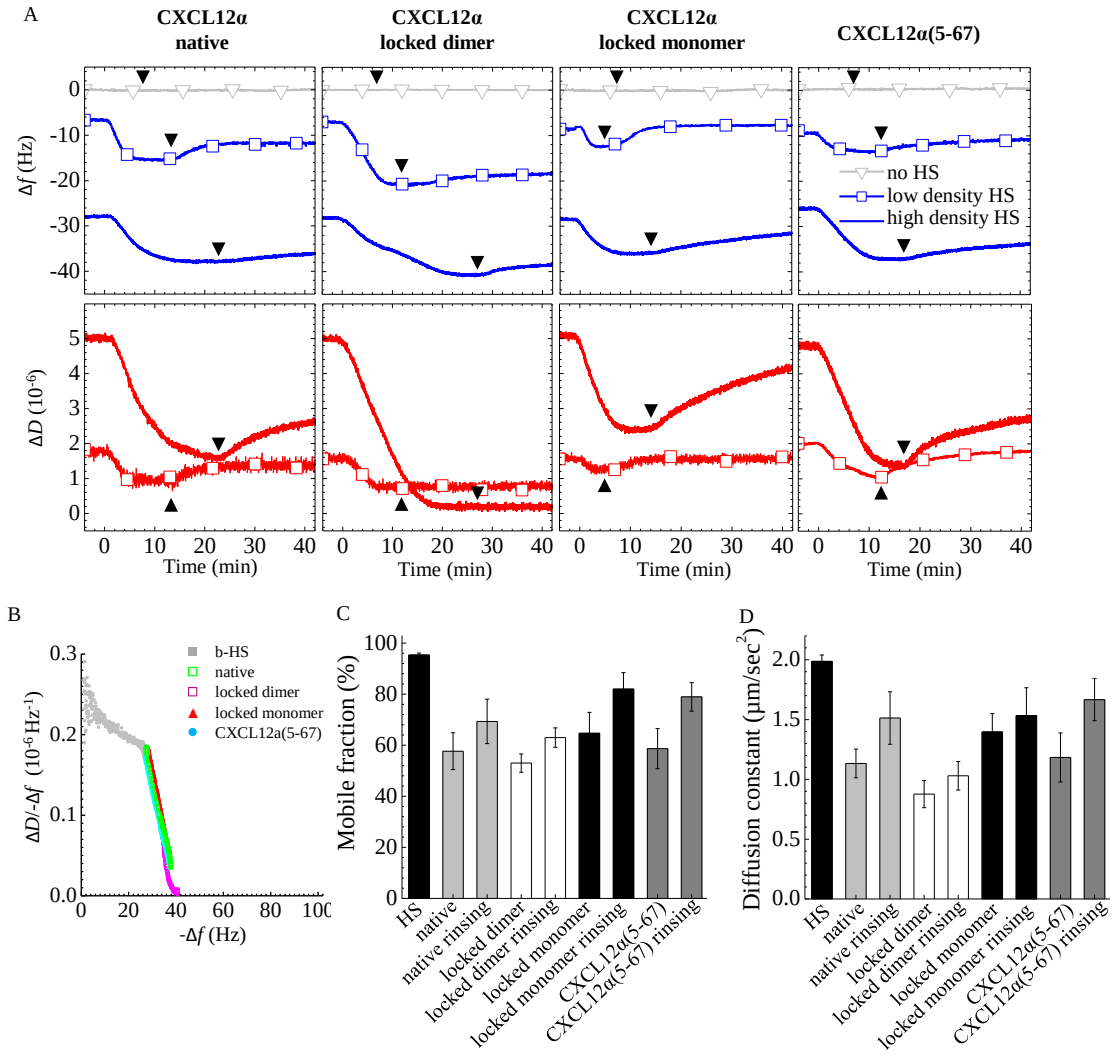

Figure 4. Dimerization and N-terminal lysine are dispensable for HS cross-linking. *(A) QCM-D data for the binding of selected CXCL12α constructs to low-density (curves with square symbols) and high-density (curves without symbols) HS films on SAv on OEG monolayers. As in Fig. 2B, Δf and ΔD are shown relative to SAv-coated surfaces before b-HS binding, yet b-HS binding is not explicitly shown. All samples were injected at 0 min a concentration of 0.64 μM monomer equivalents; arrowheads indicate the start of rinsing in working buffer. Protein binding was also tested on SAv monolayers without HS (grey curves with triangle symbols; only shown for Δf) to confirm absence of non-specific binding. Frequency shifts at equilibrium and unbinding curves after rinsing differed between CXCL12α constructs, indicating that their binding affinities are distinct. However, all constructs induced dissipation decreases on low and high density films, indicating HS film rigidification. (B) Parametric plot of ΔD/-Δf for the protein-loaded HS film (a relative measure for film softness) vs. –Δf for protein binding (a relative measure for protein surface density) for the binding data on high density HS films displayed in A (with color code as indicated). The curves largely superpose for all four CXCL12α*

constructs, indicating that, for a given protein surface density, the mechanical properties of the HS films are comparable. Representative data for HS film formation (grey) is given for comparison. (C-D) Mobile fractions and their diffusion constants of b-HS (bound to fl-SAv on SLBs) before incubation with CXCL12α constructs, after incubation with the proteins at equilibrium (native CXCL12α, CXCL12α(5-67) and locked dimer at 0.64 µM monomer equivalents, partial monomer at 3.8 µM), and after elution of respective protein from the solution phase, as indicated. The fluorescent label of fl-SAv was confirmed by QCM-D not to induce any measurable non-specific binding of any of the CXCL12α constructs (not shown). The mobility data confirm that all CXCL12α constructs can cross-link HS.

Effect of CXCL12α on HS oligomers. Having established that CXCL12α cross-links HS, we next tested if there is a minimal length of HS chains required for cross-linking. CXCL12α binding to HS oligosaccharides of different size was analyzed by QCM-D, to determine the minimum number of saccharides necessary for CXCL12α binding and cross-linking (Fig. 5A). No response was observed on hexasaccharides (dp6), while clear binding was present on dp8, dp10 and dp12, confirming that an octasaccharide but not a hexasaccharde is sufficient for efficient binding, in agreement with the literature (22). The dissipation decreased only slightly yet significantly (-0.1×10^{-6}) for dp8, while films of dp10 and dp12 showed pronounced dissipation decreases upon CXCL12α binding. Clearly, the chemokine induced a rigidification of the oligosaccharide HS layers, suggesting that even rather short HS chains can be cross-linked.

Consistent with this interpretation, FRAP measurements on dp12 revealed significant decreases in the mobile fraction and its diffusion constant with CXCL12α (Figs. 5B-C). No significant effect was observed with dp6, as expected, demonstrating specificity of the assay. The effect of CXCL12α on the mobility of dp12 was, however, rather weak. This indicates that the oligosaccharides assemble into relatively small clusters with largely retained lateral mobility. In other words, longer HS chains are required for a sufficient amount of CXCL12α to bind to each chain and thus to induce effective cross-linking of many HS chains.

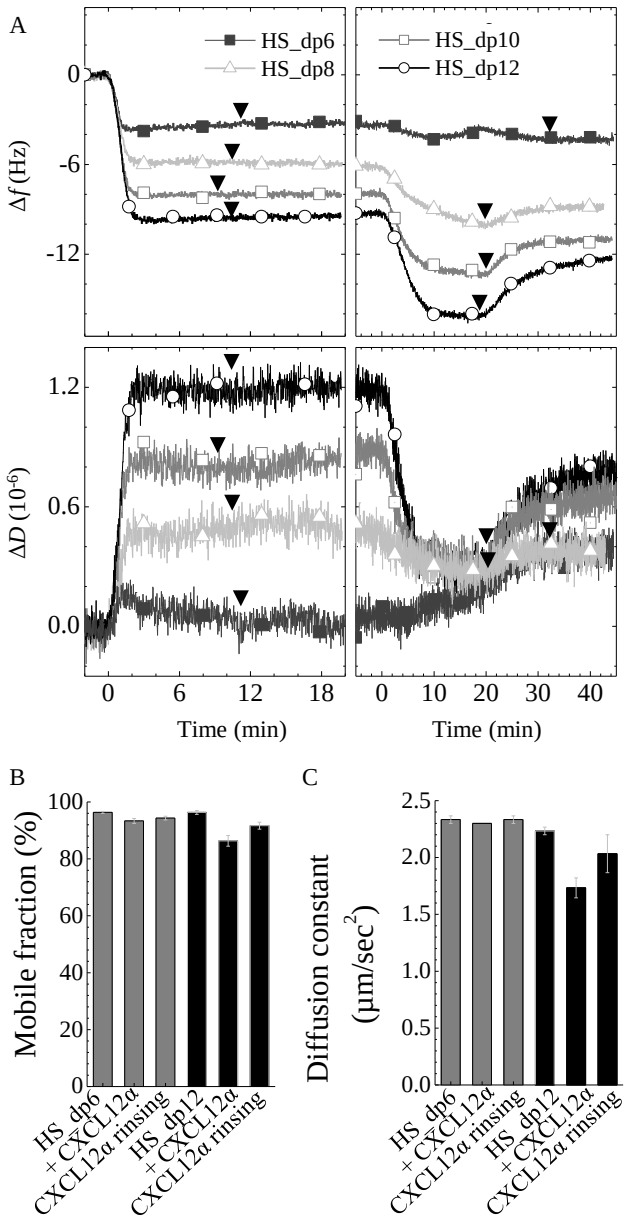

Figure 5. CXCL12α binding to and rigidification of films of oligomeric HS*. (A) CXCL12α binding to monolayers of b-HS oligosaccharides of different lengths (as indicated; dp = degree of polymerization), immobilized on a SAv monolayer on OEG (see Fig. 2) was monitored by QCM-D to test the minimal length needed for the chemokine to bind and to cross-link HS. Injection of b-HS oligosaccharides (at 50 μg/mL; left panels) and CXCL12α (at 0.64 μM; right panels) started at 0 min, and arrowheads indicate the start of rinsing with working buffer. Clear binding of CXCL12α is only observed for HS of dp8 (Δf = -4 Hz) and larger, indicating that a hexasaccharide it not sufficiently long for protein binding. Pronounced dissipation decreases for HS as small as dp8 indicate that even films of oligomeric HS are rigidified. (B-C) Mobile fractions and their diffusion constants of b-HS oligosaccharides (bound to fl-SAv on SLBs) either bare or in the presence of 0.64 μM*

CXCL12α, as indicated. The moderate reduction in dp12 mobility suggests that oligosacharides can by cross-linked into relatively small clusters by CXCL12α.

Effect of other HS-binding proteins on HS films. To test whether HS-cross-linking is unique to CXCL12α, we extended our study and systematically investigated the effect of several other HS-binding proteins, namely CXCL12γ, interferon γ (IFNγ) and the fibroblast growth factors FGF-2 and FGF-9, on high-density and low-density HS surfaces by QCM-D, and on low-density HS surfaces by FRAP (Fig. 6). The structures of all tested proteins are known and HS binding sites have been identified (14, 34–37) (Fig. 1B-E). As expected, none of the proteins exhibited any significant non-specific binding to the SAv monolayer (Fig. 6A, grey curves with triangle symbols).

Compared to CXCL12α (Fig. 1A), CXCL12γ (Fig. 1B) features 30 additional amino acids at the C-terminus, which are known to have HS binding activity and enhance the affinity of CXCL12 for HS: dissociation constants K_D of 200 nM and 1.5 nM have been reported for the α and γ isoforms, respectively (14). Indeed, CXCL12γ bound more stably and more rapidly than CXCL12α (Figs. 6A and 4A, respectively, blue curves). The decrease in dissipation for CXCL12γ was pronounced at low and high HS coverage (Fig. 6A, red curves). The $\Delta D/-\Delta f$ *vs.* $-\Delta f$ plot (Fig. 6B) confirms that this protein also has a strong propensity to rigidify the HS film. In this plot, differences between CXCL12γ and CXCL12α were small, albeit significant compared to the variations between CXCL12α and its mutants (Fig. 4B), suggesting that there are subtle differences in the morphology of the protein-loaded HS films. Nevertheless, CXCL12γ reduced the HS mobile fraction and its diffusion constant (Fig. 6C-D) somewhat stronger than native CXCL12α, i.e. to a similar extent as the locked dimer of CXCL12α (Fig. 4C-D). We conclude that CXCL12γ is also a potent HS cross-linker and that this potency is enhanced by the HS binding stability.

IFNγ is a homodimeric cytokine known to strongly interact with HS (K_D ~ 1 nM (38)). The known HS binding site is located at the C terminus and the two C termini in the homodimer are spatially separated (Fig. 1C). At present, it is not clear, if the two binding loci bind to a single or to two distinct HS chains. IFNγ readily bound to the HS films and binding was very stable as shown by the QCM-D frequency response (Fig. 6A). In high-density HS films, IFNγ induced a negative shift in dissipation (Fig. 6A) albeit with a reduced magnitude compared to CXCL12α (Fig. 4A). However, IFNγ generated a slight increase in dissipation in low-density HS films. FRAP (Figs. 6E-F, left plots) revealed that IFNγ induces only moderate reductions in the mobile fraction of HS (by 15%) and in the diffusion coefficient of this mobile fraction (by 25%). The lack of dissipation decrease and the weak reduction in HS mobility thus correlate, and indicate that IFNγ does not cross-link HS strongly, at least at low surface density. Under these conditions, the two HS binding sites on the IFNγ homodimer apparently bind within a single HS chain (intra-HS-chain bond).

To test if the decrease in dissipation at high HS surface density (Fig. 4A) is an indicator for the formation of inter-HS-chain bonds by IFNγ when HS chains are densely packed,

we performed additional FRAP measurements at high HS surface densities (Figs. 6E-F, right plots). To this end, the fraction of biotinylated lipids used to form the SLB was increased (from 0.5% to 5%) to enable formation of a dense fl-SAv monolayer. Under these conditions, the lateral mobility of the bare HS films was largely retained (i.e. the mobile fraction was only slightly reduced, to 90%) although crowding of fl-SAv entailed a marked reduction of the diffusion constant (from 2 $\mu m^2/s$ to 0.5 $\mu m^2/s$). Interestingly, the mobile fraction as well as its diffusion constant decreased only weakly in the presence of IFNγ (by 12% and 20%, respectively). This indicates that the IFNγ homodimer prefers to form intra-HS rather than inter-HS-chain bonds even at high HS concentrations, and supports the previously proposed model in which IFNγ binds to two adjacent N-sulphated domains along a single HS chain (39).

FGF-2 and FGF-9 were selected because of their well-characterized HS-binding sites (Fig. 1D-E). FGF-2 has 3 HS-binding sites, of which two are located on the same face and the third on the opposite face of the protein (36, 37, 40, 41). In contrast, only one (rather extended) HS-binding site has been identified for FGF-9 (26). FGF-2 and FGF-9 were reported to have affinities of 10 and 620 nM, respectively, to heparin dp8 (i.e. a representative of high affinity binding sites on HS) (26, 42). Both FGFs bound readily to HS films (Fig. 6A), as expected. The frequency shifts on high-density HS films exceeded those observed for the previously investigated chemokines (Figs. 4 and 6), indicating extensive binding. FGF-2 generated pronounced decreases in dissipation for high-density and low-density HS films. In stark contrast, the dissipation remained largely unchanged and increased drastically, respectively, for FGF-9. This contrast is also apparent in the $\Delta D/-\Delta f$ *vs.* $-\Delta f$ plot (Fig. 6B), where the curve for FGF-9 is located above the curve for FGF-2, thus indicating that FGF-2 is more potent in rigidifying HS films. FRAP revealed a drastic reduction (by 80%) in the mobile fraction with FGF-2 (Fig. 6C), i.e. this protein essentially immobilized HS. FGF-9, on the other hand, did not affect the mobile fraction at all (Fig. 6C) and the diffusion constant of the mobile fraction was only weakly affected (Fig. 6D).

Clearly, FGF-2, but not FGF-9, has a strong propensity to cross-link and to rigidify HS films. In light of the distinct structural features of these two growth factors, we propose that FGF-2 cross-links HS by accommodating at least two different chains simultaneously in its multiple HS binding sites, whereas only one HS chain at a time can bind to the extended binding site on FGF-9. The results with FGFs highlight that not all HS-binding proteins cross-link HS and that the cross-linking propensity can vary distinctly among proteins of the same family.

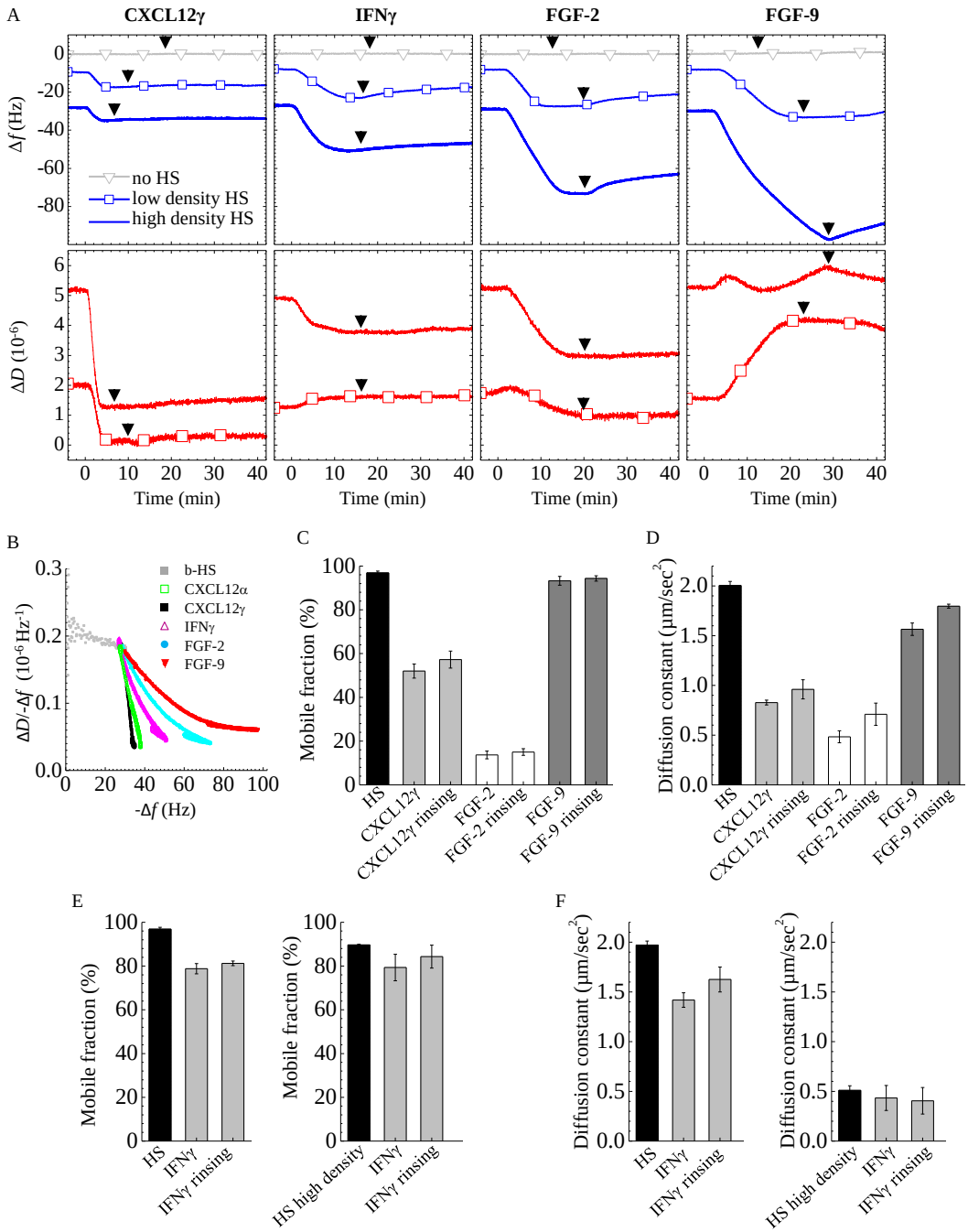

Figure 6: Correlation between structure and HS cross-linking propensity of HS-binding proteins. *(A) QCM-D data for binding of proteins to HS films are displayed analogous to Fig. 4A. CXCL12γ, as CXCL12α, induced strong negative shifts in dissipation irrespective of HS film density; FGF-2, but not FGF-9, induced negative dissipation shifts irrespective of HS film density; for IFNγ, the dissipation decreased only on high-density HS films, indicating distinct, protein-specific degrees of HS film rigidification. (B) Parametric plot of*

ΔD/-Δf for the protein-loaded HS film vs. –Δf for protein binding for the binding data on high density HS films displayed in A; the curves show that HS film rigidification depends on protein type and coverage. (C-D) Mobile fractions and their diffusion constants of b-HS (bound to fl-SAv on SLBs at low surface density) either bare or in the presence of CXCL12γ, FGF-2 or FGF-9, as indicated. (E-F) Mobile fractions and their diffusion constants of b-HS (bound to fl-SAv on SLBs at low surface density (left graphs) and high surface density (right graphs)) either bare or in the presence of IFNγ, as indicated. The fluorescent label of fl-SAv was confirmed by QCM-D not to induce any measurable non-specific binding of any of the HS-binding proteins (not shown). Protein concentrations used throughout were 0.43 μM for CXCL12γ, 0.29 μM for IFNγ, 0.28 μM for FGF-2 and 0.17 μM for FGF-9. The mobility and rigification data correlate, confirming that FGF-2 is a potent cross-linker whereas FGF-9 does not cross-link, that CXCL12γ cross-links HS film similarly to CXCL12α locked dimer, and that IFNγ may be a weak cross-linker.

Discussion

What are the molecular mechanisms behind HS cross-linking? One may argue that a protein with an HS-binding surface large enough to accommodate more than one HS chain should be able to cross-link HS. Yet, we found the extension of the HS-binding surface alone to be a poor predictor of a protein's cross-linking propensity. This is illustrated by the limited cross-linking propensity of the IFNγ homodimer (Fig. 6), but also by the negligible effects of the elongated C-terminal of CXCL12γ, compared to CXCL12α, on HS film rigidification and cross-linking (Figs. 4 and 6). Apparently, the formation of multiple bonds with the same HS chain is more favourable in these cases than the inter-connection of several distinct HS chains.

FGF-2, in contrast, exhibited strong cross-linking activity (Fig. 6). A detailed inspection of the protein's surface reveals that the three HS-binding patches containing basic amino acids are separated from each other by acidic and hydrophobic amino acids. Such HS-repelling rims are not present in any of the other proteins tested. From the correlation with our experimental data, we thus propose multiple HS-binding patches separated by HS-repelling borders as a distinct structural feature conducive to HS cross-linking.

Mutation of the primary binding site reduces binding of FGF-2 to HS substantially (43), i.e. the affinities of the secondary HS binding sites on FGF-2 are rather weak. Yet, FGF-2 apparently is a potent HS cross-linker. This effect is not surprising if one takes into consideration that, once FGF is sequestered into the matrix through its primary high-affinity binding site, the local concentration in HS is high such that even weak interactions can occur frequently. Thus, the example of FGF-2 illustrates how rather weak secondary binding sites can fulfil functions.

CXCL12 is also a potent HS cross-linker (Figs. 4-6), yet the molecular mechanism of cross-linking must be different since this protein does not feature several clearly separated binding sites. It is instructive to consider the quaternary structure of this

protein. Upon HS binding, CXCL12 readily forms homodimers through the association of β-sheets (22), but our tests with partial monomer and locked dimer (Fig. 4) demonstrated that this 'β-sheet' dimer is not directly involved in HS cross-linking. Crystallographic studies (44) though revealed that CXCL12α can form another homodimer through the association of two N-termini, analogous to what is commonly observed for chemokines of the CC family (45), although the functional significance of the 'N-terminal' dimer has so far remained unclear.

We propose that β-sheet and N-terminal dimers co-exist in the HS matrix, potentially forming dimers of dimers. In this scenario, the two dimerization mechanisms would have distinct functions, i.e. dimerization through β-sheets enhances the affinity of the protein for HS whereas dimerization through N-termini induces HS cross-linking. Our experimental data are fully consistent with such a scenario. In particular, arginines at positions 8 and 12 were found to be involved in the formation of the N-terminal dimer (44). These are present in all mutants (including the truncated CXCL12α(5-67) form), and it is thus not surprising that all our CXCL12α constructs exhibited a similar propensity to rigidify and cross-link HS films once the differences in affinity were adjusted for (Figs. 4B-D). Moreover, an N-terminal dimer can also readily cross-link short HS oligosaccharides (Fig. 5), whereas such an effect would be difficult to explain with β-sheet dimers alone: in the current binding model, dp8 is just long enough to fit the HS-binding interface in the β-sheet dimer (20); it would be conceivable that a single dp8 binds two β-sheet dimers (i.e. one on each face of the oligosaccharide), but not the opposite. Future studies with other CXCL12α mutants should be useful to test if the arginines at positions 8 and 12 are indeed crucial for dimerization-mediated cross-linking and how HS-binding (20, 33) and CXCL12α oligomerization interplay to promote cross-linking.

The methodological approach presented in this study is novel. HS films as model matrices present HS at controlled orientation and lateral mobility and at tuneable surface density thus enabling supramolecular interaction studies under well-defined conditions. The two characterization techniques, QCM-D and FRAP, provide complementary information and together enable identification of the protein's binding and cross-linking activity. Specifically, QCM-D provides information about binding kinetics, and about HS/protein film morphology (thickness) and rigidity, whereas FRAP enables quantification of the lateral mobility of HS chains. The assay does not require any labelling of the protein and is thus broadly applicable to assess the propensity of proteins to cross-link HS and other GAGs.

GAG-on-chip devices are increasingly used to probe the interaction of GAGs with proteins. On such devices, the extent of protein-mediated GAG cross-linking will depend sensitively on the presentation and surface density of GAGs. As a consequence, the binding behaviour of proteins may also vary strongly, calling for care in the interpretation of the read out and comparison of data between different GAG-on-chip-

based assays. The method developed here should be very useful to evaluate how GAG presentation and surface density affect binding.

What is the functional relevance of HS cross-linking by extracellular signalling proteins? Cross-linking of HS requires the spatial proximity of HS chains. This criterion was met in our well-defined model matrices. Based on the typical length of HS chains and the typical density of HS-bearing proteoglycans, Yanagishita and Hascall estimated that the ensemble of HS chains on cells can readily explore the entire cell surface (15). HS cross-linking thus may also be a frequent phenomenon at the cell surface and in extracellular matrix, spatio-temporally controlled through the sequestration of chemokines or growth factors in the course of specific biological processes (e.g. angiogenesis (46), inflammation (47), cell proliferation (6, 42, 48)). This may have consequences at different levels.

On the level of the matrix, the proteins can promote changes in structure that parallel their signalling activity. The ensuing changes in physical properties of peri- and extracellular matrices, such as permeability, rigidity or thickness, may elicit a range of additional cellular responses. For example, a reduction in the thickness of pericellular coats may facilitate inter-cellular contacts through membrane-bound cell adhesion receptors/ligands (49), or the cross-linking of HS displayed by two distinct pericellular coats could be important in the initial stage of cell-cell adhesion. Moreover, changes in the rigidity of the cellular glycocalyx through HS-crosslinking may provide a physical cue that guides the behaviour of cells.

On the local scale, cross-linking of HS could promote clustering of cell-surface proteoglycans (PGs) to which the HS chains are attached, thereby activating signalling. Clustering of the HSPG syndecan-4, for example, is important for the binding to and activation of protein kinases which ultimately determine the assembly of focal adhesions and the organization of the actin cytoskeleton (50). In this regard, it has been demonstrated that a syndecan-4 dimer requires a minimum of four HS chains to be functional, whereas a mutated form of syndecan-4 with a single HS chain was not functional unless a cluster of multiple syndecan-4 dimers was formed. This suggests that multiple HS chains must associate in the presence of a ligand, to form a signalling unit (51). In this scenario, HS-cross-linking proteins would elicit signalling activity in a way that has thus far not been appreciated.

It has also been proposed that the HS chains of syndecan control the formation of exosomes, with an impact on the trafficking and confinement of FGF signals (52). In particular, the interaction between FGFs and syndecans has been demonstrated to promote receptor clustering, translocation to cholesterol-rich membrane domains and eventually internalization (53). Here, future studies comparing the effect of proteins that cross-link HS (such as FGF-2, CXCL12α or CXCL12γ) with those that do not (such as IFNγ or FGF-9) would provide a direct test if HS-cross-linking is important for exosome formation.

Last but not least, the proteins themselves would also be affected by HS cross-linking, in that the attachment through multiple binding sites reduces their mobility. This may contribute, for example, to the substantial fraction of FGF-2 that is observed to undergo confined, rather than diffusive motion in pericellular matrix (54).

Conclusions

In summary, we have demonstrated that extracellular signalling proteins can cross-link GAGs and propose that several binding sites, well separated either through GAG-repellent borders on the protein's surface (e.g. FGF-2) or through spatial separation in quaternary protein structures (e.g. N-terminal CXCL12 dimers), are required for GAG cross-linking. This prediction can now readily be tested with other GAG-binding proteins using the here-presented GAG cross-linking assay. The ability of extracellular signaling proteins to influence matrix organization and physico-chemical properties implies that the functions of these proteins may not simply be confined to the activation of cognate cellular receptors. This may have far-reaching implications for cell-cell and cell-matrix communication, and our predictions can be tested in future cell and *in vivo* assays.

Author information

Author's contributions. E.M. and D.T. carried out surface preparation, QCM-D and FRAP measurements; D.T., R.S., D.P.D., Y.L., C.S. and B.F.V. prepared heparan sulphate conjugates and proteins; J.K. developed data analysis methods; E.M., D.T., L.C.-G. and R.P.R. participated in data analysis; E.M., D.P.D., T.M.H., L.C.-G., D.G.F. and H.L.-J. helped design the study and draft the manuscript; L.C.-G. helped coordinate the study; E.M. and R.P.R. wrote the manuscript; R.P.R. conceived of and coordinated the study. All authors gave final approval for publication.

Acknowledgements. We thank Severin Ehret (CIC biomaGUNE, San Sebastian, Spain) for the preparation of small unilamellar vesicles and support for FRAP measurements and data analysis, Catherine Picart and Fabian Dalonneau (LMGP, Grenoble, France) for access to and support for the confocal microscope, respectively, Damien Maurin (IBS, Grenoble, France) for the purification of IFNγ and CXCL12γ, and Françoise Baleux (Institut Pasteur, Paris, France) for providing the CXCL12α(5-67) mutant.

Funding. We acknowledge funding by the Nanoscience Foundation Chair of Excellence Project "GAG2D" to R.P.R., the National Institute of Health (NIH, USA) grant R01 AI37113 to T.M.H., the North West Cancer Research (UK) and the Cancer and Polio Research Fund (UK) to D.F., NIH grant R01 AI058072 to B.F.V., the NanoBio programme, and the French National Research Agency via Labex ARCANE (ANR-11-LABX-0003-01).

Competing interests. We have no competing interests.

References

1. Rapraeger, A. C., Krufka, A., and Olwin, B. B. (1991) Requirement of heparan sulfate for bFGF-mediated fibroblast growth and myoblast differentiation. *Science* **252**, 1705–1708
2. Aviezer, D., and Yayon, A. (1994) Heparin-dependent binding and autophosphorylation of epidermal growth factor (EGF) receptor by heparin-binding EGF-like growth factor but not by EGF. *Proc. Natl. Acad. Sci. U.S.A.* **91**, 12173–12177
3. Zioncheck, T. F., Richardson, L., Liu, J., Chang, L., King, K. L., Bennett, G. L., Fügedi, P., Chamow, S. M., Schwall, R. H., and Stack, R. J. (1995) Sulfated oligosaccharides promote hepatocyte growth factor association and govern its mitogenic activity. *J. Biol. Chem.* **270**, 16871–16878
4. Amara, A., Lorthioir, O., Valenzuela, A., Magerus, A., Thelen, M., Montes, M., Virelizier, J. L., Delepierre, M., Baleux, F., Lortat-Jacob, H., and Arenzana-Seisdedos, F. (1999) Stromal cell-derived factor-1alpha associates with heparan sulfates through the first beta-strand of the chemokine. *J. Biol. Chem.* **274**, 23916–23925
5. Broxmeyer, H. E., Cooper, S., Hangoc, G., and Kim, C. H. (2005) Stromal cell-derived factor-1/CXCL12 selectively counteracts inhibitory effects of myelosuppressive chemokines on hematopoietic progenitor cell proliferation in vitro. *Stem Cells Dev.* **14**, 199–203
6. Turbic, A., Leong, S. Y., and Turnley, A. M. (2011) Chemokines and inflammatory mediators interact to regulate adult murine neural precursor cell proliferation, survival and differentiation. *PLoS ONE* **6**, e25406
7. Migliorini, E., Thakar, D., Sadir, R., Pleiner, T., Baleux, F., Lortat-Jacob, H., Coche-Guerente, L., and Richter, R. P. (2014) Well-defined biomimetic surfaces to characterize glycosaminoglycan-mediated interactions on the molecular, supramolecular and cellular levels. *Biomaterials* **35**, 8903–8915
8. Bass, M. D., and Humphries, M. J. (2002) Cytoplasmic interactions of syndecan-4 orchestrate adhesion receptor and growth factor receptor signalling. *Biochem. J.* **368**, 1–15
9. Li, J.-P., and Vlodavsky, I. (2009) Heparin, heparan sulfate and heparanase in inflammatory reactions. *Thromb. Haemost.* **102**, 823–828
10. Blackhall, F. H., Merry, C. L., Davies, E. J., and Jayson, G. C. (2001) Heparan sulfate proteoglycans and cancer. *Br. J. Cancer* **85**, 1094–1098
11. Vanhaverbeke, C., Simorre, J.-P., Sadir, R., Gans, P., and Lortat-Jacob, H. (2004) NMR characterization of the interaction between the C-terminal domain of interferon-gamma and heparin-derived oligosaccharides. *Biochem. J.* **384**, 93–99
12. Plotnikov, A. N., Hubbard, S. R., Schlessinger, J., and Mohammadi, M. (2000) Crystal structures of two FGF-FGFR complexes reveal the determinants of ligand-receptor specificity. *Cell* **101**, 413–424

13. Weber, M., Hauschild, R., Schwarz, J., Moussion, C., De Vries, I., Legler, D. F., Luther, S. A., Bollenbach, T., and Sixt, M. (2013) Interstitial dendritic cell guidance by haptotactic chemokine gradients. *Science* **339**, 328–332
14. Laguri, C., Sadir, R., Rueda, P., Baleux, F., Gans, P., Arenzana-Seisdedos, F., and Lortat-Jacob, H. (2007) The novel CXCL12gamma isoform encodes an unstructured cationic domain which regulates bioactivity and interaction with both glycosaminoglycans and CXCR4. *PLoS ONE* **2**, e1110
15. Yanagishita, M., and Hascall, V. C. (1992) Cell surface heparan sulfate proteoglycans. *J. Biol. Chem.* **267**, 9451–9454
16. Mulloy, B., Gee, C., Wheeler, S. F., Wait, R., Gray, E., and Barrowcliffe, T. W. (1997) Molecular weight measurements of low molecular weight heparins by gel permeation chromatography. *Thromb. Haemost.* **77**, 668–674
17. Sadir, R., Imberty, A., Baleux, F., and Lortat-Jacob, H. (2004) Heparan sulfate/heparin oligosaccharides protect stromal cell-derived factor-1 (SDF-1)/CXCL12 against proteolysis induced by CD26/dipeptidyl peptidase IV. *J. Biol. Chem.* **279**, 43854–43860
18. Thakar, D., Migliorini, E., Coche-Guerente, L., Sadir, R., Lortat-Jacob, H., Boturyn, D., Renaudet, O., Labbe, P., and Richter, R. P. (2014) A quartz crystal microbalance method to study the terminal functionalization of glycosaminoglycans. *Chem. Commun.* **50**, 15148–15151
20. Laguri, C., Sapay, N., Simorre, J.-P., Brutscher, B., Imberty, A., Gans, P., and Lortat-Jacob, H. (2011) 13C-labeled heparan sulfate analogue as a tool to study protein/heparan sulfate interactions by NMR spectroscopy: Application to the CXCL12α chemokine. *J. Am. Chem. Soc.* **133**, 9642–9645
21. Denoyer, A., Godefroy, D., Célérier, I., Frugier, J., Degardin, J., Harrison, J. K., Brignole-Baudouin, F., Picaud, S., Baleux, F., Sahel, J. A., Rostène, W., and Baudouin, C. (2012) CXCR3 antagonism of SDF-1(5-67) restores trabecular function and prevents retinal neurodegeneration in a rat model of ocular hypertension. *PLoS ONE* **7**, e37873
22. Sadir, R., Baleux, F., Grosdidier, A., Imberty, A., and Lortat-Jacob, H. (2001) Characterization of the stromal cell-derived factor-1alpha-heparin complex. *J. Biol. Chem.* **276**, 8288–8296
23. Ziarek, J. J., Getschman, A. E., Butler, S. J., Taleski, D., Stephens, B., Kufareva, I., Handel, T. M., Payne, R. J., and Volkman, B. F. (2013) Sulfopeptide probes of the CXCR4/CXCL12 interface reveal oligomer-specific contacts and chemokine allostery. *ACS Chem. Biol.* **8**, 1955–1963
24. Veldkamp, C. T., Seibert, C., Peterson, F. C., De la Cruz, N. B., Haugner, J. C., 3rd, Basnet, H., Sakmar, T. P., and Volkman, B. F. (2008) Structural basis of CXCR4 sulfotyrosine recognition by the chemokine SDF-1/CXCL12. *Sci. Signal.* **1**, ra4
25. Saesen, E., Sarrazin, S., Laguri, C., Sadir, R., Maurin, D., Thomas, A., Imberty, A., and Lortat-Jacob, H. (2013) Insights into the mechanism by which interferon-γ basic

amino acid clusters mediate protein binding to heparan sulfate. *J. Am. Chem. Soc.* **135**, 9384–9390

26. Xu, R., Ori, A., Rudd, T. R., Uniewicz, K. A., Ahmed, Y. A., Guimond, S. E., Skidmore, M. A., Siligardi, G., Yates, E. A., and Fernig, D. G. (2012) Diversification of the structural determinants of fibroblast growth factor-heparin interactions: implications for binding specificity. *J. Biol. Chem.* **287**, 40061–40073
27. Richter, R., Mukhopadhyay, A., and Brisson, A. (2003) Pathways of lipid vesicle deposition on solid surfaces: a combined QCM-D and AFM study. *Biophys. J.* **85**, 3035–3047
28. Domack, A., Prucker, O., Ruhe, J., and Johannsmann, D. (1997) Swelling of a polymer brush probed with a quartz crystal resonator. *Phys. Rev. E* **56**, 680–689
29. D. Johannsmann http://www2.pc.tu-clausthal.de/dj/software_en.shtml.
30. Eisele, N. B., Andersson, F. I., Frey, S., and Richter, R. P. (2012) Viscoelasticity of thin biomolecular films: a case study on nucleoporin phenylalanine-glycine repeats grafted to a histidine-tag capturing QCM-D sensor. *Biomacromolecules* **13**, 2322–2332
31. Reviakine, I., Johannsmann, D., and Richter, R. P. (2011) Hearing what you cannot see and visualizing what you hear: interpreting quartz crystal microbalance data from solvated interfaces. *Anal. Chem.* **83**, 8838–8848
32. Kühnle, J. (2007) in Diploma Thesis, Faculty of Phsyics and Astronomy, University of Heidelberg
33. Ziarek, J. J., Veldkamp, C. T., Zhang, F., Murray, N. J., Kartz, G. A., Liang, X., Su, J., Baker, J. E., Linhardt, R. J., and Volkman, B. F. (2013) Heparin oligosaccharides inhibit chemokine (CXC motif) ligand 12 (CXCL12) cardioprotection by binding orthogonal to the dimerization interface, promoting oligomerization, and competing with the chemokine (CXC motif) receptor 4 (CXCR4) N terminus. *J. Biol. Chem.* **288**, 737–746
34. Ealick, S. E., Cook, W. J., Vijay-Kumar, S., Carson, M., Nagabhushan, T. L., Trotta, P. P., and Bugg, C. E. (1991) Three-dimensional structure of recombinant human interferon-gamma. *Science* **252**, 698–702
35. Plotnikov, A. N., Eliseenkova, A. V., Ibrahimi, O. A., Shriver, Z., Sasisekharan, R., Lemmon, M. A., and Mohammadi, M. (2001) Crystal structure of fibroblast growth factor 9 reveals regions implicated in dimerization and autoinhibition. *J.Biol.Chem.* **276**, 4322–4329
36. Faham, S., Hileman, R. E., Fromm, J. R., Linhardt, R. J., and Rees, D. C. (1995) Heparin structure and interactions with basic fibroblast growth factor. *Science* **271**, 1116–1120
37. Ori, A., Free, P., Courty, J., Wilkinson, M. C., and Fernig, D. G. (2009) Identification of heparin-binding sites in proteins by selective labeling. *Mol. Cell Proteomics* **8**, 2256–2265

38. Lortat-Jacob, H., Kleinman, H. K., and Grimaud, J. A. (1991) High-affinity binding of interferon-gamma to a basement membrane complex (matrigel). *J. Clin. Invest.* **87**, 878–883
39. Lortat-Jacob, H., Turnbull, J. E., and Grimaud, J. A. (1995) Molecular organization of the interferon gamma-binding domain in heparan sulphate. *Biochem. J.* **310 (Pt 2)**, 497–505
40. Kinsella, L., Chen, H. L., Smith, J. A., Rudland, P. S., and Fernig, D. G. (1998) Interactions of putative heparin-binding domains of basic fibroblast growth factor and its receptor, FGFR-1, with heparin using synthetic peptides. *Glycoconj. J.* **15**, 419–422
41. Baird, A., Schubert, D., Ling, N., and Guillemin, R. (1988) Receptor- and heparin-binding domains of basic fibroblast growth factor. *Proc. Natl. Acad. Sci. U.S.A.* **85**, 2324–2328
42. Delehedde, M., Lyon, M., Gallagher, J. T., Rudland, P. S., and Fernig, D. G. (2002) Fibroblast growth factor-2 binds to small heparin-derived oligosaccharides and stimulates a sustained phosphorylation of p42/44 mitogen-activated protein kinase and proliferation of rat mammary fibroblasts. *Biochem. J.* **366**, 235–244
43. Thompson, L. D., Pantoliano, M. W., and Springer, B. A. (1994) Energetic characterization of the basic fibroblast growth factor-heparin interaction: identification of the heparin binding domain. *Biochemistry* **33**, 3831–3840
44. Murphy, J. W., Yuan, H., Kong, Y., Xiong, Y., and Lolis, E. J. (2009) Heterologous quaternary structure of CXCL12 and its relationship to the CC chemokine family. *Proteins* **78**, 1331–1337
45. Lortat-Jacob, H., Grosdidier, A., and Imberty, A. (2002) Structural diversity of heparan sulfate binding domains in chemokines. *Proc. Natl. Acad. Sci. U S A* **99**, 1229–1234
46. Cao, R., Bråkenhielm, E., Pawliuk, R., Wariaro, D., Post, M. J., Wahlberg, E., Leboulch, P., and Cao, Y. (2003) Angiogenic synergism, vascular stability and improvement of hind-limb ischemia by a combination of PDGF-BB and FGF-2. *Nat. Med.* **9**, 604–613
47. Poznansky, M. C., Olszak, I. T., Foxall, R., Evans, R. H., Luster, A. D., and Scadden, D. T. (2000) Active movement of T cells away from a chemokine. *Nat. Med.* **6**, 543–548
48. Sahni, A., Sporn, L. A., and Francis, C. W. (1999) Potentiation of endothelial cell proliferation by fibrin(ogen)-bound fibroblast growth factor-2. *J. Biol. Chem.* **274**, 14936–14941
49. Weinbaum, S., Tarbell, J. M., and Damiano, E. R. (2007) The structure and function of the endothelial glycocalyx layer. *Annu. Rev. Biomed. Eng.* **9**, 121–167
50. Couchman, J. R. (2003) Syndecans: proteoglycan regulators of cell-surface microdomains? *Nat. Rev. Mol. Cell Biol.* **4**, 926–937

51. Gopal, S., Bober, A., Whiteford, J. R., Multhaupt, H. A. B., Yoneda, A., and Couchman, J. R. (2010) Heparan Sulfate Chain Valency Controls Syndecan-4 Function in Cell Adhesion. *J. Biol. Chem.* **285**, 14247–14258
52. Baietti, M. F., Zhang, Z., Mortier, E., Melchior, A., Degeest, G., Geeraerts, A., Ivarsson, Y., Depoortere, F., Coomans, C., Vermeiren, E., Zimmermann, P., and David, G. (2012) Syndecan-syntenin-ALIX regulates the biogenesis of exosomes. *Nat. Cell Biol.* **14**, 677–685
53. Tkachenko, E., and Simons, M. (2002) Clustering induces redistribution of syndecan-4 core protein into raft membrane domains. *J. Biol. Chem.* **277**, 19946–19951
54. Duchesne, L., Octeau, V., Bearon, R. N., Beckett, A., Prior, I. A., Lounis, B., and Fernig, D. G. (2012) Transport of fibroblast growth factor 2 in the pericellular matrix is controlled by the spatial distribution of its binding sites in heparan sulfate. *PLoS Biol.* **10**, e1001361
55. Schlessinger, J., Plotnikov, A. N., Ibrahimi, O. A., Eliseenkova, A. V., Yeh, B. K., Yayon, A., Linhardt, R. J., and Mohammadi, M. (2000) Crystal structure of a ternary FGF-FGFR-heparin complex reveals a dual role for heparin in FGFR binding and dimerization. *Mol. Cell* **6**, 743–750

V. Myoblast behavior on biomimetic surfaces

This chapter constitutes a manuscript in preparation:

The mode of chemokine display determines myoblast adhesion and motility

Dhruv Thakar[1,2], Fabien Dalonneau[3,4], Elisa Migliorini[1,2], Hugues Lortat-Jacob[5,6,7], Didier Boturyn[1,2], Liliane Coche-Guerente[1,2], Catherine Picart[3,4] and Ralf P. Richter[1,2,8,9]

[1]Université Grenoble Alpes, Departement de Chimie Moléculaire (DCM), 38000 Grenoble, France; [2]CNRS, DCM, 38000 Grenoble, France; [3]CNRS UMR 5628 (LMGP), 3 parvis Louis Néel, 38016 Grenoble, France; [4]Université Grenoble Alpes, LMGP, 3 parvis Louis Néel, 38016 Grenoble, France; [5]Université Grenoble Alpes, Institut de Biologie Structurale (IBS), 38027 Grenoble, France; [6]CNRS, IBS, 38027 Grenoble, France; [7]CEA, DSV, IBS, 38027 Grenoble, France; [8]CIC biomaGUNE, San Sebastian, Spain; [9]Max Planck Institute for Intelligent Systems, Stuttgart, Germany.

Significance: This chapter demonstrates the potential of the biomimetic GAG-presenting surfaces (described in Chapter III) for mechanistic studies on cell-matrix interactions. The determinant role of the mode of chemokine presentation (i.e. presentation *via* GAGs) on myoblast behavior is demonstrated. In addition, we apply the biomimetic surfaces to study the inter-play of two cellular receptors in determining cell adhesion and motility.

My contribution: I co-designed research (together with Liliane Coche-Guerente, Didier Boturyn, Catherine Picart and Ralf P. Richter). I performed and analyzed all the measurements, and contributed to data interpretation and figure preparation. I wrote the first draft of the manuscript.

Résumé

Les chimiokines sont des molécules de signalisation qui guident la migration des cellules. Les glycosaminoglycanes (GAGs) aident à maintenir les gradients de chimiokines dans la matrice extracellulaire, le long duquel les cellules (par exemple des myoblastes au cours de la régénération musculaire) peuvent migrer. On a peu d'information à ce jour, sur la façon dont la présentation des chimiokines affecte le comportement des cellules. Pour étudier ceci, nous avons conçu des surfaces biomimétiques multifonctionnelles qui présentent les chimiokines (CXCL12α), les glycosaminoglycanes (l'héparane sulfate, HS) et des ligands favorisant l'adhésion cellulaire (RGD) avec une orientation contrôlée et des densités de surface modulables. Ces surfaces fonctionnelles ont été utilisées pour étudier les réponses cellulaires aux signaux extracellulaires dans un environnement bien défini.

Sur ces surfaces modèles, les myoblastes répondent à la chimiokine CXCL12α liée de façon réversible à son ligand naturel le HS par l'adhésion et une motilité accrue. En revanche, la chimiokine CXCL12α liée irréversiblement à la surface améliore l'adhésion, mais altère la motilité cellulaire. Ceci démontre que la présentation des chimiokines, en particulier la présence des HS, est importante pour la régulation du comportement cellulaire. En augmentant la complexité, nous avons conçu des surfaces multifonctionnelles, qui présentent le ligand d'adhésion cellulaire RGD (Arg-Gly-Asp) avec la chimiokine CXCL12α liée au HS, comme mimes de l'interface entre les myoblastes et la matrice extracellulaire au cours de la régénération et de la réparation musculaire. La co-présentation du RGD avec la chimiokine CXCL12α liée au HS conduit à améliorer l'adhésion, l'étalement et la motilité d'une manière distincte de la réponse à chaque signal individuel. Cela indique que le récepteur cellulaire de la chimiokine CXCL12α, CXCR4 et le récepteur cellulaire du RGD, l'intégrine peuvent agir en synergie. Ces surfaces biomimétiques sont prometteuses pour accroître les connaissances concernant le rôle des chimiokines CXCL12α dans la myogenèse et la réparation musculaire.

The presentation mode of chemokine display determines myoblast adhesion and motility

Dhruv Thakar[1,2], Fabien Dalonneau[3,4], Elisa Migliorini[1,2], Hugues Lortat-Jacob[5,6,7], Didier Boturyn[1,2], Liliane Coche-Guerente[1,2], Catherine Picart[3,4] and Ralf P. Richter[1,2,8,9]

[1] Université Grenoble Alpes, Département de Chimie Moléculaire (DCM), 38000 Grenoble, France;

[2] CNRS, DCM, 38000 Grenoble, France

[3] CNRS UMR 5628 (LMGP), 3 parvis Louis Néel, 38016 Grenoble, France

[4] Université Grenoble Alpes, LMGP, 3 parvis Louis Néel, 38016 Grenoble, France

[5] Université Grenoble Alpes, Institut de Biologie Structurale (IBS), 38027 Grenoble, France

[6] CNRS, IBS, 38027 Grenoble, France

[7] CEA, DSV, IBS, 38027 Grenoble, France

[8] CIC biomaGUNE, San Sebastian, Spain

[9] Max Planck Institute for Intelligent Systems, Stuttgart, Germany

Abstract

Chemokines are signaling molecules that guide the migration of cells. Glycosaminoglycans (GAGs) help maintaining gradients of chemokines in the extracellular matrix, along which cells can migrate. Chemokines are important in the migration of muscle precursors during myogenesis and muscle regeneration. Little is known to date, as to how the molecular presentation of chemokines affects cell behavior. To study this, we designed multifunctional biomimetic surfaces that present the CXCL12α chemokine, the heparan sulfate (HS) glycosaminoglycan and RGD as cell adhesion ligand with controlled orientation and at tunable densities. We used these surfaces to study the response of myoblasts to extracellular cues in a highly defined environment. Myoblasts responded to CXCL12α reversibly bound to its natural ligand HS through enhanced adhesion and motility. In contrast, CXCL12α that was quasi-irreversibly surface-bound in the absence of HS enhanced adhesion but impaired motility. This demonstrates that the presentation of chemokines, in particular the presence of HS, is essential for regulating cellular behavior, in particular adhesion and motility. Co-presentation of RGD along with HS-bound CXCL12α led to enhanced adhesion, spreading and motility, in a way that is distinct from the response to each individual cue alone. This indicates that cell-surface CXCR4 (i.e. the CXCL12α receptor) and integrins (the RGD receptors) can act in synergy. These novel biomimetic surfaces hold promise in generating novel insights in the field of glycobiology, e.g. in dissecting the function of HS in the chemokine-mediated migration of myoblasts during myogenesis and muscle repair.

Keywords

Glycosaminoglycan; heparan sulfate; chemokine; CXCL12α; SDF-1α; C2C12 myoblast adhesion and motility; biomimetic surfaces; spectroscopic ellipsometry

1. Introduction

Muscle development and repair are crucial for body function. It is a highly organized process, orchestrated by muscle progenitor cells called satellite cells [1]. These cells are normally quiescent but undergo a number of modifications including activation, differentiation and proliferation, in response to muscle injury. *In vitro* studies have shown that the migration of myoblasts, i.e. satellite cell progenitors, is crucial for myogenesis and muscle regeneration [2-4]. Migration along with cell adhesion is crucial to achieve cell–cell contacts, which is essential for the alignment of myotubes, their subsequent fusion and formation of myotubes [2, 4-6].

Migration is a complex process. It is initiated by signalling molecules secreted in response to injury. These signalling molecules, small proteins called chemokines, have chemoattractant properties [7]. They are required for the migration of muscle precursor cells during embryonic myogenesis [6]. In particular, the stromal cell-derived factor-1α (SDF-1α: also called CXCL12α) chemokine and its major receptor, CXCR4 have been shown to be important during myogenesis and muscle regeneration, both *in vivo* [6, 8-10] and *in vitro* [11-13].

Chemokines once secreted, are trapped and presented to the cells *via* glycosaminoglycans (GAGs) [14]. GAGs are linear polysaccharides which are ubiquitously present at the cell surface and in the extracellular matrix. They are usually found attached covalently through their reducing end to core proteins, forming the proteoglycan family [15, 16]. GAGs interact with a plethora of proteins and *via* these interactions they regulate matrix assembly and remodelling, as well as cell-matrix and cell-cell interactions [17]. GAGs and heparan sulfate (HS) in particular, help organizing and maintaining the haptotactic gradients of chemokines on the cell surface and in the extracellular matrix, thus providing directional cues for migrating cells [18-20].

An important factor for a cell to migrate is controlled adhesion and release, cell binds and detaches from the substrate in a coordinated manner with extension and retraction of pseudopods executing the directional migration [21, 22]. To control this, the extracellular matrix and the surface of cells possess cell-adhesion ligands. These ligands bind to specific transmembrane receptors called integrins.

Many works have focused on the role of CXCL12α *in vitro* in muscle development and regeneration, mostly by presenting CXCL12α in solution [6, 11-13]. It is only very recently that it has been presented in a matrix-bound manner to cells, i.e. physically trapped in a biopolymeric film [23]. However, no study has aimed to investigate if CXCL12α presented *via* a biomimetic matrix made of GAGs, its native matrix ligand, can be perceived differently by the cells.

For mechanistic studies, it is desirable to arrange biomolecules in such a way that the orientation, density and lateral mobility of the exposed biomolecules can be controlled and tuned. To this end, the biofunctionalization of solid surfaces i.e. designing biomimetic surfaces is an attractive route. We have previously demonstrated the

formation of multifunctional biomimetic surfaces that present chemokines (CXCL12α), GAGs (HS in particular) and ligands promoting cell adhesion with controlled orientation and at tunable densities, in a background of low non-specific binding [24]. In the present study, we have adapted this approach to study the response of myoblasts, by using a distinct cell-adhesion ligand i.e. RGD peptide. RGD peptide has been used to study myogenic differentiation of C2C12 myoblasts [25]. Our surfaces were designed to reproduce selected features of muscle extracellular matrix, i.e. the supramolecular arrangement of ECM and cell-surface GAGs, which was attached to the surface through the reducing end, thus mimicking the native attachment of HS to its proteoglycan core, chemokines (bound to GAGs) and cell adhesion ligands. We designed biomimetic surfaces presenting chemokines in two different ways: either HS-bound CXCL12α or immobilized CXCL12α, the immobilized protein being available for binding to the receptors but not for uptake by the cells. We evaluated the response of myoblasts towards these different presentations, to test if and how the presentation of chemokines affects cellular adhesion, spreading and motility. In addition, we studied the differential response of myoblasts towards the co-presentation of chemokines and cell adhesion ligands. We demonstrate how surfaces that mimic selected aspects of the muscle extracellular and cellular surface enable cellular mechanistic studies on early stages of *in vitro* muscle regeneration in an environment that is well-defined and tunable.

2. Materials and methods

2.1. Buffer, heparan sulfate, proteins and other molecular building blocks

The working buffer used for all experiments and for protein dilution was made of 10 mM Hepes (Fisher, Illkirch, France) and 150 mM NaCl (Sigma Aldrich, Saint-Quentin Fallavier, France) at pH 7.4 in ultrapure water. Heparan sulphate (HS) derived from porcine intestinal mucosa with an average molecular weight of 12 kDa and a polydispersity of 1.6 (Celsus Laboratories, Cincinnati, OH, USA) was conjugated with biotin, site-specifically attached to the reducing end by oxime ligation [26]. Recombinant CXCL12α (amino acids 1 to 68; 8.1 kDa) was prepared as previously reported [27]. The same protein with a biotin conjugated to the C-terminal lysine through a tetraethylene glycol linker (b-CXCL12α; 8.6 kDa) was produced by solid-phase peptide synthesis as previously reported [28]. Lyophilized streptavidin (SAv, 60 kDa) and bovine serum albumin (BSA) were purchased from Sigma Aldrich. All proteins were diluted to 0.2 mg/mL in autoclaved working buffer and stored at -20°C. Thawed protein solutions were used within 5 days and further diluted as desired. AMD3100 was purchased from Sigma (France). Polyethylene glycol (PEG, 3.2 kDa) with a biotin at one end and an OH group at the other (b-PEG) was purchased from Iris Biotech (France). b-cRGD (3.9 kDa) was obtained by amide-coupling of linear PEG (3.2 kDa) with a biotin at one end and an

activated acid group at the other end (b-PEG-NHS; Iris Biotech) to a RGD-containing cyclic pentapeptide c[-RGD*f*K-] at lysine side-chain [29].

2.2. Surfaces and surface functionalization

QCM-D sensors with gold coating (QSX301) were purchased from Biolin Scientific (Västra Frölunda, Sweden). Appropriately sized wafers with an optically opaque gold coating (100 nm, sputter-coated) were used for SE measurements. Glass cover slips (24 × 24 mm^2; Menzel Gläser, Braunschweig, Germany) with a semi-transparent gold film (~5 nm) were prepared, as described previously [24]. To create a biotin-displaying and otherwise inert background, the gold-coated surfaces were conditioned with UV/ozone (Jelight, Irvine, CA, USA) for 10 min and then immersed overnight in an ethanolic solution (Fisher, Illkirch, France) of OEG disulfide and biotinylated OEG thiol (Polypure, Oslo, Norway) at a total concentration of 1 mM and a molar ratio of thiol equivalents of 999:1.

2.3. Assembly of biomimetic surface coatings

A monolayer of streptavidin on a gold-supported biotinylated OEG monolayer (Fig. 1A) served as a 'molecular breadboard' onto which the desired molecules were sequentially assembled. To prepare chemokine-presenting surfaces (Fig. 1B), the following concentrations and exposure times were used: b-HS - 50 µg/mL, 30 min; CXCL12α – 5 µg/mL, 30 min; b-CXCL12α – 5 µg/mL, 30 min. Under these conditions, binding is expected to saturate or equilibrate, irrespective of whether the solution is flown (in QCM-D measurements), or still (in SE measurements and for cell assays). To prepare multifunctional surfaces (Fig. 3), the following concentrations and incubation times were used: b-HS - 1 µg/mL, 30 min; b-cRGD - 1 µg/mL, 5 min (Fig. 3A-C) or 90 s (Fig. 3D); b-PEG - 50 µg/mL, 20 min; CXCL12α – 5 µg/mL, 30 min. Here, the reduced concentrations and/or incubation times of HS and cRGD were chosen to obtain the desired sub-monolayer surface densities (Fig. 3 and Table 1); b-PEG was incubated to back-fill the remaining biotin-binding pockets on the SAv monolayer, and eventually CXCL12α was incubated until equilibrium were desired.

2.4. Quartz crystal microbalance with dissipation monitoring (QCM-D)

QCM-D measures the changes in resonance frequency, Δf, and dissipation, ΔD, of a sensor crystal upon molecular adsorption on its surface. The QCM-D response is sensitive to the mass (including hydrodynamically coupled water) and the mechanical properties of the surface-bound layer. Measurements were performed with a Q-Sense E4 system equipped with 4 independent Flow Modules (Biolin Scientific, Vastra Frolunda, Sweden) and gold-coated QCM-D sensors functionalized with biotinylated OEG monolayers. The system was operated in flow mode with a flow rate of typically 10 µL/min, at a working temperature of 24 °C. Δf and ΔD were measured at six overtones (i = 3, 5, ..., 13), corresponding to resonance frequencies of $f_i \approx$ 5, 15, 25, ..., 65 MHz; changes in dissipation and normalized frequency, $\Delta f = \Delta f_i/i$, of the third overtone (i = 3) are presented; any other overtone would have provided comparable information.

2.5. Spectroscopic ellipsometry (SE)

SE measures changes in the polarization of light upon reflection at a planar surface. SE was employed *in situ* with a M2000V system (J. A. Woollam, Lincoln, NE, USA) to quantify the surface density of adsorbed biomolecules in a time-resolved manner. Gold-coated silica wafers functionalized with biotinylated OEG monolayers were installed in a custom-built open cuvette (~120 µL) featuring a magnetic stirrer for homogenization of the cuvette content (typically for 5 s after pipetting a sample into the solution) and a flow-through system for rapid solution exchange during rinsing steps. Before use, the cuvette walls were passivated against biomolecular binding by exposure to a 10 mg/mL BSA solution in working buffer (20 min), followed by rinsing with ultrapure water and blow-drying with N_2. Biomolecular binding processes were monitored at room temperature. Surface densities were quantified through fitting of the data to optical models, as described in detail elsewhere [30]. Briefly, the opaque gold film and the OEG monolayer were treated as a single isotropic layer and fitted as a B-spline substrate. Areal mass densities were determined through de Fejter's equation, using refractive index increments, d*n*/d*c*, of 0.15 cm^3/g for b-HS, b-PEG and b-cRGD; and 0.18 cm^3/g for all proteins. All measurements were repeated twice and the data represent mean ± standard errors.

2.6. Cell culture and cell assays

The mouse myoblast cell line C2C12 (<20 passages post-delivery from ATCC) was cultured, as previously described [31]. Prior to the cell assays, serum was removed from the cell suspension, by centrifugation at 600 rpm at 25 °C for 10 min; the supernatant was then removed and the cells were exposed to serum-free 1:1 DMEM/F12 medium (Life Technology, France). Cell adhesion assays were performed with custom-made 4-well plates with ~100 µl solution per well and a functionalized glass cover slip on the bottom, prepared as described previously [24]. Surfaces with the desired biomimetic coating were sterilized for 15 min under UV light, and C2C12 cells were seeded at a density of 1.5×10^4 cells/cm^2. CXCL12α binds reversibly to HS and thus partitions between the HS-coated surface and the solution; based on the conditions employed for liquid exchange and cell seeding, we estimate the residual CXCL12α concentration in solution to be 500 nM. After incubation for 1 h and 4 h, non-adhesive (and weakly adhesive) cells were removed by gentle rinsing with sterile phosphate-buffered saline (PBS, pH 7.4; Sigma Aldrich) using a pipette. To test for the specificity of the cellular recognition of CXCL12α through the receptor CXCR4, the cell suspension was supplemented with AMD3100 at a concentration of 50 µM, which inhibits interaction of CXCR4 with CXCL12α [6, 11]. All cell assays were repeated 3 times.

Quantitative analysis of cell adhesion. 10 bright-field images of cells per sample were recorded shortly before and after gentle rinsing using an inverted microscope (Axiovert 200 M; Carl Zeiss SAS, Le Pecq, France) equipped with a 10× objective, covering a surface area of at least 2 mm^2 in total. The number of surface-proximal cells was

counted manually. The percentage of adherent cells was defined as the ratio between the number of cells after rinsing and before rinsing. Data represent the mean and standard deviation over the percentage of adherent cells across three independent experiments.

Quantitative analysis of cell spreading and morphology. Adhered cells were fixed with 3.7% formaldehyde for 20 min and permeabilized in 0.2% Triton X-100 for 4 min, incubated with rhodamine-phalloidin (1:800, Sigma, France) for labelling actin and with DAPI (1:100) for labeling the nucleus, and then imaged with an Axiovert 200 M or an LSM 700 confocal microscope (both Carl Zeiss SAS) using a 20× objective. To quantify cell spreading and morphology, fluorescence images were analyzed with ImageJ software by marking the cellular perimeter (as defined by the actin labeling) manually, to determine the projected area and circularity of the cells. Circularity is defined as $4\pi(\text{area}/\text{perimeter}^2)$, i.e. a circularity of 1 corresponds to a cell with a circular projected area and a value close to 0 to a cell with a very high perimeter. Data are presented as box-plots for a total of 120 cells, i.e. 3 independent experiments with 40 cells analyzed per sample.

Time-lapse imaging of C2C12 cells on biomimetic surfaces. To assess the motility of cells, these were imaged every 5 min for 4 h after seeding on biomimetic surfaces, using an LSM 700 confocal microscope (Carl Zeiss SAS) equipped with a 5× objective and an environmental chamber (providing 37 °C and 5% CO_2). Time-lapse image series were assembled and analyzed using ImageJ software. Individual cell tracking was performed using the "Manual tracking" plugin, which allows selecting a cell and recording its movement by following the cell position across the image frames. 80 cells were tracked per sample and experiments were repeated thrice. The motion traces were then displayed and statistically analyzed using the "Chemotaxis tool".

3. Results

3.1. *Design and preparation of well-defined biomimetic surfaces presenting GAGs and chemokines*

To directly study the response of myoblasts towards chemokines presented *via* GAGs, our approach consisted in designing biomimetic surfaces encompassing the glycosaminoglycan heparan sulfate (HS), the chemokine CXCL12α and aadhesion ligand (cyclo[-RGD*f*K-]) [32] with controlled orientation and at tunable densities into tailor-made and multifunctional model surfaces. A monolayer of streptavidin on a gold-supported biotinylated OEG monolayer served as a 'molecular breadboard' onto which the desired molecules were sequentially assembled in a background of low non-specific binding [24] (Fig. 1A). Before construction of multifunctional surfaces, we ascertained that the desired functionalities can be realized with controlled orientation. For this purpose, QCM-D was used, providing time-resolved information about the assembly process, including overall film morphology and mechanics. Figure S1 shows that all the constituents of the biomimetic surfaces can be anchored to surfaces in a specific way through site-specifically conjugated biotins for b-HS, b-CXCL12α and b-RGD, and through biospecific binding to HS for CXCL12α [33]. Thus, their presentation can be preciselly controlled.

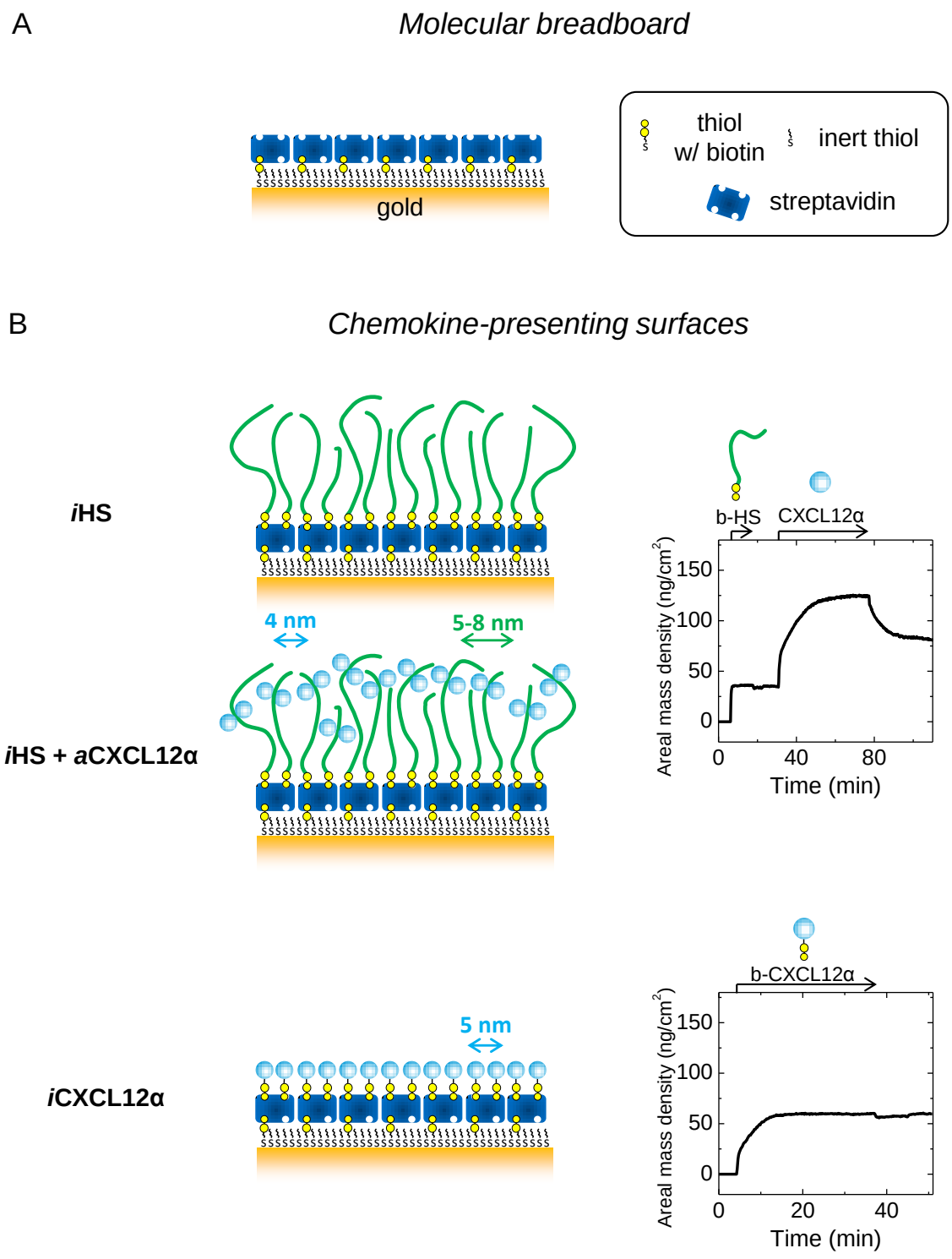

Figure 1. ***Design and preparation of well-defined biomimetic surfaces presenting GAGs and chemokine.*** *(A) Schematic presentation of a 'molecular breadboard' based on a streptavidin (SAv) monolayer immobilized on a gold-supported OEG monolayer exposing biotin at the end of a fraction of the OEG molecules, where stable attachment to the gold is mediated by thiols. The OEG monolayer (with and without SAv) confers a background of low nonspecific binding. (B) Schematic presentation of model surfaces (left) used to study the effect of chemokine presentation on myoblast adhesion and motility; functionalization of the molecular breadboard was followed by spectroscopic*

ellipsometry (SE) to quantify areal mass densities (right). The glycosaminoglycan HS is a native matrix ligand for CXCL12α, and was immobilized (iHS) through a biotin at the reducing end. The chemokine CXCL12α was presented either adsorbed (aCXCL12α) through heparan sulfate (HS) or immobilized (iCXCL12α) through a C-terminal biotin. All molecules are drawn approximately to scale. Arrows indicate the lateral root-mean-square (rms) distance between two molecules (colors of molecules and corresponding arrows are matched). Start and duration of incubation steps with different samples are indicated by arrows on top of the SE graphs; during all other times, the surface was exposed to working buffer.

In a first step, we studied how the presentation of the chemokine affects cell adhesion, by comparing CXCL12α presented either *via* reversible adsorption to its native matrix ligand heparan sulfate (*i*HS + *a*CXCl12α) or directly immobilized on the surface (*i*CXCL12α) (Fig. 1B, left). In these conditions, the molecule of interest is either reversibly adsorbed ("*a*") or quasi-irreversibly ("*i*") immobilized. To quantify the surface densities of biomolecules during the step-by-step assembly process, spectroscopic ellipsometry (SE) was used (Fig. 1B, right). Sample incubations in the SE measurements were performed in still solution, i.e. under mass-transport conditions that were identical to those subsequently used for the preparation of surfaces for cellular assays. The areal mass density for a SAv monolayer was 235 ± 5 ng/cm^2 (not shown), reproducing previous work [24]. To immobilize HS (*i*HS), b-HS was incubated to saturation, i.e. an areal mass density of 35 ± 2 ng/cm^2. This would correspond to a root-mean-square (rms) distance of 8 nm between HS anchor points on the surface, if we assume that the mean molecular weight of the surface-bound HS is 12 kDa, i.e. identical to the mean molecular weight of HS in the incubation solution. In reality, small-sized HS is likely to bind preferentially, and the average size of the surface-bound HS is thus likely to be smaller (see ref. [26] for details). Assuming that two HS chains bind per SAv at maximal coverage, we obtain an rms anchor distance of 5 nm and a mean molecular weight of 4.6 kDa. The values of 5 nm and 8 nm thus represent a lower and an upper bound, respectively, for the real rms anchor distance. Subsequent incubation of CXCL12α (*i*HS+ *a*CXCL12α) at 5 µg/mL led to adsorption at equilibrium with a surface density of 78 ± 7 ng/cm^2. To immobilize CXCL12α (*i*CXCL12α), biotinylated CXCL12α was incubated to full coverage, corresponding to 60 ± 1 ng/cm^2 or an rms distance of 5 nm. The biotin is located site-specifically at the C-terminal residue, and is thus not expected to interfere with CXCL12α binding to the cell surface receptor CXCR4 [24, 34]. The CXCL12α surface densities for the scenarios *i*HS + *a*CXCL12 (78 ± 7 ng/cm^2) and *i*CXCL12α (60 ± 1 ng/cm^2; Fig. 1B) are comparable. Table 1 summarizes the adsorbed amounts and root-mean-square (rms) anchor distances for the constituents of the biomimetic surfaces.

3.2. Effect of matrix-bound CXCL12α presentation on C2C12 myoblast adhesion

The well-defined biomimetic surfaces presenting GAGs and chemokines were used to trigger specific cellular responses. In particular, we first investigated the effects of matrix-bound CXCL12α presentation on the adhesion and spreading of C2C12 cells (Figs 1B), which was assessed by bright field imaging (Figs. 2A, C, F, H and S2A) and fluorescence staining (Figs. 2B, D, G, I and S2B). The fraction of cells that resisted gentle rinsing was quantified (Figs. 2C and H), as well as the spreading (Figs. 2D and I) and morphology (Figs. 2E and J) of the adhered cells after 1 h and 4 h of contact with the surfaces. Approximately 50% of the cells on surfaces presenting exclusively HS (*i*HS) were readily removed by gentle rinsing (Fig. 2C), the remaining cells retaining a rounded phenotype irrespective of the incubation time. This result indicates that the *i*HS surface as such is largely inert to adhesion and thus unlikely to present any specific chemical or mechanical cues to the cell. With regard to adhesion, cells did not respond significantly to the presentation of HS-bound chemokines (*i*HS + *a*CXCL12α) after 1 h of exposure but did after 4 h (Fig. 2C). The cell area increased (Fig. 2D) while the circularity decreased (Fig. 2E) significantly, demonstrating that C2C12 myoblasts do recognize and respond to HS-bound CXCL12α at sufficiently long exposure times. In contrast, the presence of CXCL12α in the bulk solution (*s*CXCL12α) did not enhance cell adhesion to a bare breadboard (Fig. S4A-C).

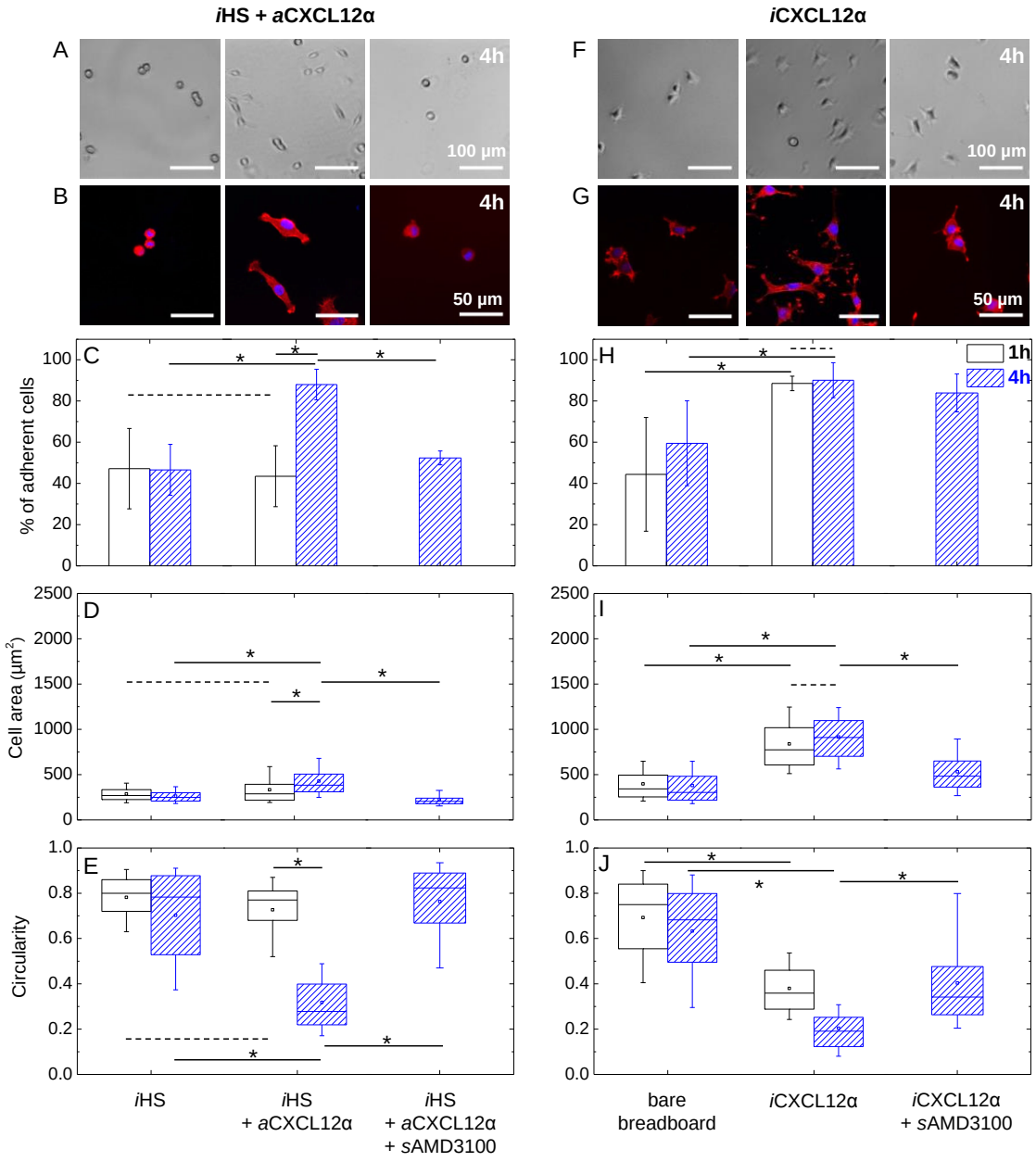

Figure 2. ***Effect of matrix-bound CXCL12α presentation on C2C12 myoblast adhesion, spreading and circularity.*** *A to E: adsorbed CXCL12α; F to J: immobilized CXCL12α. Bright-field images of live cells (A and F) and representative fluorescence staining of fixed cells (cell nuclei labeled in blue and actin in red; B and G) for C2C12 myoblasts exposed to surfaces presenting different surface functionalizations for 4 h. (C and H) Quantitative analysis of the percentage of adherent cells that remain after gentle rinsing following 1 h (black) and 4 h (blue, hatched) of exposure to different surface functionalizations. The area (D and I) and circularity (E and J) of the adhered cells are displayed as box plots; the small square and the horizontal line inside the box indicate the mean and the median, respectively, the box delimits the 25% to 75% percentile of data, and the error bar represents the lower 10% limit and the upper 90% limit. An ANNOVA test was performed to obtain p-values (lines with an asterisk indicate $p < 0.05$; dotted lines indicate no significant difference).*

Moreover, when CXCL12α binding to the cell-surface receptor CXCR4 was blocked with the soluble CXCR4 antagonist AMD3100 (*s*AMD3100), the fraction of adhered cells, the cell area and the circularity returned to the levels of HS alone (Figs. 2C-E), demonstrating that the adhesion of C2C12 myoblasts to surfaces presenting HS-bound CXCL12α is mediated by the specific binding of CXCL12α to CXCR4.

Next, we evaluated how the presentation of CXCL12α affected the C2C12 cell response. For this purpose we immobilized CXCL12α in a quasi-irreversible manner in comparison to reversibly bound CXCL12α in the case of HS-bound CXCL12α. When cells were exposed to CXCL12α immobilized quasi-irreversibly (*i*CXCL12α) and in the absence of HS, they responded strongly to the chemokine already after 1 h of exposure with increased adhesion (Fig. 2H) and spreading (Fig. 2I), and reduced circularity (Fig. 2J) compared to the bare breadboard. Thus, matrix-bound presentation of CXCL12α increased cell spreading. Prolonged exposure did not enhance spreading and circularity further (Fig. 2I-J). Interestingly, the adhered cells showed unusual finger-like protrusions that appeared to mature over time and the tips of which were particularly rich in actin (compare Figs. 2G and S2B). These protrusions were not observed on surfaces with HS-bound *a*CXCL12α (Figs. 2B and S2B). The stark difference in the temporal response and in the cell morphology demonstrates that the mode of CXCL12α presentation plays an important role in myoblast adhesion. Apparently, distinct mechanisms are involved in cellular recognition and internal signaling. A significant decrease in adhesion and spreading of cells on *i*CXCL12α (although not a full return to the base level found for a bare breadboard) was though observed with *s*AMD3100 (Figs. 2H-J), indicating that adhesion to *i*CXCL12α was specific and mediated by CXCR4.

3.3. Design and preparation of multifunctional biomimetic surfaces

Next, we aimed at investigating the response of C2C12 cells to the co-presentation of chemokines and cell adhesion ligands. For this purpose we aimed at designing surfaces that display an addiitonal feature of muscle extracellular matrix, i.e. adhesion ligands. Specifically, the biomimetic surfaces presented HS-bound CXCL12α together with RGD that was immobilized through a biotin to the breadboard (*i*HS + *a*CXCL12α + *i*RGD, Fig. 3A). With its modular design, our surface functionalization platform (i.e. the SAv monolayer) can readily accommodate multiple biotinylated compounds, generating multifunctional surfaces. The densities of different compounds can be tuned by adjusting the incubation time of each component on the surface. To form these co-funtionalized surfaces, b-HS was first incubated with reduced concentration and for a controlled time to reach a surface coverage of 13 ± 1 ng/cm^2 (Fig. 3A), corresponding to an rms anchor distance of 8 nm to 13 nm (following the rationale outlined above). This was followed by b-RGD incubation with conditions adjusted to obtain an areal mass density of 9 ± 2 ng/cm^2, which corresponds to an rms distance of 8 nm (Fig. 3A). b-PEG was then incubated to back-fill the remaining free biotin-binding pockets, if any, on the

SAv breadboard. Onto this mutifunctional surface, CXCL12α bound with an equilibrium surface density of 37 ± 3 ng/cm^2 (Fig. 3A). As controls, we prepared surfaces that lacked one or two of the biofunctional components (i.e. HS, CXCL12α, or RGD) with the surface density of all remaining biofunctional components unchanged (Fig. 3B-D) and vacant biotin-binding sites back-filled by b-PEG. SE analysis (Fig. 3B-D, right) demonstrates that comparable surface densities of *i*HS and *i*RGD could indeed be obtained, straightforwardly for *i*HS (Fig. 3B) and *i*HS + *i*RGD (Fig. 3C), and through a further modification of incubation conditions (i.e. a reduction in incubation time to 90 s) for *i*RGD (Fig. 3D; dotted lines). The surface density of *a*CXCL12α on a sub-monolayer of *i*HS without *i*RGD was around 30 ng/cm^2 at equilibrium (Fig. 3B), comparable to the values observed in the presence of *i*RGD. The incubation conditions established in Fig. 3 were subsequently used for the construction of biomimetic surfaces for the cellular assays.

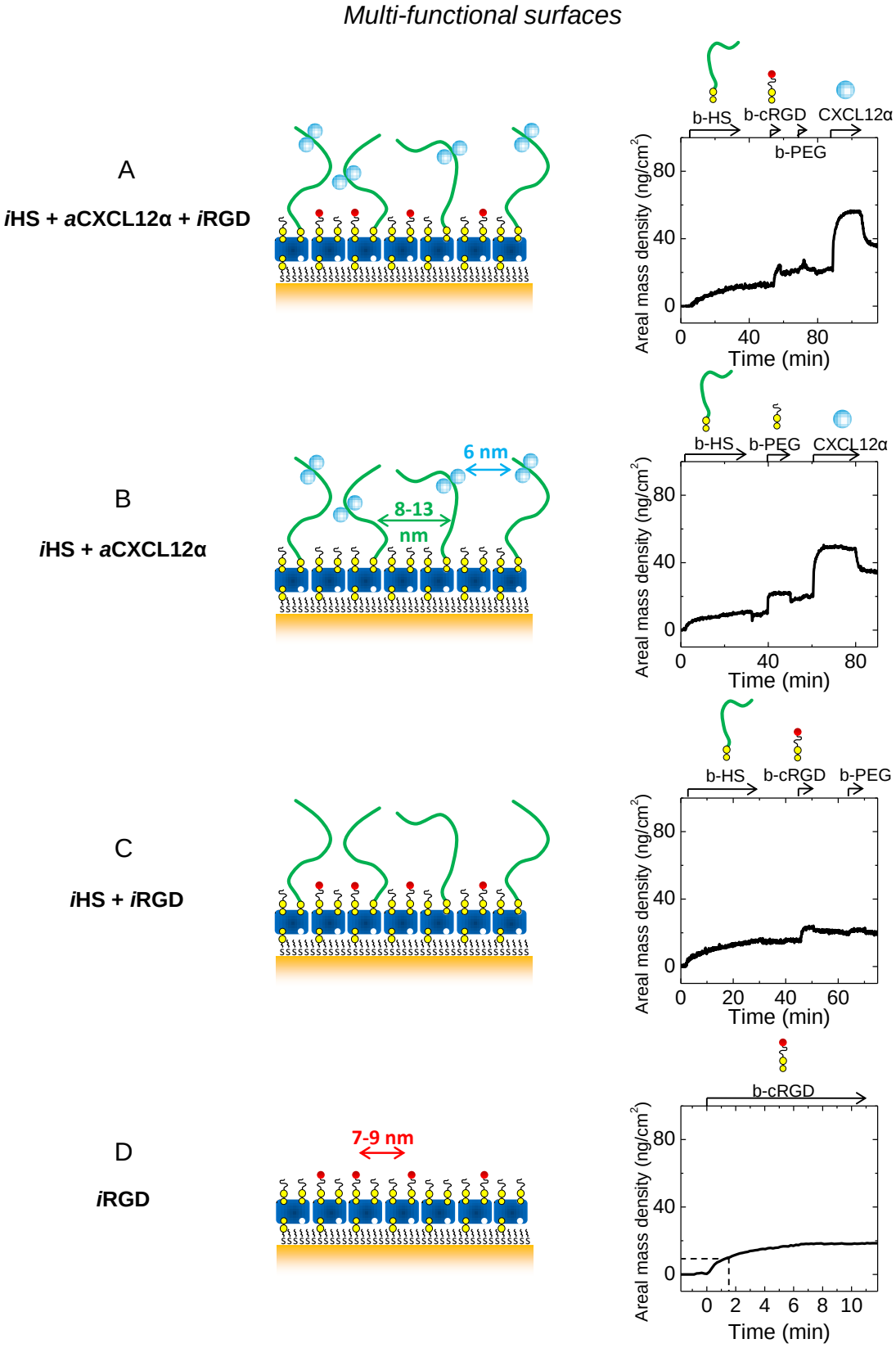

Figure 3. ***Design and preparation of multifunctional biomimetic surfaces presenting GAG-bound chemokine and cell adhesion ligands.*** *Schematic presentation of model surfaces (left) used to study the joint effect of HS-bound CXCL12α (iHS + aCXCL12α) and the immobilized cell adhesion ligand RGD (iRGD) on myoblast adhesion and motility;*

surface functionalization was followed by SE to quantify areal mass densities (right). Schemes and SE data are displayed analogous to Fig. 1B. Next to surfaces displaying iHS, aCXCL12α and iRGD (A), controls displaying only one or two of the three components (B-D) at comparable surface densities were also prepared. RGD was immobilized through a PEG-linked biotin; b-PEG was used to back-fill the remaining free biotin-binding pockets, if any, on the breadboard.

Table 1. ***Adsorbed amounts (Γ) and root-mean-square anchor distances r_{rms} for the constituents of biomimetic surfaces.*** *Data was extracted from SE measurements. Mean values and standard errors are presented.*

	b-HS		CXCL12α		b-CXCL12α		b-RGD	
	Γ (ng/cm^2)	r_{rms} (nm)	Γ (ng/cm^2)	r_{rms} (nm)	Γ (ng/cm^2)	r_{rms} (nm)	Γ (ng/cm^2)	r_{rms} (nm)
			Chemokine-presenting surfaces					
*i*HS + *a*CXCL12α	35 ± 2	5 - 8 [a)]	78 ± 7	4				
*i*CXCL12α					60 ± 1	5		
			Multi-functional surfaces					
*i*HS + *a*CXCL12α + *i*RGD [b)]	13 ± 1	8 - 13 [a)]	37 ± 3	6			9 ± 2	7 - 9 [a)]

[a)] Upper bounds are determined by assuming that the average molecular mass of surface-bound molecules is identical to the average solution-phase molecular mass; lower bounds are determined assuming a stoichiometry of two biotinylated molecules per SAv at maximal coverage.

[b)] All the controls, i.e. surfaces that lacked one or two of the biofunctional components (i.e. HS, CXCL12α, or RGD) present all remaining biofunctional components with surface densities and rms distances unchanged.

3.4. Effect of co-presentation of HS-bound CXCL12α with RGD, on myoblast adhesion

Cell adhesion to multifunctional surfaces presenting additionally RGD was analyzed analogously to the chemokine-presenting surface (Figs. 4 and S3). The responses on the control surface presenting only HS-bound CXCL12α were similar to those shown in Fig. 2, for 1 h as well as 4 h of exposure, i.e. the moderate reduction in HS and CXCL12α surface density on the control surfaces shown in Fig. 4 (by roughly 3-fold and 2-fold, respectively, compared to Fig. 2) did only slightly affected the cellular responses. Cells adhered and spread significantly on RGD presenting surfaces either alone (*i*RGD) or in the presence of HS (*i*HS + *i*RGD) with a pronounced formation of actin stress-fibers (Fig. 4B), as expected for integrin-mediated adhesion. Interestingly when the cells were exposed to surfaces co-presenting HS-bound CXCL12α and RGD (*i*HS + *a*CXCL12α + *i*RGD), there was a significant further increase in the spreading of cells. This

demonstrates that HS-bound CXCL12α and RGD promote cell adhesion and spreading synergistically. It is particularly interesting that the combined presentation of HS-bound CXCL12α and RGD enhances cell spreading already after 1h of exposure, i.e. under conditions at which HS-bound CXCL12α alone did not have any appreciable effect. This suggests that the enhanced spreading is more than the simple superposition of two independent adhesion-promoting cellular processes. Co-presentation of HS with RGD (*i*HS + *i*RGD) did not affect cell spreading compared to RGD alone (*i*RGD). This demonstrates that the synergistic effect observed on surfaces co-presenting HS-bound CXCL12α and RGD requires CXCL12α. When CXCL12α binding to its cell-surface receptor CXCR4 was blocked with *s*AMD3100, cell spreading was also reduced to the levels observed for RGD alone (Fig. 4D), demonstrating that the synergistic effect requires the binding of CXCL12α to CXCR4. In addition, the presence of sCXCL12α with *i*RGD did not lead to enhanced cell spreading (Fig. S4D-F), i.e. the synergistic effect requires HS-bound CXCL12α. This assay thus demonstrates that the co-presentation of an integrin ligand and a GAG-bound chemokine elicits a cellular response that is distinct from the response to each individual cue alone.

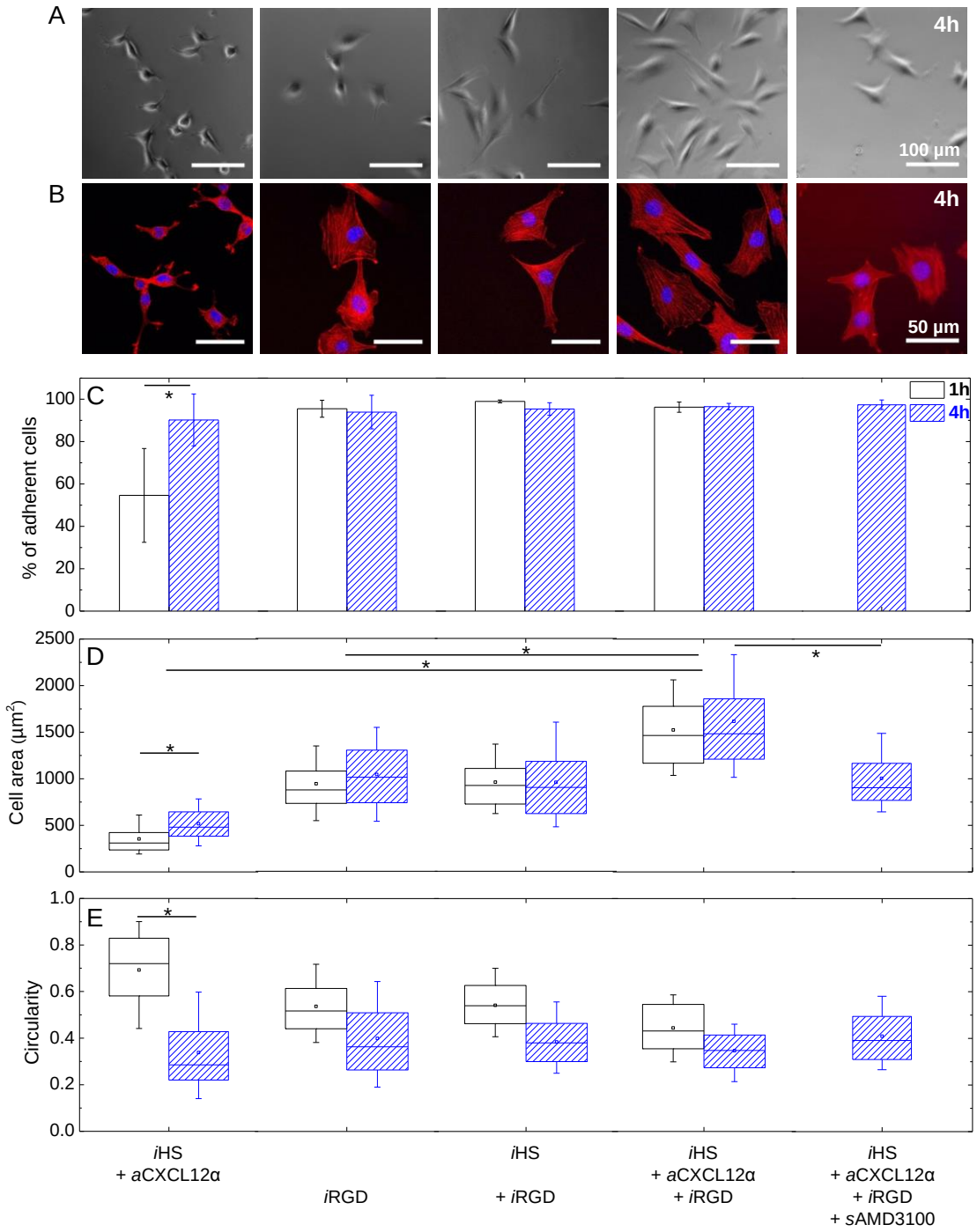

Figure 4. ***Effect of RGD, and co-presentation of HS-bound CXCL12α with RGD, on myoblast adhesion, spreading and circularity.*** *Adhesion and spreading of C2C12 myoblasts on model surfaces presenting HS (iHS) or HS-bound chemokine (aCXCL12α) with or without cell adhesion ligand (iRGD), each at comparable surface densities. Data are displayed analogous to Fig. 2.*

3.5. Effect of CXLC12α, RGD and their combination on cell migration

As CXCL12α plays a key role in trafficking, by regulating the migration of both proliferative and terminally differentiated muscle cells, [6, 9, 35] we next addressed the question whether matrix-bound CXCL12α, in particular HS-bound, initiates cell migration. At first, we investigated whether the CXCL12α presentation mode ("*a*" or "*i*") affected cell migration. The motility of C2C12 myoblasts on surfaces with different CXCL12α presentations was assessed by recording time-lapse images over 4 h and tracking individual cells (Fig. 5). Fig. 5A-B demonstrates that the cells are essentially immotile on *i*HS alone as the cell tracks remain confined to a narrow area around the starting point and the mean velocity is low. A significant increase in the mean velocity (Fig 5B) was observed when CXCL12α was additionally presented through HS (*i*HS + *a*CXCL12α), demonstrating that *a*CXCL12α promotes myoblast motility. In striking contrast, the cells were immotile on *i*CXCL12α, indicating that the mode of CXCL12α presentation is a crucial factor for motility. Fig. 5C provides insight into temporal variations in the cellular motility. It can be seen that cells respond to HS-bound CXCL12α (as compared to *i*HS alone or to *i*CXCL12α) already within the first 30 min after exposure, yet about 2 h are required to reach the maximal response. The maximal response was then largely retained for the remainder of the exposure.

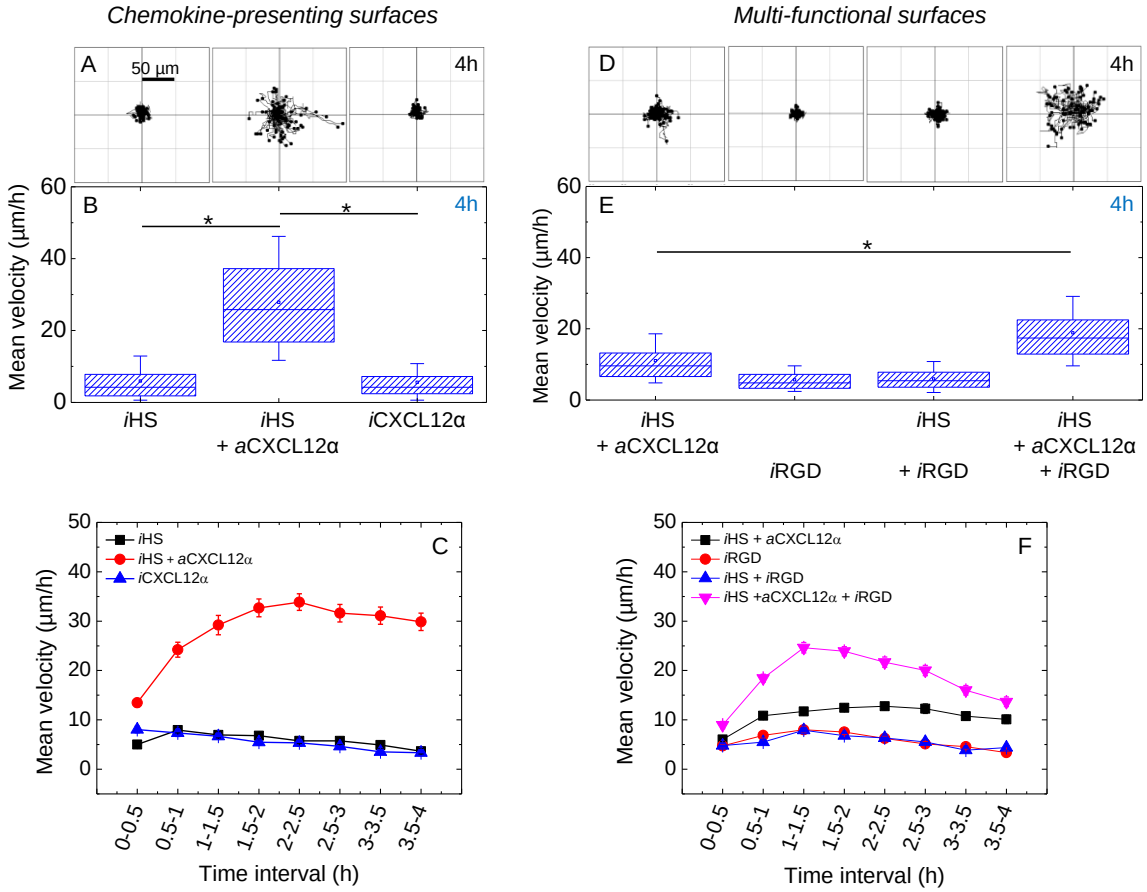

Figure 5. ***Effect of CXLC12α, RGD and their combination on cell migration.*** *(A, D) Trajectories of the nucleus of C2C12 myoblasts over a period of 4 h after plating on*

surfaces presenting different surface functionalizations (chemokine presenting surfaces – A; multifunctional surfaces – D; 80 trajectories are shown in each panel, all taken from one representative measurement). (B, E) Corresponding box plots of the mean velocity (µm/h) throughout 4 h of exposure, computed for a total of 240 cells from three independent measurements. (C, F) Corresponding variations in the mean velocity as a function of time; here, the mean velocity was computed over intervals of 0.5 h and data represent the average and standard errors of the mean (S.E.M.) over 240 cells taken from three independent measurements.

Next, we investigated if the co-presentation of the cell-adhesion ligand with HS-bound CXCL12α affected cell migration. For this purpose, we performed motility assays on multi-functional surfaces presenting HS-bound CXCL12α jointly with *i*RGD. Figure 5D-F demonstrates that the motility of cells is retained (although reduced in magnitude) on surfaces that present a roughly 2-fold reduced density of HS-bound CXCL12α compared to HS-saturated surfaces (Fig. 5A-C). In contrast, cells were immotile on surfaces presenting *i*RGD irrespective of the presence of *i*HS. Strikingly, HS-bound CXCL12α in combination with RGD (*i*HS + *a*CXCL12α + *i*RGD) promoted a level of motility that was even higher than that observed for HS-bound CXCL12α alone. Clearly, HS-bound CXCL12α and RGD also have a synergistic effect on motility. Notably, the mean velocity of the cells on HS-bound CXCL12α in the presence of RGD rose to a maximum within the first 1.5 hours, and then decreased again (Fig. 5F). This is in contrast to HS-bound CXCL12α alone, where a stabilization of the motility at an elevated level is observed (Figs. 5C and F). Taken together, HS-bound CXCL12α (*i*HS + *a*CXCL12α) but not *i*CXCL12α promotes C2C12 myoblast motility, both alone and in combination with *i*RGD.

4. Discussion

CXCL12α and its receptor CXCR4 have been shown to play a key role in tissue development and regeneration [36] as mice deficient in CXCR4 exhibited impaired myogenesis [10]. CXCR4 activation upon CXCL12α binding induces various signalling pathways that regulate the adhesion and migration of muscle progenitors [9]. Hence, CXCL12α is a suitable signalling molecule for studying *in vitro* muscle development and repair.

To understand the cellular behavior in response to specific molecular cues, it is desirable to create well-defined model surfaces. Our approach consisted in designing biomimetic surfaces that display HS with chemokines and other ECM components, e.g. integrin ligands promoting cell adhesion. These model surfaces are well-defined with a controlled orientation of the ligand, in a background of low non-specific binding. The surface density of each ligand can be quantitatively tuned. SE was used to characterize and control the densities of biomolecules. The biofunctionality of the biomolecules was assessed by their effects on cellular adhesion and motility. These biomimetic surfaces mimic muscle extracellular matrix in that they reproduce the supramolecular

arrangement of ECM and cell-surface GAGs (attached to the surface through the reducing end, thus mimicking the native attachment of HS to its proteoglycan core), and chemokines (bound to GAGs).

The adhesion observed on HS-bound *a*CXCL12α is quite remarkable, considering that no cell adhesion ligand was involved, suggesting that CXCL12α alone also promotes adhesion. In addition, the adhesion on HS-bound *a*CXCL12 suggests that CXCL12α interacts simultaneously and in trans with HS and CXCR4, which is consistent with the observation that in CXCL12α, the binding domains for GAG and CXCR4 are spatially distant and do not interfere functionally [14].

It has been previously shown that cell lines derived from satellite cells such as C2C12 cells possess the CXRC4 receptor [12]. Moreover, blocking CXCL12α binding to the cell-surface receptor CXCR4 with the CXCR4 antagonist sAMD3100 impaired cellular adhesion (Figs. 2C-E), demonstrating that the adhesion of C2C12 myoblasts to surfaces presenting CXCL12α is mediated by the specific binding of CXCL12α to CXCR4. Besides CXCR4, CXCR7 was also recently reported as another CXCL12α receptor involved in C2C12 myoblast response to CXCL12α [13, 37]. However, Dalonneau *et al.* [23] have recently shown that only CXCR4 was the major CXCL12α receptor expressed in C2C12 cells in our culture conditions, CXCR7 being not visible in these experimental conditions [23].

With these well-defined model surfaces in hand, we studied the response of myoblasts to surfaces presenting the chemokine CXCL12α in two different presentation modes. C2C12 myoblasts responded to CXCL12α reversibly bound to its natural ligand HS with pronounced adhesion and motility (Figs. 2 and 5). In contrast, irreversibly surface-bound CXCL12α (in the absence of HS) promoted adhesion but impaired motility (Figs. 2 and 5). This demonstrates that the way in which the chemokine is presented, and in particular the presence of HS, is important for regulating cellular behaviour. At the molecular level, HS has been shown to dimerize CXCL12α upon binding [33, 38, 39]. In addition, *a*CXCL12α was reversibly bound to HS, as CXCL12α can be eluted in high salt concentrations [28]. In contrast, *i*CXCL12α which is monomeric in this presentation was bound *via* strong and stable SAv-biotin bonds and hence quasi-irreversibly bound (Fig. S1B). The presentations of CXCL12α presented though HS (i.e. *a*CXCL12α) and in the form of *i*CXCL12α are distinct: *a*CXCL12α is dimeric [33] and reversibly bound whereas *i*CXCL12α is monomeric and quasi-irreversibly immobilized. These differences might account for the differences in cellular responses observed on the two presentations. We hypothesize that the cells prefer the reversibly bound *a*CXCL12α facilitating its internalization, which could initiate internal signalization inducing motility which was lacking in the quasi-irreversibly bound *i*CXCL12α. Indeed, internalization of CXCL12α has been shown to induce downstream signalling [40]. Future studies should investigate if there is a potential internalization of the reversibly HS-bound CXCL12α which leads to distinct downstream effects that are not analysed here.

We investigated the response of C2C12 cells to the co-presentation of chemokines and cell adhesion ligands. For this purpose we designed surfaces that present cell adhesion ligand RGD along with chemokines (bound to GAGs). We observed a significant enhancement in adhesion, spreading and motility on surfaces co-presenting RGD with HS-bound *a*CXCL12α compared to each individual cue alone. Apparently, CXCR4 (the chemokine receptor) and integrins (the RGD receptors) on the cell surface can act synergistically to control cellular adhesion and migration. This remarkable effect suggests a potential cross-talk between the two receptors. In fact, integrins have been shown to mediate phosphorylation of growth factor receptors even in the absence of growth factor ligands [41]. Based on this, it is possible that integrins may also activate CXCR4 receptors, which could explain the fact that even in the absence of cellular response to CXCL12α alone after 1h we still observed a synergistic effect between the two receptors (both the integrins and the activated CXCR4) on co-presentation of two ligands. This is however a hypothesis, future studies should focus on elucidation of this cross-talk between the two receptors. To this end, studies could focus on the different signalization events that are involved in the inter-play between the two receptors. For example, Moro *et al.* have reported that integrins induce a phosphorylation of specific tyrosine residues of growth factor receptor during its activation, which is distinct from that induced during activation by the normal growth factor ligand [42].

5. Conclusion

The strategy to design biomimetic surfaces developed here represents a versatile experimental platform for mechanistic studies of chemokine-(GAG-bound)-mediated cell-cell and cell-matrix communication. The mode of CXCL12α presentation plays an important role in myoblast adhesion and adhesion. Chemokine presentation *via* GAGs is a requisite for myoblast motility but not adhesion. These surfaces mimicking the muscle extracellular matrix provide insights into the role of GAG-bound CXCL12α presented under physiological (i.e. natural) conditions, in muscle development and repair. A synergistic effect, suggesting cross-talk between CXCR4 and integrin was observed on co-presentation of GAG-bound chemokines and cell adhesion ligands. Elucidation of this cross-talk would lead to further expansion of the already broad functions of integrins. This may have far-reaching implications for cell-cell and cell-matrix communications during controlled adhesion and migration of myoblasts in muscle development and repair. Our future studies will aim to study the directed migration of C2C12 cells on gradients of HS-bound CXCL12α. The strategy to create multifunctional biomimetic surfaces should find applications as mimics of the extracellular matrix by presenting different matrix or cell surface components in a well-defined way.

Acknowledgements

We gratefully acknowledge Françoise Baleux (Institut Pasteur, Paris, France) for providing b-CXCL12α, Rabia Sadir (Institut de Biologie Structurale, Grenoble, France) for providing CXCL12α, Luis Yate (CIC biomaGUNE) for surface coatings and Xi Qiu Liu (LMGP) for fruitful discussions. We acknowledge funding by the Nanoscience Foundation Chair of Excellence Project “GAG2D” to R.P.R., the NanoBio programme, the ICMG FR 2607, and the French National Research Agency via Labex ARCANE (ANR-11-LABX-0003-01). CP is grateful to the European Commission for funding via an ERC Starting Grant (GA259370).

References

[1] Yin H, Price F, Rudunicki MA. Satellite cells and the muscle stem cell niche. Physiol Rev. 2013;93:23-67.

[2] Jansen KM, Pavlath GK. Mannose receptor regulates myoblast motility and muscle growth. J Cell Biol. 2006;174:403-13.

[3] Thorsteinsdottir S, Deries M, Cachaco AS, Bajanca F. The extracellular matrix dimension of skeletal muscle development. Dev Biol. 2011;354:191-207.

[4] Mylona E, Jones KA, Mills ST, Pavlath GK. CD44 regulates myoblast migration and differentiation. J Cell Physiol. 2006;209:314-21.

[5] O'Connor RS, Mills ST, Jones KA, Ho SN, Pavlath GK. A combinatorial role for NFAT5 in both myoblast migration and differentiation during skeletal muscle myogenesis. J Cell Sci. 2006;120:149-59.

[6] Griffin CA, Apponi LH, Long KK, Pavlath GK. Chemokine expression and control of muscle cell migration during myogenesis. J Cell Sci. 2010;123:3052-60.

[7] Luster AD. Chemokines - Chemotactic cytokines that mediate inflammation. N Engl J Med. 1998;338:436-45.

[8] Yusuf F, Rehimi R, Moros¸an-Puopolo G, Dai F, Zhang X, Brand-Saberi B. Inhibitors of CXCR4 Affect the Migration and Fate of CXCR4 Progenitors in the Developing Limb of Chick Embryos. Dev Dyn. 2006;235:3007-15.

[9] Vasyutina E, Stebler J, Brand-Saberi B, Schulz S, Raz E, Birchmeier C. CXCR4 and Gab1 cooperate to control the development of migrating muscle progenitor cells. Genes Dev. 2005;19:2187-98.

[10] Odemis V, Lamp E, Pezeshki G, Moepps B, Schilling K, Gierschik P, et al. Mice deficient in the chemokine receptor CXCR4 exhibit impaired limb innervation and myogenesis. Mol Cell Neurosci. 2005;30:494-505.

[11] Odemis V, Boosmann K, Dieterlen MT, Engele J. The chemokine SDF1 controls multiple steps of myogenesis through atypical PKC. J Cell Sci. 2007;120:4050-9.

[12] Ratajczak MZ, Majka M, Kucia M, Drukala J, Pietrzkowski Z, Peiper S, et al. Expression of Functional CXCR4 by Muscle Satellite Cells and Secretion of SDF-1 by Muscle-Derived Fibroblasts is Associated with the Presence of Both Muscle Progenitors in Bone Marrow and Hematopoietic Stem/Progenitor Cells in Muscles. Stem Cell. 2003;21:363-71.

[13] Melchionna R, Di Carlo A, De Mori R, Cappuzzello C, Barberi L, Musaro A, et al. Induction of myogenic differentiation by SDF-1 via CXCR4 and CXCR7 receptors. Muscle Nerve. 2010;41:828-35.

[14] Laguri C, Arenzana-Seisdedos F, Lortat-Jacob H. Relationships between glycosaminoglycan and receptor binding sites in chemokines-the CXCL12 example. Carbohydr Res. 2008;343:2018-23.

[15] Hacker U, Nybakken K, Perrimon N. Heparan sulphate proteoglycans: the sweet side of development. Nat Rev Mol Cell Biol. 2005;6:530-41.

[16] Sarrazin S, Lamanna WC, Esko JD. Heparan sulfate proteoglycans. Cold Spring Harb Perspect Biol. 2011;3.
[17] Bernfield M, Gotte M, Park PW, Reizes O, Fitzgerald ML, Lincecum J, et al. Functions of cell surface heparan sukfate proteoglycans. Annu Rev Biochem. 1999;68:729-77.
[18] Lortat-Jacob H. The molecular basis and functional implications of chemokine interactions with heparan sulphate. Curr Opin Struct Biol. 2009;19:543-8.
[19] Massena S, Christoffersson G, Hjertstrom E, Zcharia E, Vlodavsky I, Ausmees N, et al. A chemotactic gradient sequestered on endothelial heparan sulfate induces directional intraluminal crawling of neutrophils. Blood. 2010;116:1924-31.
[20] Rueda P, Balabanian K, Lagane B, Staropoli I, Chow K, Levoye A, et al. The CXCL12gamma chemokine displays unprecedented structural and functional properties that make it a paradigm of chemoattractant proteins. PloS one. 2008;3:e2543.
[21] Ward SG, Bacon K, Westwick J. Chemokines and T Lymphocytes: More than an Attraction. Immunity. 1998;9:1-11.
[22] Bokoch GM. Chemoattractant Signaling and Leukocyte Activation. Blood. 1995;86:1649-60.
[23] Dalonneau F, Liu XQ, Sadir R, Almodovar J, Mertani HC, Bruckert F, et al. The effect of delivering the chemokine SDF-1alpha in a matrix-bound manner on myogenesis. Biomaterials. 2014;35:4525-35.
[24] Migliorini E, Thakar D, Sadir R, Pleiner T, Baleux F, Lortat-Jacob H, et al. Well-defined biomimetic surfaces to characterize glycosaminoglycan-mediated interactions on the molecular, supramolecular and cellular levels. Biomaterials. 2014;35:8903-15.
[25] Gribova V, Gauthier-Rouviere C, Albiges-Rizo C, Auzely-Velty R, Picart C. Effect of RGD functionalization and stiffness modulation of polyelectrolyte multilayer films on muscle cell differentiation. Acta Biomater. 2013;9:6468-80.
[26] Thakar D, Migliorini E, Coche-Guerente L, Sadir R, Lortat-Jacob H, Boturyn D, et al. A quartz crystal microbalance method to study the terminal functionalization of glycosaminoglycans. Chem Commun. 2014;50:15148-51.
[27] Laguri C, Sapay N, Simorre JP, Brutscher B, Imberty A, Gans P, et al. 13C-labeled heparan sulfate analogue as a tool to study protein/heparan sulfate interactions by NMR spectroscopy: application to the CXCL12alpha chemokine. J Am Chem Soc. 2011;133:9642-5.
[28] Amara A, Lorthioir O, Valenzuel A, Magerus A, Thelen M, Montes M, et al. Stromal Cell-derived Factor-1a Associates with Heparan Sulfates through the First b-Strand of the Chemokine. J Biol Chem. 1999;274:23916-25.
[29] Boturyn D, Dumy P. A convenient access to aVb3:aVb5 integrin ligand conjugates: regioselective solid-phase functionalisation of an RGD based peptide. Tetrahedron Lett. 2001;42:2787-90.
[30] Dubacheva GV, Curk T, Mognetti BM, Auzely-Velty R, Frenkel D, Richter RP. Superselective targeting using multivalent polymers. J Am Chem Soc. 2014;136:1722-5.

[31] Ren K, Fourel L, Rouviere CG, Albiges-Rizo C, Picart C. Manipulation of the adhesive behaviour of skeletal muscle cells on soft and stiff polyelectrolyte multilayers. Acta Biomater. 2010;6:4238-48.
[32] Pfaff M, Tangemann K, Muller B, Gurrath M, Muller G, Kessler H, et al. Selective Recognition of Cyclic RGD Peptides of NRlR Defined Conformation by aIIbb3, aVb3, and a5bl Integrins. J Biol Chem. 1994;269:20233-8.
[33] Sadir R, Baleux F, Grosdidier A, Imberty A, Lortat-Jacob H. Characterization of the stromal cell-derived factor-1alpha-heparin complex. J Biol Chem. 2001;276:8288-96.
[34] Sadir R, Imberty A, Baleux F, Lortat-Jacob H. Heparan sulfate/heparin oligosaccharides protect stromal cell-derived factor-1 (SDF-1)/CXCL12 against proteolysis induced by CD26/dipeptidyl peptidase IV. J Biol Chem. 2004;279:43854-60.
[35] Yusuf F, Rehimi R, Morosan-Puopolo G, Dai F, Zhang X, Brand-Saberi B. Inhibitors of CXCR4 affect the migration and fate of CXCR4+ progenitors in the developing limb of chick embryos. Dev Dyn. 2006;235:3007-15.
[36] Avigdor A, Goichberg P, Shivtiel S, Dar A, Peled A, Samira S, et al. CD44 and hyaluronic acid cooperate with SDF-1 in the trafficking of human CD34+ stem/progenitor cells to bone marrow. Blood. 2004;103:2981-9.
[37] Hunger C, Odemis V, Engele J. Expression and function of the SDF-1 chemokine receptors CXCR4 and CXCR7 during mouse limb muscle development and regeneration. Exp Cell Res. 2012;318:2178-90.
[38] Fermas S, Gonnet F, Sutton A, Charnaux N, Mulloy B, Du Y, et al. Sulfated oligosaccharides (heparin and fucoidan) binding and dimerization of stromal cell-derived factor-1 (SDF-1/CXCL 12) are coupled as evidenced by affinity CE-MS analysis. Glycobiology. 2008;18:1054-64.
[39] Murphy JW, Cho Y, Sachpatzidis A, Fan C, Hodsdon ME, Lolis E. Structural and functional basis of CXCL12 (stromal cell-derived factor-1 alpha) binding to heparin. J Biol Chem. 2007;282:10018-27.
[40] Hatse S, Balzarini J, Liekens S. Stromal cell-derived factor 1 (CXCL12) binds to endothelial cells and signals through a receptor different from CXCR4. Biochem Biophys Res Commun. 2006;348:192-9.
[41] Yamada KM, Even-Ram S. Integrin regulation of growth factor receptors. Nat Cell Biol. 2002;4:E75-E6.
[42] Moro L, Dolce L, Cabodi S, Bergatto E, Boeri Erba E, Smeriglio M, et al. Integrin-induced epidermal growth factor (EGF) receptor activation requires c-Src and p130Cas and leads to phosphorylation of specific EGF receptor tyrosines. J Biol Chem. 2002;277:9405-14.

Supplementary Information

The presentation mode of chemokine display determines myoblast adhesion and motility

Dhruv Thakar, Fabien Dalonneau, Elisa Migliorini, Hugues Lortat-Jacob, Didier Boturyn, Liliane Coche-Guerente, Catherine Picart and Ralf P. Richter

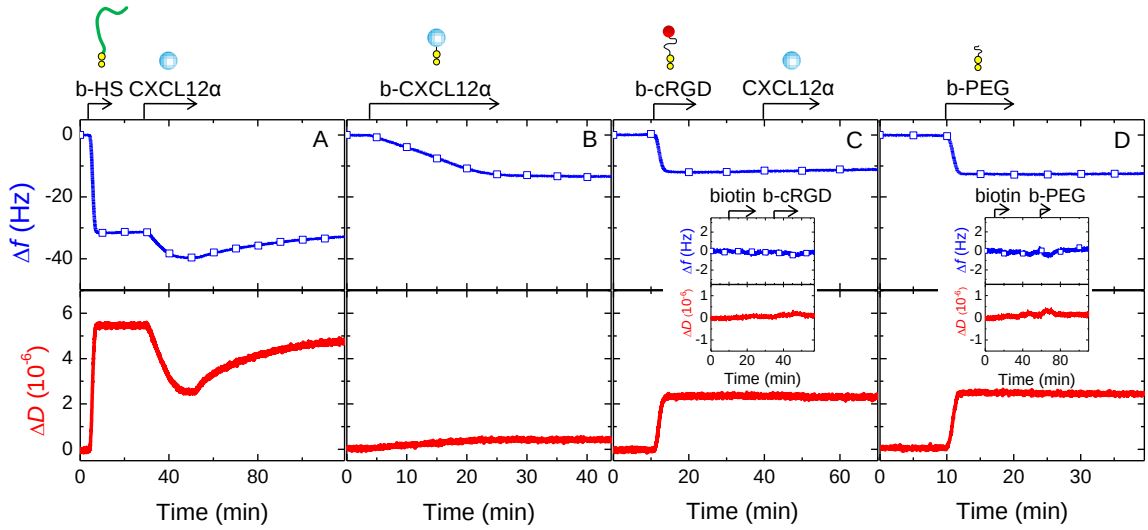

Figure S1. ***Controls for specific and oriented immobilization of functional molecules.*** *Binding of functional molecules to the molecular breadboard, i.e. SAv monolayers on gold-supported monlayers of biotinylated OEG thiols was followed by quartz crystal microbalance (QCM-D; frequency shifts, Δf – blue lines with square symbols, dissipation shifts, ΔD – red lines). Start and duration of incubation steps with different samples are indicated by arrows; during all other times, the surface was exposed to working buffer. Responses for b-HS and CXCL12α on b-HS (A; incubated at 50 µg/mL) and for b-CXCL12α (B; incubated at 5 µg/mL) are comparable to those previously reported and analyzed in detail by Migliorini et al. [1] Briefly, the data indicate that: b-HS is immobilized specifically through its reducing-end biotin and forms a soft and hydrated HS film of approximately 12 nm thickness; CXCL12α binds specifically to HS and rigidifies the HS film, this binding is partially reversible, i.e. some CXCL12α is released over experimentally accessible time scales whereas a sizeable fraction remains rather stably bound and displayed by HS; b-CXCL12α is immobilized specifically and stably through its C-terminal biotin thus displaying its binding sites for HS and the cell surface receptor CXCR4 towards the solution. Immobilization of b-RGD (C; incubated at 10 µg/mL) and b-PEG (D; incubated at 50 µg/mL): monotonous QCM-D responses, binding to saturation and full stability upon rinsing in buffer are consistent with the formation of monolayers of b-RGD and b-PEG. Neither b-RGD nor b-PEG bound to a SAv monolayer that had previously been saturated with biotin (insets in C and D, respectively), confirming specific immobilization. Final responses of Δf = -13 ± 1 Hz and ΔD = 2.5 ± 0.2 × 10^{-6} for b-RGD, and Δf = -12 ± 1 Hz and ΔD = 2.4 ± 0.2 × 10^{-6} for b-PEG, are consistent with a soft and hydrated layer of a few nm in thickness, expected for monolayers based on the molecules' dimensions and flexible structure. Surfaces presenting b-RGD remain inert to non-specific binding of CXCL12α (C).*

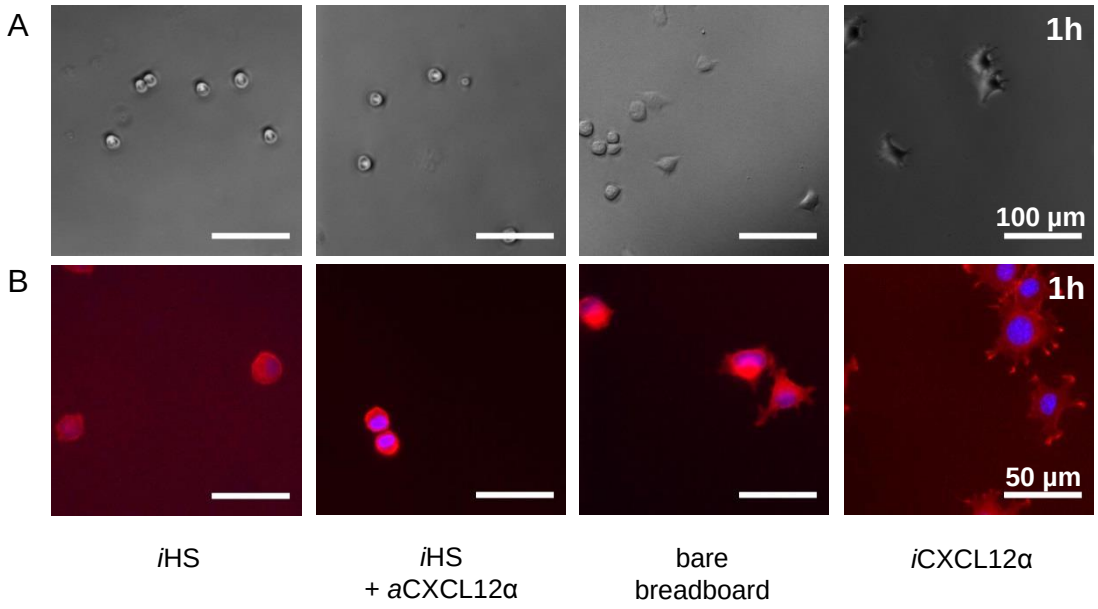

Figure S2. ***Complementary images for Fig. 2, showing cells after 1 h of exposure.*** *Images in A are displayed analogous to Fig. 2A and F, and images in B analogous to Fig. 2B and G.*

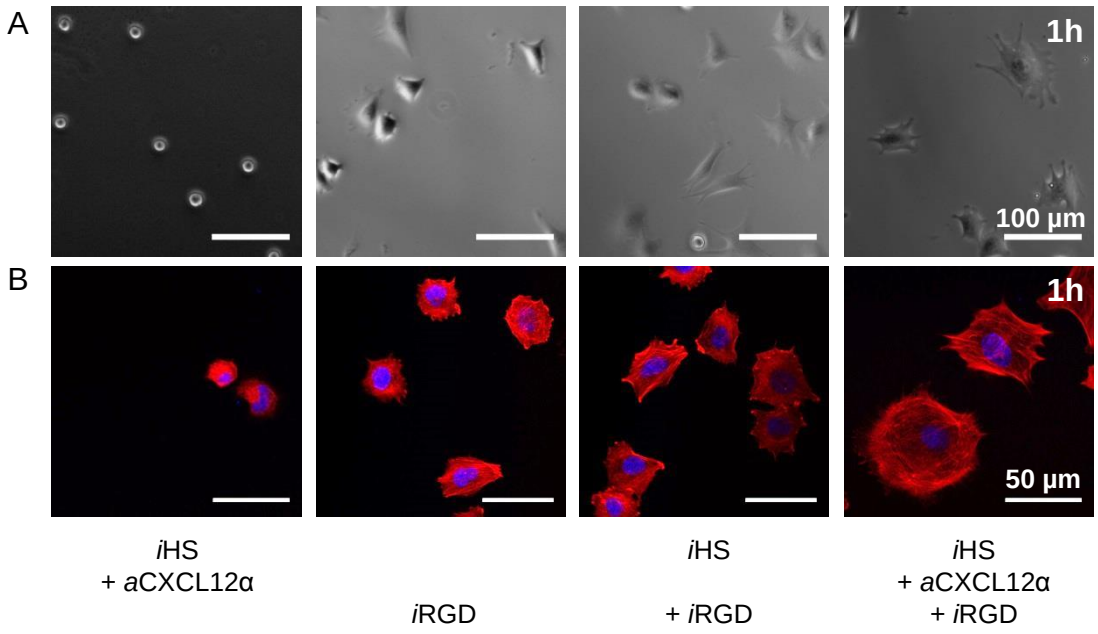

Figure S3. ***Complementary images for Fig. 4, showing cells after 1 h of exposure.*** *Images are displayed analogous to Fig. 4A-B.*

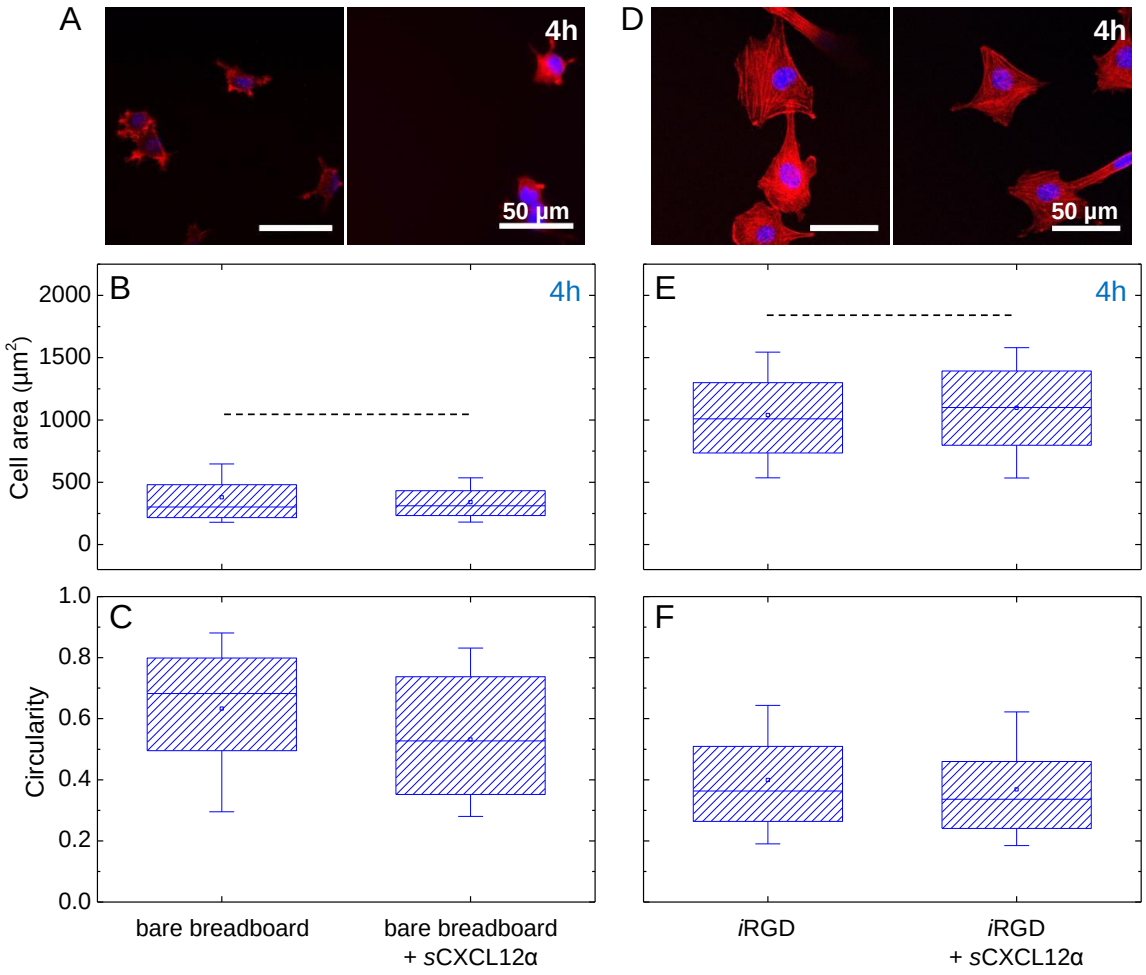

Figure S4. ***Effect of CXCL12α in solution (sCXCL12α) on cytoskeleton organization and cell spreading.*** *C2C12 myoblasts were plated for 4 h on the bare SAv breadboard (c.f. fig. 1A) (A-C) or on iRGD (c.f. Fig. 3D) (D-F) with or without solution-phase CXCL12α (sCXCL12α, 5µg/mL). (A, D) Representative fluorescence micrographs of fixed cells with the nuclei labeled in blue and actin in red reveal no clear effect of sCXCL12α on cytoskeleton organization. Moreover, box plots (analogous to Fig. 2) of the mean cell area (B, E) and circularity (C, F) also demonstrate no significant effect of sCXCL12α. Thus, the enhanced myoblast spreading observed in Figs. 2 and 4 requires CXCL12α in matrix-bound forms.*

Supplementary references

[1] Migliorini E, Thakar D, Sadir R, Pleiner T, Baleux F, Lortat-Jacob H, et al. Well-defined biomimetic surfaces to characterize glycosaminoglycan-mediated interactions on the molecular, supramolecular and cellular levels. Biomaterials. 2014;35:8903-15.

VI. Concluding remarks and perspectives

The objective of this PhD thesis was to develop biomimetic surfaces that are highly defined and tunable, for mechanistic studies of GAG-protein interactions on the molecular and supramolecular levels, and to probe cellular responses to defined biochemical and biophysical cues to better understand GAG-mediated cell-cell and cell-matrix communications. In the following, main achievements and their potential extension for further studies are summarized.

VI.1. Terminal functionalization of glycosaminoglycans

We have established oxime ligation as a facile, one-step method for the selective conjugation of GAGs at the reducing end. The method is superior in yield and stability to the commonly used hydrazone ligation, and versatile in that it can be applied to GAGs of various (most likely any) types and sizes. In addition, we have demonstrated QCM-D to be an instrumental technique for the characterization of conjugates made from chemically complex molecules such as GAGs, providing information about reaction yields, sample degradation and sample composition that is difficult to assess using conventional analytical techniques, in particular when the amount of sample is limited to a few micrograms.

This method could be extended for creating GAG conjugates with more complex, multi-functional ligands, for example GAG conjugates carrying a fluorescent label (ATTO) together with biotin, which would find applicability in a wide range of applications such as imaging, immobilization or enzymatic detection (e.g. with streptavidin-horseradish peroxidase).

Another possible application is the design of GAG mimics where different saccharides are artificially attached with a particular conformation. For example, two different oligosaccharides presenting sulfate groups at particular distances can be joined, providing a control over the distance between sulfate groups. These conjugates can be exploited to study the effect of distance between sulfate groups on their interaction with proteins. For this purpose, a bifunctional linker presenting two oxyamine groups can be exploited to attach two different oligo or polysaccharides.

In conclusion, the method should find broad use, as a tool in the glycosciences and in biotechnological applications. In particular, the control over and stability of GAG conjugates are crucial for the reliable preparation of GAG-functionalized surfaces and scaffolds for tissue engineering and fundamental biological studies. Indeed, these conjugates were used in separate although related research project of the group of Ralf Richter at CIC biomaGUNE, Spain, which has led to a publication on which I am co-author (N. Baranova *et al.*, *J. Biol. Chem., 2*89 (2014) 30481–98).

VI.2. Preparation of well-defined biomimetic surfaces

We have presented a versatile strategy to create biomimetic surfaces that present GAGs together with other cell surface or extracellular matrix molecules in a background of low non-specific binding. These biomimetic surfaces are based on a 'molecular breadboard' i.e. a SAv monolayer, grafted either on OEG monolayers or on SLBs. We have demonstrated that the orientation of the immobilized molecules can be controlled and their surface density tuned, thanks to the surface design and quantitative characterization by surface sensitive techniques. In addition, we have demonstrated the potential of this platform for functional studies on the molecular, supramolecular and cellular levels.

These biomimetic surfaces mimicking the muscle extracellular matrix provided insights into the role of CXCL12α presented under physiological conditions, in muscle development and repair. However, these biomimetic surfaces are not limited to only studying muscle development and repair; they also hold potential for applications well beyond what is exploited during this thesis. In fact, any biomolecule can be grafted to these surfaces, presenting a biotin tag being a requisite, and cellular mechanistic studies can be performed to interrogate its biological function. These surfaces should also find broad applicability in cellular mechanistic studies where cellular responses to different presentations of biomolecules are to be studied. The strategy to create multifunctional biomimetic surfaces that present different biomolecules should be broadly applicable for interrogating the cross-talk between two cellular receptors.

VI.3. Supramolecular HS-chemokine interactions

The biomimetic surfaces were used to study supramolecular HS-protein interactions. We demonstrate that chemokines and other growth factors cross-link HS chains, and this cross-linking ability is a generic feature of these proteins, which depends on the architecture of their HS binding sites. We propose that several binding sites well separated either through GAG-repellent borders on the protein's surface or through spatial separation in quaternary protein structures, are required for GAG cross-linking. In the case of the chemokine CXCL12, we propose a mechanism behind HS cross-linking which is based on the co-existence of two types of dimers i.e. β-sheet and N-terminal dimers, in the HS matrix, where the dimerization through β-sheets enhances the affinity of the protein for HS whereas dimerization through N-termini induces HS cross-linking, potentially forming dimers of dimers.

The ability of extracellular signaling proteins to influence matrix organization and physico-chemical properties implies that the functions of these proteins may not simply be confined to the activation of cognate cellular receptors. HS cross-linking on the cell surface or in ECM may lead to a reduction in the thickness of pericellular coats which

may render the cell-adhesion ligands visible that were usually hidden in the matrix, thus facilitating cell-cell and cell-matrix contacts. This adhesion is particularly important as it provides traction to the moving cell (on the surface), in the absence of which the cells may be dragged away, e.g. by the blood flow in the context of the leukocyte migration at the inner walls of blood vessels. Moreover, changes in the rigidity of the cellular glycocalyx through HS-crosslinking may provide a physical cue that guides the behaviour of cells.

The effect demonstrated here may have far-reaching implications for cell-cell and cell-matrix communication, and our predictions can be tested in future *in vitro* and *in vivo* assays.

VI.4. Response of myoblasts to biomimetic surfaces

The strategy to create biomimetic surfaces developed here represents a versatile experimental platform for mechanistic studies of chemokine-mediated cell-cell and cell-matrix communication, and of the role of GAGs in chemokine presentation. We have demonstrated that the way in which the chemokine is presented, and in particular the presence of HS, is important for regulating myoblast behavior. Myoblasts respond to CXCL12α reversibly bound to its natural ligand HS with pronounced adhesion and motility. In contrast, irreversibly surface-bound CXCL12α (in the absence of HS) promoted adhesion but impaired motility. Perhaps, the cells prefer the reversibly bound CXCL12α facilitating its internalization, which could initiate internal signalization inducing specific behavior. Indeed, internalization of CXCL12α has been shown to induce downstream signalling [1]. Future studies should investigate if there is a potential internalization of the reversibly HS-bound CXCL12α which leads to distinct downstream effects that are not detectable in the cell adhesion and motility assays used here. To this end, fluorescently labelled chemokine can be used. Another configuration of irreversibly bound CXCL12α can be used where chemokine instead of directly immobilized to the surface, is covalently attached to HS, thus similar to HS-bound chemokine, but with impaired CXCL12α release and consequently impaired internalization. This could provide further insights into the molecular origin of the distinct cellular behaviours observed.

This thesis has provided novel insights in the role of GAGs in chemokine-mediated myoblast behaviour. In addition, the work has raised many other questions that will require further work for which the biomimetic surfaces are very useful. Several possible directions of future study are described below. To understand the origin of different cellular responses on HS-bound and immobilized CXCL12α, cellular responses on surfaces that present HS and immobilized CXCL12α, where CXCL12α instead of being adsorbed to HS is directly immobilized on the surface, can be studied, and compared to HS-bound CXCL12α at similar surface density. The comparison in the responses would

provide further insights in the importance of presentation of chemokines and the role of HS in cellular responses.

The motility observed on reversibly HS-bound CXCL12α raises another question: do cells get polarised during movement? Future studies can be focused on studying the mechanism involved in cellular motility. Next, we observed a strikingly distinct morphology of the cells on *i*CXCL12α (i.e. CXCL12α quasi-irreversibly immobilized to the surface in the absence of HS), i.e. the formation of actin-rich protrusions. Future studies can be focused on understanding whether these protrusions are integrin rich and if integrins are also involved in the profound cellular adhesion observed on *i*CXCL12α. To this end, integrin labelling can be done, to identify if and which integrins are involved. Other important questions that arise are: are these protrusions static or dynamic, and do these protrusions belongs to filopodia or lamellipodia type? Future studies can be focused in finding answers to these questions.

We next designed multifunctional surfaces that mimic certain aspects of *in vivo* conditions. We report a significant enhancement in adhesion, spreading and motility on surfaces co-presenting RGD with HS-bound CXCL12α compared to each individual cue alone. This demonstrates that the cell receptors CXCR4 (CXCL12α receptor) and integrins (RGD receptor) can act synergistically in controlling cellular adhesion and migration. This suggests a cross-talk between CXCR4 and integrin. Future studies can be focused on elucidation of this phenomenon. For this purpose, biochemical signaling assays exploiting the biomimetic surfaces developed here can be performed to follow the up/down regulation of certain proteins and factors during the communication between the two receptors.

VI.5. Application to study directed cellular migration on gradients of signaling molecules

During this PhD thesis, model biomimetic surfaces were designed, which are well-defined (i.e. the orientation of ligands can be controlled, thus guaranteeing their functionality, in a background of low non-specific binding), and the surface density of each ligand can be quantitatively tuned, thus fulfilling the goal of the thesis. In addition, the PhD thesis has also demonstrated the potential of these biomimetic surfaces in interrogating the role of HS in chemokine-mediated myoblast behavior in the context of muscle development and repair. An important process involved in muscle development and repair is the migration of myoblasts in response to gradients of HS-bound chemokines. These biomimetic surfaces open the door to mechanistic studies of myoblast migration. To this end, these surfaces present excellent platforms for the preparation of gradients of HS-bound chemokines. In particular, micro-fluidic systems can be combined with our surface-functionalization strategy to immobilize HS in the form of a density gradient thus generating a gradient of HS-bound chemokine. Studies

with these gradients would further enhance the understanding of the role of HS, which was interrogated during the thesis, and provide further insights into physiological and pathological processes such as muscle development and repair, and inflammation.

VI. Concluding remarks and perspectives (en français)

Lobjectif de cette thèse concerne le développement de surfaces biomimétiques parfaitement définies et modulables, pour l'étude mécanistique des interactions protéine-GAG aux niveaux moléculaires et supramoléculaires, et pour sonder la réponse cellulaire aux signaux biochimiques et biophysiques afin de mieux comprendre les communications cellule-cellule et cellule-matrice induites par les GAGs. Dans les paragraphes suivants, les principales réalisations et les perspectives pour de plus amples études sont résumées.

VI.1. Fonctionnalisation des glycosaminoglycanes à leur extréminité réductrice

Nous avons établi que le lien oxime constitue une méthode simple qui permet de réaliser la conjugaison sélective des GAG à leur extrémité réductrice en une seule étape. La méthode conduit à des rendements supérieurs et à une meilleure stabilité par rapport au lien hydrazone qui est couramment utilisé. La méthode est polyvalente puisqu'elle peut être appliquée à une grande variété de GAGs (probablement à tous les GAGs quels qu'ils soient). De plus, nous avons démontré que la QCM-D est une technique instrumentale utile à la caractérisation des conjugués fabriqués à partir de molécules chimiquement complexes tels que les GAGs. La QCM-D fournit en effet des informations sur les rendements de réaction, la dégradation de l'échantillon et sa composition qui est difficile à évaluer en utilisant des techniques analytiques classiques, notamment lorsque la quantité de l'échantillon est limitée à quelques microgrammes.

Cette méthode pourrait être étendue pour créer des conjugués de GAG plus complexes, des ligands multifonctionnels, par exemple des GAGs portant à la fois un marqueur fluorescent (ATTO) et un groupe biotine. Ce mode de conjugaison pourra être appliqué dans de nombreux domaines tels que l'imagerie, l'immobilisation ou la détection enzymatique (par exemple avec l'utilisation de la streptavidine fonctionnalisée par la peroxydase de raifort).

Une autre application possible est la conception de mime de GAGs où différents saccharides sont fixés artificiellement avec une conformation particulière. Par exemple, deux oligosaccharides présentant des groupes sulfate à des distances particulières pourraient être couplés avec un contrôle de la distance entre les groupes sulfate. Ces conjugués pourraient être exploitées pour étudier l'effet de la distance entre des groupes sulfate sur leur interaction avec des protéines. A cet effet, un espaceur bifonctionnel présentant deux groupes oxyamine pourrait être exploité pour coupler deux oligo ou polysaccharides différents.

En conclusion, la technique de couplage devrait être largement utilisée comme outil dans le domaine des glycosciences et pour des applications biotechnologiques. Dans le cadre d'applications telles que l'ingénierie tissulaire ou pour des études biologiques fondamentales, le contrôle et la stabilité de conjugués de GAG sont fondamentaux pour la préparation fiable des surfaces et des substrats fonctionnalisés par les GAGs. Ces conjugués ont été utilisés dans un projet de recherche du groupe de Ralf Richter au CIC biomaGUNE, dans lequel j'ai été impliqué et qui a donné lieu à une publication dont je suis co-auteur (N. Baranova *et al.*, *J. Biol. Chem., 2*89 (2014) 30481–98).

VI.2. Préparation des surfaces biomimétiques

Nous avons présenté une stratégie polyvalente pour créer des surfaces biomimétiques portant des GAGs et d'autres composantes de la surface cellulaire ou des matrices extracellulaires, sur un substrat résistant aux interactions non-spécifiques. Ces surfaces biomimétiques sont basées sur une plateforme constituée d'une monocouche de SAv, fixée sur une monocouche d'OEG ou sur une SLB. Nous avons démontré que l'orientation des molécules immobilisées peut être contrôlée et leur densité de surface ajustée, grâce à l'architecture de l'assemblage et à la caractérisation quantitative par des techniques sensibles de surface. De plus, nous avons démontré le potentiel de cette plateforme pour des études fonctionnelles aux niveaux moléculaires, supramoléculaires et cellulaires.

Ces surfaces biomimétiques reproduisant la matrice extracellulaire des muscles ont permis de comprendre le rôle de la chimiokine CXCL12α présentés dans des conditions physiologiques, dans le développement et la réparation musculaire. Cependant, ces surfaces biomimétiques ne sont pas limitées uniquement à l'étude du développement et de la réparation musculaire; elles recèlent également un potentiel d'applications bien au-delà ce qui est exploitée dans cette thèse. En fait, toutes les biomolécule peuvent être greffées sur ces surfaces, à condition d'être préalablement biotinylées. Des études mécanistiques cellulaires peuvent alors être effectuées pour interroger leur fonction biologique. Ces surfaces devraient également trouver une large applicabilité dans les études mécanistiques où les réponses cellulaires à différentes présentations de biomolécules sont à étudier. La stratégie visant à créer des surfaces biomimétiques multifonctionnelles qui présentent différentes biomolécules devraient être largement applicables pour interroger le crosstalk entre deux récepteurs cellulaires.

VI.3. Interactions supramoléculaire HS-chimiokines

Les surfaces biomimétiques ont été utilisés pour étudier les interactions supramoléculaires protéine-HS. Nous démontrons que les chimiokines et d'autres facteurs de croissance réticulent les chaines de HS. Cette capacité à réticuler les HS est une caractéristique générique de ces protéines, qui dépend de l'architecture de leurssites de liaison aux HS. Nous proposons que les sites de liaison de la protéine soient

séparés d'une part par des régions répulsives aux charges négatives des GAGs , et par la séparation spatiale due à la structure quaternaire des protéines. Ces séparations entre les sites de liaison sont nécessaires à la réticulation des GAGs. Dans le cas de la chimiokine CXCL12, nous proposons un mécanisme deréticulation des HS qui est basé sur la co-existence de deux types de dimères, les dimères résultant de par l'association de feuillets β ou des extréminté N-terminales de la protéine, dans la matrice de HS. La dimérisation par les feuillets β améliore l'affinité de la protéine pour les HS alors que la dimérisation par les extrémités N-terminales induit la réticulation des HS, qui peut potentiellement former des dimères de dimères.

La capacité des protéines extracellulaires de signalisation à influencer l'organisation et les propriétés physico-chimiques de la matrice implique que leurs fonctions ne sont pas limitées simplement à l'activation des récepteurs cellulaires apparentés. La réticulation des HS sur la surface cellulaire ou de l'ECM conduit à une réduction de l'épaisseur des couches péricellulaires. Cette diminution d'épaisseur rendrait accessibles les ligands d'adhésion cellulaire alors qu'ils sont habituellement enfouies dans la matrice, ce qui faciliterait les contacts cellule-cellule et cellule-matrice. Cette adhésion est particulièrement importante car elle provoque la traction nécessaire aux cellules dans leur mouvement (sur la surface), en l'absence de laquelle les cellules seraient e emportées par le flux sanguin par exemple, dans le contexte de la migration des leucocytes au niveau des parois internes des vaisseaux sanguins. De plus, des changements de rigidité du glycocalyx cellulaire par la réticulation des HS peuvent fournir un signal physique qui guide le comportement des cellules.

L'effet démontré ici peut avoir des implications profondes pour les communications cellule-cellule et cellule-matrice, et nos prédictions peuvent être évaluées à l' avenir par des tests cellulaire in vivo.

VI.4. Réponse des myoblastes sur les surfaces biomimétiques

La stratégie développée ici pour créer des surfaces biomimétiques conduit à la conception d'une plate-forme expérimentale polyvalente pour la réalisation d'études mécanistiques de communication cellule-cellule et cellule-matrice induites par les chimiokines, et pour analyser le rôle des GAGs dans la présentation des chimiokines. Nous avons démontré que la manière dont la chimiokine est présentée, et en particulier la présence du HS, est importante dans la régulation du comportement des myoblastes. Les myoblastes répondent à la chimiokine CXCL12α liée réversiblement à son ligand naturel le HS par une adhésion et une motilité accrues. En revanche, la CXCL12α fixée irréversiblement à la surface (en l'absence de HS) favorise l'adhésion mais diminue la motilité. Les cellules préfèrent peut-être les CXCL12α liées réversiblement, ce qui faciliteraite son internalisation et déclencherait la signalisation interne induisant ainsi un comportement spécifique. En effet, il a été démontré que l'internalisation des

CXCL12α permet d'induire la signalisation en aval [1]. Des études ultérieures pourraient explorer l'influence d'une internalisation potentielle de la CXCL12α lié réversiblement au HS sur la signalisation qui n'est pas détectée dans les tests utilisés ici d'adhésion cellulaire et de motilité. A cet effet, la chimiokine marquée par fluorescence pourra être utilisée. Une autre configuration de la CXCL12α liée irréversiblement pourra être impliquée, il s'agit de la chimiokine fixée de manière covalente aux chaînes de HS. Ce mode de fonctionnalisation sera plus proche de celui correspondant à la chimiokine liée réversiblement au HS mais sans la possibilité de libérer la CXCL12α ni son internalisation par la cellule. Cela pourrait permettre de mieux comprendre l'origine moléculaire des comportements cellulaires distincts observés.

Cette thèse a permis d'approfondir les connaisssances sur le rôle des GAGs dans le comportement des myoblastes induits par les chimiokines. De plus, cette étude a soulevé de nombreuses autres questions qui nécessiteraient la poursuite des travaux pour lesquels les surfaces biomimétiques seront très utiles. Plusieurs directions possibles pourraient être explorées, elles sont décrites ci-dessous. Pour comprendre l'influence de la présentation de la chimiokine sur les différentes réponses cellulaires une étude pourra être réalisée sur des surfaces qui présentent d'une part le HS et la CXCL12α fixée irréversiblement sur la surface et d'autre part des surfaces où la CXCL12α est liée au HS avec des densités surfaciques similaires. La comparaison des réponses fournirait de nouvelles informations sur l'importance de la présentation des chimiokines et le rôle du HS dans les réponses cellulaires.

La mobilité cellulaire observée sur les surfaces fonctionnalisées par la CXCL12α liée réversiblement au HS soulève une autre question: les cellules sont-elles polarisées pendant le mouvement? Les futures études pourraient être axées sur l'étude du mécanisme impliqué dans la motilité cellulaire. Nous avons observé une morphologie cellulaire bien distincte sur *i*CXCL12α (CXCL12α quasi-irréversiblement immobilisée sur la surface en l'absence de HS), la formation de protrusions riches en actine. Ces futures études pourraient permettre de comprendre si si ces protrusions sont riches en intégrine et si les intégrines sont également impliquées dans l'adhésion cellulaire très prononcée sur *i*CXCL12α. A cet effet, le marquage de l'intégrine pourra être réalisé pour identifier si les intégrines sont impliquées et le type d'intégrine impliqué. D'autres questions importantes se posent : ces protrusions sont-elles statiques ou dynamiques, et de quelle nature sont ces protrusions, filopodes ou lamellipodes? Les futures études pouront répondre à ces questions.

Nous avons ensuite conçu des surfaces multifonctionnelles qui miment certains aspects des conditions in vivo. Nous décrivons des améliorations significatives de l'adhésion, de l'etalement et de la motilité sur des surfaces portant le ligand RGD et la CXCL12α liée au HS, par rapport à chaque signal pris individuellement. Cela démontre que les récepteurs des cellules le CXCR4 (récepteur de la CXCL12α) et l'intégrine (récepteur du RGD)

peuvent agir en synergie dans le contrôle de l'adhésion et de la migration cellulaire. Ceci suggère un cross-talk entre le CXCR4 et l'intégrine. Les futures études pourraient être axées sur l'élucidation de ce phénomène. A cet effet, des tests biochimiques de signalisation exploitant les surfaces biomimétiques développées ici pourront être effectuées pour suivre le la régulation (positive ou négative) de certaines protéines et des facteurs au cours de la communication entre les deux récepteurs.

VI.5. Application à l'étude dirigée de la migration cellulaire sur les gradients de molécules de signalisation

Au cours de cette thèse, des surfaces biomimétiques modèles bien définies ont été conçues (par exemple l'orientation des ligands peut être contrôlée ce qui garantit leur fonctionnalité sur des surfaces passivées qui limitent l'adsorption non-spécifique des cellules), et la densité de surface de chaque ligand peut être quantitativement modulée, remplissant ainsi l'objectif de la thèse. De plus, ces travaux ont également démontré le potentiel de ces surfaces biomimétiques à interroger le rôle des HS dans le comportement des myoblastes induit par la chimiokine dans le contexte du développement et de la réparation musculaire. Un processus important impliqué dans le développement et la réparation musculaire est la migration des myoblastes en réponse à des gradients de chimiokines liés au HS. Ces surfaces biomimétiques ouvrent la porte à des études mécanistiques concernant la migration des myoblastes. A cet effet, ces surfaces constituent d'excellentes plates-formes pour la préparation de gradients de chimiokines liés au HS. En particulier, les systèmes micro-fluidiques peuvent être combinés avec notre stratégie de fonctionnalisation de surface pour immobiliser les HS sous la forme d'un gradient de densité, générant ainsi un gradient de chimiokine liée au HS. Des études avec ces gradients permettraient d'améliorer la compréhension du rôle des HS, qui a été interrogé au cours de la thèse, et de fournir de nouvelles informations sur les processus physiologiques et pathologiques tels que le développement,la réparation musculaire, et l'inflammation.

References:

[1] Hatse S, Balzarini J, Liekens S. Stromal cell-derived factor 1 (CXCL12) binds to endothelial cells and signals through a receptor different from CXCR4. Biochem Biophys Res Commun. 2006;348:192-9.

Publications

Publications and manuscripts in preparation related to the PhD project work:

1. **D. Thakar**,* E. Migliorini,* R. Sadir, T. Pleiner, F. Baleux, H. Lortat-Jacob, L. Coche-Guerente and R. P. Richter. Well-defined biomimetic surfaces to characterize glycosaminoglycan-mediated interactions on the molecular, supramolecular and cellular levels. *Biomaterials*, 35 (2014) 8903-8915.
2. **D. Thakar**, E. Migliorini, L. Coche-Guerente, R. Sadir, H. Lortat-Jacob, D. Boturyn, O. Renaudet, P. Labbé and R. P. Richter. A Quartz Crystal Microbalance Method to Study the Terminal Functionalization of Glycosaminoglycans. *Chem. Commun.,* 50 (2014) 15148-51.
3. N. S. Baranova, A. Inforzato, D. C. Briggs, V. Tilakaratna, J. J. Enghild, **D. Thakar**, C. M. Milner, A. J. Day and R. P. Richter. Incorporation of Pentraxin 3 into Hyaluronan Matrices is Tightly Regulated and Promotes Matrix Cross-Linking. *J. Biol. Chem., 2*89 (2014) 30481–98.
4. E. Migliorini, **D. Thakar**, J. Kühnle, R. Sadir, D. P. Dyer, Y. Li, C. Sun, B. F. Volkman, T. M. Handel, L. Coche-Guerente, D. G. Fernig, H. Lortat-Jacob, and R. P. Richter. Cytokines and growth factors cross-link heparan sulfate, *submitted to Open Biol.*
5. **D. Thakar**, F. Dalonneau, E. Migliorini, R. Sadir, H. Lortat-Jacob, D. Boturyn, L. Coche-Guerente, C. Picart and R. P. Richter. The mode of chemokine display determines myoblast adhesion and motility, manuscript in preparation.

Other publications:

6. **D. Thakar**, L. Coche-Guérente, M. Claron, C. Wenk, J. Dejeu, P. Dumy, P. Labbé and D. Boturyn. Redox-driven host-guest interactions allow the controlled release of captured cells on RGD-functionalized surfaces. *ChemBioChem* 2014; 15(3):377-81.
7. L. Sandrine, **D. Thakar**, C. Goyer, P. Labbé, D. Boturyn and L. Coche-Guérente. Controlled surface density of RGD ligands for cell adhesion: evidence for a ligand specificity by using QCM-D. *J. Mater. Chem. B* 2015; DOI: 10.1039/C5TB00420A.
8. R. Medwal, K. Gogia, **D. Thakar**, V. Vibhu, J. R. Mohan, N. Sehdev and S. Annapoorni. Effect of functionalization on positional ordering of 3 nm FePt nanoparticles: Langmuir–Blodgett monolayer. *Surf. Coat. Technol. 258* (2014) 509-514.
9. L. Kumar, R. Gupta, **D. Thakar**, V. Vibhu and S. Annapoorni. A New Route to Glucose Sensing Based on Surface Plasmon Resonance Using Polyindole. *Plasmonics* 8 (2013) 487–494.

* - authors contributed equally

Communications

Oral communications:

- *Design of biomimetic surfaces to interrogate the role of glycosaminoglycans in chemokine-induced myoblast behavior.* **D. Thakar**, E. Migliorini, F. Dalonneau, R. Sadir, O. Renaudet, H. Lortat-Jacob, D. Boturyn, L. Coche-Guérente, C. Picart, R. P. Richter. 2015 MRS spring meeting, San Francisco, USA; 06-10/04/2015.

- *Design of biomimetic surfaces to interrogate the role of glycosaminoglycans in chemokine-induced myoblast behavior.* **D. Thakar**, E. Migliorini, L. Coche-Guérente, R. Sadir, F. Dalonneau, C. Laguri, D. Boturyn, O. Renaudet, C. Picart, H. Lortat-Jacob, P. Labbé, R. P. Richter. Journée des Doctorants – Nanoscience Foundation, Grenoble, France; 01/04/2014.

- *The sweet spot - How sugars make cells behave.* **D. Thakar**, E. Migliorini, L. Coche-Guérente, R. Sadir, F. Dalonneau, C. Laguri, D. Boturyn, O. Renaudet, C. Picart, H. Lortat-Jacob, P. Labbé, R. P. Richter. Journée des Doctorants - Ecole Doctorale Chimie & Sciences du Vivant (EDCSV), Grenoble, France; 24/04/2014.

- *Biomimetic surfaces with nano scale control to study cell migration processes.* **D. Thakar**, E. Migliorini, L. Coche-Guérente, R. Sadir, F. Dalonneau, D. Boturyn, O. Renaudet, C. Picart, H. Lortat-Jacob, P. Labbé, R. P. Richter. Scientific Council – Nanoscience Foundation, Grenoble, France; 02-03/06/2014.

- *Biomimetic surfaces with nano scale control to study cell migration processes.* ***D.*** **Thakar**, E. Migliorini, L. Coche-Guérente, R. Sadir, F. Dalonneau, D. Boturyn, O. Renaudet, C. Picart, H. Lortat-Jacob, P. Labbé, R. P. Richter. Assemblée Generale – DCM, Grenoble, France; 03/07/2014.

Communications by poster:

- *Design of biomimetic surfaces to interrogate the role of glycosaminoglycans in chemokine-induced myoblast behavior.* **D. Thakar**, E. Migliorini, F. Dalonneau, R. Sadir, O. Renaudet, H. Lortat-Jacob, D. Boturyn, L. Coche-Guérente, C. Picart, R. P. Richter. ERC BIOMIM Meeting, Grenoble, France; 11-13/03/2015.

- *Morphogens cross-link heparan sulphate.* E. Migliorini, **D. Thakar**, R. Sadir, H. Lortat-Jacob, D. Fernig, L. Coche-Guérente, R. P. Richter. Proteoglycans Gordon Research Seminar and Conference, Andover, USA; 06-11/07/2014.

- *Design of biomimetic surfaces to interrogate the role of glycosaminoglycans in chemokine-induced myoblast behaviour.* **D. Thakar**, E. Migliorini, L. Coche-

Guérente, R. Sadir, C. Laguri, F. Dalonneau, C. Picart, H. Lortat-Jacob, O. Renaudet, D. Boturyn, P. Labbé, R. P. Richter. FEBS Workshop "Biological Surfaces and Interfaces", Sant Feliu de Guixols, Spain; 30/06-05/07/2013.

- *Glycosaminoglycan-presenting surfaces to study lymphocyte trafficking during immune response.* E. Migliorini, **D. Thakar**, L. Coche-Guérente, R. Sadir, H. Lortat-Jacob, L. Leroy, P. Labbé, R. P. Richter. FEBS Workshop "Biological Surfaces and Interfaces", Sant Feliu de Guixols, Spain; 30/06-05/07/2013.

- *Design of biomimetic surfaces to interrogate the role of glycosaminoglycans in chemokine-induced myoblast behaviour.* **D. Thakar**, E. Migliorini, L. Coche-Guérente, R. Sadir, C. Laguri, F. Dalonneau, C. Picart, H. Lortat-Jacob, O. Renaudet, D. Boturyn, P. Labbé, R. P. Richter. 18th Congress – Groupe Français des Peptides et des Protéines, Sète, France; 26-31/05/2013.

- *Glycosaminoglycan-presenting surfaces to study lymphocyte trafficking during immune response.* E. Migliorini, **D. Thakar**, L. Coche-Guérente, R. Sadir, H. Lortat-Jacob, L. Leroy, P. Labbé, R. P. Richter. ERC BIOMIM Meeting, Grenoble, France; 10-12/04/2013.

Annex

A.1. Biotinylation of cell adhesion ligand (cRGD)

To graft the cell adhesion ligand onto biomimetic surfaces, a biotin tag was attached to cRGD. b-cRGD was obtained by amide-coupling of linear PEG with a biotin at one end and an activated acid group (an N-Hydroxysuccinimide (NHS) group) at the other (b-PEG-NHS) to a cyclic pentapeptide containing RGD and with a pendant NH_2 group ((RGD*f*K)-NH_2, previously synthesized in the lab [1]) (Figure A.1). A PEG linker with M_w = 3kDa, between biotin and cRGD was used to control the thickness of cRGD film adsorbed on the molecular breadboard. These PEG chains adopt a random coil conformation on the surface and a PEG chain with M_W 3 kDa and corresponding radius of gyration, R_g ~ 2.3 nm [2], would occupy a surface area of ~ 17 nm^2. This surface area is less than half the surface area of SAv (~ 40 nm^2) suggesting two PEG chains can be grafted on each SAv, which a longer PEG chain would fail to do. Hence, we chose this PEG chain length to saturate the binding sites on SAv based molecular breadboard.

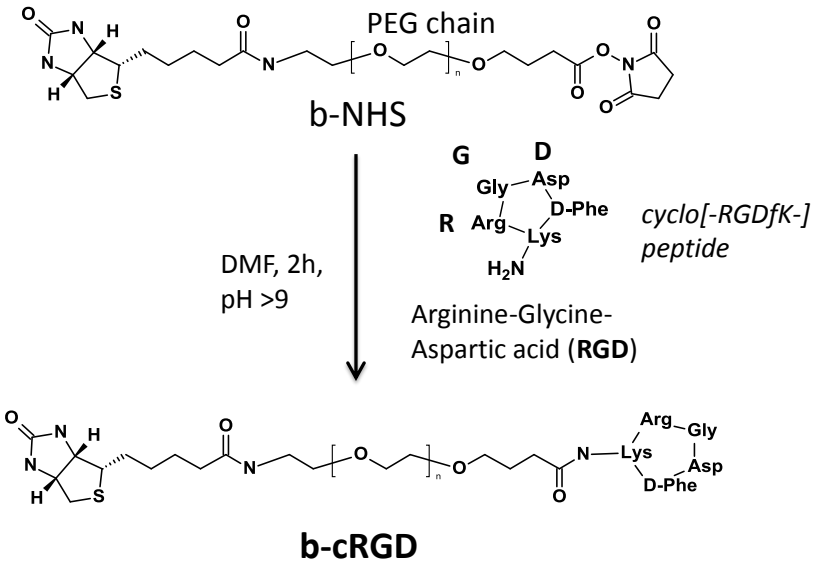

Figure A.1: Strategy adopted for the biotinylation of cRGD.

References:

[1] Boturyn D, Dumy P. A convenient access to aVb3:aVb5 integrin ligand conjugates: regioselective solid-phase functionalisation of an RGD based peptide. Tetrahedron Lett. 2001;42:2787-90.

[2] Linegar KL, Adeniran AE, Kostko AF, Anisimov MA. Hydrodynamic radius of polyethylene glycol in solution obtained by dynamic light scattering. Colloid Journal. 2010;72:279-81.

Well-defined biomimetic surfaces to characterize glycosaminoglycan-mediated interactions on the molecular, supramolecular and cellular levels

The oriented migration and controlled adhesion of cells is fundamental to many physiological and pathological processes. A family of linear polysaccharides, known as glycosaminoglycans (GAGs), help organizing and presenting signaling proteins, so-called chemokines, on the cell surface and in the extracellular matrix thus regulating cellular behavior. The objective of this PhD thesis was to develop biomimetic surfaces that are highly defined and tunable, for mechanistic studies of GAG-protein interactions on the molecular and supramolecular levels, and to probe cellular responses to defined biochemical and biophysical cues to better understand GAG-mediated cell-cell and cell-matrix communications.

Applying oxime ligation, GAGs could be stably functionalized with biotin at the reducing end, and these features proved crucial for the reliable preparation of GAG-functionalized surfaces. A streptavidin monolayer served as a 'molecular breadboard' to sequentially assemble biotinylated molecules with controlled orientation and surface densities. GAGs (heparan sulfate (HS) in particular), chemokines and other ECM components (e.g. integrin ligands promoting cell adhesion, RGD) were assembled into multifunctional surfaces that recapitulate selected aspects of the *in vivo* situation. Quartz crystal microbalance (QCM-D) and spectroscopic ellipsometry permitted us to characterize and control the supramolecular presentation of HS and RGD. These model surfaces were used to study the supramolecular interactions between HS and the selected chemokine stromal derived factor SDF-1α/CXCL12α and to analyze cellular responses to extracellular cues. Our data provide evidence that CXCL12α binding rigidifies HS assemblies, and that this effect is due to protein-mediated cross-linking of HS chains. The kinetics of chemokine binding to HS was quantified using surface plasmon resonance (SPR). We also demonstrate that the way in which the chemokine is presented, and in particular the presence of HS, is important for regulating myoblast behavior. Our data shows that the cell surface receptors CXCR4 (the CXCL12α receptor) and integrins (the RGD receptor) can act synergistically in controlling cellular adhesion and migration. These surfaces can generate novel insights in the field of glycobiology, e.g. in dissecting the function of GAGs in chemokine-mediated cellular migration.

Keywords: Heparan sulfate, chemokine, biomimetic surfaces, HS-protein interactions, cell-matrix interactions

Surfaces biomimétiques pour caractériser les interactions induites par les glycosaminoglycanes aux niveaux moléculaire, supramoléculaire et cellulaire

L'adhésion contrôlée et la migration orientée des cellules est fondamentale pour plusieurs processus physiologiques et pathologiques. Une famille de polysaccharides linéaires, connus sous le nom de glycosaminoglycanes (GAG) est impliquée dans l'organisation et la présentation des protéines de signalisation, les chimiokines, à la surface des cellules et dans la matrice extracellulaire (ECM). Les travaux concernent le développement de surfaces biomimétiques bien définies aux niveaux moléculaires et supramoléculaires pour l'étude des mécanismes d'intéractions protéines-GAG et l'analyse de la réponse cellulaire à des signaux biochimiques et biophysiques spécifiques. L'objectif de cette étude est de mieux comprendre les communications cellule-cellule et cellule-matrice induites par les GAGs.

En utilisant la ligation oxime, les GAGs peuvent être fonctionnalisés de manière stable par la biotine à leur extrémité réductrice, ce mode de couplage s'est avéré déterminant pour préparer des surfaces fonctionnalisées par les GAGs de manière stable. Une monocouche de streptavidine est utilisée comme plateforme modulable pour assembler séquentiellement les molécules biotinylées, avec une orientation et des densités de surface contrôlées. Des GAGs (les héparane sulfate (HS), en particulier), des chimiokines et d'autres composants de l'ECM (par exemple un ligand d'adhésion cellulaire, RGD) ont été assemblés reconstituant certains aspects des surfaces *in vivo* (cellules ou de l'ECM). La microbalance à quartz (QCM-D) et l'ellipsométrie spectroscopique nous ont permis de caractériser et de contrôler la présentation supramoléculaire du HS et du RGD. Ces surfaces modèles ont été utilisées pour étudier les interactions supramoléculaires entre le HS et la chimiokine SDF-1α/CXCL12α facteur d'origine stromale et pour analyser les réponses cellulaires aux signaux extracellulaires. Nos données apportent la preuve que la chimiokine, CXCL12α rigidifie les assemblages de HS, et que cet effet est dû à la réticulation des chaînes de HS induite par la protéine. La cinétique des interactions HS-chimiokine a été quantifiée en utilisant la résonance plasmonique de surface (SPR). Nous avons également démontré que le mode de présentation de la chimiokine sur la surface, en particulier la présence des HS, influence le comportement des myoblastes. Nos données montrent que les récepteurs cellulaires CXCR4 (récepteur de la CXCL12α) et l'intégrine (récepteur du RGD) peuvent agir en synergie pour contrôler l'adhésion et la migration cellulaire. Ces surfaces modèles fournissent des indications précieuses qui pourront être appliquées au domaine de la glycobiologie, par exemple, pour étudier le rôle des GAGs dans la migration cellulaire induite par les chimiokines.

Mot clés: Heparane sulfate, chimiokine, surface biomimétique, interactions HS-protéine, interactions cellule-matrice